



5-2017

Thermally Robust and Redox Active Catalysts: Studying Their Behavior for Ethylene and L-lactide Polymerization

Lauren Ashley Brown

University of Tennessee, Knoxville, lbrown75@vols.utk.edu

Recommended Citation

Brown, Lauren Ashley, "Thermally Robust and Redox Active Catalysts: Studying Their Behavior for Ethylene and L-lactide Polymerization." PhD diss., University of Tennessee, 2017.
https://trace.tennessee.edu/utk_graddiss/4387

This Dissertation is brought to you for free and open access by the Graduate School at Trace: Tennessee Research and Creative Exchange. It has been accepted for inclusion in Doctoral Dissertations by an authorized administrator of Trace: Tennessee Research and Creative Exchange. For more information, please contact trace@utk.edu.

To the Graduate Council:

I am submitting herewith a dissertation written by Lauren Ashley Brown entitled "Thermally Robust and Redox Active Catalysts: Studying Their Behavior for Ethylene and L-lactide Polymerization." I have examined the final electronic copy of this dissertation for form and content and recommend that it be accepted in partial fulfillment of the requirements for the degree of Doctor of Philosophy, with a major in Chemistry.

Brian K. Long, Major Professor

We have read this dissertation and recommend its acceptance:

Michael D. Best, Ziling Xue, S. Michael Kilbey II

Accepted for the Council:

Dixie L. Thompson

Vice Provost and Dean of the Graduate School

(Original signatures are on file with official student records.)

Thermally Robust and Redox Active Catalysts: Studying Their Behavior for Ethylene and L- lactide Polymerization

**A Dissertation Presented for the
Doctor of Philosophy
Degree
The University of Tennessee, Knoxville**

**Lauren Ashley Brown
May 2017**

Copyright © 2017 by Lauren A. Brown
All rights reserved.

DEDICATION

This dissertation is dedicated to my parents, nana, and granny. Without your love and support, I would not have made it this far.

ACKNOWLEDGEMENTS

First, I want to thank my research advisor Dr. Brian K. Long. Your guidance over the past several years has been instrumental in shaping my chemistry career. You motivated me to be a better chemist, leader, and co-worker. I am eternally grateful for all the guidance and inspiration you have provided. If I had to do it all over again, I would still choose the Long research group.

Special thanks to my doctoral committee: Prof. Michael Best, Prof. Mike Kilbey, Prof. Ben Xue, and Prof. Bruce Bursten. Your time, guidance, comments, and critiques of my work have made me a better scientist for which I am truly grateful. To the chemistry faculty at Wofford College, I am proud to say that my chemistry education started with you. This work would not be possible without the financial support from the U.S. Army Research Office.

The Long research group (past and present members) became my Knoxville family. Thank you for your friendship, advice, and support. Specifically, I would like to thank Dr. Jennifer Rhinehart and Dr. Costyl Njiojob for their synthetic advice. Kevin (and Jennie) Gmernicki, your friendship was instrumental in making these past five years successful, and I am glad that we were the trailblazers for the Long group. And of course, a special thanks to Team Redox, Curtis Anderson, Jordan Kaiser, and Alicia Doerr. I think the lab would have been a lot quieter without us.

Finally, I want to thank my family and my friends for always being there for me. Especially, I want to thank my parents, Jeff and Jan, who have given their endless love, support, and encouragement. I can never repay you. I also want to thank Curtis Anderson for love, advice, and support throughout this journey. I would also like to give a special shout out to my doggies, Louis and Bear, who have given me their love, support, and cuddles throughout this journey.

ABSTRACT

The development of homogenous single-site catalysts has significantly impacted the field of organometallic chemistry. The well-defined structures of homogenous catalysts make it less cumbersome to understand and develop methods to tailor these compounds for specific catalytic processes. Currently, polymerization catalysis is a major division in organometallic chemistry due to the global demand for polymeric materials such as polyethylene (PE) and polypropylene (PP), based on their low-cost feedstock, remarkable mechanical properties, and their use in a wide range of applications. However, bioplastics have become a highly sought-after alternative to conventional petrochemical-based plastics due to their biodegradability and derivatization from renewable resources. Specifically, polylactic acid (PLA) has shown tremendous promise for a variety of applications including medical and packaging products. With such a high demand for these materials, there is a great desire to understand and to be able to control the polymerizations of monomers such as ethylene and lactide.

This dissertation will describe several advances the Long group has taken toward designing advanced single-site catalysts for the polymerization of ethylene and L-lactide. In our studies, we have determined that catalyst design can have a major impact on polymerization behavior and catalyst stability. More specifically, our group has been particularly successful in (1) designing thermally robust catalysts for ethylene polymerization and (2) designing redox-switchable catalysts for L-lactide polymerization. To date, our group has published several fundamental studies encompassing thermally robust catalysts for polyethylene and the development of redox-switchable catalysts for PLA. A portion of these results will be described herein.

TABLE OF CONTENTS

CHAPTER 1– INTRODUCTION TO ETHYLENE POLYMERIZATION CATALYSIS.....	1
1.1 MOTIVATION	2
1.2 EARLY POLYETHYLENE CATALYSIS	2
1.2.1 Ziegler/Natta Catalysis.....	2
1.2.2 Homogenous Catalysis.....	4
1.3 INTRODUCTION TO GROUP 10 ETHYLENE POLYMERIZATION CATALYSTS.....	5
1.4 RESEARCH OBJECTIVES	9
CHAPTER 2– THERMALLY ROBUST NICKEL (II) CATALYSTS FOR ETHYLENE POLYMERIZATIONS.....	11
2.1 ABSTRACT.....	12
2.2 INTRODUCTION	12
2.3 RESULTS AND DISCUSSION.....	14
2.4 CONCLUSIONS.....	22
2.5 EXPERIMENTAL.....	23
2.5.1 General Methods and Materials.....	23
2.5.2 Synthesis of <i>N,N'</i> -bis(2,6-dibenzhydryl-4-methylphenyl) butane-2,3-diimine (1b).....	24
2.5.3 Synthesis of $NiBr_2(ArN=CC=NAr)$ (<i>Ar</i> = 2,6 bis(diphenylmethyl)-4-methylbenzene) (2a).....	24
2.5.4 Synthesis of $NiBr_2(ArN=C(Me)C(Me)=NAr)$ (<i>Ar</i> = 2,6 bis(diphenylmethyl)-4-methylbenzene) (2b).....	24
2.5.5 General Polymerization Conditions.....	25
CHAPTER 3– CONTROLLED/LIVING THERMALLY ROBUST NICKEL (II) CATALYST FOR ETHYLENE POLYMERIZATION	26
3.1 ABSTRACT.....	27
3.2 INTRODUCTION	27
3.3 RESULTS AND DISCUSSION.....	28
3.4 CONCLUSIONS.....	39
3.5 EXPERIMENTAL.....	40
3.5.1 General Methods and Materials.....	40

3.5.2 General Ethylene Polymerization Procedure.....	40
CHAPTER 4– INTRODUCTION TO REDOX-SWITCHABLE CATALYSIS FOR CYCLIC ESTER POLYMERIZATIONS.....	42
4.1 MOTIVATION	43
4.2 REDOX SWITCHABLE CATALYSIS	44
4.3 REDOX SWITCHABLE POLYMERIZATION CATALYSIS	44
4.4 RESEARCH OBJECTIVES	49
CHAPTER 5– REDOX ACTIVE TITANIUM (IV) SALFEN CATALYST FOR L-LACTIDE POLYMERIZATIONS.....	52
5.1 ABSTRACT.....	53
5.2 INTRODUCTION	53
5.3 RESULTS AND DISCUSSION.....	56
5.4 CONCLUSIONS.....	69
5.5 EXPERIMENTAL.....	69
5.5.1 General Materials and Methods.....	69
5.5.2 Synthesis of (salfen)Ti(O ⁱ Pr) ₂ (5 _{red})	70
5.5.3 General Procedure for NMR Scale Polymerizations.....	71
C.5.3.1 Oxidation/reduction of 5 in the absence of L-lactide.....	71
C.5.3.2 Oxidation/reduction of 5 in the presence of L-lactide	71
5.5.4 In situ Switching Polymerization	71
5.5.5 General Procedure for Scale-up of Polymerizations	72
CHAPTER 6– CONCLUSIONS AND FUTURE WORK	73
6.1 SUMMARY AND CONCLUSIONS.....	74
6.2 FUTURE WORK.....	75
6.3 EXPERIMENTAL.....	80
6.3.1 General Materials and Methods.....	80
6.3.2 NMR Scale Polymerization Procedure.....	80
6.3.3 Synthesis of 2-(bromomethyl)-4,6-di-tert-butylphenol	80
6.3.4 Synthesis of monoferrocenyl salalen (9).....	81
6.3.4 Synthesis of monoferrocenyl (salalen)Ti(O ⁱ Pr) ₂ (14)	81
6.3.2 Synthesis of Ethynylferrocene (13).....	82

6.3.3 Synthesis of 3-tert-butyl-5-iodo-2-hydroxybenzaldehyde (14)	82
6.3.4 Synthesis of 3-tert-butyl-5-ethynylferrocene-2-hydroxybenzaldehyde (15)	83
6.3.5 Synthesis of Bis(3-tert-butyl-5-ethynylferrocene-salicylidene)-1,2-ethylenediamine (16).....	83
6.3.6 Synthesis of 6,6'-((ethane-1,2-diylbis(azanediyl))bis(methylene))bis(2-(tert-butyl)-4-ethynylferrocenephenol (17)	83
6.3.7 Synthesis of dimethyl ethane-1,2-diylbis((3-tert-butyl)-5-ethynylferrocene-2-hydroxybenzyl)carbamate) (18)	84
6.3.8 Synthesis of 6,6'-((ethane-1,2-diylbis(methylazanediyl))bis(methylene))bis(2-(tert-butyl)-4-ethynylferrocenephenol (11)	84
REFERENCES.....	85
APPENDICES	100
APPENDIX A –PROGRESS TOWARD OTHER REDOX ACTIVE LIGANDS	101
A.1 INTRODUCTION	102
A.2 RESULTS AND DISCUSSION	103
A.3 CONCLUSIONS	106
A.4 EXPERIMENTAL	107
A.4.1 General Considerations.....	107
A.4.9 Synthesis of Iodoferrocene (19).....	107
A.4.10 Synthesis of N-ferrocenyl phthalimide (20).....	107
A.4.11 Synthesis of Aminoferrocene (21)	108
A.4.12 Synthesis of Ferrocenyldimethyl(2,3,4,5-tetramethylcyclopenta-2,4-dien-1-yl)silane (22)	108
A.4.13 Synthesis of (E)-2-(tert-butyl)-6-(((2,6-diisopropylphenyl)imino)methyl-4-ethynylferrocenephenol (23).....	108
A.4.14 Synthesis of (E)-2,4-di-tert-butyl-6-(((ethynylferrocene)imino)methyl)phenol (24).....	109
APPENDIX B –POLYMERIZATION OF LACTIDE WITH AN IRON CATALYST	110
B.1 ABSTRACT.....	111
B.2 INTRODUCTION	111
B.3 RESULTS AND DISCUSSION	113
B.3.1 Synthesis and Characterization of BIAN-Fe(C ₆ H ₆).....	113
B.3.2 L-lactide Polymerization.....	113
B.4 CONCLUSIONS	120
B.5 EXPERIMENTAL	121

<i>B.5.1 General Considerations</i>	121
<i>B.5.2 X-ray crystallography</i>	122
<i>B.5.3 Preparation of BIAN-Fe(C₆H₆)</i>	122
<i>B.5.4 General Procedure for NMR Scale Polymerizations</i>	123
<i>B.5.5 General Procedure for Larger Scale Polymerizations</i>	123
<i>B.5.6 PROCEDURE FOR BIAN-Fe(C₆H₆) DECOMPOSITION STUDY</i>	123
B.6 SUPPORTING INFORMATION	124
<i>B.6.1 ¹H NMR Spectroscopy</i>	124
<i>B.6.2 Gel Permeation Chromatography</i>	127
APPENDIX C – EXPERIMENTAL AND SUPPORTING INFORMATION	131
C.1 SUPPORTING INFORMATION – CHAPTER 2	132
<i>C.1.1 X-ray Crystallography Data</i>	132
<i>C.1.2 NMR Spectroscopy</i>	133
C.2 SUPPORTING INFORMATION – CHAPTER 3	135
<i>C.2.1 NMR Spectroscopy</i>	135
<i>C.2.2 Gel Permeation Chromatography</i>	137
C.3 SUPPORTING INFORMATION – CHAPTER 5	154
<i>C.3.1 X-ray Crystallography Data</i>	154
<i>C.3.2 Gel Permeation Chromatography</i>	155
VITA	156

LIST OF TABLES

Table 2.1 Ethylene Polymerization Results for Temperature Screening of Catalyst 2a	17
Table 2.2 Ethylene Polymerization Results for Temperature Screening of Catalyst 2b ^a	17
Table 2.3 Ethylene Polymerization Results at 100 psi for 2b ^a	19
Table 3.1 Ethylene Polymerizations using Catalyst 3 ^a	32
Table 3.2 Ethylene Polymerizations Using Catalyst 3 and Cobaltocene ^a	39
Table 5.1 Polymerization Data for Catalyst 5_{red} after Rereduction in the Presence of Monomer ^a	62
Table B.1 L-lactide Polymerization using BIAN-Fe(C₆H₆) ^a	120

LIST OF FIGURES

Figure 1.1 Karl Ziegler (left) and Giulio Natta (right) who performed ethylene and propylene polymerizations with a TiCl_4 heterogeneous catalyst. Box represents open coordination site.....	3
Figure 1.2 Timeline for ethylene polymerization catalysis.	5
Figure 1.3 Representation of a nickel α -diimine catalyst generating PE with various branching contents with only ethylene as a feedstock.....	6
Figure 1.4 Coordination-insertion mechanism for ethylene polymerization with a cationic metal catalyst that has the ability to undergo chain-walking.....	7
Figure 1.5 Representation of a late transition metal catalyst incorporating polar comonomers during ethylene polymerization.	7
Figure 1.6 Increasing the thermal stability of a Ni α -diimine catalyst during ethylene polymerization by changing the N-aryl moiety or the ligand backbone.....	8
Figure 2.1 <i>N</i> -heterocyclic carbene (NHC) catalyst that contains <i>iPr</i> * moieties.	14
Figure 2.2 ORTEP drawing of precatalyst 2b with thermal ellipsoids drawn at 50% probability.....	16
Figure 2.3 Plot of M_n (squares) and M_w/M_n (open circles) versus yield for catalyst 2b at (a) 80 °C, 100 psi, (b) 90 °C, 100 psi, and (c) 100 °C, 100 psi.	20
Figure 2.4 Plots of (a) turnover frequency (TOF) versus time and (b) productivity versus time for catalyst 2b at 80 °C (green diamonds), 90 °C (red circles), and 100 °C (blue squares).....	21
Figure 3.1 Catalyst 3 used for ethylene polymerizations.....	28
Figure 3.2 Representative GPC of polyethylene produced with complex 3 containing an impurity.	29
Figure 3.3 LC-MS of <i>iPr</i> * aniline in DCM prior to purification.....	30
Figure 3.4 LC-MS of <i>iPr</i> * aniline in DCM after four recrystallizations from isopropanol.....	31
Figure 3.5 (a) Plot of M_n (blue circle) and \bar{D} (red triangles) as a function of polymerizations time when using 3 /PMAO-IP at 75 °C. (b) GPC traces (viscometer signal) of polymerizations at 75 °C as a function of polymerization time (black = 60 min, purple = 45 min, green = 30 min, orange = 15 min).....	33

Figure 3.6 (a) Plot of M_n (blue circles) and \bar{D} (red triangles) as a function of polymerization time using 3 /PMAO-IP at 70 °C. (b) GPC traces (viscometer detector) of polymerizations run at 70 °C at various polymerization times (black = 60 min, purple = 45 min, green = 30 min, orange = 15 min).....	34
Figure 3.7 Plot of activity versus reaction time for ethylene polymerizations using 3 /PMAO-IP at 75 °C.	35
Figure 3.8 (a) Plot of M_n (blue circle) and \bar{D} (red triangles) as a function of polymerizations time when using 3 /PMAO-IP at 80 °C. (b) GPC traces (viscometer signal) of polymerizations at 80 °C as a function of polymerization time (black = 60 min, purple = 45 min, green = 30 min, orange = 15 min).....	35
Figure 3.9 Plot of M_n (blue circles) and \bar{D} (red triangles) as a function of polymerization yield using 3 /PMAO-IP at 70 °C.	36
Figure 3.10 Plot of M_n (blue circles) and \bar{D} (red triangles) as a function of polymerization yield using 3 /PMAO-IP at 75 °C.	37
Figure 3.11 Plot of M_n (blue circles) and \bar{D} (red triangles) as a function of polymerization yield using 3 /PMAO-IP at 80 °C.	37
Figure 3.12 Cyclic voltammogram of 3 (0.01 mmol) recorded at a scan rate of 100 mV/s in dichloromethane (5 mL) and (<i>n</i> Bu) ₄ NPF ₆ buffer (0.20 M), referenced versus Fc/Fc+.	38
Figure 4.1 A redox-switchable rhodium stabilized catalyst that is 16 times more active for the hydrogen of alkenes when in its reduced form. The reduced form is represented by the solid line. The oxidized form is represented by the dotted line. "Reprinted with permission from (<i>J. Am. Chem. Soc.</i> , 1995 , 117 (12), pp 3617–3618). Copyright (1995) American Chemical Society." ⁷⁵	45
Figure 4.2 Plot of percent conversion versus time for Gibson’s titanium-based salen catalyst. The reduced species (blue) and the oxidized species (red) display varying polymerization rates during the <i>in situ</i> polymerization switch. "Reprinted with permission from (<i>J. Am. Chem. Soc.</i> , 2006 , 128 (23), pp 7410–7411). Copyright (2006) American Chemical Society." ⁷²	46
Figure 4.3 (left) Plot of L-lactide conversion versus time using the zirconium salfan catalyst. The reduced species (red) was active for polymerization while the oxidized complex (blue) was inactive for polymerization of L-lactide. (right) Plot of ε-caprolactone	

conversion versus time mediated by a zirconium salfan catalyst. The oxidized species (blue) was active for ϵ -caprolactone polymerization while the reduced complex was inactive for ϵ -caprolactone polymerization. "Adapted with permission from (<i>J. Am. Chem. Soc.</i> , 2014 , <i>136</i> (32), pp 11264–11267). Copyright (2014) American Chemical Society." ⁷³	48
Figure 4.4 (left) Fe-based catalyst oxidized to the Fe ^{III} species with ferrocenium hexafluorophosphate (FcPF ₆) and rereduced to the Fe ^{II} version with CoCp ₂ . (right) A plot of percent lactide conversion versus time with the reduced species (blue) and the inactive, oxidized species (red). The catalyst is "Reprinted with permission from (<i>J. Am. Chem. Soc.</i> , 2013 , <i>135</i> (44), pp 16553–16560). Copyright (2013) American Chemical Society." ⁷⁴	48
Figure 4.5 Representation of the catalysts designed in Chapters 5 and 6 that contain a redox active moiety within the ligand scaffold, a group 4 metal, which is active for L-lactide polymerization, and labile alkoxide ligands, which will become the end-groups of the polymer chain.....	50
Figure 5.1 Coordination-insertion mechanism for the polymerization of L-lactide.....	55
Figure 5.2 Comparison of catalysts bearing redox-active ferrocenyl moieties distal to the active metal site (4) and a ferrocenyl moiety proximal to the active metal center (5) (L = OiPr).....	56
Figure 5.3 ORTEP representation of complex 5 . Thermal-ellipsoids were drawn at 50% probability and all hydrogen atoms were omitted for clarity.....	57
Figure 5.4 Cyclic voltammogram of catalyst 5 (0.01 mmol) recorded at a scan rate of 50 mV/s in dichloromethane (5 mL), (<i>n</i> Bu) ₄ NPF ₆ (0.20 M), (<i>E</i> _{1/2} = -0.085 V) versus Fc/Fc ⁺	58
Figure 5.5 Plot of conversion versus time for the polymerization of L-lactide (100 equiv, 1 M) in C ₆ D ₆ at 90 °C using catalyst 5 _{red} (red squares) or 5 _{ox} (blue circles) (NOTE: the oxidation of catalyst 5 _{red} → 5 _{ox} was performed prior to monomer addition).	59
Figure 5.6 Plot of conversion versus time for the polymerization of L-lactide (100 equiv, 1 M) in C ₆ D ₆ at 90 °C with <i>in situ</i> redox-switching, starting with catalyst 5 . Times at which oxidant ([ox] = ^A cFcBAR ^F , 1 eq.) or reductant ([red] = CoCp ₂ , 1 eq.) were added are denoted at the top, and time-periods between additions are labeled as (A), (B), (C), (D), and (E).	60

Figure 5.7 Plot of conversion versus time for the polymerization of L-lactide (100 equiv, 1 M) in C ₆ D ₆ at 90 °C using catalyst 5 _{red} (red squares), oxidized catalyst 5 _{ox} (blue circles), and rereduced catalyst 5 _{red} (green triangles) (NOTE: oxidation of catalyst 5 _{red} → 5 _{ox} , and its rereduction from 5 _{ox} → 5 _{red} , were performed in the presence of lactide monomer)....	62
Figure 5.8 ¹ H NMR spectra (400 MHz, 90 °C, C ₆ D ₆) highlighting the imino and aryl proton region of catalyst 5 (for protons highlighted in blue and red in Figure 5.10) during an L-lactide polymerization <i>in situ</i> redox switch. Spectra 1-4 corresponds to catalyst 5 _{red} during time period A, Figure 5.6 spectra 5-8 represents catalyst 5 _{ox} during time period B, Figure 5.6 , and spectra 8-10 is represents re-reduced catalyst 5 _{red} during time period C, Figure 5.6	63
Figure 5.9 ¹ H NMR spectra (400 MHz, 90 °C, C ₆ D ₆) highlighting the imino and aryl proton region of catalyst 5 (for protons highlighted in blue and red in Figure 5.10) during an L-lactide polymerization <i>in situ</i> redox switch. The bottom trace corresponds to time period A, Figure 5.6 . The top trace represents rereduced catalyst 5 _{red} during time period C, Figure 5.6	64
Figure 5.10 Possible conformations for catalyst 5 , L = OiPr.....	65
Figure 5.11 Cyclic voltammogram of catalyst 5 _{ox} (0.01 mmol) with L-lactide (5 equiv.) after heating for 15 minutes at 90 °C recorded at a scan rate of 50 mV/s in dichloromethane (5 mL), (nBu) ₄ NPF ₆ (0.20 M), (<i>E</i> _{1/2} = -0.143 V) versus Fc/Fc ⁺ . Catalyst 5 was oxidized with AgPF ₆	66
Figure 5.12 Cyclic voltammogram of catalyst 5 _{ox} (0.01 mmol) with L-lactide (5 equiv.) after heating for 15 minutes at 90 °C recorded at a scan rate of 50 mV/s in dichloromethane (5 mL), (nBu) ₄ NPF ₆ (0.20 M), (<i>E</i> _{1/2} = -0.230 V) versus Fc/Fc ⁺ . Catalyst 5 was oxidized with AgPF ₆	66
Figure 5.13 Cyclic voltammogram of catalyst 5 _{ox} (0.01 mmol) with L-lactide (5 equiv.) after heating for 30 minutes at 90 °C recorded at a scan rate of 50 mV/s in dichloromethane (5 mL), (nBu) ₄ NPF ₆ (0.20 M), (<i>E</i> _{1/2} = -0.230 V) versus Fc/Fc ⁺ . Catalyst 5 was oxidized with AgPF ₆	67
Figure 5.14 <i>In situ</i> switching polymerization of 100 equivalents of L-lactide in C ₆ D ₆ at 90 °C starting from rereduced catalyst 5 _{red} and switching at 1 h increments (green circles = 5 _{red} and blue squares = 5 _{ox}).	68

Figure 5.15 Plot of $\ln(L\text{-lactide}_0/L\text{-lactide}_t)$ versus time to study the polymerization kinetics before (green triangles) and after switch (black squares).....	68
Figure 6.1 Proposed [ONNO] ligand library to study their redox effects during the polymerization of L-lactide. More specifically, the proposed ligands contain either one or two ferrocenyl moieties. In addition, the redox innocent functionality of the ligand will be examined, namely the functionality of the nitrogen within the ONNO ligand scaffold to be either a diimine, a diimine, or an imine/amine.....	76
Figure 6.2 Plot of percent conversion of L-lactide versus time with 14_{red} (red circles) and 14_{ox} (blue squares). 14 was oxidized with $\text{AcFcBAR}^{\text{F}}$	78
Figure 6.3 Cyclic voltammogram of catalyst 14 (0.01 mmol) recorded at a scan rate of 100 mV/s in dichloromethane (5 mL), $(n\text{Bu})_4\text{NPF}_6$ (0.20 M), ($E_{1/2} = 0.047$ and 0.317 V) versus Fc/Fc ⁺	78
Figure A.1 Ligands synthesized which contain redox-active, ferrocenyl moieties.....	103
Figure B.1 ¹ H NMR spectrum of BIAN-Fe(C₆H₆) illustrating η^6 -bound benzene and apparent diamagnetic nature of complex.....	114
Figure B.2 Molecular structure of BIAN-Fe(C₆H₆) . Thermal ellisoids are drawn at the 30% level for optimal viewing. Hydrogen atoms are excluded for clarity.....	114
Figure B.3 Plot of percent conversion versus time for the polymerization of L-lactide (50 equiv) at 90 °C using BIAN-Fe(C₆H₆) as the catalyst with varying concentrations of monomer 0.75 M (blue), 0.5 M (black), and 0.25 (red) in C ₆ D ₆	115
Figure B.4 Plot of percent conversion versus time for the polymerization of lactide (50 equiv, 0.5 M) in C ₆ D ₆ at 90 °C using BIAN-Fe(C₆H₆) with either 2 equiv (triangle), 1 equiv (square), or 0.5 equiv (x) or 4-methoxyphenol present.....	117
Figure B.5 ¹ H NMR spectrum of end-group analysis for polymer obtained with L-lactide (50 equiv, 0.5 M) in C ₆ D ₆ at 90 °C using BIAN-Fe(C₆H₆) (1 equiv) and 4-methoxyphenol (2 equiv).....	118
Figure B.6 Kinetic study L-lactide polymerization using BIAN-Fe(C₆H₆) and either 2 equiv (square), 1 equiv (triangle), or 0.5 equiv (x) of 4-methoxyphenol.....	119
Figure B.7 ¹ H NMR spectrum of BIAN-Fe(C₆H₆) (1 equiv, 9 μmol) and 4-methoxyphenol (2 equiv) in C ₆ D ₆ after being heated for 90 °C for 5 h.....	119

Figure B.8 Representative ^1H NMR spectrum (400 MHz, 90 °C, C_6D_6) of polymerization with 50 equiv. of L-lactide and BIAN-Fe(C_6H_6)	124
Figure B.9 ^1H NMR spectrum of BIAN-Fe(C_6H_6) (1 equiv, 9 μmol) and 4-methoxyphenol (2 equiv) in C_6D_6 after being heated for 90 °C for 30 minutes.	125
Figure B.10 ^1H NMR spectrum of PLA (Table B.1 , entry 2) produced with BIAN-Fe(C_6H_6) (1 equiv, 9 μmol) and 4-methoxyphenol (0.5 equiv) in C_6D_6 . Used to calculate M_n^{NMR}	125
Figure B.11 ^1H NMR spectrum of PLA (Table B.1 , entry 3) produced with BIAN-Fe(C_6H_6) (1 equiv, 9 μmol) and 4-methoxyphenol (1.0 equiv) in C_6D_6 . Used to calculate M_n^{NMR}	126
Figure B.12 ^1H NMR spectrum of PLA (Table B.1 , entry 4) produced with BIAN-Fe(C_6H_6) (1 equiv, 9 μmol) and 4-methoxyphenol (2.0 equiv) in C_6D_6 . Used to calculate M_n^{NMR}	126
Figure B.13 GPC trace of PLA formed with BIAN-Fe(C_6H_6) . Samples measured in THF at 40 °C and referenced to polystyrene standards (Table B.1 , Entry 1).	127
Figure B.14 GPC trace of PLA formed with BIAN-Fe(C_6H_6) and 0.5 equiv of 4-methoxyphenol. Samples measured in THF at 40 °C and referenced to polystyrene standards (Table B.1 , Entry 2).	128
Figure B.15 GPC trace of PLA formed with BIAN-Fe(C_6H_6) and 1 equiv of 4-methoxyphenol. Samples measured in THF at 40 °C and referenced to polystyrene standards (Table B.1 , Entry 3).	129
Figure B.16 GPC trace of PLA formed with BIAN-Fe(C_6H_6) and 2 equiv of 4-methoxyphenol. Samples measured in THF at 40 °C and referenced to polystyrene standards (Table B.1 , Entry 4).	130
Figure C.1 ORTEP representation of precatalyst 2b with thermal ellipsoids drawn at 50% probability. Hydrogens were omitted for clarity. X-ray quality single crystals of complex 2b were grown overnight at ambient temperature by layering a saturated methylene chloride solution with pentanes. The observed bond lengths are typical for α -diimine Ni^{II} complexes with $\text{N1-Ni} = 1.9978(15)$ Å and $\text{N2-Ni} = 2.0020(15)$ Å. The Ni-Br bond lengths were 2.3286(3) and 2.3351(3) Å for Ni-Br1 and Ni-Br2, respectively. Complex 2b displayed a distorted tetrahedral geometry with a N1-Ni-N2 angle of 80.76(6)° and a Br1-Ni-Br2 angle of 125.767(12)°. Crystal data for $\text{C}_{70}\text{H}_{60}\text{Br}_2\text{N}_2\text{Ni}$ (1147.77 g/mol); monoclinic; space group $\text{P2}_1/\text{c}$; $a = 18.3734(8)$ Å; $b = 18.2988(8)$ Å; $c = 17.9527(8)$ Å; α	

= 90°; β = 98.511(2)°; γ = 90°. Data for this structure can be obtained free of charge from the Cambridge Crystallographic Data Center (CCDC) under CCDC1570782.	132
Figure C.2 ¹ H NMR spectrum of polyethylene made by catalyst 2b (Table 2.3 , Entry 4)..	133
Figure C.3 ¹ H NMR spectrum of polyethylene made by catalyst 2b (Table 2.3 , Entry 8)..	133
Figure C.4 ¹ H NMR spectrum of polyethylene made by catalyst 2b (Table 2.3 , Entry 12).	134
Figure C.5 ¹³ C NMR Spectrum of polyethylene made by catalyst 2b (Table 2.3 , Entry 8).	134
Figure C.6 Representative ¹ H NMR of polyethylene at 70 °C. (Table 3.1 , Entry 3).....	135
Figure C.7 Representative ¹ H NMR of polyethylene at 75 °C. (Table 3.1 , Entry 8).....	136
Figure C.8 Representative ¹ H NMR of polyethylene at 80 °C. (Table 3.1 , Entry 11).....	136
Figure C.9 GPC of polyethylene. (Table 3.1 , Entry 1).....	137
Figure C.10 GPC of polyethylene. (Table 3.1 , Entry 2).....	138
Figure C.11 GPC of polyethylene. (Table 3.1 , Entry 3).....	139
Figure C.12 GPC of polyethylene. (Table 3.1 , Entry 4).....	140
Figure C.13 GPC of polyethylene. (Table 3.1 , Entry 5).....	141
Figure C.14 GPC of polyethylene. (Table 3.1 , Entry 6).....	142
Figure C.15 GPC of polyethylene. (Table 3.1 , Entry 7).....	143
Figure C.16 GPC of polyethylene. (Table 3.1 , Entry 8).....	144
Figure C.17 GPC of polyethylene. (Table 3.1 , Entry 9).....	145
Figure C.18 GPC of polyethylene. (Table 3.1 , Entry 10).....	146
Figure C.19 GPC of polyethylene. (Table 3.1 , Entry 11).....	147
Figure C.20 GPC of polyethylene. (Table 3.1 , Entry 12; Table 3.2 , Entry 3).....	148
Figure C.21 GPC of polyethylene. (Table 3.1 , Entry 13).....	149
Figure C.22 GPC of polyethylene. (Table 3.1 , Entry 14).....	150
Figure C.23 GPC of polyethylene. (Table 3.2 , Entry 1).....	151
Figure C.24 GPC of polyethylene. (Table 3.2 , Entry 2).....	152
Figure C.25 GPC of polyethylene. (Table 3.2 , Entry 4).....	153
Figure C.26 ORTEP representation of (salfen)Ti(O ⁱ Pr) ₂ (5_{red}) with thermal ellipsoids drawn at 50% probability. Hydrogens were omitted for clarity. X-ray quality single crystals of complex 5_{red} were grown overnight at ambient temperature from a concentrated hexanes solution. Crystal data for C ₄₆ H ₆₄ FeN ₂ O ₄ Ti (812.74 g/mol); orthorhombic; space	

group P-2₁; $a = 10.8375(13) \text{ \AA}$; $b = 14.8073(18) \text{ \AA}$; $c = 27.377(3) \text{ \AA}$; $\alpha = 90^\circ$; $\beta = 90^\circ$; $\gamma = 90^\circ$; $V = 4393.3(9) \text{ \AA}^3$; $Z = 4$; $T = 273(2) \text{ K}$; $\lambda = 0.71073 \text{ \AA}$; $\mu = 0.554 \text{ mm}^{-1}$; $R_1 = 0.0505$, $wR_2 = 0.1255$ for 8408 reflections; GOF = 0.901. Data for this structure can be obtained free of charge from the Cambridge Crystallographic Data Center (CCDC) under CCDC1570783..... 154

Figure C.27 Representative GPC trace of PLA formed with rereduced catalyst **5_{red}**. Samples measured in THF at 40 °C and referenced to polystyrene standards (**Table 5.1**, Entry 6) 155

LIST OF SCHEMES

Scheme 1.1 Early transition metal based metallocene catalyst that can produce linear ethylene from ethylene as a single feedstock and branched polyethylene using ethylene along with higher α -olefins as the feedstock.	4
Scheme 2.1 Synthesis of α -diimine precatalysts 2a and 2b	15
Scheme 3.1 Modification of the synthetic route to obtain complex 3 in ultrahigh purity.	32
Scheme 4.1 Titanium-based catalyst with two ferrocenyl redox active moieties at the outer extremity of the complex. The complex is easily oxidized with silver triflate (AgOTf) to the Fe ^{III} species (red) and rereduced back to the Fe ^{II} species (blue) using decemethylferrocene (Fe(Cp*) ₂). "Adapted with permission from (<i>J. Am. Chem. Soc.</i> , 2006 , <i>128</i> (23), pp 7410–7411). Copyright (2006) American Chemical Society." ⁷²	45
Scheme 4.2 Zirconium-based redox-switchable catalyst containing a ferrocenyl moiety close to the active metal center. The catalyst was oxidized from the Fe ^{II} species to the Fe ^{III} species using ^{Ac} FcBAR ^F and rereduced using CoCp ₂ . "Reprinted with permission from (<i>J. Am. Chem. Soc.</i> , 2014 , <i>136</i> (32), pp 11264–11267). Copyright (2014) American Chemical Society." ⁷³	47
Scheme 5.1 Synthesis of redox-active catalyst 5	57
Scheme 5.2 Redox-switch between catalysts 5_{red} and 5_{ox}	58
Scheme 6.1 Synthesis of the imine/amine titanium-based catalyst 14 , which contains a single ferrocenyl moiety off the imine portion of the ligand.	77
Scheme 6.2 Synthesis of tetradentate [ONNO] ligand 11 , which contains two ferrocenyl substituents at the outer extremity of the ligand scaffold.	79
Scheme A.1 Synthesis of constrained geometry ligand 22	105
Scheme A.2 Synthesis of FI ligand 23 , which contains a single ferrocenyl unit located on the phenol section of the ligand.	106
Scheme A.3 Synthesis of FI ligand 24 , which contains a single ferrocenyl moiety located in the imine portion of the ligand.	106

LIST OF ABBREVIATIONS AND SYMBOLS

α	alpha
AcFcBAR ^F	acetylferrocenium tetrakis(3,5-bis(trifluoromethyl)phenyl)borate
AcOH	acetic acid
AgOTf	silver triflate
AgPF ₆	silver hexafluorophosphate
β	beta
<i>B</i>	branching content per 1000 carbons
NaBAR ^F	sodium tetrakis(3,5-bis(trifluoromethyl)phenyl)borate
BIAN	bis(aryl)acenaphthenequinonediimine (aryl = 2,6-diisopropylaniline)
CGC	constrained geometry catalyst
CL	ϵ -caprolactone
CoCp ₂	cobaltocene
Cp	cyclopentadienyl
CTA	chain transfer agent
CV	cyclic voltammetry
\bar{D}	polymer dispersity
DCM	dichloromethane (methylene chloride)
dppc	1,1'-bis(diphenylphosphino)(cobaltocene)
DSC	differential scanning calorimetry
Fc	ferrocene
Fc ⁺	ferrocenium
FcPF ₆	ferrocenium hexafluorophosphate
Fc*PF ₆	decamethyl ferrocenium hexafluorophosphate
Fe(Cp*) ₂	decamethyl ferrocene
FI	phenoxyimine
GPC	gel permeation chromatography
HDPE	high-density polyethylene
<i>i</i> Pr	isopropyl
<i>i</i> Pr*	1,3-bis(2,6-bis(diphenylmethyl)-4-methylphenyl)imidazo-2-ylidene
LA	lactic acid or lactide
LDA	lithium diisopropylamide
LDPE	low-density polyethylene
LLDPE	linear low-density polyethylene
MAO	methylaluminoxane
Me	methyl
MeOH	methanol
M_n	number average molecular weight
M_w	weight average molecular weight
M_w/M_n	polymer dispersity
OTf	triflate
PDI	polydispersity index
PE	polyethylene
Ph	phenyl

PLA.....poly(lactic acid) or polylactide
PMAO-IP.....polymethylaluminoxane-improved performance
PP.....polypropylene
ROP.....ring-opening polymerization
RSC.....redox-switchable catalysis
RSP.....redox-switchable polymerization
salen.....bis(3-*tert*-butyl-5-ethynylferrocene-salicylidene)-1,2-ethylenediamine
salfan.....1,1'-di(2,4,-di-*tert*-butyl-6-*N*-methylmethylenephenol)ferrocene)
salfen.....1,1'-di(2,4,-di-*tert*-butyl-salicylimino)ferrocene)
*t*Bu.....*tert*-butyl
THF.....tetrahydrofuran
TMB.....1,3,5-trimethoxybenzene
TOF.....turn-over frequency
 T_mpolymer melting transition temperature

Chapter 1– INTRODUCTION TO ETHYLENE POLYMERIZATION CATALYSIS

1.1 Motivation

Few synthetic products have had a profound impact on the world's economy, but commodity plastics, which are comprised mostly of polyolefins, have become a vital part of our everyday lives. From plastic containers for food and medicine to industrial materials, people have come to depend upon plastics, like polyethylene (PE), which is the most common of the commodity plastics. PE is produced globally on a multibillion pound per year scale, and its mechanical and thermal properties can vary depending on the density of the polymer. Typically, in order to vary the density or change the branching content of PE, the use of higher α -olefin comonomers is required. While this method is effective, it dramatically increases the cost of polymer production due to the increased price of larger α -olefins, which are usually synthesized by ethylene oligomerization processes.

Another consideration for the industrial generation of PE materials are the catalysts, which must withstand elevated temperatures (70 – 120 °C).¹ However, most of the catalysts that polymerize at these higher temperatures provide little control over the polymerization process. Controlled ethylene polymerizations offer a way to modulate copolymer incorporation, regioselectivity, stereoselectivity, and end-group functionalization.²⁻⁵ Many variations of catalysts have been studied over the years; however, fundamental understanding of how the catalyst can be controlled to achieve advanced polyethylene materials is still ongoing. The development of catalysts that are thermally stable and that have the ability to modulate their polymerization behavior and resulting polymers are of utmost importance to advance the frontiers of polyolefin-based materials. In this portion of the dissertation, we will discuss how we targeted and designed advanced catalysts in order to study their thermal robustness, their controllability during ethylene polymerizations, and to characterize their resultant polymers.

1.2 Early Polyethylene Catalysis

1.2.1 Ziegler/Natta Catalysis

Catalysts for ethylene polymerization often can be divided into heterogeneous and homogenous species. The first revolutionary discovery in the world of polyolefins came from

Karl Ziegler and Giulio Natta in the 1950s with their implementation of a TiCl_4 heterogeneous catalysts (**Figure 1.1**).^{6,7} Using these heterogeneous catalysts, they were able to synthesize high molecular weight polyethylene and polypropylene with a wide range of mechanical and thermal properties from cheap starting materials. This work eventually earned them the Nobel Prize in 1953 for their pivotal discoveries.⁸ Ziegler-Natta catalysts are still used commercially today to produce high density polyethylene (HDPE). While Ziegler-Natta catalysts are extremely effective in producing long chain hydrocarbons, heterogeneous catalytic systems are extremely difficult to study due to their multiple open coordination sites. Multiple coordination sites can lead to polymers with broad dispersities, unpredictable tacticities, and widely varying kinetics of polymerization. Though industrially useful, heterogeneous catalyst systems do not facilitate the fundamental understanding of polymerization catalysis, and it is difficult to intuitively design catalysts in order to target specific PE materials. Therefore, it was not until the discovery of methylaluminoxane (MAO) in 1980 that scientists could study homogenous single-site catalyst systems for the polymerization of ethylene, which enabled fundamental studies to better understand the catalytic processes occurring during ethylene polymerizations and how these catalysts could be used to make advanced materials.⁹

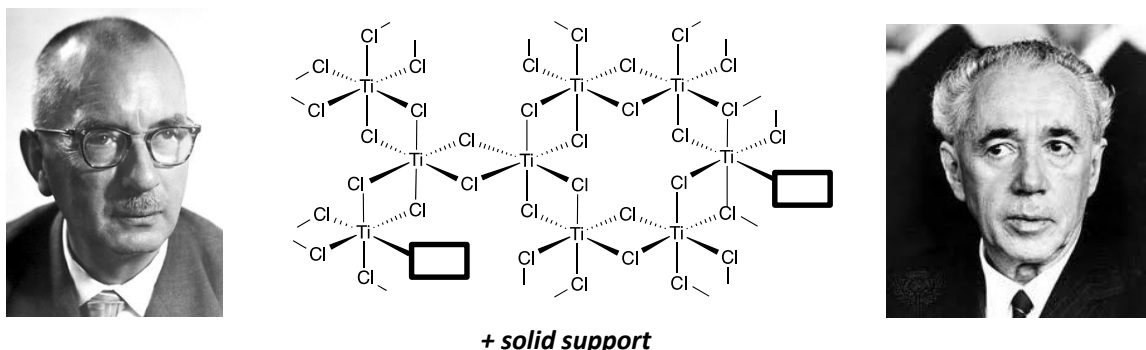
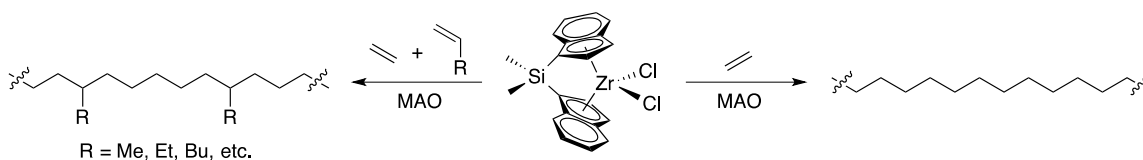


Figure 1.1 Karl Ziegler (left) and Giulio Natta (right) who performed ethylene and propylene polymerizations with a TiCl_4 heterogeneous catalyst. Box represents open coordination site

1.2.2 Homogenous Catalysis

The discovery of MAO as an initiating species for homogenous single-site catalysts for ethylene polymerization was instrumental in understanding of how ethylene polymerizations proceed.⁹ Initially, most of the catalysts studied were metallocene-based group 4 catalysts. While these catalysts are highly reactive with ethylene to produce linear polyethylene, in order to vary the polymer density and branching content, the addition of higher α -olefin comonomers is needed (**Scheme 1.1**).



Scheme 1.1 Early transition metal based metallocene catalyst that can produce linear ethylene from ethylene as a single feedstock and branched polyethylene using ethylene along with higher α -olefins as the feedstock.

Because metallocene-based catalysts generally include early transition metals, group 4 metals to be more specific, they are extremely oxophilic. Therefore, their tolerance to comonomers that contain polar moieties is poor.¹⁰ Expanding the ligand library beyond metallocene-based catalysts and integration of late-transition metals offered advantages like the ability to incorporate a wider variety of comonomers to create more advanced polymer materials. In 1995, the first highly active group 10 catalysts for ethylene polymerizations were introduced.¹¹ Because these catalysts are less oxophilic, they provide the possibility to include polar comonomers; they also can produced variation in polyethylene topology from a single feedstock of ethylene, eliminating the use of higher α -olefin comonomers. An overview of the timeline for ethylene polymerization catalysis is presented in **Figure 1.2**.

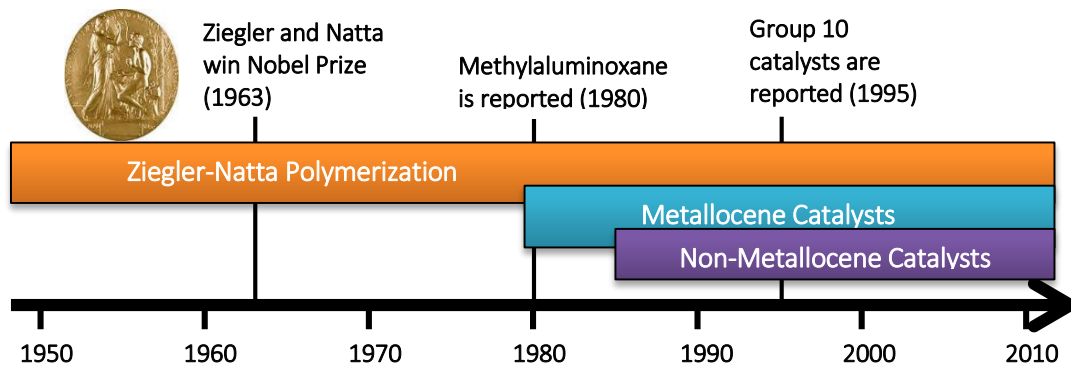


Figure 1.2 Timeline for ethylene polymerization catalysis.

1.3 Introduction to Group 10 Ethylene Polymerization Catalysts

When the ligand library was expanded to include post-metallocene complexes, scientists began to understand how the ligand around the active metal center can be tuned to enhance the catalyst's polymerization behavior.¹² With the invention of Brookhart's nickel α -diimine catalyst, the ability to create polyethylene with varying branching content from a single polymer feedstock was realized (**Figure 1.3**).¹¹ This ability to modulate the branching content occurs via a phenomenon known as "chain-walking", which leverages the catalyst's propensity to undergo β -hydride elimination and reinsertion back into the polymer chain. To better understand this phenomenon, **Figure 1.4** displays the coordination-insertion mechanism of a late transition metal-based catalyst for ethylene polymerization. First, the active catalytic species must be generated. Typically, late transition metal-based catalysts bear two halide ligands, or a halide and an alkyl ligand, which must be reacted with an activator to produce a cationic metal center containing an alkyl substituent and an open coordination site. Once the active species is generated, ethylene can coordinate to the catalyst which will subsequently undergo a migratory insertion. The repeated coordination/insertion of monomer eventually generates high molecular weight linear polyethylene. However, in

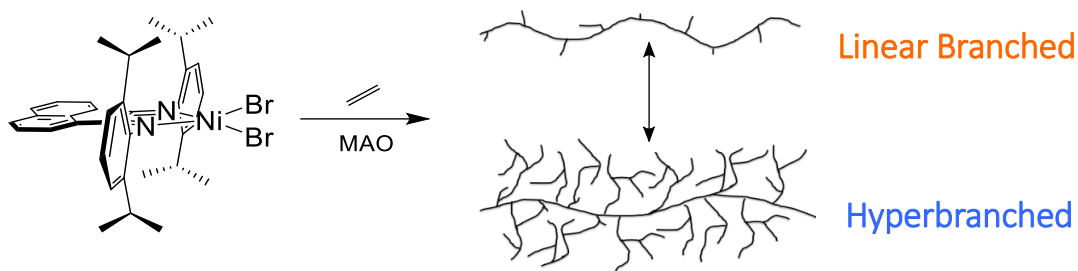


Figure 1.3 Representation of a nickel α -diimine catalyst generating PE with various branching contents with only ethylene as a feedstock.

some cases, instead of coordinating another monomer, the catalyst appended polymer chain may undergo β -hydride elimination, which can result in three outcomes: (1) the polymer chain can undergo 1,2-insertion, which negates the β -hydride elimination to produce a linear polymer chain; (2) the polymer chain can dissociate leading to a chain transfer event; and (3) the polymer chain can undergo a 2,1-insertion, which forms a methyl branch on the polymer chain. Chain-walking can be modulated by a variety of external factors including but not limited to reaction temperature and pressure.¹³⁻¹⁵ Another possible advantage of using late transition metal-based catalysts, namely Pd, is the opportunity to explore the incorporation of polar comonomers due to their increased functional group tolerance when compared to early transition metal-based catalysts (**Figure 1.5**).

While group 10 metal catalysts offer several advantages over other classes of catalysts, there are still issues related to the implementation of late transition metal-based catalysts in an industrial setting. Most of the reported late transition metal catalysts have poor thermal stability, which often result in their decomposition or deactivation at temperatures exceeding 25 °C. This lack of thermal stability, particularly in regards to Ni α -diimine catalysts, is attributed to *N*-aryl rotation, which has been linked to detrimental events such as: (1) catalyst deactivation, (2) chain transfer, and (3) chain termination.^{10,11} In addition, Ni- and Pd-based catalysts often produce lower molecular weight materials when polymerization temperature is increased. Therefore, several fundamental studies on how to alleviate the *N*-aryl rotation has been conducted, and several of these studies revolve around

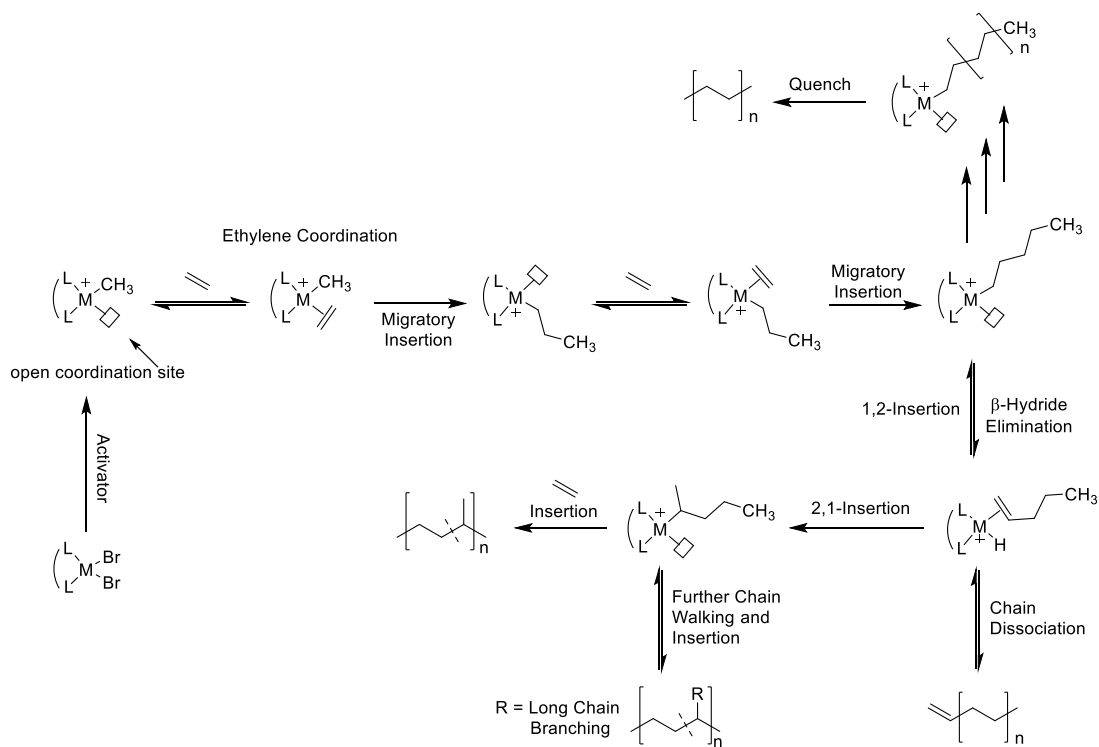


Figure 1.4 Coordination-insertion mechanism for ethylene polymerization with a cationic metal catalyst that has the ability to undergo chain-walking.

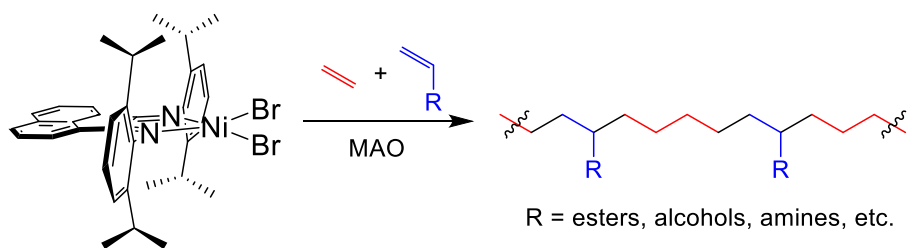


Figure 1.5 Representation of a late transition metal catalyst incorporating polar comonomers during ethylene polymerization.

either (1) increasing the steric bulk of the ligand backbone or (2) increasing the bulk of the *ortho* position of the *N*-aryl moiety (**Figure 1.6**).¹⁶⁻¹⁸

In 2004, Guan and coworkers showed that connecting the *ortho* positions of the *N*-aryl moieties of a nickel α -diimine catalyst could help inhibit *N*-aryl rotation and thereby increase the catalyst's thermal stability.¹⁶ Their use of a cyclophane linker between the *N*-aryl moieties of the nickel catalyst allowed for the active species during ethylene polymerization to remain stable for 10 minutes at 70 °C. A separate study performed by Wu and coworkers in 2009 showed that when the bulkiness of a Ni α -diimine's backbone was increased by using a camphorquinone-derived backbone, the thermal stability of the catalyst during ethylene polymerization increased from ambient conditions to 80 °C; however, the catalyst underwent slow decomposition at these temperatures.¹⁸ While there has been some success in increasing the thermal stability of these Ni α -diimine catalysts, most of the temperatures fall below the acceptable range for use in industrial gas-phase ethylene polymerizations.

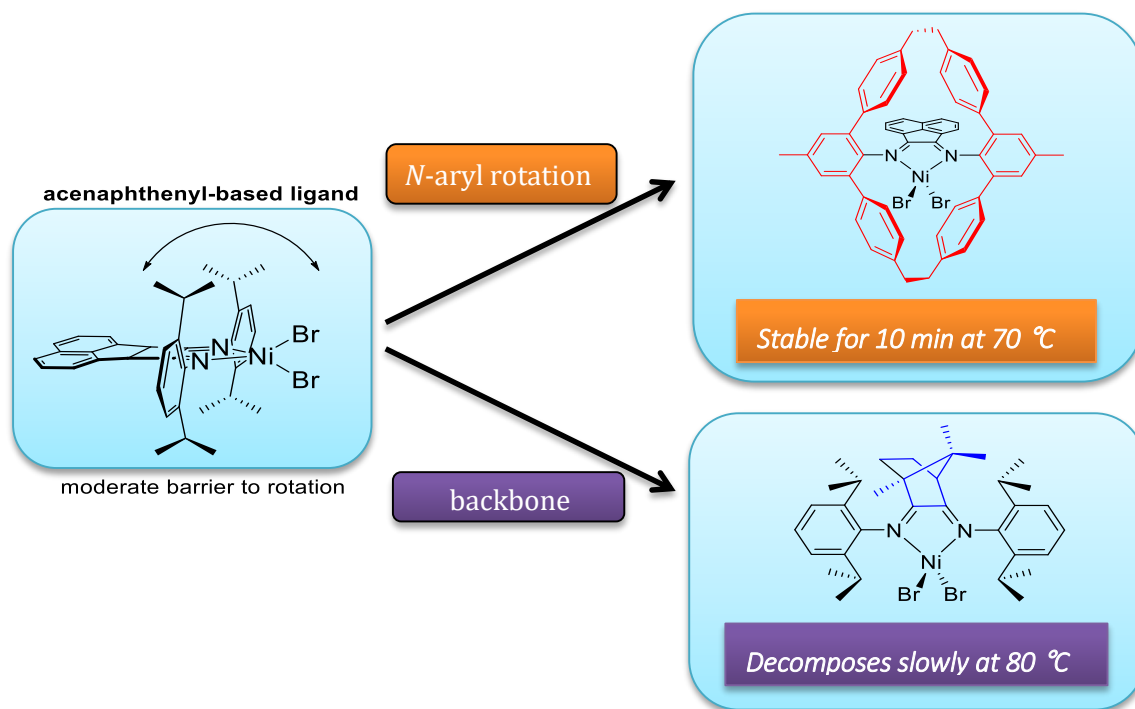


Figure 1.6 Increasing the thermal stability of a Ni α -diimine catalyst during ethylene polymerization by changing the *N*-aryl moiety or the ligand backbone.

1.4 Research Objectives

The overall aim of this portion of the dissertation is to explore strategies designed to enhance the thermal stability of late transition metal-based catalysts, namely nickel α -diimine catalysts, and possibly identify catalysts that display controlled/"living" behavior during the polymerize ethylene at temperatures exceeding ambient conditions. These strategies will be dependent on the synthesis and characterization of several nickel α -diimine catalysts designed to withstand elevated temperatures and directly affect ethylene polymerization behavior. The scope of this project will include:

- I. Design and synthesis of new precatalysts;
- II. Characterization of the new catalytic species by NMR spectroscopy and single-crystal X-ray diffraction;
- III. Polymerization of ethylene at various conditions with the newly synthesized Ni α -diimine complexes; and
- IV. Characterization of polyethylene produced at elevated temperatures via high temperature gel permeation chromatography (GPC) and NMR spectroscopy

While studying PE materials serve as motivation for this portion of the dissertation research, it is emphasized that the efficacy of this research focuses on the design of thermally robust and controlled/"living" ethylene polymerization catalysts. It is expected that the results described herein will provide insight into methodologies for controlling ethylene polymerizations at superambient temperatures, which will provide fundamental knowledge for late transition metal-based catalyst design and their potential to be used in industrial ethylene polymerizations in the future. Chapters 2 and 3 will discuss the fundamental research performed to enhance the thermal stability of late transition metal-based ethylene polymerization catalysts.

In Chapter 2, a detailed catalytic study of two nickel α -diimine complexes are performed during PE production at temperatures ranging from 80 to 100 °C. The synthesis and characterization of the Ni precatalysts are discussed. A survey of their performance at the elevated temperatures will be discussed in detail. These catalysts are shown to be thermally robust at elevated temperatures while producing high molecular weight, moderately branched materials with relatively low dispersities.

In Chapter 3, a third nickel α -diimine catalyst will be discussed in an effort to improve upon the results discussed in Chapter 2. The synthesis of this Ni catalyst will be discussed as well as a comprehensive study of catalyst activity for ethylene polymerization temperatures ranging from 70 to 80 °C. The Ni α -diimine catalyst discussed in this chapter was shown to be controlled/"living" at elevated temperatures, produce high molecular weight polyethylene, and maintain extremely low polymer dispersities.

Following these chapters are an examination of redox active catalysts for the polymerization of L-lactide (Chapter 4-6). References for all chapters will be presented after Chapter 6. Presentation of data that is secondary to the project goals for Chapters 2 and 3 will be provided in Appendix C, which will include representative NMR spectra, representative gel permeation chromatography (GPC), and X-ray crystallography data.

Chapter 2– THERMALLY ROBUST NICKEL (II) CATALYSTS FOR ETHYLENE POLYMERIZATIONS

A version of this chapter was originally published by Jennifer L. Rhinehart, Lauren A. Brown and Brian K. Long in the peer-reviewed publication:

Jennifer L. Rhinehart, Lauren A. Brown, Brian K. Long. "A Robust Ni(II) α -Diimine Catalyst for High Temperature Ethylene Polymerization." *Journal of the American Chemical Society*. **2013** 135 (44) 16316-16319, DOI: 10.1021/ja408905t

I was responsible for the synthesis and characterization of the precatalysts presented in the manuscript and aided in the preparation of the manuscript. Dr. Jennifer Rhinehart synthesized all of the polymers studied in the work and contributed to the preparation of the manuscript. Dr. Brian Long advised this work.

2.1 Abstract

Sterically demanding Ni^{II} α -diimine precatalysts were synthesized utilizing 2,6-bis(diphenylmethyl)-4-methyl aniline. When activated with methylaluminoxane, the catalyst NiBr₂(ArN=C(Me)-C(Me)=NAr) (Ar = 2,6-bis(diphenylmethyl)-4-methylbenzene) was highly active, produced well-defined polyethylene at temperatures up to 100 °C ($M_w/M_n = 1.09$ -1.46), and demonstrated remarkable thermal stability at temperatures appropriate for industrially used gas-phase polymerizations (80-100 °C).

2.2 Introduction

Over the past three decades, there has been an explosion of research dedicated to the design and development of homogeneous, single-site olefin polymerization catalysts. Single-site catalysts provide tremendous flexibility in ligand design and have revolutionized the field of polyolefin research by establishing new opportunities for mechanistic understanding, catalyst control, and tailored polyolefin synthesis that were impossible using heterogeneous catalyst systems.^{10,12,19-21} Perhaps one of the most significant advances during this time period was the development of highly active, late transition metal-based olefin polymerization catalysts by Brookhart and co-workers.^{11,22} These Ni- and Pd-based α -diimine catalysts were capable of producing high molecular weight polyethylene (PE), were tolerate

to incorporation of numerous polar comonomers,²³⁻²⁶ and could produce multiple polymer topologies ranging from linear to hyperbranched by simply varying ethylene pressure.^{13,27-32}

Despite these advantages, these Ni- and Pd-based catalysts generally exhibit poor thermal stability at elevated temperatures that are required for industrially used gas-phase polymerizations (70–110 °C).^{1,27} As a result, the commercialization and overall industrial appeal of α -diimine-derived catalyst systems has been greatly hindered. For example, typical Pd^{II}- and Ni^{II}-based α -diimine catalyst systems have been shown to undergo rapid catalyst decomposition at temperatures ≥ 60 °C. This phenomenon has been attributed to increased *N*-aryl rotations perpendicular to the ligand backbone, which leads to events such as C–H activation of the ligand itself and increased associative chain transfer, as well as potential decomposition pathways arising from *in situ* generated Ni-hydride species.^{18,27,31,33} In addition, ethylene polymerizations that utilize Ni- and Pd-based catalysts often produce PE with decreased molecular weights as reaction temperatures are elevated. This phenomenon, which is attributed to increased rates of chain transfer (via β -hydride elimination) relative to chain propagation and to the decreased solubility of ethylene in toluene at elevated temperatures, further compounds the need for thermally robust catalysts, as extended reaction times are required to produce polymers of sufficient molecular weight.²⁷ Consequently, the development of late transition metal-based α -diimine catalysts with enhanced temperature stability is of tremendous importance to the field of olefin polymerization.^{5,27,34}

To date, few examples of α -diimine-based catalysts with improved thermal stability have been reported.^{16,18,35,36} To address these temperature sensitivities, researchers have examined the effects that ligand backbone modifications and *N*-aryl moiety substitutions have on the thermal stability of α -diimine-based catalysts. For example, catalysts bearing α -diimine ligands with camphor-derived backbones have displayed modest activity at temperatures as high as 80 °C, yet their turnover frequency (TOF) was shown to decay as a function of time and the polymers produced had broad molecular weight distributions ($M_w/M_n \geq 2.0$) and were highly branched (no T_m was observed).¹⁸ In contrast, Ni^{II}-based catalysts developed by Guan and coworkers, which featured cyclophane-derived *N*-aryl substituents, have demonstrated remarkable activities for ethylene polymerization (TOFs = 1,000,000–1,400,000 h⁻¹), produced well-defined polymers ($M_w/M_n = 1.2$ –1.7), and showed

constant TOFs at 70 and 90 °C for 10 min; however, the catalysts did show decomposition upon extended reaction times.¹⁶ In addition, while an elegant example of synthetic chemistry, cyclophane-based ligands require an elaborate multistep synthesis involving three separate transition metal catalyzed reactions to construct the ligand alone.

In an effort to develop a complementary, yet readily accessible alternative to cyclophane-derived catalysts, we sought to design and synthesize α -diimine catalysts featuring sterically demanding *iPr** moieties (*iPr** = 1,3-bis(2,6-bis(diphenylmethyl)-4-methylphenyl)imidazo-2-ylidene). The *iPr** functionality has recently gained popularity in the field of bulky N-heterocyclic carbenes and is structurally related to several reported olefin polymerization catalysts (**Figure 2.1**).³⁷⁻³⁹ We envisioned that the steric bulk of the *iPr** moieties would greatly inhibit *N*-aryl rotations of the α -diimine ligand and thereby dramatically enhance their thermal stability. Herein, we report the successful synthesis and high temperature polymerization of ethylene by a bulky, thermally robust Ni^{II} α -diimine catalyst bearing symmetrical *iPr** moieties. To the best of our knowledge, this represents the most thermally stable Ni^{II} α -diimine catalyst reported to date.

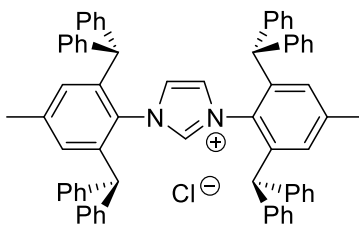
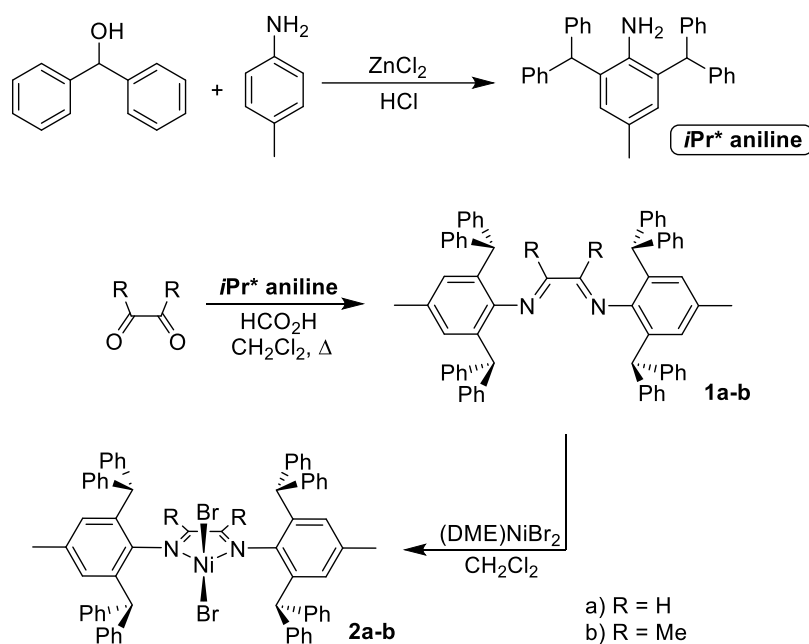


Figure 2.1 *N*-heterocyclic carbene (NHC) catalyst that contains *iPr** moieties.

2.3 Results and Discussion

The synthesis of Ni^{II} precatalysts **2a** and **2b** were completed in three steps from commercially available starting materials (**Scheme 2.1**). *p*-Toluidine was alkylated using 2 equiv of biphenylmethanol in the presence of stoichiometric HCl and ZnCl₂ to yield 2,6-dibenzhydryl-4-methylaniline (*iPr** aniline), which was subsequently condensed onto glyoxal to form ligand **1a**.³⁸ In an analogous reaction, 2,6-dibenzhydryl-4-methylaniline was condensed onto 2,3-butadione using magnesium sulfate as a desiccant and purified via

column chromatography to afford α -diimine ligand **1b**. Ligand **1a** was metallated in methylene chloride at room temperature using the nickel(II) dibromide dimethoxyethane adduct to form precatalyst **2a**. In contrast, ligand **1b** required gentle heating at 30 °C for 5 h to form precatalyst **2b**. Both complexes **2a** and **2b** displayed paramagnetic ^1H NMR spectra, which was indicative of tetrahedral coordination geometries about their Ni^{II} centers.



Scheme 2.1 Synthesis of α -diimine precatalysts **2a** and **2b**.

X-ray quality crystals of precatalyst **2b** were grown by layering a saturated methylene chloride solution with pentane (**Figure 2.2**). The observed bond lengths are typical for α -diimine Ni^{II} complexes with $\text{N1-Ni} = 1.9978(15)$ Å and $\text{N2-Ni} = 2.0020(15)$ Å. The Ni-Br bond lengths were $2.3286(3)$ and $2.3351(3)$ Å for Ni-Br1 and Ni-Br2, respectively. Complex **2b** displayed a distorted tetrahedral geometry with a N1-Ni-N2 angle of $80.76(6)^\circ$ and a Br1-Ni-Br2 angle of $125.767(12)^\circ$.

Ethylene polymerizations using precatalysts **2a** and **2b** were evaluated using polymethylaluminumoxane-improved performance (PMAO-IP) as an activator. Catalyst **2a** displayed good activity toward ethylene polymerization at 20 °C producing high molecular

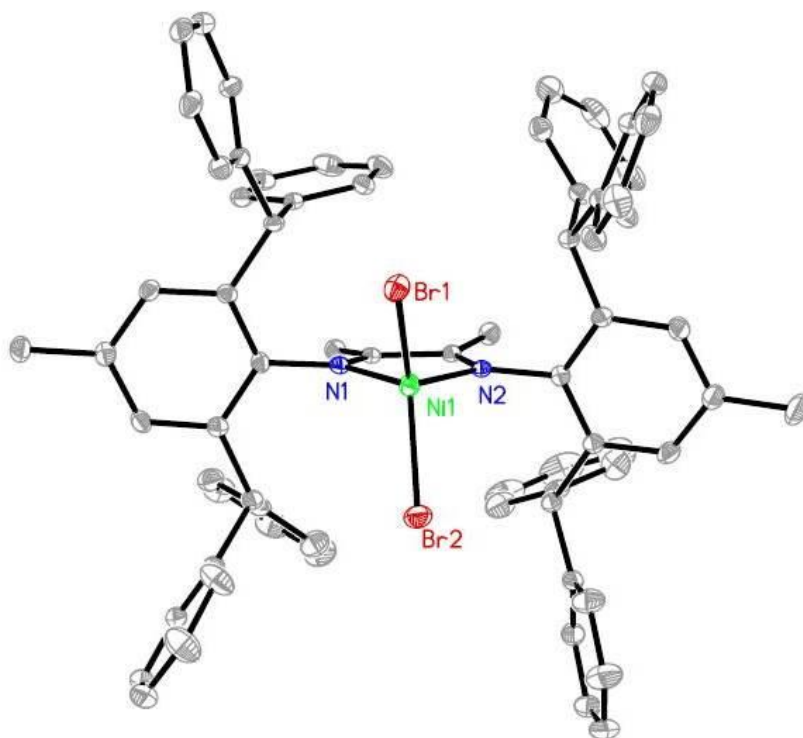


Figure 2.2 ORTEP drawing of precatalyst **2b** with thermal ellipsoids drawn at 50% probability.

weight PE ($M_n = 165,000$ g/mol) with a $T_m = 109$ °C; however, the polymer displayed broad molecular weight distribution ($M_w/M_n = 2.64$) (**Table 2.1**). In contrast, catalyst **2b** exhibited slightly lower activity at 20 °C, but the molecular weight of the PE produced was in perfect agreement with those theoretically calculated ($M_n^{\text{exp}} = 44,000$ g/mol, $M_n^{\text{theo}} = 44,000$ g/mol) (**Table 2.2**, entry 5), and the resultant PE displayed a remarkably narrow molecular weight distribution ($M_w/M_n = 1.09$) and a $T_m = 60$ °C. These observations suggested that catalyst **2b** underwent rapid initiation, could produce branched PE and that little to no chain termination or chain transfer events were detected during the polymerization. Encouraged by this result, all subsequent polymerizations were conducted using catalyst **2b**.

A temperature-dependent study was performed at 15 psi of ethylene using catalyst **2b** (**Table 2.2**). Polymerizations conducted at temperatures ≤ -20 °C (entries 1–3) exhibited low activities (i.e. turnover frequency, TOF), broad molecular weight distributions ($M_w/M_n \geq 1.55$), and produced highly linear polymer with $T_m = 132, 127,$ and 111 °C respectively

Table 2.1 Ethylene Polymerization Results for Temperature Screening of Catalyst **2a**

entry	T_{rxn} (°C)	time (min)	yield (mg)	TOF ^b (h ⁻¹)	M_n^c (g/mol)	M_w/M_n^c	T_m^d (°C)
1	-60	390	38	120	33200	1.08	ND
2	-40	45	65	1800	61500	1.08	ND
3	-20	15	189	15800	132500	1.62	ND
4	0	15	301	25400	205100	1.97	129 ^e
5	20	15	833	70400	165700	2.64	109
6	40	15	863	72900	129200	2.83	ND
7	60	20	732	46900	94600	2.24	ND

^aPolymerization conditions: [**2a**] = 1.69 μ mol, 100 mL of toluene, 15 psi, and 100 equiv of methyl aluminiumoxane (PMAO-IP). ^bTurnover frequency (TOF) = mol of ethylene/(mol of cat. x h). ^cDetermined using gel permeation chromatography at 145 °C in 1,2,4-trichlorobenzene. ^dDetermined by differential scanning calorimetry, second heating. ^eSecond heating showed a bimodal melting temperature of 129 and 133 °C. ND = not determined.

Table 2.2 Ethylene Polymerization Results for Temperature Screening of Catalyst **2b**^a

entry	T_{rxn} (°C)	time (min)	yield (mg)	TOF ^b (h ⁻¹)	M_n^c (kg/mol)	M_w/M_n^c	T_m^d (°C)
1	-60	1050	190	277	118	3.25	132
2	-40	110	190	2363	115	2.00	127
3	-20	60	187	4258	102	1.55	111
4	0	45	120	3652	91	1.15	77
5	20	15	69	6297	44	1.09	60
6	40	15	55	4959	47	1.12	39
7	60	15	45	4076	63	1.02	39
8	80	15	22	2029	82	1.22	32
9	100	20	38	2578	94	1.21	30

^aPolymerization conditions: [**2b**] = 1.57 μ mol, 100 mL of toluene, 15 psi, and 100 equiv of methyl aluminiumoxane (PMAO-IP). ^bTurnover frequency (TOF) = mol of ethylene/(mol of cat.*h). ^cDetermined using gel permeation chromatography at 145 °C in 1,2,4-trichlorobenzene. ^dDetermined by differential scanning calorimetry, second heating. ^eSecond heating showed a bimodal melting temperature of 127 and 130 °C.

(entries 1–3). In contrast, polymerizations performed at temperatures ≥ 0 °C (entries 4–7) produced lower molecular weight PEs; however, all PEs were well-defined with narrow molecular weight distributions ($M_w/M_n \leq 1.22$). It should be noted that decreased PE yields and molecular weights were observed at elevated temperatures, which is an observation that is attributed to increased rates of chain transfer (via β -hydride elimination) relative to chain propagation and to the decreased solubility of ethylene in toluene at elevated temperatures.^{27,34,40}

To evaluate the thermal stability of catalyst **2b** and to overcome the limitations associated with elevated reaction temperatures, additional polymerizations were performed at 100 psi of ethylene at 80, 90, and 100 °C (**Table 2.3**). Polymerizations were run for durations up to 20 min in 5 min intervals, and the polymers obtained were thoroughly characterized. As can be seen in **Figure 2.3**, polymerizations conducted at 80 and 90 °C displayed nearly linear growth of molecular weight with time, reached molecular weights of over 600,000 g/mol, and maintained narrow molecular weight distributions ($M_w/M_n \leq 1.31$, **Table 2.3**, entries 1–8). In contrast, polymerizations conducted at 100 °C clearly deviate from this behavior displaying nonlinear growth of molecular weight with time and noticeable increases in molecular weight distribution after polymerization times of just 10 min (**Table 2.3**, entries 9–12). Each of these PE samples displayed melting transitions just above room temperature (37–46 °C) suggesting that the PE was moderately branched. This was confirmed by NMR spectroscopy in which branching contents of 63–75 branches per 1000 carbons were observed (see **Figure C.**) and consisted of both short- and long-chain branches.

Additionally, TOFs and productivities of catalyst **2b** were plotted as a function of polymerization time (**Figure 2.4**). At 80 °C, the turnover frequency of catalyst **2b** was found to slightly increase with polymerization time, which could be attributed to the slight exothermicity of the polymerization, and TOFs at 90 °C remained almost perfectly constant for the entire polymerization supporting their stability at these temperatures. At 100 °C, TOFs remained relatively constant up to 15 min; however, a dramatic decrease was observed upon extended polymerization times. An identical trend was also observed in plots of productivity (productivity = kg of PE/mol of catalyst) versus time (**Figure 2.4**) in which catalyst **2b** remained highly productive throughout the entire 20 min polymerization at 80 and 90 °C,

Table 2.3 Ethylene Polymerization Results at 100 psi for **2b**^a

<i>entry</i>	<i>T_{rxn}</i> (°C)	<i>time</i> (min)	<i>yield</i> (mg)	<i>TOF^b</i> (× 10 ³ h ⁻¹)	<i>M_n^c</i> (kg /mol)	<i>M_w/M_n^c</i>	<i>T_m^d</i> (°C)	<i>B^e</i>
1	80	5	241	66	208	1.13	46	63
2	80	10	538	74	376	1.18	45	67
3	80	15	831	76	508	1.25	44	70
4	80	20	1144	79	625	1.27	43	69
5	90	5	303	83	260	1.10	43	71
6	90	10	652	89	377	1.26	42	68
7	90	15	972	88	516	1.31	40	74
8	90	20	1273	88	605	1.31	42	70
9	100	5	346	95	235	1.19	40	73
10	100	10	746	102	422	1.24	39	71
11	100	15	1100	100	459	1.42	38	74
12	100	20	1139	79	564	1.46	37	75

^aPolymerization conditions: [**2b**] = 1.57 μmol, 100 mL of toluene, 100 psi of ethylene, and 300 equiv of PMAO-IP. ^bTOF = mol of ethylene/(mol of cat.*h). ^cDetermined using gel permeation chromatography at 145 °C in 1,2,4-trichlorobenzene. ^dDetermined by differential scanning calorimetry, second heating. ^eDetermined by ¹H NMR spectroscopy.

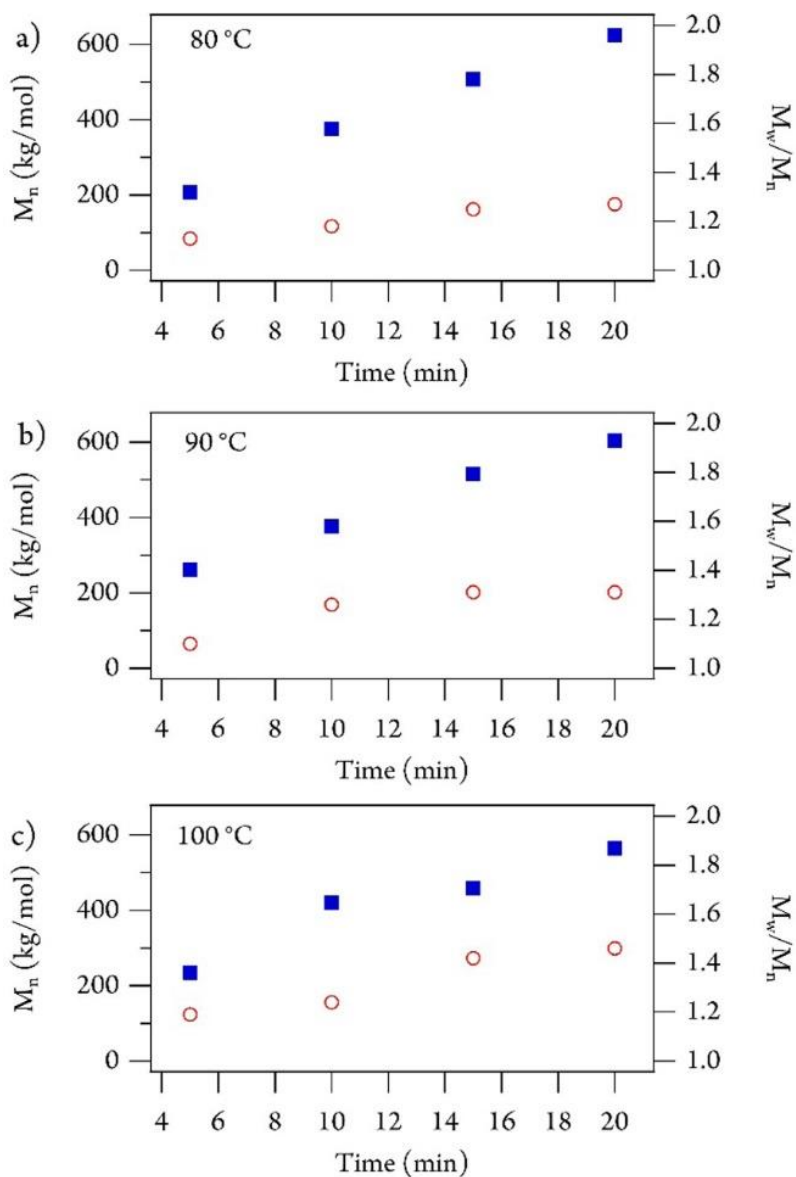


Figure 2.3 Plot of M_n (squares) and M_w/M_n (open circles) versus yield for catalyst **2b** at (a) 80 °C, 100 psi, (b) 90 °C, 100 psi, and (c) 100 °C, 100 psi.

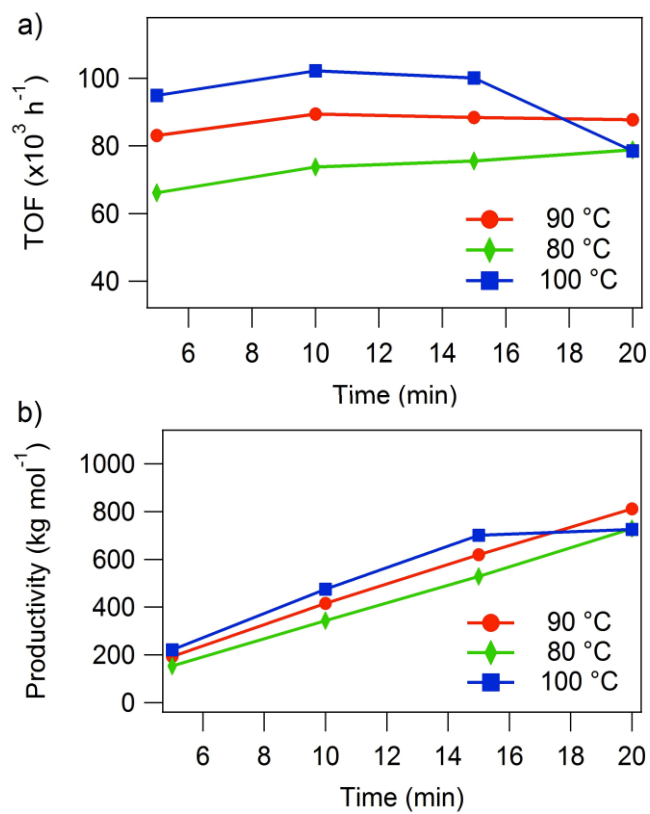


Figure 2.4 Plots of (a) turnover frequency (TOF) versus time and (b) productivity versus time for catalyst **2b** at 80 °C (green diamonds), 90 °C (red circles), and 100 °C (blue squares).

while productivities at 100 °C did not increase upon polymerization times longer than 15 min. This indicates significant catalyst decomposition at this temperature. Polymerization times extending beyond 20 min were performed; however, polymer precipitation from solution became problematic, making TOF and productivity calculations unreliable.

2.4 Conclusions

The molecular weight, molecular weight distribution, TOF, and productivity data all strongly support that catalyst **2b** is remarkably stable at both 80 and 90 °C and that it is moderately stable at 100 °C for polymerizations up to 15 min. This enhanced stability represents a dramatic improvement over other reported α -diimine-based systems, and we attribute this behavior to the unique nature of the *iPr** *N*-aryl moieties. The steric demand of the *iPr** moieties greatly inhibits *N*-aryl rotation preventing premature catalyst decomposition while effectively blocking the axial sites of the active Ni^{II} center, thereby preventing associative chain transfer that can drastically limit polymer molecular weight.

In summary, we report a synthetically simple, Ni^{II} α -diimine precatalyst that demonstrates remarkable thermal stability for ethylene polymerization. Precatalyst **2b** was activated with PMAO-IP and found to produce moderately branched PE with narrow molecular weight distributions ($M_w/M_n \leq 1.22$) at temperatures up to 100 °C at 15 psi of ethylene pressure. To circumvent issues related to elevated polymerization temperatures, the thermal stability of catalyst **2b** was evaluated using increased ethylene pressures (100 psi) and found to exhibit virtually no catalyst decomposition at temperatures as high as 90 °C for polymerization times up to 20 min. The PE produced demonstrated well-defined molecular weight distributions ($M_w/M_n \leq 1.31$), was of high molecular weight ($M_n > 600,000$ g/mol), and was moderately branched (63–75 branches per 1000 carbons). Stable turnover frequencies and a nearly linear increase in productivity were also observed at 100 °C for polymerization times ≤ 15 min, though extended reaction times did clearly show that catalyst decomposition could be problematic. The enhanced thermal stability of catalyst **2b**, as well as its ability to make high molecular weight PE with narrow molecular weight distributions, provides a significant advance toward developing Ni- and Pd-based catalysts suitable for industrially used gas-phase polymerizations.

2.5 Experimental

2.5.1 General Methods and Materials

All reactions were performed under a dry nitrogen atmosphere using an MBraun UniLab drybox or standard Schlenk techniques unless otherwise noted. Solvents were dried on an Innovative Technologies PureSolv Solvent Purification System and degassed by three freeze-pump-thaw cycles. Toluene was passed through alumina and copper columns. CD_2Cl_2 was dried over activated molecular sieves (4Å) and degassed by three freeze-pump-thaw cycles prior to use. 2,6-bis(diphenylmethyl)-4-methylaniline and *N,N'*-bis(2,6-dibenzhydryl-4-methylphenyl)ethane-1,2-diimine (**1a**) were prepared as previously reported.³² PMAO-IP was purchased from Akzo Nobel. All other reagents were purchased from commercial vendors and used without further purification. ^1H and ^{13}C NMR spectra were recorded at ambient temperature on a Varian Mercury 300 MHz or Varian VNMRS 500 MHz narrow-bore broadband system. ^1H and ^{13}C NMR chemical shifts were referenced to the residual solvent. Elemental microanalyses were carried out by Atlantic Microlab, Inc. (Norcross, GA). All mass spectrometry analyses were performed using a JEOL AccuTOF-D time-of-flight (TOF) mass spectrometer with a DART (direct analysis in real time) ionization source. X-Ray diffraction measurements were performed on single crystals coated with Paratone oil, mounted on a loop, and frozen under a stream of N_2 while data was collected on a Bruker APEX diffractometer. Reflections were merged and corrected for Lorentz and polarization effects, scan speed, and background using SAINT 4.05. The structure was solved by direct methods with the aid of successive difference Fourier maps, and were refined against all data using the SHELXTL 5.0 software package. All of the solvent molecules were squeezed. Gel permeation chromatography was performed at 145 °C in 1,2,4-trichlorobenzene at 1.0 mL/min on a Polymer Labs GPC220 equipped with refractive index and two-angle light-scattering detectors (Precision Detectors). Weight average molecular weights (M_w) were obtained from GPC light scattering data and molecular weight distributions (M_w/M_n) were obtained from GPC refractive index data relative to polystyrene standards. Number average molecular weights (M_n) were calculated using M_w , obtained from light scattering, and molecular weight distributions (M_w/M_n) obtained from RI. Polymer melting point transition temperatures (T_m)

were measured on a TA Instruments Q1000 differential scanning calorimeter equipped with an autosampler on the second heating cycle at a heating rate of 10 °C/min.

2.5.2 Synthesis of *N,N'*-bis(2,6-dibenzhydryl-4-methylphenyl) butane-2,3-diimine (1b)

2,6-bis(diphenylmethyl)-4-methyl-aniline (544.9 mg, 1.23 mmol) and 2,3-butadione (52 μ L, 0.59 mmol) were charged in a round bottom flask with methylene chloride (20 mL). Formic acid (10 drops) and magnesium sulfate were added and the reaction heated to reflux for 3 days open to air. The reaction was filtered and washed with excess methylene chloride. The purified product was obtained by column chromatography. Yield 8.6% (100 mg). R_f = 0.48 (hexanes/dcm, 50:50). ^1H NMR (CD_2Cl_2 , 500 MHz), δ , ppm: 7.35 – 7.12 (m, 24H), 7.06 (d, J = 7.4 Hz, 8H), 6.97 (d, J = 6.9 Hz, 8H), 6.70 (s, 4H), 5.15 (s, 4H), 2.14 (s, 6H), 1.23 (s, 6H). ^{13}C NMR (CDCl_3 , 125 MHz), δ , ppm: 169.91, 145.74, 143.94, 143.20, 131.97, 130.98, 129.88, 129.59, 129.13, 128.54, 128.25, 126.52, 126.23, 51.82, 21.50, 16.82. DART (m/z)(calc.): 929.58 (928.48).

2.5.3 Synthesis of $\text{NiBr}_2(\text{ArN}=\text{CC}=\text{NAr})$ ($\text{Ar} = 2,6$ bis(diphenylmethyl)-4-methylbenzene) (2a)

A solution of *N,N'*-bis(2,6-dibenzhydryl-4-methylphenyl)ethane-1,2-diimine (99.6 mg, 0.11 mmol) in methylene chloride (5 mL) was added to nickel(II) dibromide dimethoxyethane adduct (66.0 mg, 0.21 mmol) in a Schlenk flask and stirred overnight at room temperature. The reaction was filtered through a pad of celite and the solvent removed in vacuo. The precatalyst was used without further purification. Yield 96% (107.2 mg). ^1H NMR (CD_2Cl_2 , 500 MHz), δ , ppm: 24.77 (s, 6H, Ar-Me), 21.02 (s, 4H, CH), 7.30, 7.15, 7.04, 6.83. ^{13}C NMR (CD_2Cl_2 , 125 MHz), δ , ppm: 136.74, 130.83, 129.4, 128.85, 127.26, 105.43, 103.07.

2.5.4 Synthesis of $\text{NiBr}_2(\text{ArN}=\text{C}(\text{Me})\text{C}(\text{Me})=\text{NAr})$ ($\text{Ar} = 2,6$ bis(diphenylmethyl)-4-methylbenzene) (2b)

A solution of *N,N'*-bis(2,6-dibenzhydryl-4-methylphenyl)butane-2,3-diimine (239.4 mg, 0.25 mmol) in methylene chloride (5 mL) was added to a Schlenk flask containing

nickel(II) dibromide dimethoxyethane adduct (79.1 mg, 0.25 mmol). The reaction mixture was heated to 30 °C and stirred for five hours. The reaction was filtered through a pad of celite and layered with pentane to induce crystallization. The solvent was decanted and dried in vacuo. Yield 86% (247.8 mg). ¹H NMR (CD₂Cl₂, 500 MHz): δ 32.78 (s, 6H, Ar-Me), 21.94 (s, 4H, CH), 12.05 (2H), 7.98 (8H), 7.02 (8H), 6.86 (4H), 6.55 (14H), 4.52 (8H), -18.97 (6H, CH₃). ¹³C NMR (CD₂Cl₂, 125 MHz): δ 132.99, 132.29, 129.51, 128.58, 127.18, 127.10. Anal. Calc'd for C₇₀H₆₀N₂Br₂Ni (1146.25): C 73.25, H 5.27, N 2.44; found C 73.55, H 5.50, N 2.55.

2.5.5 General Polymerization Conditions

Under an inert atmosphere, a Fisher Porter bottle was charged with nickel catalyst **2a** or **2b** (1.57 μmol), 100 mL of toluene, and a magnetic stir bar. The bottle was sealed and placed in an oil bath at the desired temperature. The vessel was pressurized with ethylene and allowed to equilibrate under constant pressure for 10 minutes with stirring. PMAO-IP was injected to initiate polymerization and stirred continuously for the desired time. The polymerization was quenched via the addition of MeOH (5 mL) and the polymer was precipitated using excess acidic MeOH (5% HCl in MeOH) and dried in a vacuum oven to constant weight.

**Chapter 3– CONTROLLED/LIVING THERMALLY
ROBUST NICKEL (II) CATALYST FOR ETHYLENE
POLYMERIZATION**

A version of this chapter has been submitted by Lauren A. Brown, W. Curtis Anderson, Jr., Nolan E. Mitchell and Brian K. Long to a peer-reviewed journal and is currently under review.

Lauren A. Brown, W. Curtis Anderson, Jr., Nolan E. Mitchell, Brian K. Long. "High Temperature, Living Polymerization of Ethylene by a Sterically Demanding Ni α -Diimine Catalyst"

I was responsible for the synthesis and characterization of the catalyst, synthesis of the polymers, analysis of the polymers, and preparation of the manuscript. W. Curtis Anderson, Jr. and Nolan E. Mitchell aided with the characterization of the polymers. Dr. Brian Long advised this work.

3.1 Abstract

Catalysts employing late transition metals, namely Ni and Pd, have been extensively studied for their use in olefin polymerizations, copolymerizations, and for their synthesis of advanced polymeric species such as block copolymers. Unfortunately, many of these catalysts often exhibit poor thermal stability and/or non-living polymerization behavior that limits their ability to synthesize tailored polymer structures and overall industrial appeal. Because of this, the development of catalysts that display controlled/living behavior at elevated temperatures is vital. In this manuscript, we will describe a Ni -diimine complex capable of polymerizing ethylene in a living manner at temperatures as high as 75 °C, which is the highest temperature reported for the living polymerization of ethylene by a late transition metal-based catalyst.

3.2 Introduction

Controlled/living polymerizations offer a precise means to tailor polymer structure, comonomer incorporation levels, block copolymer synthesis, and even regio- and stereoselectivity.^{2-5,41-43} Living polymerization methodologies are those that are free of deleterious chain termination and irreversible chain transfer events.⁴⁴ Specifically for α -olefins polymerizations, these chain transfer and termination events are often suppressed by

low temperatures, and for this reason, most living polymerizations of ethylene occur at or below ambient temperature.^{2,22,29,45-48} However, due to the growing demand for polymers with tailored structure and because industrial olefin polymerizations are often conducted at elevated temperatures (70 – 115 °C), the overall utility of most known late transition metal-based catalysts is severely limited.^{1,49}

To date, only a few examples of Ni- and Pd-based olefin polymerization catalysts that are controlled/living at superambient temperatures have been reported.⁵⁰⁻⁵⁵ Furthermore, most of these polymerizations are not performed using ethylene as the feedstock, but rather higher α -olefins. This lack of Ni- and Pd-based catalysts capable of performing living ethylene polymerizations at elevated temperatures represents a fundamental gap in current knowledge. To address this issue, herein we report that Ni-based α -diimine catalyst **3** readily polymerizes ethylene in a living fashion at temperatures as high as 75 °C (**Figure 3.1**). To the best of our knowledge, this is the highest temperature, living ethylene polymerization using a Ni- or Pd-based catalyst reported to date.

3.3 Results and Discussion

Catalyst **3**, which contains an acenaphthenequinone-based backbone bearing sterically demanding *N*-aryl moieties (*iPr**), was previously developed by our group and its time-resolved thermal stability studied.⁵⁶ Though this catalyst was found to be remarkably thermally robust at temperatures as high as 90 °C, we noted that the polymer produced often exhibited a slight high molecular weight shoulder when analyzed by gel permeation chromatography (GPC) (**Figure 3.2**), which was almost undetectable via refractive index. This high molecular weight shoulder resulted in polymer samples with dispersities broader

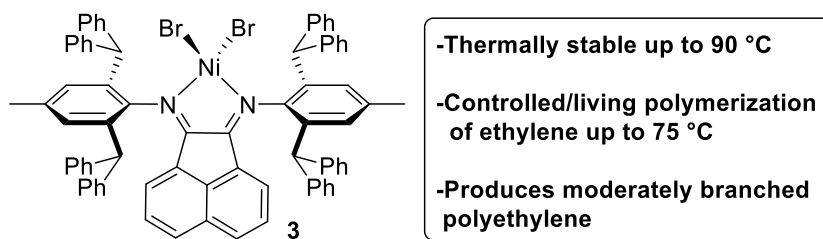


Figure 3.1 Catalyst **3** used for ethylene polymerizations.

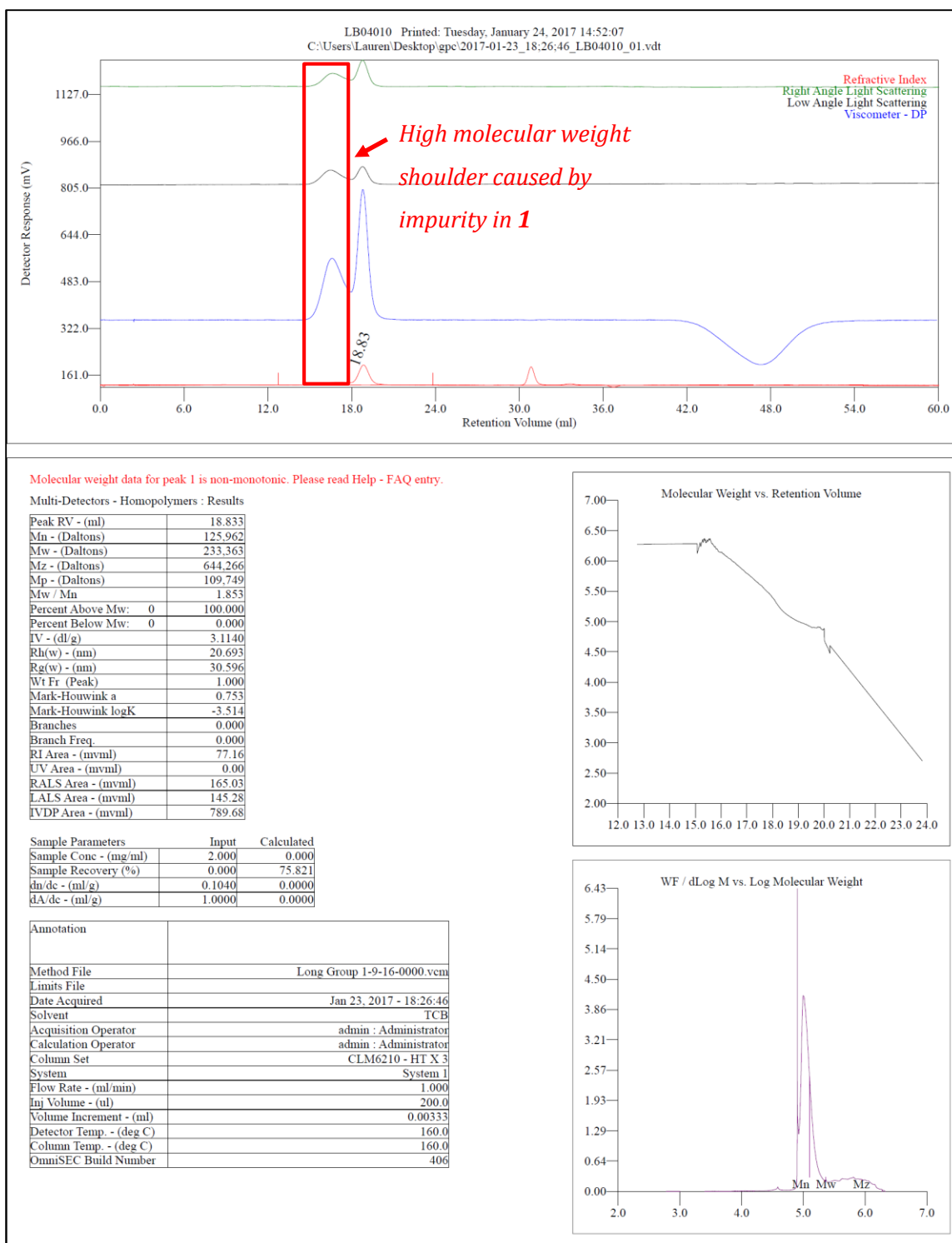


Figure 3.2 Representative GPC of polyethylene produced with complex **3** containing an impurity.

than typically desired for a controlled/living polymerization, albeit still relatively narrow as compared to many commonly employed olefin polymerization catalysts.⁵⁶

Encouraged by the promising behavior of this catalyst, and after further investigation, we have now been able to attribute this high molecular weight shoulder to a catalyst impurity that initially was not detectable via ¹H NMR spectroscopy. More specifically, we discovered that the problematic impurity was an asymmetric analogue of catalyst **3** in which only three benzhydryl (*i*Pr*) *N*-aryl moieties are present. This asymmetric ligand precursor was identified via liquid chromatography-mass spectrometry (LC-MS) prior to metalation and is a result of incomplete conversion during the synthesis of the bulky 2,6-disubstituted aniline moieties (**Figure 3.3**).

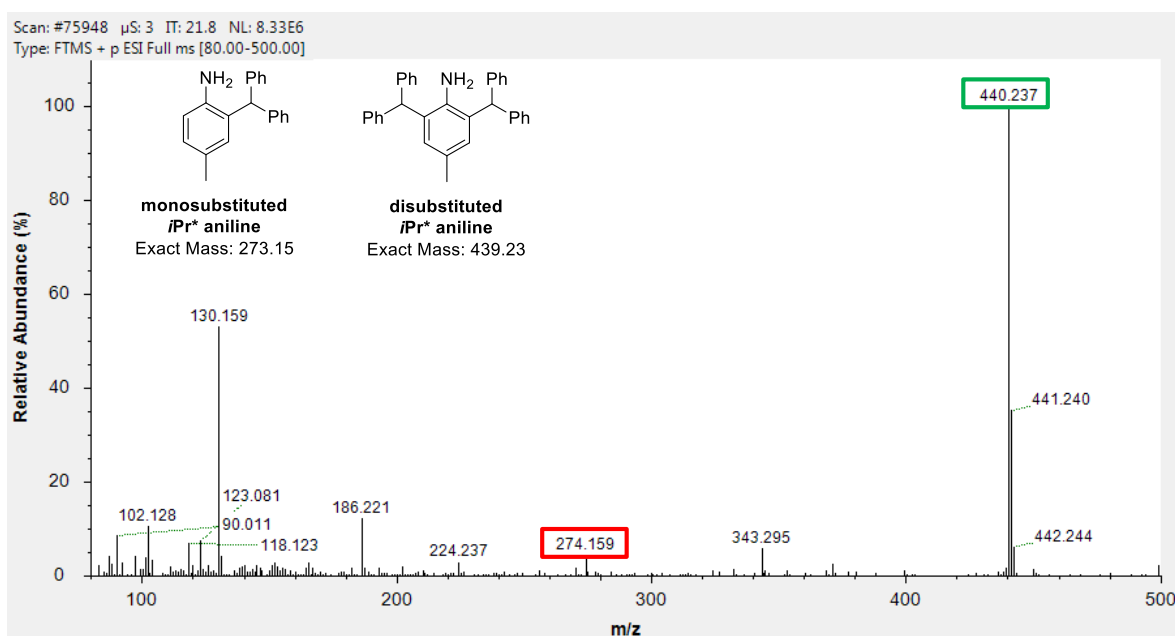


Figure 3.3 LC-MS of *i*Pr* aniline in DCM prior to purification.

Ultimately, high purity Ni complex **3** was synthesized according to our previously reported procedure.⁵⁶ However, in order to eliminate any undesired monosubstituted ligand impurities, which result following the double Friedel-Crafts alkylation of *p*-toluidene using benzhydrol (diphenylmethanol) and ZnCl₂,⁵⁷ the reaction product was recrystallized in quadruplicate from isopropanol. These additional recrystallizations completely removed the

monosubstituted aniline, and this removal was subsequently confirmed via LC-MS (**Figure 3.4**). This high purity aniline was then condensed onto acenaphthenequinone using a two-step, one-pot reaction and subsequently metallated using NiBr₂ (dimethoxyethane adduct) to yield high purity catalyst **3**, which is used exclusively in the following studies (**Scheme 3.1**).

Ethylene polymerization trials were conducted using catalyst **3** (5 μmol) and activated with PMAO-IP (100 equiv) (**Table 3.1**). Polymerizations were performed at 70, 75, and 80 °C and were monitored as a function of time up to 1 h. Catalyst **3** was found to be highly active over the entire 1 h trial (TOF = 6,300 – 8,700) even at the low ethylene pressure (15 psi) and elevated temperatures (70-80 °C) studied. The resultant polymers were analyzed via gel permeation chromatography (GPC) and ¹H NMR. The number average molecular weights (*M_n*) of the polymers produced by **3**/MAO were found to increase steadily over time reaching final molecular weights ranging from 193,000-253,000 g/mol, depending on reaction temperature (**Table 3.1**). Polymer dispersities (*D*) remained below 1.2 for polymerizations at both 70 and 75 °C, which suggested that this catalyst might indeed be living at these temperatures. In contrast, polymers produced by **3**/MAO at 80 °C

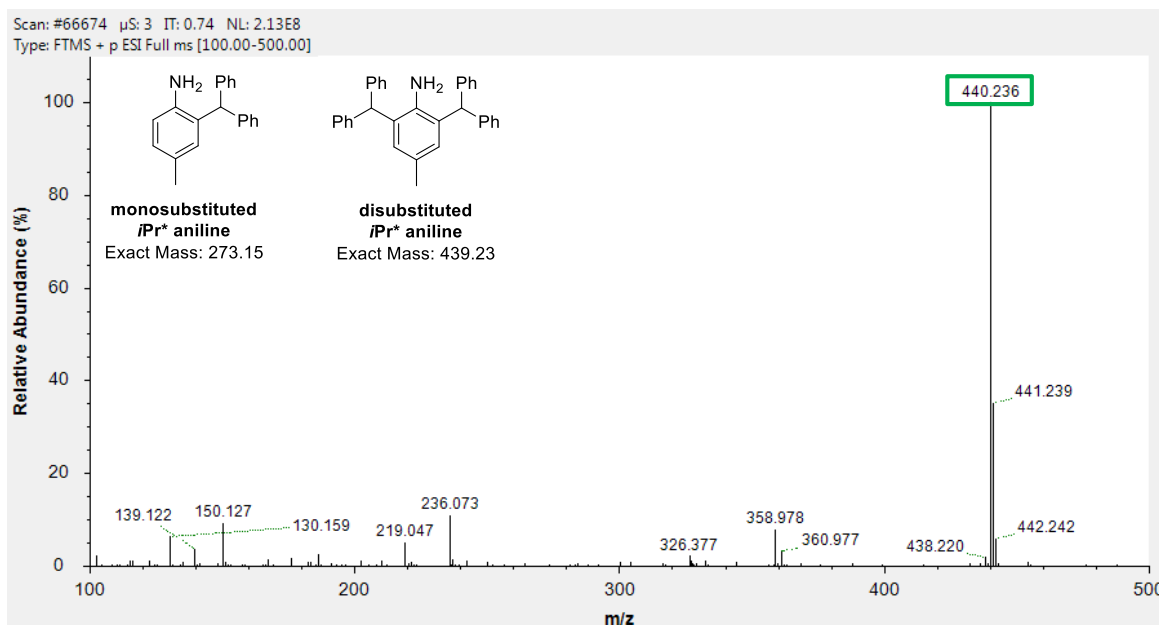
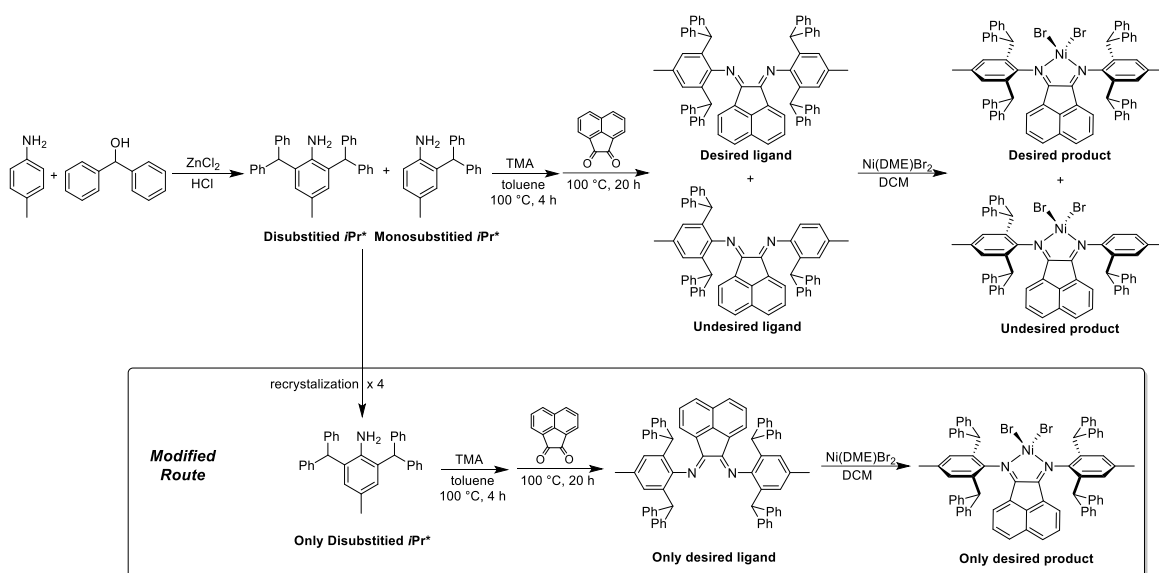


Figure 3.4 LC-MS of *iPr** aniline in DCM after four recrystallizations from isopropanol.



Scheme 3.1 Modification of the synthetic route to obtain complex **3** in ultrahigh purity.

Table 3.1 Ethylene Polymerizations using Catalyst **3**^a

entry	T_{rxn} (°C)	time (min)	yield (g)	TOF ^b	M_n ^c (kg/mol)	\bar{D} ^c	B^d (°C)
1	70	10	0.16	6900	44	1.35	47
2	70	15	0.22	6300	50	1.22	48
3	70	30	0.49	7000	128	1.14	48
4	70	45	0.77	7300	164	1.18	47
5	70	60	0.96	6900	244	1.17	48
6	75	10	0.17	7300	40	1.37	47
7	75	15	0.23	6600	67	1.20	49
8	75	30	0.49	7000	155	1.17	47
9	75	45	0.85	8100	191	1.14	50
10	75	60	1.07	7600	253	1.15	46
11	80	15	0.30	8600	70	1.10	48
12	80	30	0.61	8700	114	1.17	49
13	80	45	0.72	6900	162	1.24	50
14	80	60	0.93	6600	193	1.33	45

^aEthylene polymerization conditions: 5.0 μ mol of catalyst **3**, 15 psi of ethylene, 98 mL of toluene, 2 mL of dichloromethane, and 100 equiv of PMAO-IP. ^bTurnover frequency (TOF) = mol of ethylene/(mol of cat. \times h). ^cDetermined using gel permeation chromatography at 160 °C in 1,2,4-trichlorobenzene. ^dBranches per 1000 total carbons determined via ¹H NMR.

exhibited broadening dispersities as a function of time (**Table 3.1**, entries 11–14) suggesting that **3**/MAO may deviate from living behavior at temperatures exceeding 75 °C. While our previous work established that catalyst **3** remains active at temperatures as high as 90 °C,⁵⁶ the broadening dispersities observed at 80 °C are attributed to increased chain transfer or chain termination events. Lastly, ¹H NMR analysis showed that all of the polymers produced by complex **3** contained 45-50 branches per 1000 total carbons (*B*).

To determine if catalyst **3** is indeed living at these elevated temperatures, we plotted their progression of molecular weight and dispersity as a function of polymerization time. **Figure 3.5** clearly shows that catalyst **3** provides a linear increase in polyethylene molecular weight at 75°C, ultimately reaching over 250,000 g/mol after 1 h. Moreover, GPC analysis showed that the polymers produced at 75 °C remained monomodal during the course of the polymerization and their dispersities narrowed as the polymerization progressed ($\mathcal{D} = 1.37 \rightarrow 1.15$) (**Table 3.1**, entries 6–10). We see the same trends for polymerizations conducted at 70 °C (**Figure 3.6**).

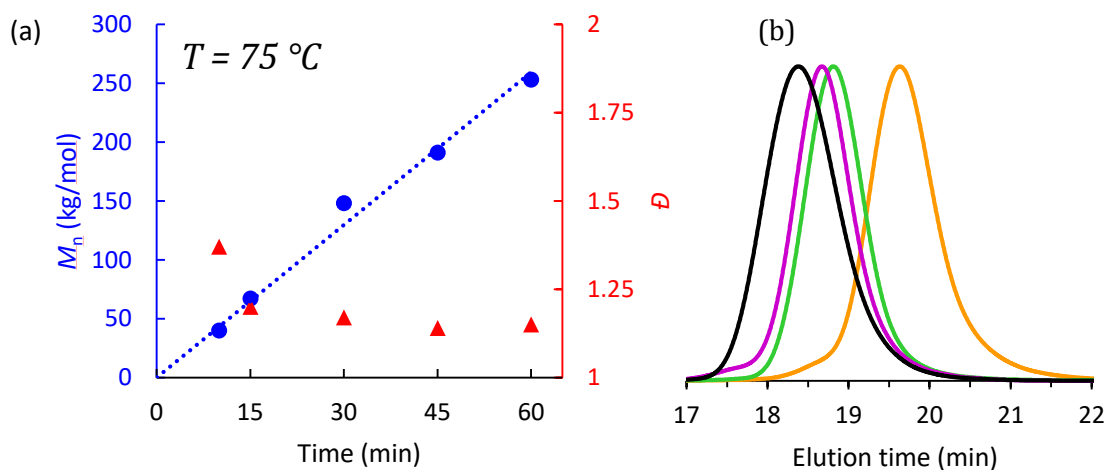


Figure 3.5 (a) Plot of M_n (blue circle) and \mathcal{D} (red triangles) as a function of polymerizations time when using **3**/PMAO-IP at 75 °C. (b) GPC traces (viscometer signal) of polymerizations at 75 °C as a function of polymerization time (black = 60 min, purple = 45 min, green = 30 min, orange = 15 min).

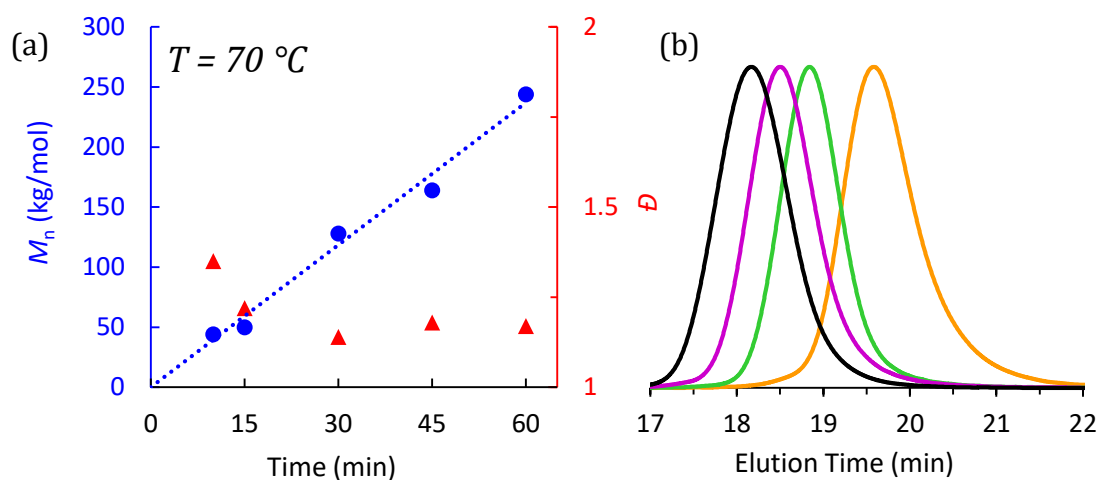


Figure 3.6 (a) Plot of M_n (blue circles) and \bar{D} (red triangles) as a function of polymerization time using **3**/PMAO-IP at 70 °C. (b) GPC traces (viscometer detector) of polymerizations run at 70 °C at various polymerization times (black = 60 min, purple = 45 min, green = 30 min, orange = 15 min).

To further emphasize the controlled/living character of the polymerization run with catalyst **3** we calculated its activity (kg of PE/mol of **3** x h) during polymerization at 75 °C to ensure no loss of activity was observed as a function of time. As expected, **Figure 3.7** demonstrates that complex **3** retains constant activity during ethylene polymerizations at 75 °C for the full hour monitored. From these results, we conclude that catalyst **3** does polymerize ethylene in a controlled/living manner at both 70 and 75 °C. To the best of our knowledge, this is the highest temperature reported for the living polymerization of ethylene mediated by any late transition metal-based catalyst.

When examining ethylene polymerizations using **3**/MAO at 80 °C, we initially noted that molecular weights increased steadily and that polymer dispersity values were low (**Table 3.1**, entries 11-12). However, after 30 minutes of polymerization, significant deviation from linear molecular weight growth was evident and polymer dispersity values steadily increasing over the 1 h polymerization ($\bar{D} = 1.10 \rightarrow 1.33$). This was also observed from their respective GPC traces in which the resultant polymer samples broadened as a function of time at 80 °C (**Figure 3.8**). Therefore, we concluded that while **3**/MAO maintains

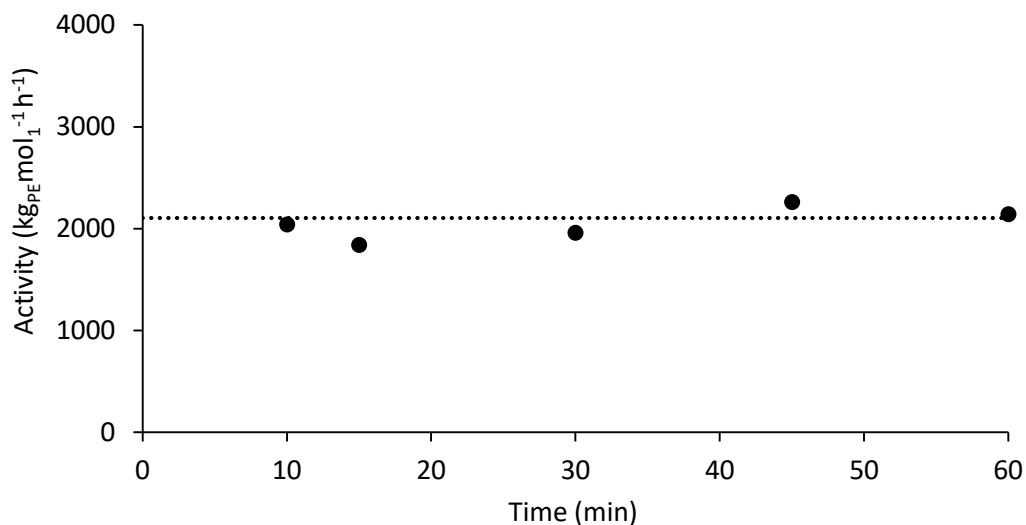


Figure 3.7 Plot of activity versus reaction time for ethylene polymerizations using **3**/PMAO-IP at 75 °C.

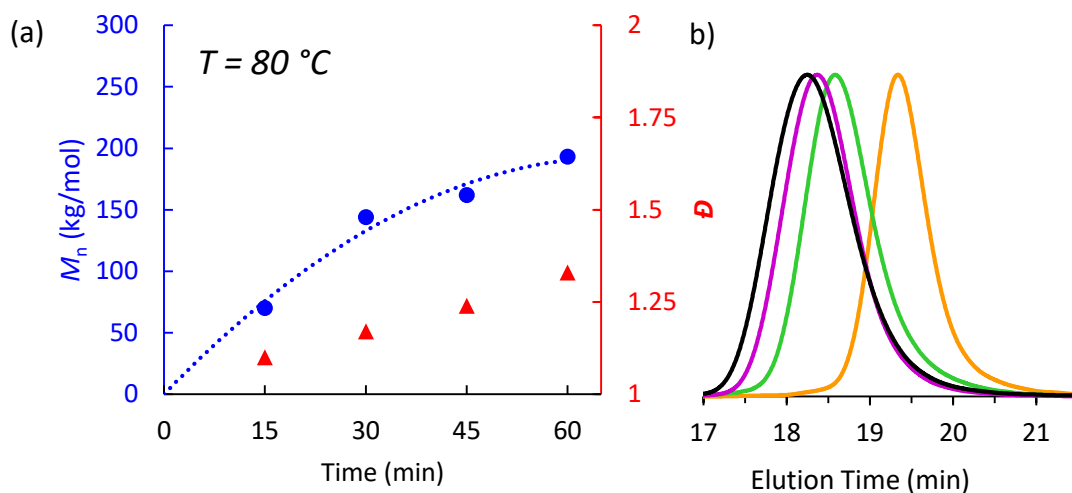


Figure 3.8 (a) Plot of M_n (blue circle) and D (red triangles) as a function of polymerizations time when using **3**/PMAO-IP at 80 °C. (b) GPC traces (viscometer signal) of polymerizations at 80 °C as a function of polymerization time (black = 60 min, purple = 45 min, green = 30 min, orange = 15 min).

living polymerization behavior at 75 °C, it begins to diverge from controlled behavior at temperatures ≥ 80 °C. Lastly, we would like to note that though polymerizations with catalyst **3** are not living at these higher temperatures (≥ 80 °C), our previous studies have conclusively shown that it remains active for ethylene polymerizations up to 90 °C.⁵⁶ This suggests that catalyst decomposition or deactivation is minimal between 80–90 °C, and that undesirable chain transfer and/or chain termination hinders controlled/living polymerization behavior.

Lastly, because living behavior of a polymerization is often evaluated by comparing progression of polymer molecular weight versus monomer conversion, rather than time, we have also evaluated our data with respect to the amount of polymer produced at 70, 75, and 80 °C, which can be seen in **Figure 3.9**, **Figure 3.10**, and **Figure 3.11**, respectively. Again, we see that catalyst **3** polymerizes ethylene in a living fashion at both 70 and 75 °C, which is displayed by the linear increase of polymer yield as the molecular weight is increased. However, when the polymerization temperature is increased to 80 °C, the polymerizations begins to deviate from living behavior at 80 °C.

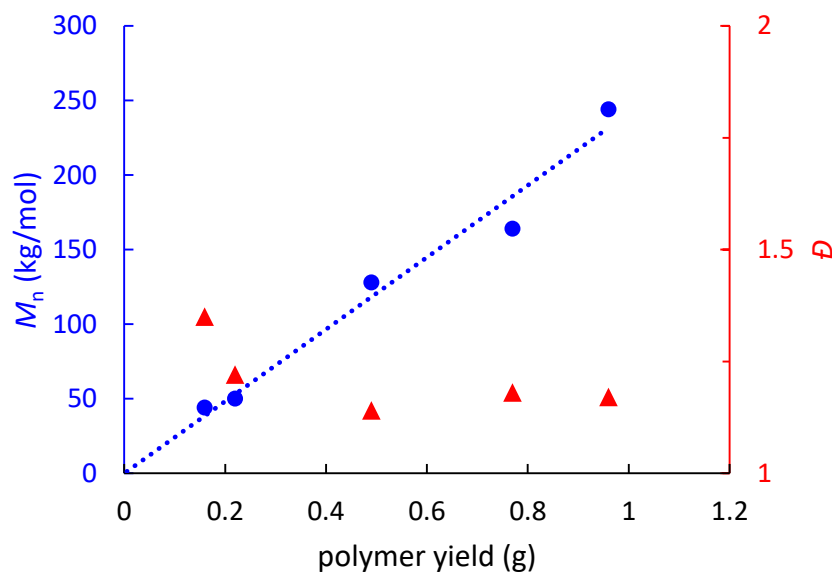


Figure 3.9 Plot of M_n (blue circles) and D (red triangles) as a function of polymerization yield using **3**/PMAO-IP at 70 °C.

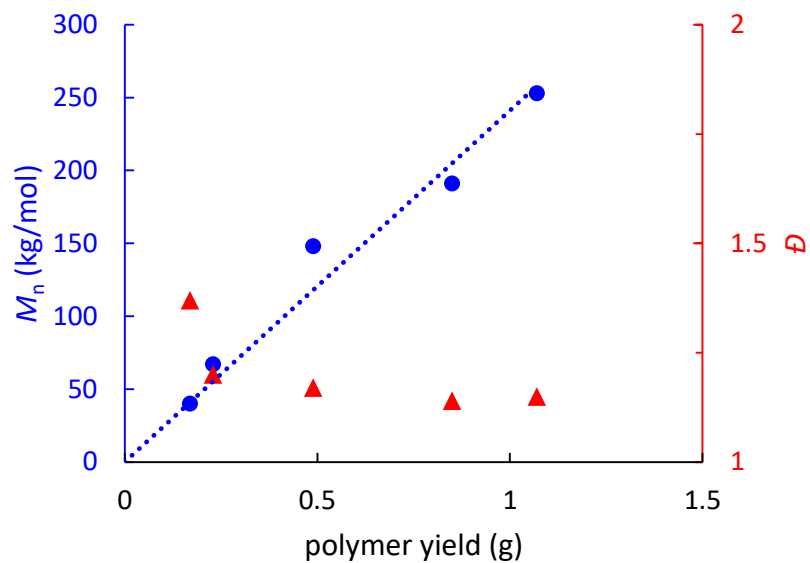


Figure 3.10 Plot of M_n (blue circles) and D (red triangles) as a function of polymerization yield using **3**/PMAO-IP at 75 °C.

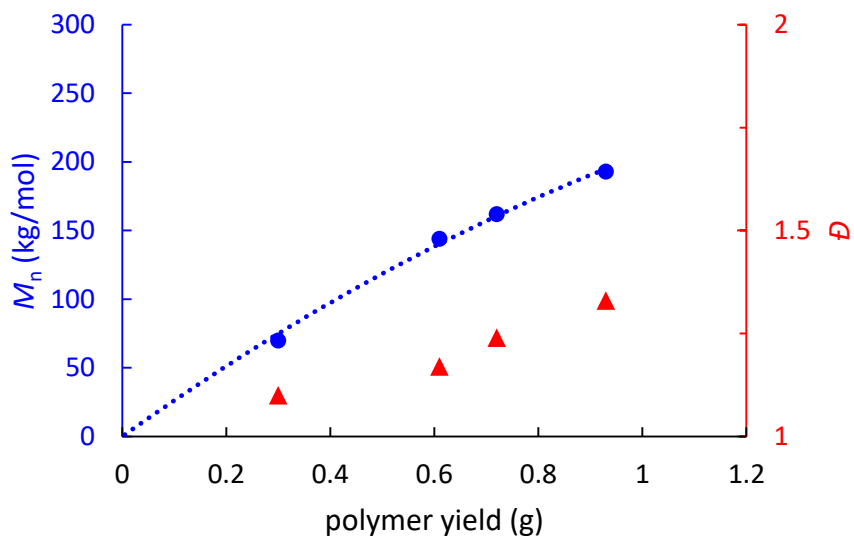


Figure 3.11 Plot of M_n (blue circles) and D (red triangles) as a function of polymerization yield using **3**/PMAO-IP at 80 °C.

To further elucidate this catalyst's full polymerization capabilities, we decided to examine the redox activity of catalyst **3** in hopes of controlling polyethylene microstructure via redox manipulation. Ni α -diimine catalysts are well-known to undergo a phenomenon known as 'chain-walking' during ethylene polymerization, which may be modulated via temperature, pressure, and, as recently discovered, redox state of the catalyst.^{13,14,42,58-60} Those recent reports show that a related Ni α -diimine catalyst also containing an acenaphthequinone-based ligand is readily reduced using a chemical reductant, and that polyethylenes with tailored microstructures can be produced.⁵⁹ Because complex **3** also bears an acenaphthequinone-based ligand we chose to evaluate its redox-activity for the polymerization of ethylene.

In order to examine the redox activity of complex **3**, we performed cyclic voltammetry (CV) in dichloromethane (DCM) using [n Bu₄N][PF₆] (0.1 M) as the electrolyte (**Figure 3.12**). The CV trace was referenced to a ferrocene standard (Fc/Fc⁺), and it revealed that complex **3**

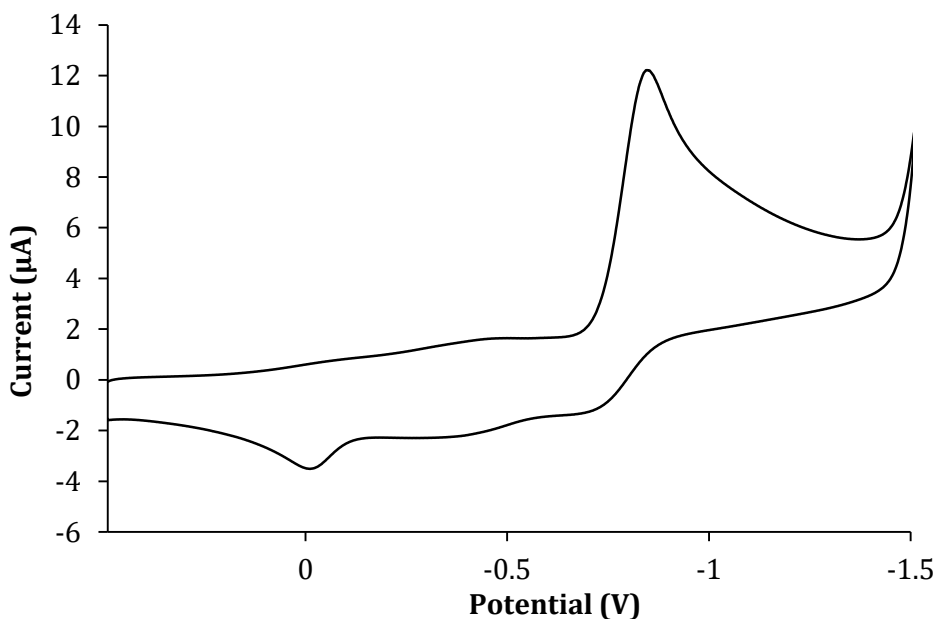


Figure 3.12 Cyclic voltammogram of **3** (0.01 mmol) recorded at a scan rate of 100 mV/s in dichloromethane (5 mL) and (n Bu)₄NPF₆ buffer (0.20 M), referenced versus Fc/Fc⁺.

displayed a non-reversible reduction potential at $E^{\text{red}} = -0.86$ V. Though not reversible, we proceeded to examine how reduction of catalyst **3** would affect ethylene polymerizations and cobaltocene (CoCp_2) was chosen as an appropriate reductant ($E^{\circ} = -1.3$ V).⁶¹

Ethylene polymerizations using complex **3** and 3 equiv of added CoCp_2 reductant did produce polymer at 20 and 80 °C; however, the difference in the microstructure of polyethylene produced by **3** and **3** with added CoCp_2 (1 equiv) was negligible at both room temperature and elevated temperatures (**Table 3.2**). Due to the lack of difference in polyethylene microstructure, further redox studies were not pursued. We attribute the similarities in polymer branching content between polymers produced by **3** and **3**/reductant to be a result of the remarkably bulky $i\text{Pr}^*$ moieties. While these bulky substituents are needed to inhibit N -aryl rotation and enhance thermal stability,^{56,62} it is believed to also hinder chain transfer, chain walking, and chain termination events of this active species.^{16,36,63}

Table 3.2 Ethylene Polymerizations Using Catalyst **3** and Cobaltocene^a

entry	$[\text{CoCp}_2]$	$T_{\text{rxn}}(^{\circ}\text{C})$	yield (g)	TOF ^b	M_n^c (kg/mol)	\bar{D}^c	B^d ($^{\circ}\text{C}$)
1	0	20	0.98	7000	204	1.13	47
2	5	20	0.69	4929	177	1.25	45
3	0	80	0.93	6624	193	1.33	45
4	5	80	1.33	9500	207	1.66	47

^aEthylene polymerization conditions: 5.0 μmol of catalyst **3**, 15 psi of ethylene, 98 mL of toluene, 2 mL of dichloromethane, and 100 equiv of PMAO-IP for 60 min. ^bTurnover frequency (TOF) = mol of ethylene/(mol of cat. x h). ^cDetermined using gel permeation chromatography at 160 °C in 1,2,4-trichlorobenzene. ^dBranches per 1000 total carbons determined via ^1H NMR.

3.4 Conclusions

The bulky $i\text{Pr}^*$ catalyst **3** is the first α -diimine complex capable of polymerizing ethylene in a living fashion at temperatures significantly above room temperature. More specifically, when activated with PMAO-IP, complex **3** exhibits living behavior at temperatures as high as 75 °C as evidenced by narrowing polymer dispersities and linearly increasing molecular weights as a function of polymerization time and conversion. To the best of our knowledge, this is the highest temperature reported for a living polymerization of

ethylene using a late transition-metal complex. Lastly, **3**/MAO was found to deviate from living behavior at temperatures ≥ 80 °C, though the catalytically active species remains thermally robust up to temperatures as high as 90 °C.⁵⁶ We attribute this deviation from living behavior to undesired chain transfer and chain termination events.

3.5 Experimental

3.5.1 General Methods and Materials

All experiments were performed under a dry nitrogen atmosphere using standard Schlenk techniques or MBraun inert-gas glove box, unless otherwise noted. Solvents were purified using a two-column solid-state Innovative Technologies PureSolv Solvent Purification System and degassed via three freeze-pump-thaw cycles. NMR solvents were purchased from Cambridge Isotope Laboratories. Catalyst **3** was prepared according to literature.⁶⁴ The liquid chromatography- mass spectroscopy experiments of the *iPr** aniline were performed on a Thermo Fisher Scientific Exactive Plus Orbitrap MS using direct injection, full scan, electrospray ionization. PMAO-IP was purchased from the Akzo Nobel and used as received. All other reagents were purchased from commercial vendors and used without further purification. Cyclic voltammetry measurements were performed on a CH Instruments potentiostat using 0.01 mmol of compound **3** in 5 ml DCM solution (0.002 M) with supporting electrolyte 0.2 M (*n*Bu)₄NPF₆, and using a Ag reference electrode, 2 mm Au working electrode, and a tungsten counter electrode at a scan rate of 100 mV•s⁻¹. All potentials are referenced to the ferrocene-ferrocenium (Fe^{II}/Fe^{III}) redox couple. Gel permeation chromatography (GPC) was performed at 160 °C in 1,2,4-trichlorobenzene at a flow rate of 1.0 mL/min on a Malvern Viscotek HT-GPC equipped with triple detection. Polymer ¹H NMR spectra were obtained in CDCl₃ using a Bruker 400 MHz NMR at 25 °C. All NMR spectra are referenced relative to their residual solvent signal. Branching content was determined by ¹H NMR spectroscopy using the formula $(\text{CH}_3/3)/[(\text{CH} + \text{CH}_2 + \text{CH}_3)/2] \times 1000$.⁶⁵

3.5.2 General Ethylene Polymerization Procedure

Under an inert atmosphere, a Fisher-Porter bottle was charged with catalyst **3** (5 μmol) dissolved in dichloromethane (DCM) (2 mL), toluene (98 mL), and a magnetic stir bar.

The Fisher-Porter bottle was sealed and placed in an oil bath set to the desired temperature. The vessel was pressurized with ethylene gas while stirring and equilibrated for 10 min. PMAO-IP (100 equiv) was injected to initiate the polymerization and was stirred continuously for the desired time. All polymerizations were quenched via the addition of MeOH (10 mL). The polymer was precipitated using excess acidic MeOH (5% HCl in MeOH) and dried to constant weight in a vacuum oven. Polymerizations requiring the reduced catalyst form were performed using the same procedure except cobaltocene (1 equiv) was added to the DCM/toluene solution prior to activation with PMAO-IP.

**Chapter 4– INTRODUCTION TO REDOX-
SWITCHABLE CATALYSIS FOR CYCLIC ESTER
POLYMERIZATIONS**

4.1 Motivation

Bioplastics have become a highly sought-after alternative to conventional petrochemical-based plastics due to their biodegradability and derivatization from renewable resources.⁶⁶ For these reasons, polylactic acid (PLA) is a viable alternative for a variety of applications that include medical and packaging products.⁶⁷⁻⁶⁹ Though PLA may be directly synthesized from lactic acid, this route typically leads to materials with low molecular weight and poor mechanical properties. In contrast, the use of lactide, the dimeric bislactone of lactic acid, as a monomer readily produces high molecular weight PLA via ring-opening polymerization (ROP). ROP can be conducted by a variety of methods, but one that shows tremendous success is the utilization of metal-based catalysts, most commonly stannous octanoate (also known as Tin(II) 2-ethylhexanoate, or $\text{Sn}(\text{Oct})_2$).^{70,71} By using metal-based catalysts, PLA can be produced in a controlled fashion and can even be incorporated into advanced architectures, such as block copolymers, making it a truly diverse material.⁶⁹

In an effort to further develop methods of enhancing polymerization control, we chose to study the use of redox-switchable catalysts, which can be used to alter the electrophilicity of the propagating metal center. With redox active catalysts, the polymerization behavior may be changed using a single catalytically active species, which could one day be industrially relevant by controlling polymerization rate and/or monomer incorporation. In fact, previous studies show that modulating the electronic nature of a catalyst drastically alters the rate of polymerization as well as the reactivity toward individual monomers.⁷²⁻⁷⁴ To advance fundamental understanding within this area of polymerization catalysis, this portion of the dissertation will discuss which aspects of the redox active catalysts must be modulated in order to achieve a targeted polymerization effect. We will examine the effect that the proximity of the redox active moiety to the active polymerization site has on achieving optimal “on-off-on” switching in L-lactide polymerizations to modulate, which oscillates the catalyst between an active and a dormant state. To this end, group 4 transition metal-based catalysts containing a redox active moiety will be synthesized and monitored for their polymerization of L-lactide and discussed herein.

4.2 Redox Switchable Catalysis

The first example of redox-switchable catalysis (RSC) was performed by Wrighton and coworkers in 1995 where they showed that the redox state of the catalyst would affect its affinity for different reactions *in situ*.⁷⁵ Their study was conducted with a rhodium stabilized dppc (dppc = 1,1'-bis(diphenylphosphino)(cobaltocene)) catalyst that was 16 times more reactive toward alkene hydrogenation when in its reduced state compared to its oxidized form. **Figure 4.1** shows the redox events of this catalyst were easily reversible upon the addition of chemical oxidants and reductants. The reaction was initially monitored with the reduced species, which is highly active for the hydrogenation of cyclohexene, but after the addition of decamethyl ferrocenium hexafluorophosphate (Fc^+PF_6^-), the catalyst was converted to the oxidized species, which was much less reactive. However, after addition of cobaltocene (CoCp_2), the catalyst was converted back to the reduced form and once again extremely active in the reaction. While the oxidized species was not reactive for the hydrogenation of alkenes, the oxidized form of the Rh-based catalyst was much more active for hydrosilylation of ketones compared to the reduced species. This work showed that it was possible to modulate the reaction behavior *in situ* with a single catalyst by changing its electronic state. This work inspired researchers to explore if RSC could be implemented in other reactions

4.3 Redox Switchable Polymerization Catalysis

The first example of a single-site, redox-switchable catalyst for polymerization was reported by Gibson and coworkers in 2006.⁷² Their redox active catalyst was a titanium-based salen bis(isopropoxide) complex, which represents a class of catalysts that has been examined for polymerization of lactide;⁷⁶⁻⁷⁸ however, their catalyst had been modified to contain two ferrocenyl moieties at the outer extremities of the ligand scaffold. Ferrocene was chosen as the redox active moiety because it is well known that ferrocene and its derivatives display a highly reversible, well-understood redox potential.⁶¹ Their studies showed that the catalyst containing Fe^{II} functionalities could easily be oxidized using chemical oxidant, silver triflate (AgOTf), to the dicationic Fe^{III} species and reduced back to the original form using a chemical reductant, decamethylferrocene ($\text{Fe}(\text{Cp}^*)_2$) (**Scheme 4.1**).

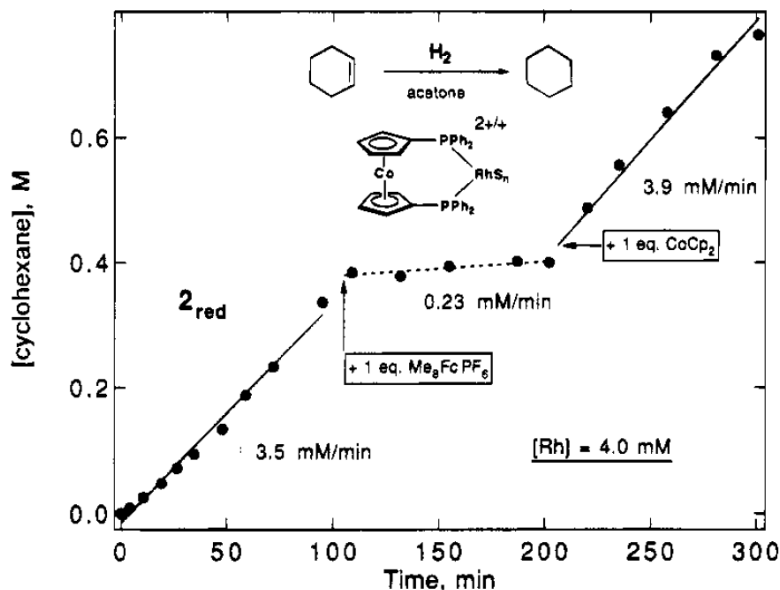
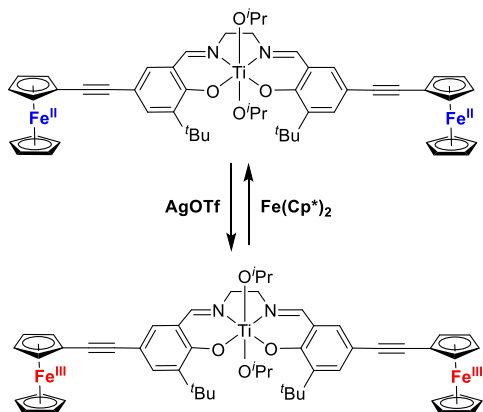


Figure 4.1 A redox-switchable rhodium stabilized catalyst that is 16 times more active for the hydrogen of alkenes when in its reduced form. The reduced form is represented by the solid line. The oxidized form is represented by the dotted line. "Reprinted with permission from (*J. Am. Chem. Soc.*, **1995**, *117* (12), pp 3617–3618). Copyright (1995) American Chemical Society."⁷⁵



Scheme 4.1 Titanium-based catalyst with two ferrocenyl redox active moieties at the outer extremity of the complex. The complex is easily oxidized with silver triflate (AgOTf) to the Fe^{III} species (red) and rereduced back to the Fe^{II} species (blue) using decemethylferrocene (Fe(Cp*)₂). "Adapted with permission from (*J. Am. Chem. Soc.*, **2006**, *128* (23), pp 7410–7411). Copyright (2006) American Chemical Society."⁷²

The titanium-based salen catalyst bearing ferrocenyl substituents was studied for its redox switchability during the polymerization of *rac*-lactide. **Figure 4.2** displays that the complex could be modulated depending on the redox state of the catalyst. The reduced species was much more active for *rac*-lactide polymerization while the oxidized species showed decreased polymerization activity.⁷² Their report showed that polymerization activity decreased with increased Lewis acidity of the metal complex. Since this first display of redox-switchable polymerization catalysis, there have been a few reports of where the RSC method has been used to altogether halt polymerization activity with one electronic species while the other remains highly active. RSC has also been used in cyclic ester polymerizations to provide control over monomer selectivity.^{73,74,79-81}

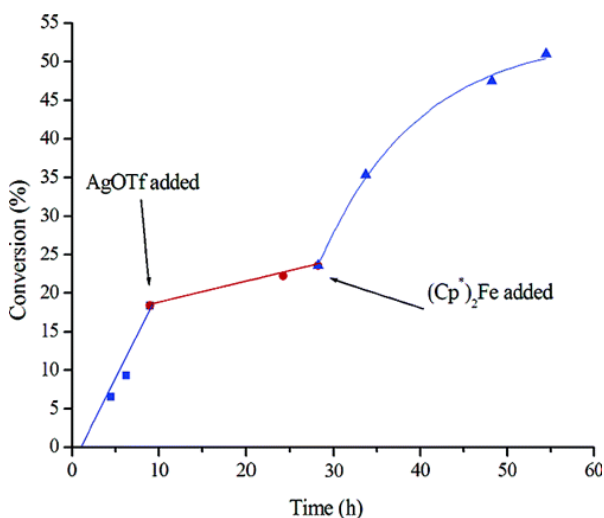
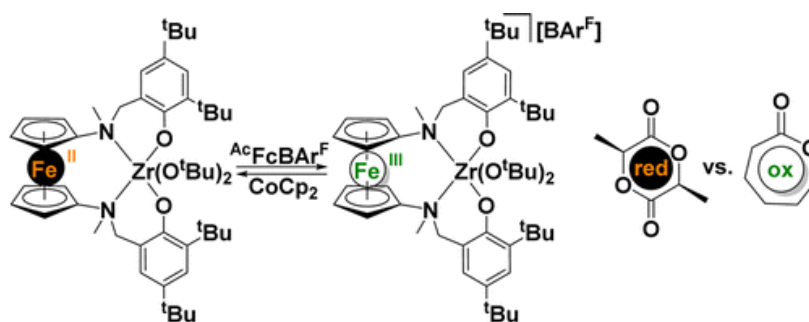


Figure 4.2 Plot of percent conversion versus time for Gibson's titanium-based salen catalyst. The reduced species (blue) and the oxidized species (red) display varying polymerization rates during the *in situ* polymerization switch. "Reprinted with permission from (*J. Am. Chem. Soc.*, **2006**, *128* (23), pp 7410–7411). Copyright (2006) American Chemical Society."⁷²

In 2014, Diaconescu and coworkers synthesized a zirconium-based salfan (salfan = (1,1'-di(2,4-di-*tert*-butyl-6-*N*-methylmethylenephenol)ferrocene)) catalyst that contained a single ferrocenyl moiety much closer to the active metal polymerization center.⁷³ The zirconium-based precatalyst showed reversible redox potential due to the ferrocenyl backbone within the ligand, and the Fe^{II} component was easily oxidized to the Fe^{III} species

with acetyl ferrocenium tetrakis[3,5-bis(trifluoromethyl)phenyl]borate ($\text{AcFcBAR}^{\text{F}}$) and rereduced with cobaltocene (CoCp_2) back to the Fe^{II} complex (**Scheme 4.2**). During their studies, they found that the reduced complex was highly reactive toward the polymerization of L-lactide while the oxidized version was virtually nonreactive toward the polymerization of L-lactide (**Figure 4.3** left). In contrast, the oxidized species was highly reactive toward a different cyclic ester monomer, ϵ -caprolactone, while the reduced catalytic complex did not display polymerization activity for ϵ -caprolactone (**Figure 4.3** right). Therefore, depending on the redox state of the salfan-based catalyst, selective polymerization of cyclic ester monomers to form block copolymers were possible via in situ redox switching with the addition of chemical redox agents.

All of the redox-switchable polymerization catalysts mentioned in this chapter contain a ferrocenyl moiety within the ligand portion of the catalyst;^{72,73} however, other redox-switchable catalysts have been synthesized for the polymerization of lactide where the redox switch occurs at the active polymerization site.^{74,80} For example, Byers and coworkers synthesized a catalyst that contained iron as the active center for polymerization,⁷⁴ so the redox switch occurred at the active metal center unlike the other catalysts previously discussed. Their findings showed that the Fe^{II} species was extremely active toward the polymerization of L-lactide while the Fe^{III} complex was virtually inactive for polymerization, which was true for all the redox active catalysts to date that contain iron. (**Figure 4.4**).



Scheme 4.2 Zirconium-based redox-switchable catalyst containing a ferrocenyl moiety close to the active metal center. The catalyst was oxidized from the Fe^{II} species to the Fe^{III} species using $\text{AcFcBAR}^{\text{F}}$ and rereduced using CoCp_2 . "Reprinted with permission from (*J. Am. Chem. Soc.*, **2014**, *136* (32), pp 11264–11267). Copyright (2014) American Chemical Society."⁷³

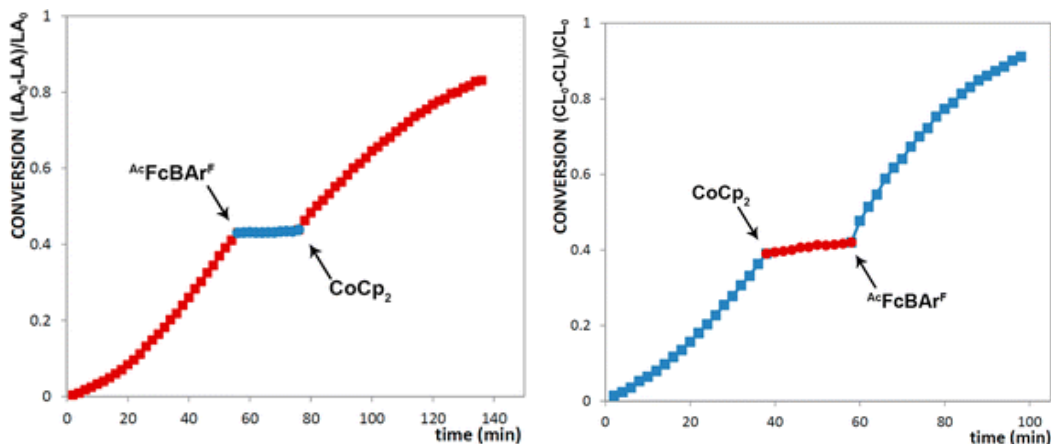


Figure 4.3 (left) Plot of L-lactide conversion versus time using the zirconium salfan catalyst. The reduced species (red) was active for polymerization while the oxidized complex (blue) was inactive for polymerization of L-lactide. (right) Plot of ϵ -caprolactone conversion versus time mediated by a zirconium salfan catalyst. The oxidized species (blue) was active for ϵ -caprolactone polymerization while the reduced complex was inactive for ϵ -caprolactone polymerization. "Adapted with permission from (*J. Am. Chem. Soc.*, **2014**, *136* (32), pp 11264–11267). Copyright (2014) American Chemical Society."⁷³

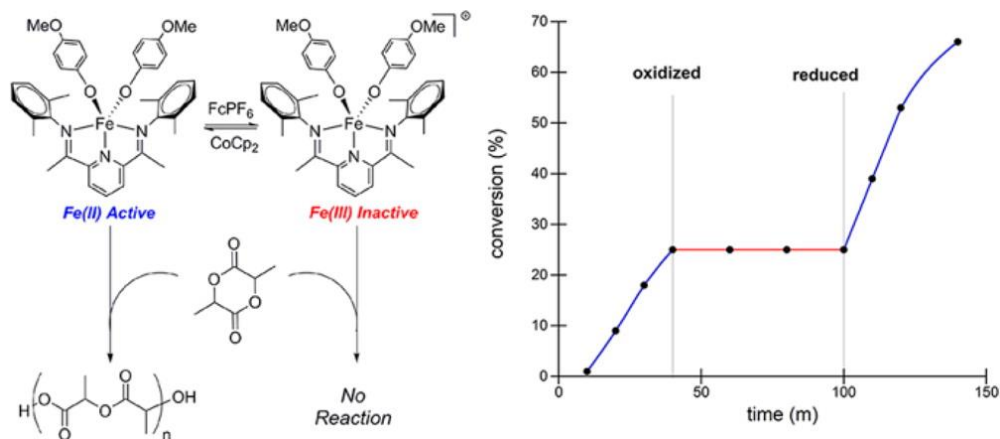


Figure 4.4 (left) Fe-based catalyst oxidized to the Fe^{III} species with ferrocenium hexafluorophosphate (FcPF₆) and rereduced to the Fe^{II} version with CoCp₂. (right) A plot of percent lactide conversion versus time with the reduced species (blue) and the inactive, oxidized species (red). The catalyst is "Reprinted with permission from (*J. Am. Chem. Soc.*, **2013**, *135* (44), pp 16553–16560). Copyright (2013) American Chemical Society."⁷⁴

Therefore, the redox events can take place within the ligand scaffold or at the polymerization site while still altering the electrophilicity of the active metal center, which alters the polymerization behavior.

While there have been several accomplishments in the realm of redox-switchable polymerization catalysis, there have been no fundamental studies as to which properties of catalyst design affect the polymerization rate and monomer selectivity. Therefore, the next portion of my dissertation will detail how our research group designed studies revolving around ligand design and how to determine which properties afford optimal control for redox switchable polymerization catalysis. Specifically, we will design catalysts to determine how the location of the redox switchable moiety to the active metal site affects polymerization activity along with tuning the redox innocent functionality located within the ligand scaffold in an effort to identify which factors contribute most to controlling redox switchable polymerizations (RSP).

4.4 Research Objectives

The overall objective for this portion of the dissertation is to describe fundamental studies that guide the development of redox active catalysts and illuminate their effect on the polymerization of L-lactide. In particular, we will monitor the oxidation and reduction environment of the catalytic species, the proximity of the redox active moiety to the active metal center, and the variation of the innocent moieties contained within the organic ligand portion of the catalyst. The scope of this project includes:

- I. Design and synthesis of redox active ligands;
- II. Synthesis of catalysts using a group 4 metals;
- III. Characterization of ligands and catalysts using NMR spectroscopy, cyclic voltammetry, single-crystal X-ray diffraction; and
- IV. Polymerization studies of L-lactide using NMR spectroscopy and gel permeation chromatography.

Though the synthesis of bioplastics, like PLA, provide a motivational aspect for this project, it is highlighted that the main purpose of this research described in the following chapters revolve around the development of redox switchable ligands and catalyst design

and their effect on polymerization behavior of cyclic esters, namely L-lactide. The results from this portion of the dissertation will provide insight into the fundamental design of redox-switchable polymerization catalysts for the possibility to create advanced PLA materials. Specifically, we will work to identify the effect of ligand design on the polymerization of L-lactide with a group 4 metal complexes that include redox active functionality within the ligand portion of the catalyst (**Figure 4.5**)

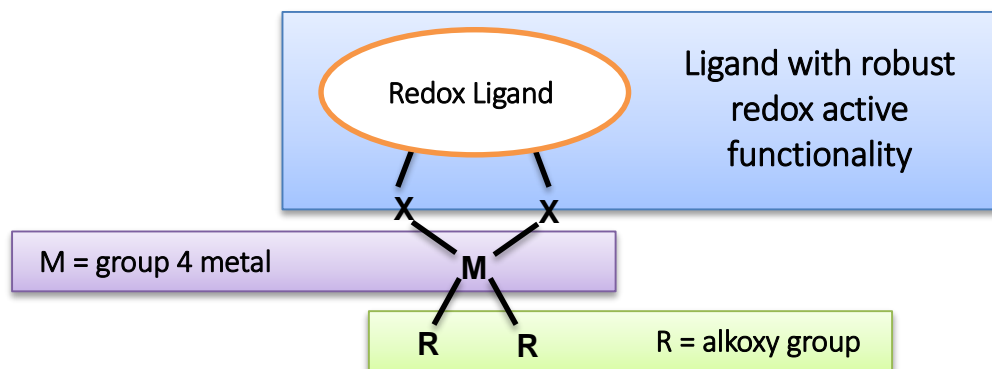


Figure 4.5 Representation of the catalysts designed in Chapters 5 and 6 that contain a redox active moiety within the ligand scaffold, a group 4 metal, which is active for L-lactide polymerization, and labile alkoxide ligands, which will become the end-groups of the polymer chain.

In Chapter 5, a new titanium-based catalyst containing a redox active ferrocenyl moiety in the ligand backbone was synthesized and studied to examine the effect of the redox active moiety placement in relation to the active metal center and how this effects the polymerization of L-lactide. The catalyst discussed in this chapter can not only alter the polymerization depending on its electronic state, but it also can drastically alter the polymerization given the oxidation environment of the catalyst, specifically if monomer is present or absent during the oxidation.

In Chapter 6, a summary of the dissertation work described in Chapters 1-5 will be provided along with a future outlook for redox active polymerization catalysis project. Chapter 6 will also include preliminary data for a proposed fundamental redox-switchable catalyst study.

Lastly, presentation of data that is subsidiary to the defined goals and discussion for the research discussed in Chapters 5 and 6, like descriptive experimental procedures, gel permeation chromatography, and X-ray crystallography data, are located in Appendix C. References are all chapters are located after Chapter 6.

Chapter 5– REDOX ACTIVE TITANIUM (IV)
SALFEN CATALYST FOR L-LACTIDE
POLYMERIZATIONS

A version of this chapter was originally published by Lauren A. Brown, Jennifer L. Rhinehart and Brian K. Long in the peer-reviewed publication:

Lauren A. Brown, Jennifer L. Rhinehart, Brian K. Long. "Effects of Ferrocenyl Proximity and Monomer Presence during Oxidation for the Redox-Switchable Polymerization of L-Lactide." *ACS Catalysis*. **2015** 5 (10), 6057-6060, DOI: 10.1021/acscatal.5b01434

I performed the catalyst synthesis and characterization addressed in the work. I also performed all the polymerizations described and discussed within this chapter and the manuscript. Dr. Jennifer Rhinehart performed some preliminary work, and Dr. Brian Long advised the work.

5.1 Abstract

A titanium (IV) salen catalyst bearing a redox-active ferrocenyl center in close proximity to the active metal site was examined for the redox-switchable polymerization of L-lactide. The catalyst displayed an atypical β -*cis* geometry in both the solid- and solution-states, and placement of the redox-active moiety in close proximity to the active metal site was shown to provide an enhancement in catalytic "on-off-on" switching behavior when the redox events were performed in the presence of lactide monomer. More importantly, when comparing oxidized and reduced catalytic species, completely contrasting trends in polymerization behavior were observed depending on whether the catalyst was oxidized in the absence or in the presence of lactide monomer. On the basis of NMR spectroscopic analysis, we propose that this unusual behavior is a result of a rapid switch in ligand coordination geometry that is facilitated by monomer coordination prior to any redox reactions. Additionally, when redox reactions were conducted in the absence of monomer, a trend in activity that contradicted those of all previously reported Ti-based redox-active catalysts was observed.

5.2 Introduction

Redox-switchable catalysis (RSC) offers a unique method by which the reactivity or selectivity of a catalytic process may be altered via modulations in the oxidation state of the

active transition-metal site or its surrounding ligands.⁸² This concept was first reported in 1995 by Wrighton and coworkers, who demonstrated that the reduced form of a diphosphinocobaltocene stabilized rhodium complex showed greater activity for the transfer hydrogenation of olefins than its oxidized analogue.⁷⁵ This difference in catalytic behavior was attributed to changes in the electron density at the active metal site as a function of ligand oxidation state and has since spawned a thriving area of research⁸²⁻⁸⁵ that has even expanded its impact to several popular polymerization methodologies, such as ring-opening polymerizations and controlled radical polymerizations.^{72-74,79,86-88}

To date, the majority of reported redox-switchable polymerizations (RSP)s have utilized single-site catalysts bearing redox-active ligands to achieve this "switch" in catalytic behavior, such as those containing ferrocenyl moieties.^{72,73,79} However, a subset of reports have shown similar results can be observed when the active transition-metal site is itself oxidized or reduced, as has been reported for certain cerium- and iron-based catalysts.^{74,80,88} A prominent example in which redox-active ligand was used to facilitate RSP was reported by Gibson and co-workers in which a catalyst (**4**) bearing two ferrocenyl moieties located on the outer extremities of the ligand scaffold was used.⁷² In that report, it was shown that the reduced form of catalyst **4** polymerized lactide at a significantly greater rate than its oxidized counterpart, an observation that was again attributed to changes in electron density at the active metal site. This observation in which the more electron-rich catalytic species displays an enhanced polymerization rate for the ring-opening polymerization of cyclic esters (as compared to their electron-deficient counterparts) is true for all early transition-metal-based catalysts bearing salen-like ligands.^{72,73,76} In contrast, initiators containing main-group metals, such as aluminum^{77,89-93} and indium,⁷⁹ typically exhibit the opposite behavior in which catalysts bearing electron-deficient ligands typically display the highest activity for the polymerization of lactide.

It is important to note that the RSCs previously studied for lactide polymerization all contain labile alkoxide ligands in addition to the ligand that contains the redox active functionality. These alkoxide ligands aid in the initiation of the monomer and become an end-group of the polymer chain (**Figure 5.1**). By attaching these alkoxide ligands to the active metal center, it eliminates the need for addition of an external initiator, like alcohols or phenols, which have also been used to aid in the initiation of the lactide polymerization.⁷⁰ The

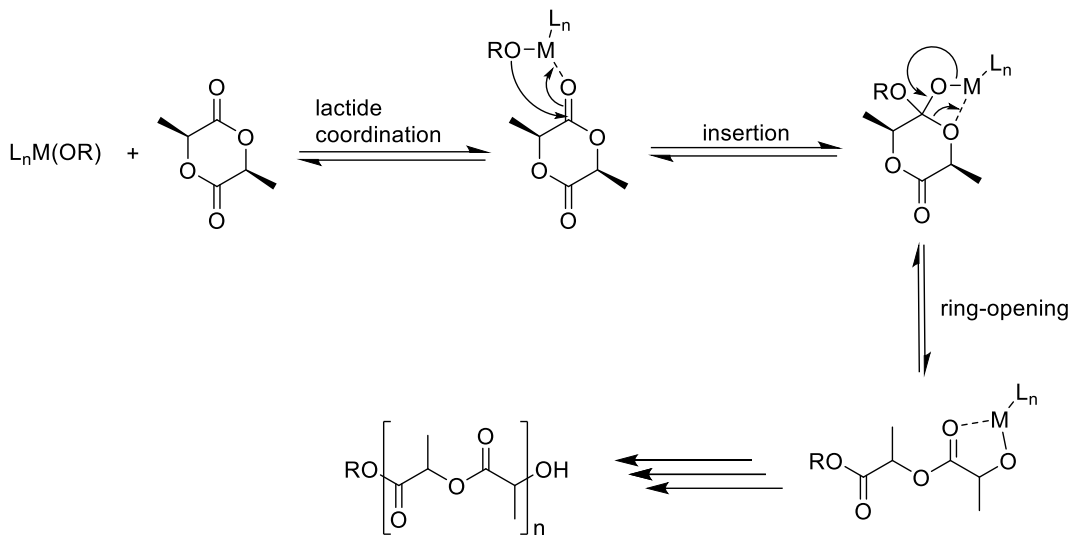


Figure 5.1 Coordination-insertion mechanism for the polymerization of L-lactide.

addition of these external initiators could lead to complications for the subsequent redox reactions performed for these catalysts; therefore, moving forward, our studies will focus on designing catalysts that contain both a redox active ligand and labile alkoxide ligands.

Given that these oscillations in catalytic behavior are directly attributed to changes in electron density at the propagating metal center, it can be surmised that the proximity of the redox-active moiety may play a significant role in the differentiation of reduced and oxidized catalytic species; however, to date, there have been no direct investigations into the effects that redox-active site proximity (to the active metal site) has on the RSP of cyclic esters. Because of the straightforward accessibility and broad success of salen-based catalysts for the polymerization of cyclic esters, we chose to synthesize and study catalyst **5** in an effort to observe the effects associated with moving the redox moiety from the ligand's outer extremities to a location proximal to the active titanium site (**Figure 5.2**). Herein, we report the synthesis and catalytic behavior of catalyst **5** for the RSP of L-lactide.

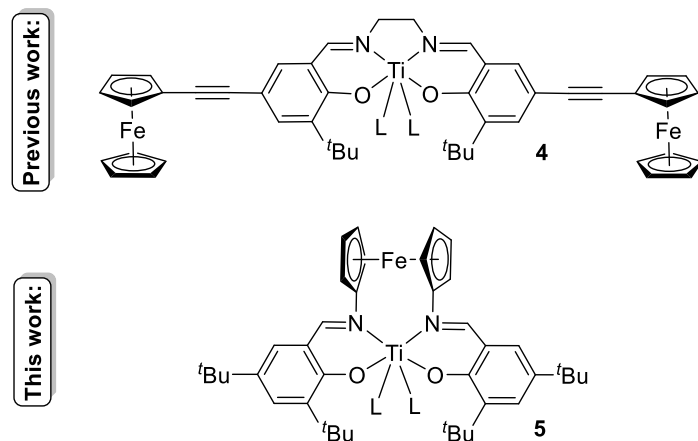
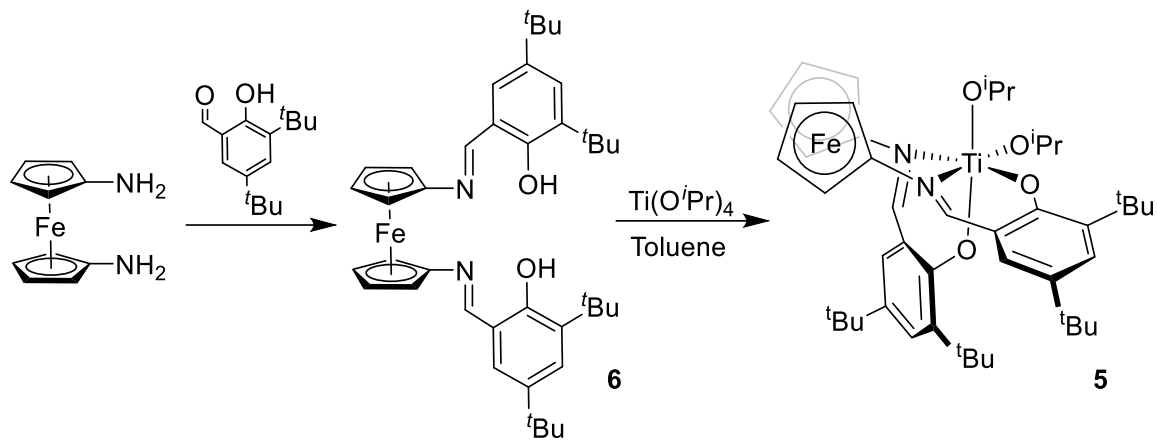


Figure 5.2 Comparison of catalysts bearing redox-active ferrocenyl moieties distal to the active metal site (**4**) and a ferrocenyl moiety proximal to the active metal center (**5**) ($L = O^iPr$).

5.3 Results and Discussion

The $H_2(\text{salfen})$ pro-ligand **6** was synthesized as previously reported⁹⁴ and metalated using $Ti(O^iPr)_4$ to yield catalyst **5** (**Scheme 5.1**). The metal complex was characterized using standard spectroscopic techniques and via solid-state, single-crystal X-ray diffraction in which suitable crystals were grown by slow evaporation of hexanes (**Figure 5.3**). As seen in **Figure 5.3**, catalyst **5** was found to adopt a distorted β -*cis* conformation in the solid state. 1H NMR spectroscopy confirmed that the catalyst's β -*cis* conformation is present in the solution state, as well, in which the asymmetry of the catalyst's β -*cis* conformation causes each proton on the aryl, imine, and isopropoxide moieties to be magnetically inequivalent. This observation is unique in that similar Ti-based catalysts, such as complex **4**, are known to adopt a *trans* configuration in both solid and solution state.^{76,95-98}



Scheme 5.1 Synthesis of redox-active catalyst 5.

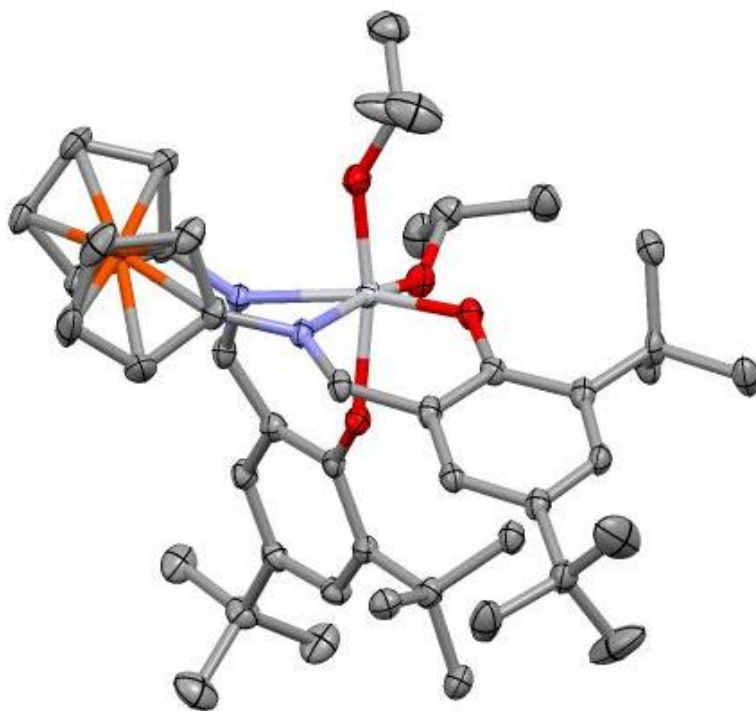


Figure 5.3 ORTEP representation of complex 5. Thermal-ellipsoids were drawn at 50% probability and all hydrogen atoms were omitted for clarity.

Cyclic voltammetry (CV) experiments were performed in DCM with $[n\text{Bu}_4\text{N}][\text{PF}_6]$ (0.2 M) as an electrolyte and scanned at a rate of 50 mV/s, which revealed that catalyst **5** had a redox half-wave potential ($E_{1/2}$) of -0.085 V versus Fc/Fc⁺ (**Figure 5.4**). From this value, silver triflate and decamethylferrocene were initially chosen as suitable oxidizing and reducing agents, respectively; however, these compounds were found to complicate our investigations, often requiring filtration to remove problematic Ag particulates after oxidation reactions. To avoid these issues, for all subsequent studies (**Scheme 5.2**), we utilized acetylferrocenium tetrakis(3,5-bis(trifluoromethyl)phenyl) borate (^{Ac}FcBAR^F) and cobaltocene (CoCp₂) as redox agents, both of which have been successfully used in other RSC reports.⁷³

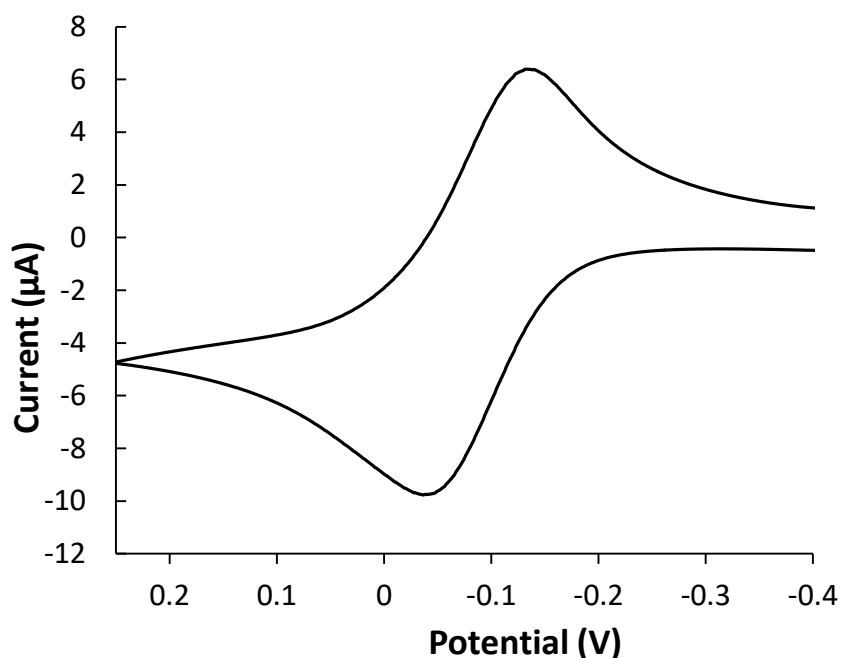
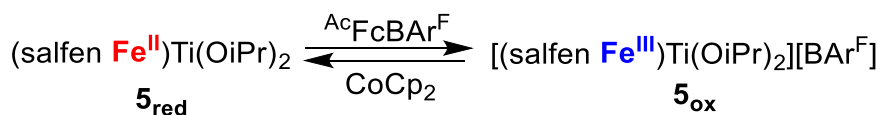


Figure 5.4 Cyclic voltammogram of catalyst **5** (0.01 mmol) recorded at a scan rate of 50 mV/s in dichloromethane (5 mL), $(n\text{Bu})_4\text{NPF}_6$ (0.20 M), ($E_{1/2} = -0.085$ V) versus Fc/Fc⁺.



Scheme 5.2 Redox-switch between catalysts **5_{red}** and **5_{ox}**.

Polymerizations of L-lactide were performed at 90 °C in either benzene- d_6 or toluene and were monitored via variable temperature NMR. A plot of monomer conversion versus time is shown in **Figure 5.5**, in which the reduced catalyst 5_{red} demonstrates a dramatically slower rate of polymerization compared with that of oxidized catalyst 5_{ox} (note: catalyst 5_{red} was oxidized using $^{\text{Ac}}\text{FcBAR}^{\text{F}}$ prior to monomer addition) reaching only 2% conversion in 3.5 h, as compared to over 50% conversion when using catalyst 5_{ox} in that same amount of time. This indicated that the more electron-deficient catalyst 5_{ox} polymerized lactide at a much greater rate than the more electron-rich catalyst 5_{red} , representing a completely opposite trend in catalytic activity as compared with catalyst **4**. Extended polymerization times up to 8 h show that catalyst 5_{ox} readily exceeds 90% conversion of monomer to polymer, whereas catalyst 5_{red} only reaches ~10% conversion to polymer. The reactivity of catalyst 5_{red} is remarkably low when compared to similar Ti-based initiators, such as **4**, and although further studies must be conducted, we postulate that this contradictory trend in catalytic activity may be related to the unusual β -*cis* conformation adopted by 5_{red} . It should also be noted that

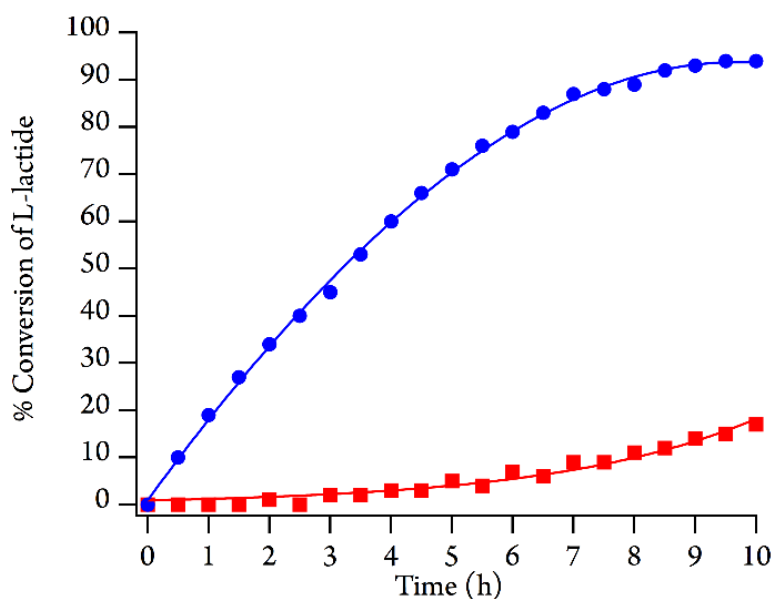


Figure 5.5 Plot of conversion versus time for the polymerization of L-lactide (100 equiv, 1 M) in C_6D_6 at 90 °C using catalyst 5_{red} (red squares) or 5_{ox} (blue circles) (NOTE: the oxidation of catalyst $5_{\text{red}} \rightarrow 5_{\text{ox}}$ was performed prior to monomer addition).

similarly low polymerization activities have been reported for related Ti-salen-based catalysts that are believed to also adopt a β -*cis* conformation.^{76,95-98}

To examine the redox-switching ability of catalyst **5**, polymerizations were conducted in which the catalyst oxidation state was modulated *in situ* via addition of $\text{AcFcBAR}^{\text{F}}$ and CoCp_2 respectively (**Figure 5.6**). In this experiment, reduced catalyst $\mathbf{5}_{\text{red}}$ was added to 100 equiv of monomer and heated to 90 °C. ^1H NMR analysis showed virtually no monomer conversion to polymer after 3 h (time-period (A), **Figure 5.6**), as was predicted by the results in **Figure 5.5**. However, upon addition of $\text{AcFcBAR}^{\text{F}}$ to oxidize the ferrocenyl moiety, the polymerization rate increased quickly as predicted, yet subsided after reaching only ~4-6% conversion (time-period (B), **Figure 5.6**). Even more remarkably, when the oxidized catalyst was re-reduced using CoCp_2 , the catalyst began to polymerize L-lactide at an even greater rate (time-period (C), **Figure 5.6**). This unexpected behavior is in complete contrast to the polymerization behavior previously observed in **Figure 5.5** for catalyst $\mathbf{5}_{\text{red}}$. Furthermore,

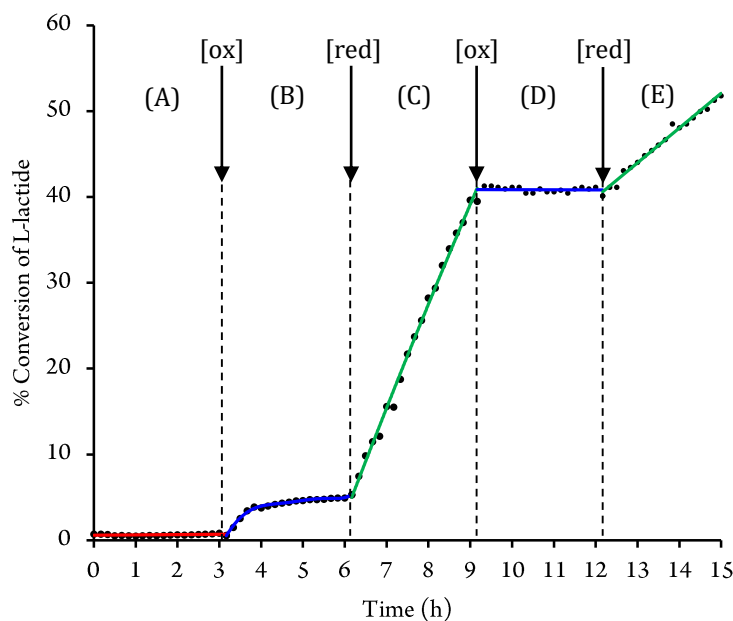


Figure 5.6 Plot of conversion versus time for the polymerization of L-lactide (100 equiv, 1 M) in C_6D_6 at 90 °C with *in situ* redox-switching, starting with catalyst **5**. Times at which oxidant ([ox] = $\text{AcFcBAR}^{\text{F}}$, 1 eq.) or reductant ([red] = CoCp_2 , 1 eq.) were added are denoted at the top, and time-periods between additions are labeled as (A), (B), (C), (D), and (E).

subsequent oxidation of this catalyst showed that virtually all polymerization activity was arrested (time-period (D), **Figure 5.6**), and after rereduction, once again proceeded at a high relative rate (time-period (E), **Figure 5.6**).

Although the results obtained in time-periods (C), (D), and (E) demonstrate that placing the redox-active ferrocenyl moiety in close proximity to the active metal site (**5_{red}**) yields an enhanced "on-off-on" switch in catalytic activity when compared to catalyst **4**, its unexpected behavior in time-periods (B) and (C) required further investigation. After careful analysis and multiple reproductions of the kinetic experiments found in **Figure 5.5** and the *in situ* switching experiments shown in **Figure 5.6**, we hypothesized that the rates of polymerization may actually be dependent upon the chemical species present during the oxidation and reduction reactions. Specifically, we noted that for the initial lactide polymerizations represented in **Figure 5.5**, catalyst **5_{red}** was oxidized using ^{Ac}FcBAR^F (in the absence of monomer) and then added to a monomer containing solution to observe its rate of polymerization. In contrast, the catalyst oxidation and reduction reactions for the *in situ* switching trials (**Figure 5.6**) were performed in the presence of excess lactide.

To support our hypothesis, polymerization trials were conducted in which the Ti-based catalyst **5_{red}** was oxidized in the presence of excess L-lactide, thereby mimicking an environment similar to what would be encountered in actual redox-switching experiments (such as those shown in **Figure 5.6**). Those results (**Figure 5.7**) indicated that when catalyst **5_{red}** is oxidized in the presence of excess L-lactide in solution, there is a rapid conversion of monomer to polymer, reaching ~4-6% conversion but then becoming virtually inactive in reactions extending up to and beyond 10 h. This result was extremely encouraging because all of our *in situ* switching experiments have shown similar behaviors in which monomer conversion essentially stops after ~4-6% lactide conversion is reached. Subsequently, when this oxidized species is rereduced using CoCp₂, once again in the presence of excess monomer, the reduced species shows dramatically increased polymerization activity, reaching over 80% conversion in only 5 h for NMR scale polymerizations (**Figure 5.7**, green triangles). Larger scale polymerizations were also performed using catalyst **5_{red}**, which was rereduced in the presence of monomer; those results are shown in **Table 5.1**. From these results, it is clear that the activity of the oxidized and reduced analogs of this Ti-based catalyst differs

Table 5.1 Polymerization Data for Catalyst **5_{red}** after Rereduction in the Presence of Monomer^a

entry	time (h)	L-lactide: 2_{red} ^a	conv ^b (%)	<i>M_n</i> ^c (g/mol)	<i>M_n</i> ^d (theor)	<i>D</i> ^c
1	6	100:1	55	6900	4000	1.11
2	12	100:1	71	7800	5100	1.15
3	18	100:1	85	12100	6100	1.28
4	24	100:1	84	11500	6100	1.20
5	24	50:1	89	7600	3200	1.69
6	24	200:1	69	13300	9900	1.20

^aPolymerization conditions: catalyst **5_{red}** was obtained after subsequent oxidation (**5_{ox}**) and reduction (**5_{red}**) in the presence of L-lactide, [monomer] = 1.0 mmol, 2 mL of toluene, 90 °C. ^bConversion was determined using ¹H NMR at 70 °C. ^cDetermined using gel permeation chromatography at 40 °C in THF. ^dTheoretical *M_n*'s were calculated on the basis of conversion and assuming dual propagating chains.

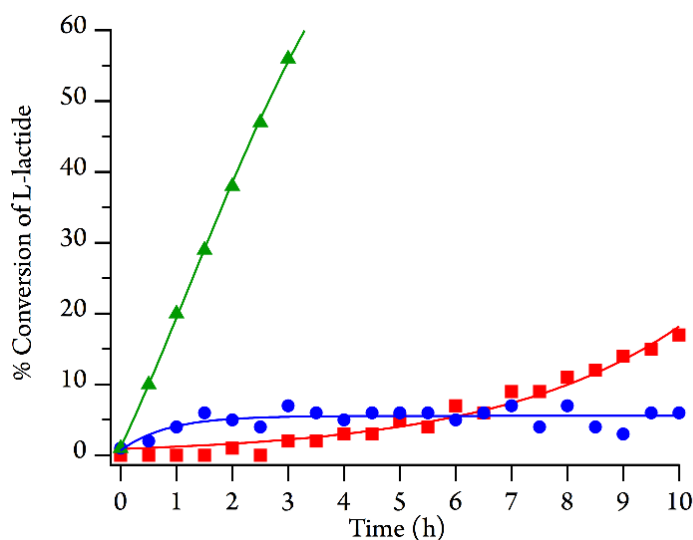


Figure 5.7 Plot of conversion versus time for the polymerization of L-lactide (100 equiv, 1 M) in C₆D₆ at 90 °C using catalyst **5_{red}** (red squares), oxidized catalyst **5_{ox}** (blue circles), and rereduced catalyst **5_{red}** (green triangles) (NOTE: oxidation of catalyst **5_{red}** → **5_{ox}**, and its rereduction from **5_{ox}** → **5_{red}**, were performed in the presence of lactide monomer).

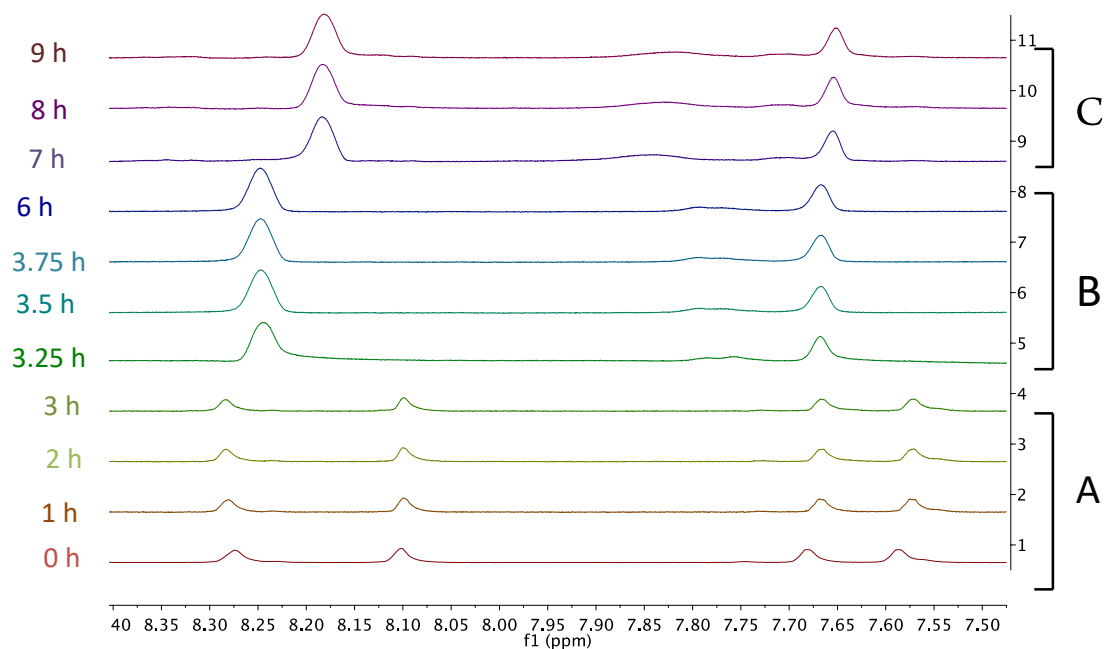


Figure 5.8 ^1H NMR spectra (400 MHz, 90 °C, C_6D_6) highlighting the imino and aryl proton region of catalyst **5** (for protons highlighted in blue and red in **Figure 5.10**) during an L-lactide polymerization *in situ* redox switch. Spectra 1-4 corresponds to catalyst **5_{red}** during time period A, **Figure 5.6** spectra 5-8 represents catalyst **5_{ox}** during time period B, **Figure 5.6**, and spectra 8-10 is represents re-reduced catalyst **5_{red}** during time period C, **Figure 5.6**.

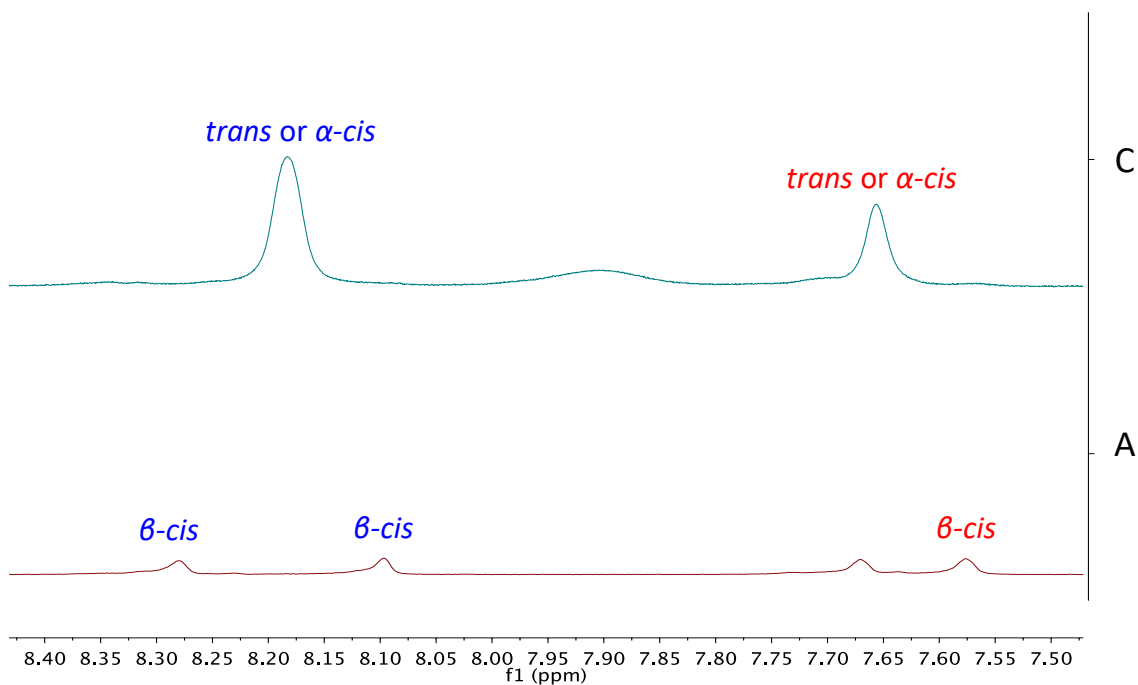


Figure 5.9 ¹H NMR spectra (400 MHz, 90 °C, C₆D₆) highlighting the imino and aryl proton region of catalyst **5** (for protons highlighted in blue and red in **Figure 5.10**) during an L-lactide polymerization in situ redox switch. The bottom trace corresponds to time period A, **Figure 5.6**. The top trace represents rereduced catalyst **5**_{red} during time period C, **Figure 5.6**.

radically, depending on whether the redox events occur in the presence or absence of L-lactide monomer.

Although further investigations are required to elucidate the source of this behavior, careful analysis of *in situ* polymerization, ^1H NMR spectra revealed that the rereduced catalyst **Figure 5.7**, green triangles) and the unperturbed catalyst 5_{red} (**Figure 5.7**, red squares) were structurally distinct from one another, as was evidenced by a change in aromatic and imine ^1H signals **Figure 5.8** and **Figure 5.9**). Likewise, CV experiments conducted in the presence of monomer showed that catalyst 5_{ox} exhibited a -0.087 V shift in the reduction potential when the catalyst was heated in the presence of monomer (**Figure 5.11**, **Figure 5.12**, and **Figure 5.13**). On the basis of these results, we propose that the observed change in catalytic behavior may be attributed to a switch in catalyst geometry from its original β -cis conformation, which shows four aromatic ^1H signals and two imine ^1H signals, to either an α -cis or trans geometry, both of which display only two aromatic signals and one imine ^1H NMR signal. The possible conformations for catalyst **5** can be seen in **Figure 5.10** We believe this geometry change is promoted in the presence of monomer during the *in situ* oxidation reaction, and although both the α -cis or *trans* geometries are plausible, the large number of previously reported catalysts adopt a *trans* configuration making it the most likely form.^{76,95-98} Several attempts were made to isolate the Fe(III) complex with 5 equiv of lactide; however, single crystals could not be obtained.

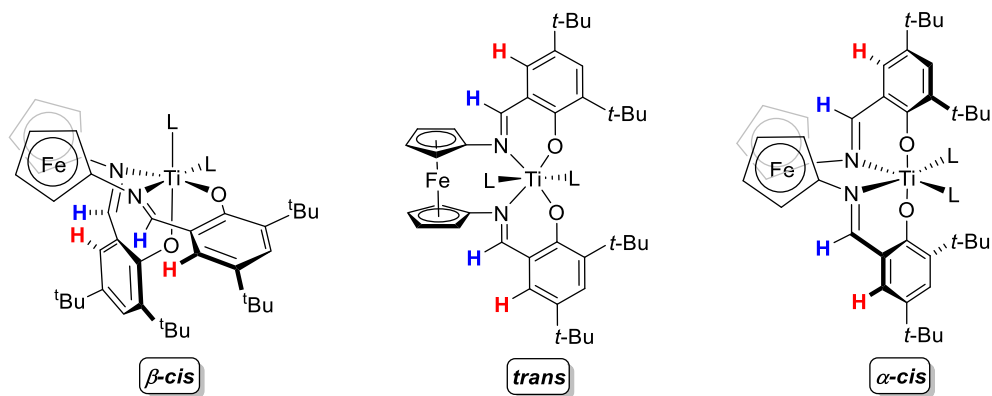


Figure 5.10 Possible conformations for catalyst **5**, L = OiPr.

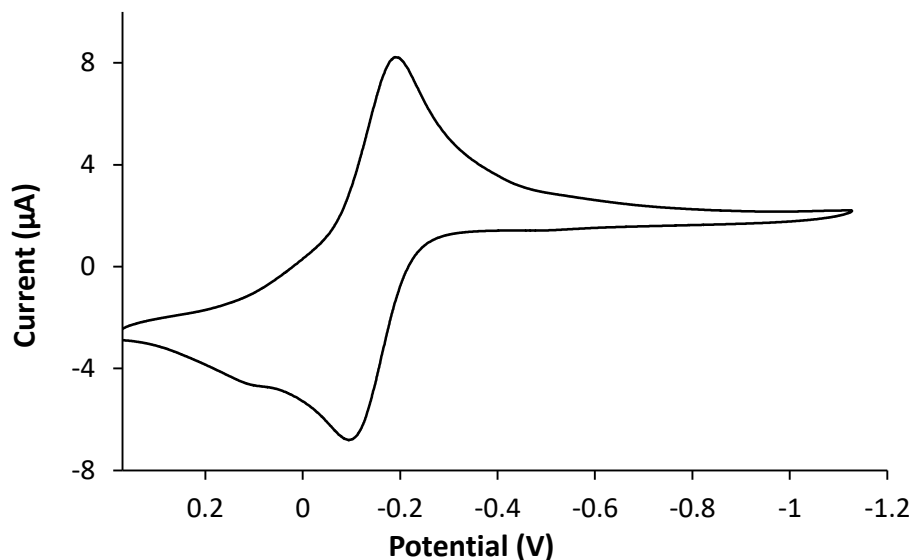


Figure 5.11 Cyclic voltammogram of catalyst **5_{ox}** (0.01 mmol) with L-lactide (5 equiv.) after heating for 15 minutes at 90 °C recorded at a scan rate of 50 mV/s in dichloromethane (5 mL), (*n*Bu)₄NPF₆ (0.20 M), ($E_{1/2} = -0.143$ V) versus Fc/Fc⁺. Catalyst **5** was oxidized with AgPF₆.

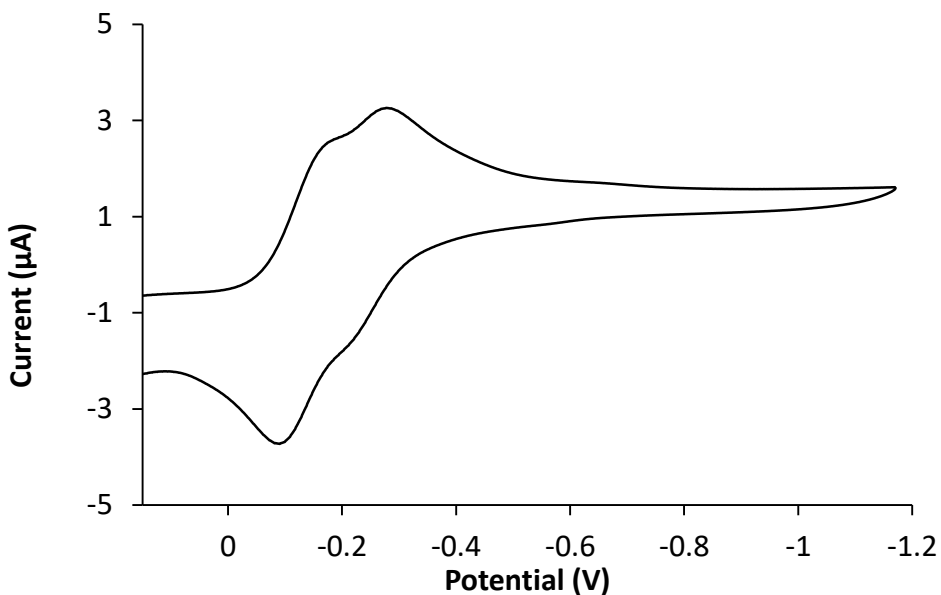


Figure 5.12 Cyclic voltammogram of catalyst **5_{ox}** (0.01 mmol) with L-lactide (5 equiv.) after heating for 15 minutes at 90 °C recorded at a scan rate of 50 mV/s in dichloromethane (5 mL), (*n*Bu)₄NPF₆ (0.20 M), ($E_{1/2} = -0.230$ V) versus Fc/Fc⁺. Catalyst **5** was oxidized with AgPF₆.

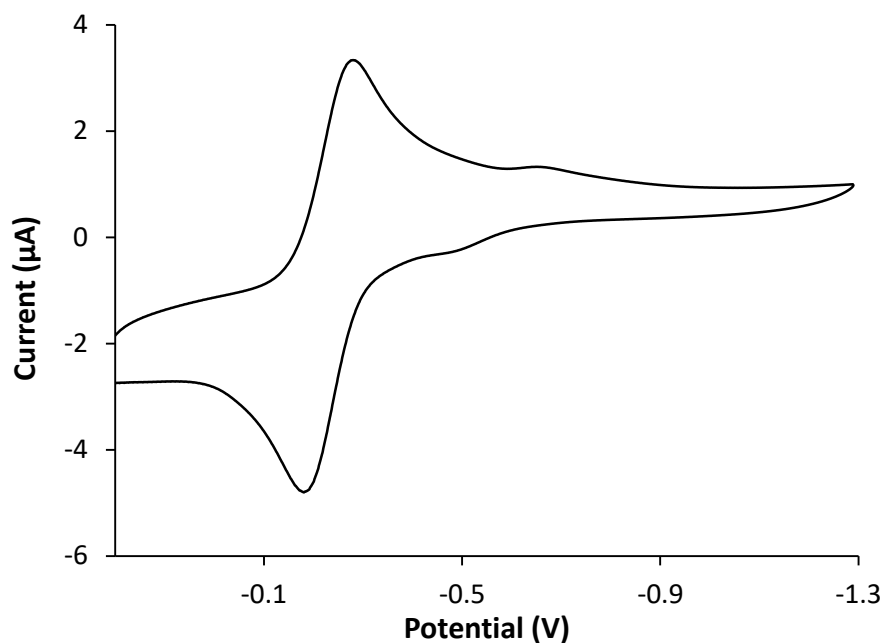


Figure 5.13 Cyclic voltammogram of catalyst 5_{ox} (0.01 mmol) with L-lactide (5 equiv.) after heating for 30 minutes at 90 °C recorded at a scan rate of 50 mV/s in dichloromethane (5 mL), $(nBu)_4NPF_6$ (0.20 M), ($E_{1/2} = -0.230$ V) versus Fc/Fc⁺. Catalyst **5** was oxidized with AgPF₆.

We also proceeded to study the activity of complex **5** for its catalytic activity after several oxidation and reduction reactions. Therefore, complex **5** was oxidized and reduced in the presence of monomer and then monitored for its polymerization activity (**Figure 5.14**). The monomer conversion had already reached approximately 15% given that the proposed geometry switch occurs in the presence of monomer at elevated temperature, which also initiates the polymerization. The polymerization was halted after 60 minutes with the addition of $^{Ac}FcBAR^F$ but heated at 90 °C monitored for 60 minutes until $CoCp_2$ was added to the reduced the catalyst and continue the polymerization (**Figure 5.14**). The natural log of monomer conversion was plotted as a function of time (**Figure 5.15**) in order to determine that the 5_{red} displays the same activity before and after oxidation and subsequent reduction reactions. The slopes of both kinetics data prior to the first switch and after the rereduction are equivalent; therefore, the catalyst does not undergo any deactivation pathways and can withstand multiple oxidation and reductions reactions.

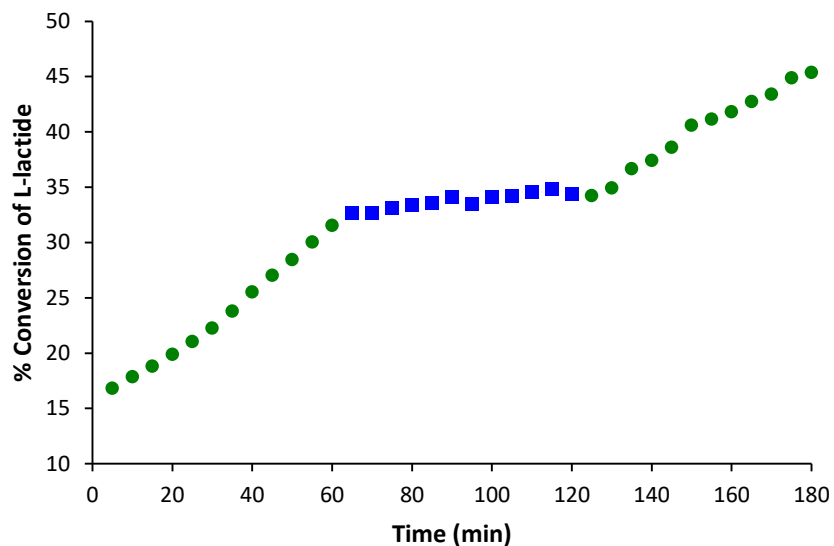


Figure 5.14 *In situ* switching polymerization of 100 equivalents of L-lactide in C_6D_6 at 90 °C starting from rereduced catalyst 5_{red} and switching at 1 h increments (green circles = 5_{red} and blue squares = 5_{ox}).

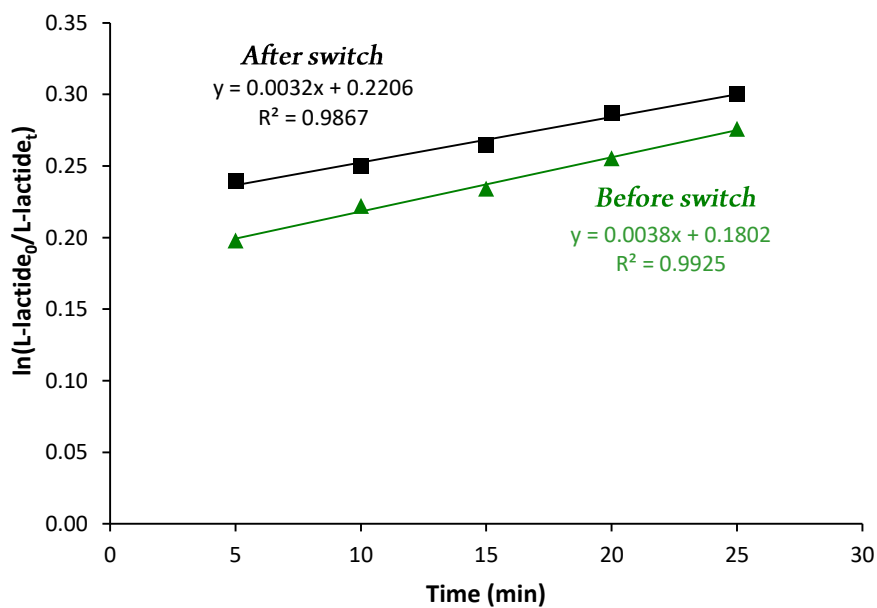


Figure 5.15 Plot of $\ln(L\text{-lactide}_0/L\text{-lactide}_t)$ versus time to study the polymerization kinetics before (green triangles) and after switch (black squares).

5.4 Conclusions

In summary, we have synthesized a new redox-active, Ti-based salfen catalyst and investigated its behavior for the RSP of L-lactide. Initial polymerizations in which catalyst **5_{red}** was oxidized in the absence of monomer showed that the oxidized catalyst **5_{ox}** proceeded at a significantly faster rate than its reduced analogue **5_{red}**, which contradicts all other reported group 4 catalysts for RSP. In contrast, when the oxidation and reduction reactions were carried out in the presence of monomer, polymerization activity was completely reversed in which the reduced species polymerized L-lactide at a much greater rate than the oxidized version.

Although the catalytic ring-opening polymerization behavior of catalysts **5_{red}** and **5_{ox}** has proven to be quite complex, requiring further investigations to elucidate the source or sources of this behavior, our results demonstrate that positioning the redox-active ferrocenyl moiety in close proximity to the active transition-metal site (**5_{red}**) produced an enhanced "on-off-on" switch (**Figure 5.6**, time periods C, D, and E) in polymerization activity when compared to catalyst **4**. Second, and more importantly, we have demonstrated that the activity of catalysts **5_{red}** and **5_{ox}** are not only dependent on the redox state of the ligand but are also dependent on the chemical species present during their *in situ* oxidation and reduction reactions. The source of this unusual behavior must be investigated further; however, these results serve as direct evidence that monomer presence and redox-active moiety placement within the ligand scaffold must be considered during redox-switching studies.

5.5 Experimental

5.5.1 General Materials and Methods

All experiments were performed under a dry nitrogen atmosphere using standard Schlenk techniques or MBraun inert-gas glove box. Solvents were purified using a two-column solid-state purification system and transferred to the glove box without exposure to air. NMR solvents were purchased from Cambridge Isotope Laboratories, dried over activated molecular sieves, and degassed prior to use. ¹H and ¹³C NMR spectra were recorded on a Varian 300 or Bruker 400 MHz spectrometer. Chemical shifts are reported with respect

to solvent residual peaks, 7.16 ppm (C_6D_6). Cobaltocene, acetyl ferrocene, bis(pentamethylcyclopentadienyl)iron, and silver triflate were purchased from Strem Chemicals and used without further purification. $NaBAR^F$, iron (III) chloride hexahydrate, and titanium(IV) isopropoxide ($Ti(O^iPr)_4$) were purchased from Fisher Scientific and used as received. 3,5-di-tert-butylsalicylaldehyde was purchased from Advanced Asymmetrics and used as received. L-lactide was purchased from Fisher Scientific and recrystallized twice in toluene prior to use. $^{Ac}FcBAR^F$ and ligand **6** were synthesized following previously reported procedures.^{94,99} Elemental microanalyses were carried out by Atlantic Microlab, Inc. (Norcross, GA). X-ray diffraction measurements were performed on single crystals using a Bruker APEX diffractometer. Cyclic voltammetry measurements were performed on a CH Instruments potentiostat using 0.01 mmol of compound **5** in 5 ml DCM solution (0.002 M) with supporting electrolyte 0.2 M $(nBu)_4NPF_6$, using Ag/AgCl as the reference electrode, a gold working electrode, and a tungsten counter electrode at a scan rate of $50\text{ mV}\cdot\text{s}^{-1}$. All potentials are given with respect to the ferrocene-ferrocenium redox couple. Molecular weights (M_n) of the polymers were determined using a Tosoh EcoSEC GPC at $40\text{ }^\circ\text{C}$ in THF and referenced to polystyrene standards.

5.5.2 Synthesis of (salfen)Ti(OⁱPr)₂ (**5_{red}**)

To a toluene solution (10 mL) of **6** (1.00 g, 1.54 mmol) at $-30\text{ }^\circ\text{C}$, $Ti(O^iPr)_4$ (0.46 mL, 1.54 mmol) was added dropwise, and the resulting mixture was stirred for 2 hours. The reaction mixture was warmed to ambient temperature and stirred for an additional 12 hours. The volatiles were removed under reduced pressure, yielding the product as a red crystalline solid. Yield: 940.0 mg, 75%. Crystals suitable for X-ray crystallography were obtained from slowly evaporating a saturated hexanes solution at ambient temperature. 1H NMR (300 MHz, $25\text{ }^\circ\text{C}$, C_6D_6), δ , ppm: 0.30-2.11 (48H), 3.78 (br, 1H), 3.84 (br, 1H), 3.87 (br, 1H), 4.00 (br, 1H), 4.01 (br, 1H), 4.19 (br, 1H), 4.47 (br, 1H), 6.04 (br, 1H), 7.05 (d, 1H), 7.15 (d, 1H), 7.63 (d, 1H), 7.73 (d, 1H), 8.10 (s, 1H), 8.23 (s, 1H). ^{13}C NMR (300 MHz, $25\text{ }^\circ\text{C}$, C_6D_6), δ , ppm: 25.65, 25.93, 27.14, 27.19, 30.62, 30.86, 32.07, 32.09, 34.57, 34.62, 35.58, 36.06, 63.98, 65.68, 67.19, 68.07, 68.53, 69.09, 70.69, 71.05, 77.43, 80.99, 108.98, 112.68, 124.06, 124.42, 127.42, 129.46, 129.59, 129.97, 137.76, 138.38, 139.45, 139.60, 161.02, 163.64, 166.81, 171.66. Elemental

analysis for $C_{46}H_{64}FeN_2O_4Ti$ (812.74 g/mol): Calc'd: 67.98% C, 7.94% H, 3.45% N; Found: 67.75% C, 8.04% H, 3.55% N.

5.5.3 General Procedure for NMR Scale Polymerizations

C.5.3.1 Oxidation/reduction of 5 in the absence of L-lactide

In a glove box, L-lactide (0.7 mmol or 0.35 mmol) was added to a J. Young NMR tube. In a separate vial, catalyst **5**_{red} (0.007 mmol) was added to C_6D_6 (0.7 mL). As appropriate, $CoCp_2$ and/or $AcFcBAR^F$ (0.007 mmol) were added to **5**, and the mixture was shaken and transferred to the J. Young NMR tube containing the monomer equipped with a Teflon valve. The NMR tube was removed from the glove box, and the polymerization was monitored by 1H NMR spectroscopy for up to 24 hours by placing the sample in a preheated Bruker Avance 400 MHz NMR at either 70 °C or 90 °C. The command “multizg” was used to collect data every 10 or 30 minutes. The data was processed with XWinNMR3.6. Conversion of L-lactide was monitored by comparing the methine peak of the monomer to the methine peak of the polymer.

C.5.3.2 Oxidation/reduction of 5 in the presence of L-lactide

In a glove box, L-lactide (0.7 mmol or 0.35 mmol), **5**_{red} (0.007 mmol), and C_6D_6 (0.7 mL) were added to a J. Young NMR tube equipped with a Teflon valve. As needed, $CoCp_2$ and/or $AcFcBAR^F$ (0.007 mmol) were added to the J. Young tube containing the monomer and complex **5**. The sealed tube was removed from the glove box, and the polymerization was monitored by 1H NMR spectroscopy for up to 24 hours by placing in a preheated Bruker Avance 400 MHz NMR at either 70 °C or 90 °C. The command “multizg” was used to collect data every 10 or 30 minutes. The data was processed with XWinNMR3.6. Conversion of L-lactide was monitored by comparing the methine peak of the monomer to the methine peak of the polymer.

5.5.4 In situ Switching Polymerization

In a glove box, L-lactide (0.7 mmol) was added to a J. Young NMR tube. To a separate 20 mL vial, **5**_{red} (0.007 mmol) was added to C_6D_6 (0.7 mL). The **5**_{red} solution was added to the monomer, and the J. Young tube was placed in a preheated (90 °C) Bruker Avance 400 MHz NMR. The polymerization was monitored by 1H NMR using the command “multizg”. $AcFcBAR^F$

or CoCp_2 (0.007 mmol) were sequentially added to the J. Young tube as prescribed (at 3 hour intervals up to 15 hours). The data was processed with XWinNMR3.6. Conversion of L-lactide was monitored by comparing the methine peak of the monomer to the methine peak of the polymer.

5.5.5 General Procedure for Scale-up of Polymerizations

In a glove box, $\mathbf{5}_{\text{red}}$ (0.01 mmol) and L-lactide (1.0 mmol) were added to a small vial, and toluene (2.0 mL) was added by syringe. The mixture was shaken to yield a homogeneous solution that was then placed on a preheated stir plate (70 or 90 °C). Once the polymerization was complete, the vial was immediately brought out of the glove box, cooled, and exposed to air. The solvent was removed, and the remaining solid was dissolved in C_6D_6 (1.0 mL) in order to determine conversion of L-lactide via ^1H NMR. The C_6D_6 was removed and the solid was dissolved in dichloromethane (10 mL) before being slowly added into approximately 80 mL methanol to yield a white solid, which was dried under reduced pressure.

Chapter 6– CONCLUSIONS AND FUTURE WORK

6.1 Summary and Conclusions

From this work, two distinct catalyst studies were performed while creating either commodity plastics like polyethylene or bioplastics like poly(lactic acid). During the first portion of the dissertation (Chapters 1-3), we laid the foundation for modifying nickel α -diimine catalysts to contain bulky *iPr** moieties on the *ortho* position of the *N*-aryl groups which inhibit *N*-aryl rotation. This ligand modification was studied in conjunction with three different ligand backbones, which resulted in the synthesis of three distinct catalysts (**2a**, **2b**, and **3**). These catalysts were determined to be thermally robust for ethylene polymerizations showing no catalyst deactivation or decomposition up to 90 °C. Additionally, catalyst **3** was shown to display living behavior up to 75 °C. These nickel α -diimine catalysts represent some of the most thermally robust ethylene catalysts reported to date, and to our knowledge, catalyst **3** is the only late transition metal-based catalyst that proceeds in the living fashion for the polymerization of ethylene above 25 °C. These catalysts provide vital evidence that inclusion of benzhydryl functionality on the *N*-aryl portion of the ligand greatly increases thermal stability of the catalyst as well as providing high molecular weight polyethylene with extremely low dispersity.

The studies presented in the second half of this dissertation (Chapters 4 and 5) reveal that our newly designed titanium-based catalysts that contain a redox active moiety for the polymerization of L-lactide showed two compelling conclusions—(1) polymerization control of the “on-off-on” switch is enhanced when the redox-active moiety is proximal to the active metal center; and (2) polymerization behavior depends on whether the monomer is absent or present during the oxidation of the catalyst. In particular, Chapter 5 described that if catalyst **5** was oxidized (or reduced from the oxidized state) in the presence of monomer prior to initiation, then the electron-rich species polymerized lactide much faster than the electron-deficient catalyst. These behaviors agree with all previous reports. However, when our catalyst is oxidized (or reduced from the oxidized state) in the absence of monomer and then injected into the polymerization reactor, the electron-deficient catalyst polymerizes lactide much faster than the electron-rich species. This behavior contradicts all previously reported polymerization behaviors for this class of catalysts. To understand this novel behavior, we have confirmed via single x -ray crystallography and ^1H NMR analysis that this catalyst is in a rare geometry conformation in the solid and solution states for this class of

catalysts. With this in mind, we attribute the remarkable contrast in polymerization behavior to a novel catalyst geometry switch that occurs when the redox state of the catalyst is changed in the presence of lactide monomer. Lastly, we observe that if this catalyst is oxidized and then rereduced in the presence of monomer, only the electron-rich catalyst is able to activate the polymerization of L-lactide. The ability to toggle the catalyst reactivity provides an optional “on-off-on” switch in reactivity, which gives control of the polymerization. These fundamental discoveries pertaining to the environment of the redox switch and the location of the redox-active moiety in the catalyst itself offer valuable insight for this area of polymerization catalysis.

6.2 Future Work

Moving forward with the redox switchable catalysis project, the first focus will be to examine other tetradentate [ONNO]-type catalysts that contain a redox-active moiety, namely ferrocene. This project will be an extension of Chapter 5; however, the focus will be shifted to understand how the number of redox moieties present within the ligand scaffold and the identity of the other functionalities that are not redox active effect the polymerization behavior. In order to achieve this goal, a systematic study of ONNO catalysts where the nitrogens within the ligand scaffold are either: (1) diimines, (2) diamines or (3) a combination of an imine and an amine. These ligands will be synthesized, metallated with a group 4 species, and observed for the polymerization of L-lactide. In addition, some of these ligands will contain either one ferrocenyl unit or two, which will determine if the amount of redox active moieties provide an advantage. The redox innocent functionalities, namely the imine or amine connections will provide insight to how these ligands should be designed in an effort to achieve the optimal properties to being able to selectively switch polymerizations on and off and also provide monomer control *in situ*. Therefore the ligand library shown in **Figure 6.1** will be synthesized and studied to better understand which aspects of ONNO redox catalysts can be tailored to obtain specific PLA materials.

As preliminary work, ligand **9** was synthesized in two steps and metallated with titanium(IV) isopropoxide to afford catalyst **14** in high yields (**Scheme 6.1**). Preliminary L-lactide polymerizations were performed in C₆D₆ at 90 °C and monitored via variable temperature ¹H NMR to determine if a difference in polymerization behavior was seen

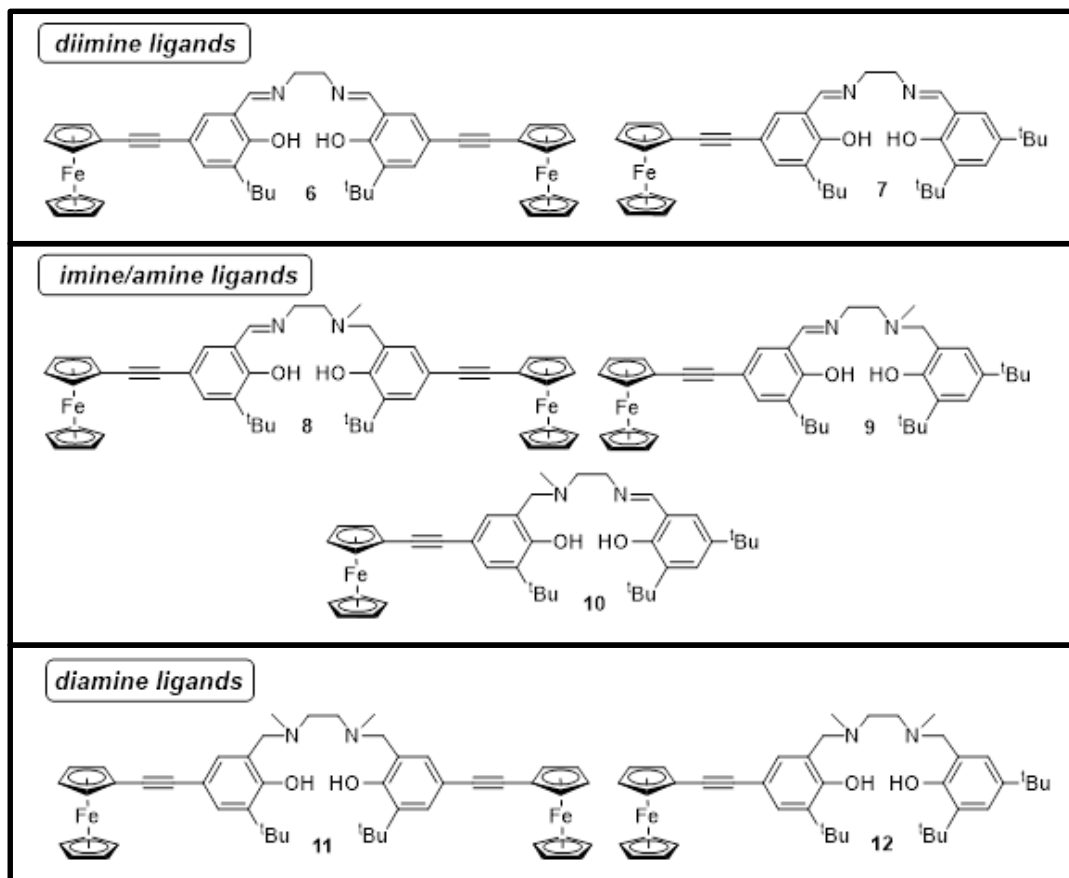
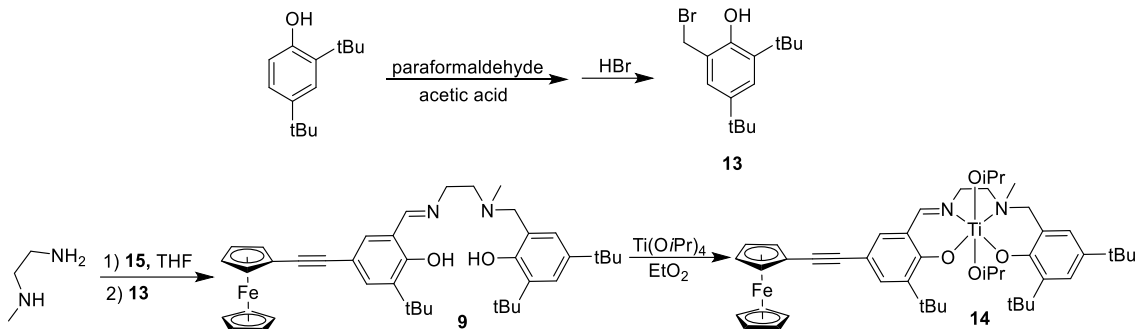


Figure 6.1 Proposed [ONNO] ligand library to study their redox effects during the polymerization of L-lactide. More specifically, the proposed ligands contain either one or two ferrocenyl moieties. In addition, the redox innocent functionality of the ligand will be examined, namely the functionality of the nitrogen within the ONNO ligand scaffold to be either a diimine, a diimine, or an imine/amine.



Scheme 6.1 Synthesis of the imine/amine titanium-based catalyst **14**, which contains a single ferrocenyl moiety off the imine portion of the ligand.

between the **14**_{red} and **14**_{ox}. **14**_{red} was oxidized with $\text{AcFcBAR}^{\text{F}}$ and rereduced with CoCp_2 . In **Figure 6.2**, a plot of percent monomer conversion versus time shows that the Fe^{II} complex (red) polymerized L-lactide at a much greater rate than the Fe^{III} species (blue). These results agreed with previous reports that the more electron-rich species polymerizes lactide at a faster rate than the electron deficient species. Notably, **14**_{red} polymerizes L-lactide at a much greater rate than **5**_{red} or **4**_{red} (Chapter 5) under the same conditions. This data seems to show evidence that having two ferrocenyl moieties on the ligand are not necessary to achieve a dramatic difference in polymerization behavior between the reduced and oxidized species.

Cyclic voltammetry (CV) experiments of **14** were performed in DCM with $[\text{nBu}_4\text{N}][\text{PF}_6]$ (0.2 M) as an electrolyte and scanned at a rate of 100 mV/s, which revealed that catalyst **14** had two quasireversible half-wave potentials ($E_{1/2}$) of 0.047 V and 0.317 when referenced versus Fc/Fc^+ (**Figure 6.3**). This redox behavior was unexpected because the only redox active functionality thought to be present in catalyst **14** was the ferrocenyl unit, which has been attributed to the signal at 0.047 V. Current investigations are underway to determine the source of the redox peak at 0.317 V.

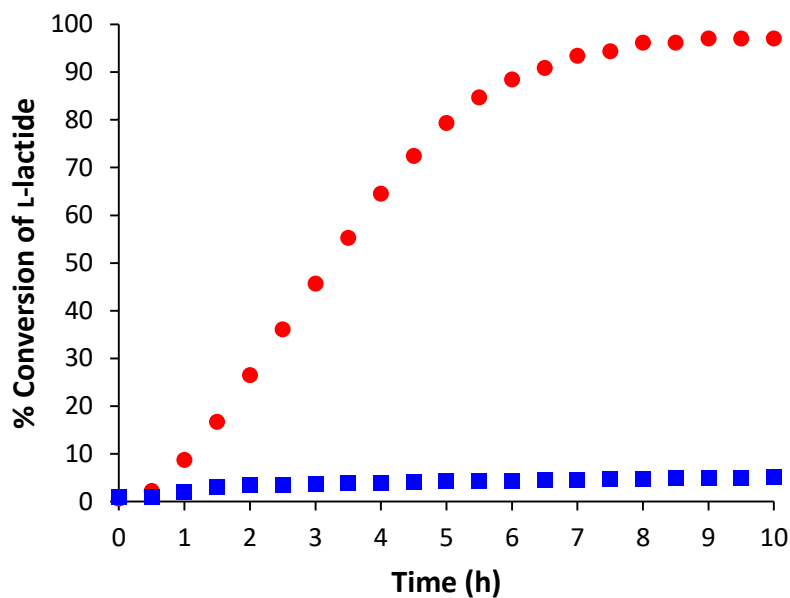


Figure 6.2 Plot of percent conversion of L-lactide versus time with **14**_{red} (red circles) and **14**_{ox} (blue squares). **14** was oxidized with ^{Ae}FcBAr^F.

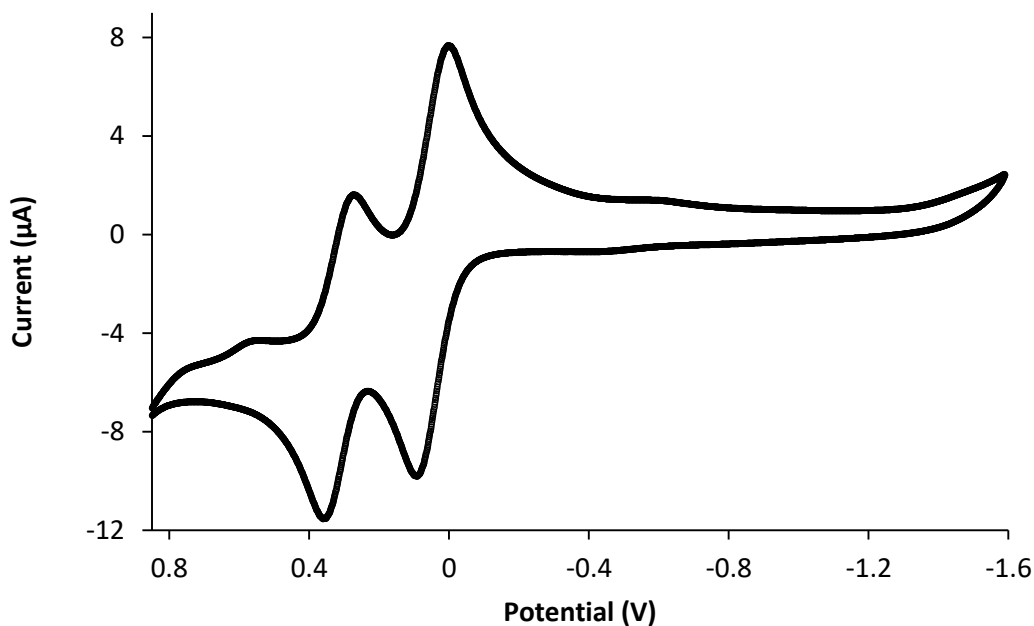
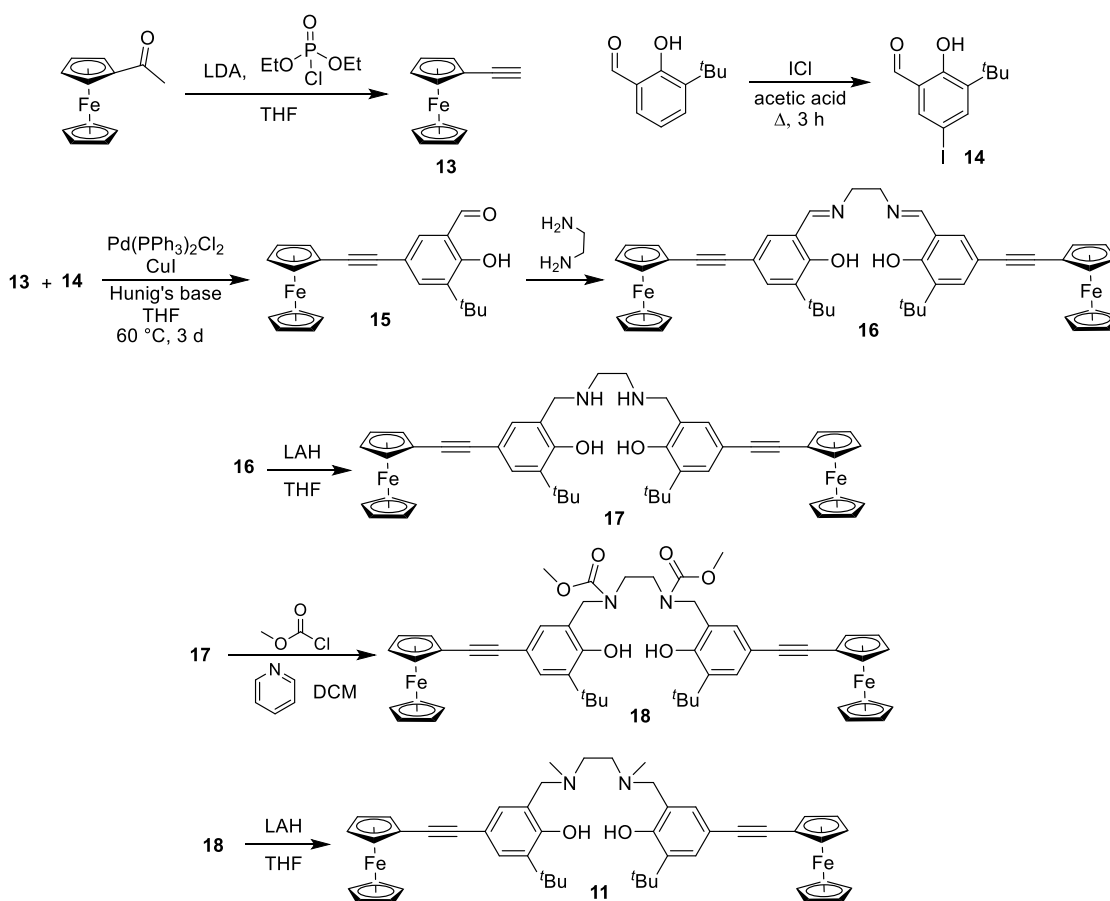


Figure 6.3 Cyclic voltammogram of catalyst **14** (0.01 mmol) recorded at a scan rate of 100 mV/s in dichloromethane (5 mL), (*n*Bu)₄NPF₆ (0.20 M), ($E_{1/2}$ = 0.047 and 0.317 V) versus Fc/Fc⁺.

Additionally, ligand **11** was synthesized from commercially available starting materials in six steps. Ethynyl ferrocene (**13**) was chosen as the redox active functionality and was synthesized from acetyl ferrocene. lithium diisopropylamide (LDA) and diethyl chlorophosphate in THF (**Scheme 6.2**).⁷² Ethynyl ferrocene underwent a Sonogashira coupling with 3-*tert*-butyl-5-iodo-2-hydroxybenzaldehyde (**14**) to produce 3-*tert*-butyl-5-ethynylferrocene-2-hydroxybenzaldehyde (**15**).⁷² To produce the diimine **16**, an imine condensation with ethylene diamine and **15** was performed.⁷² Subsequent reduction of **16** with lithium aluminum hydride (LAH) to afford the diamine **17**, which was reacted with methyl chloroformate to produce the dicarbamate **18**. Diamine ligand **11** was completed after reduction of **18** with LAH.



Scheme 6.2 Synthesis of tetradentate [ONNO] ligand **11**, which contains two ferrocenyl substituents at the outer extremity of the ligand scaffold.

6.3 Experimental

6.3.1 General Materials and Methods

All experiments were performed under a dry nitrogen atmosphere using standard Schlenk techniques or MBraun inert-gas glove box. Solvents were purified using a two-column solid-state purification system and transferred to the glove box without exposure to air. NMR solvents were purchased from Cambridge Isotope Laboratories, dried over activated molecular sieves, and degassed prior to use. ^1H and ^{13}C NMR spectra were recorded on a Varian 300 or Bruker 400 MHz spectrometer. Chemical shifts are reported with respect to solvent residual peaks, 7.16 ppm (C_6D_6). L-lactide was purchased from Fisher Scientific and recrystallized twice in toluene prior to use. $^{\text{Ac}}\text{FcBAR}^{\text{F}}$ was synthesized following previously reported procedures. All other chemicals were purchased and used as received. Cyclic voltammetry measurements were performed on a CH Instruments potentiostat using 0.01 mmol of compound **14** in 5 ml DCM solution (0.002 M) with supporting electrolyte 0.2 M ($n\text{Bu}$) $_4\text{NPF}_6$, using Ag/AgCl as the reference electrode, a gold working electrode, and a tungsten counter electrode at a scan rate of 100 $\text{mV}\cdot\text{s}^{-1}$. All potentials are given with respect to the ferrocene-ferrocenium redox couple.

6.3.2 NMR Scale Polymerization Procedure

In a glove box, L-lactide (0.7 mmol or 0.35 mmol), **14** (0.007 mmol), and C_6D_6 (0.7 mL) were added to a J. Young NMR tube equipped with a Teflon valve. As needed, $^{\text{Ac}}\text{FcBAR}^{\text{F}}$ (0.007 mmol) were added to the J. Young tube containing the monomer and complex **14**. The sealed tube was removed from the glove box, and the polymerization was monitored by ^1H NMR spectroscopy for up to 24 hours by placing in a preheated Bruker Avance 400 MHz NMR at 90 °C. The command “multizg” was used to collect data every 10 or 30 minutes. The data was processed with XWinNMR3.6. Conversion of L-lactide was monitored by comparing the methine peak of the monomer to the methine peak of the polymer.

6.3.3 Synthesis of 2-(bromomethyl)-4,6-di-tert-butylphenol

2,4-di-tert-butyl phenol (5 g, 1 equiv), and paraformaldehyde (1.11 equiv), and acetic acid are added with Schlenk flask and stirred at room temperature for 2 h. Hydrobromic acid

(3.02 equiv, 33 wt% solution) was added dropwise via syringe, and the solution was stirred for 30 min. The solvent was removed under vacuum, and the oil was stored at -30 °C for approximately 3 h until orange crystals formed. The solid was filtered and washed with diethyl ether. The solid was dried under vacuum (6.09 g, 84% yield). Characterization matched previous report.¹⁰⁰

6.3.4 Synthesis of monoferrocenyl salalen (**9**)

15 (2.0 mg, 1 equiv) was added to a Schlenk flask. THF (10 mL) was added to Schenk flask via cannula. Triethylamine (0.45 mL) was added via syringe to solution. The mixture was stirred for 12 h at room temperature. A solution of 2-(bromomethyl)-4,6-di-*tert*-butylphenol (1 equiv) in THF (10 mL) was added to the mixture via cannula. The solution was stirred for an additional 3 h. The mixture was filtered, and the solvent was removed under vacuum. The solid was washed with hot ethanol to give a light orange powder (2.7 g, 79% yield). ¹H NMR (500 MHz, 25 °C, C₆D₆), δ, ppm: 1.32 (s, 9H, C(CH₃)₃), 1.54 (s, 9H, C(CH₃)₃), 1.69 (s, 9H, C(CH₃)₃), 1.81 (s, 3H, NCH₃), 2.17 (t, 2H, CH₂NCH₂), 2.99 (t, 2H, C=N(CH₂)), 3.29 (s, 2H, NCH₂Ar), 3.98 (t, 2H, CpH), 4.16 (s, 5H, CpH), 4.57 (t, 2H, CpH), 6.90 (d, 1H, ArH), 7.31 (d, 1H, ArH), 7.50 (d, 1H, ArH), 7.61 (s, 1H, ArH), 7.79 (d, 1H, HC=N), 10.81 (s, 1H, OH).

6.3.4 Synthesis of monoferrocenyl (salalen)Ti(O^{*i*}Pr)₂ (**14**)

9 (500 mg, 1 equiv) was added to a Schlenk flask. Toluene was added to the flask via cannula. Titanium tetraisopropoxide (23 mL, 1 equiv) was added dropwise via syringe to the solution and was then stirred at room temperature for 2 h. The solution was cooled to -20 °C and filtered. The solvent was removed under vacuum to give the solid orange product (0.62 g, 92% yield). ¹H NMR (500 MHz, 25 °C, C₆D₆), δ, ppm: 1.01 (d, 3H, CH(CH₃)₂), 1.04 (d, 3H, CH(CH₃)₂), 1.31 (d, 3H, CH(CH₃)₂), 1.41 (s, 9H, C(CH₃)₃), 1.42 (s, 9H, C(CH₃)₃), 1.49 (d, 3H, CH(CH₃)₂), 1.67 (s, 9H, C(CH₃)₃), 2.30 (t, 2H, CH₂NCH₂), 2.66 (s, 3H, NCH₃), 3.96 (t, 2H, CpH), 4.12 (s, 5H, CpH), 4.39 (t, 2H, C=N(CH₂)), 4.41 (m, 1H, CH(CH₃)₂), 4.42 (s, 2H, NCH₂Ar), 4.54 (t, 2H, CpH), 5.31 (m, 1H, CH(CH₃)₂), 6.95 (s, 1H, ArH), 7.13 (s, 1H, ArH), 7.26 (s, 1H, ArH), 7.47 (s, 1H, ArH), 7.89 (s, 1H, HC=N). ¹³C NMR (500 MHz, 25 °C, C₆D₆), δ, ppm: 1.44, 26.41, 26.50, 26.77, 29.90, 30.15, 32.23, 34.37, 35.27, 35.50, 55.08, 69.03, 70.29, 71.66, 75.27, 77.50, 86.72,

87.34, 112.85, 123.15, 123.48, 123.64, 127.97, 128.16, 128.36, 135.22, 135.47, 136.66, 138.30, 139.07, 161.75, 163.50.

6.3.2 Synthesis of Ethynylferrocene (13)

Acetylferrocene (5.0 g, 1 equiv) and THF (100 mL) were added to a Schlenk flask and cooled to -78 °C. Lithium diisopropylamide (LDA) solution (2 M, 1.1 equiv) was added dropwise via syringe. The solution was stirred for 1 h and then diethyl chlorophosphate (3.3 mL, 1.05 equiv) was added dropwise via syringe and stirred for 1 h. The reaction was warmed to room temperature and stirred for 2 h. The mixture was cooled to -78 °C before LDA (2.3 equiv) was added. The solution was allowed to slowly warm to room temperature and stirred for 4 h. The reaction was quenched with water (10 mL). The organic layer was extracted with hexanes (3 x 100 mL). The combined organic layers were washed with water (2 x 100 mL) and brine (50 mL). The organic layer was dried with MgSO₄ and filtered. The solvent was removed *in vacuo* to give an orange solid. The crude material was purified via column chromatography (10:90 ethyl acetate:hexanes) and seeded to give dark orange/red crystals (3.4 g, 74% yield). Characterization matched previous literature reports.¹⁰¹

6.3.3 Synthesis of 3-*tert*-butyl-5-iodo-2-hydroxybenzaldehyde (14)

3-*tert*-butyl-5-iodo-2-hydroxybenzaldehyde (5 mL, 29.2 mmol, 1 equiv) was dissolved in acetic acid (60 mL). A solution of ICl (2.05 mL, 1.4 equiv) was added dropwise over 30 min. The mixture was refluxed for 4 h. Water (20 mL) was added to quench the reaction. The organic layer was extracted with dichloromethane (DCM) (50 mL), washed with saturated sodium thiosulfate (30 mL), dried with MgSO₄ and filtered. The solvent was removed under vacuum to afford the crude yellow solid. The crude material was purified via column chromatography (10:90 ethyl acetate:hexanes) to give a white solid (5.58 g, 63% yield). All characterization matched previous literature report.¹⁰²

6.3.4 Synthesis of 3-tert-butyl-5-ethynylferrocene-2-hydroxybenzaldehyde (15)

Ethynyl ferrocene (2.4 g, 1.1 equiv) and 3-tert-butyl-5-iodo-2-hydroxybenzaldehyde (3.15 g, 1 equiv) in THF (20 mL) was stirred in a Schlenk flask. In a glove box, copper (I) iodide (2.5 mol%) and PdCl₂(PPh₃)₂ (10 mol%) were added to a Schlenk flask. The ethynyl ferrocene mixture was added to the flask containing [Pd] via cannula. Diisopropylethylamine (3 equiv) was added to the mixture via syringe. The solution was stirred at 60 °C for 3 days. The solvent was removed under vacuum, and the crude product was purified via column chromatography (10:90 DCM:hexanes) to give an orange solid (2.8 g, 64% yield). Characterization matched previous literature reports.⁷²

6.3.5 Synthesis of Bis(3-tert-butyl-5-ethynylferrocene-salicylidene)-1,2-ethylenediamine (16)

15 (2.74 g, 1 equiv) was added to a Schlenk flask with absolute ethanol (100 mL). Ethylenediamine (0.8 equiv) was added to solution via syringe. Formic acid (3.15 equiv) was added via syringe, and the mixture was refluxed for 3 h. The solid was filtered and washed with EtOH, and dried to give a light orange solid (2.64 g, 88% yield). Characterization matched previous reports.⁷²

6.3.6 Synthesis of 6,6'-((ethane-1,2-diylbis(azanediyl))bis(methylene))bis(2-(tert-butyl)-4-ethynylferrocenophenol (17)

16 (1.0 g, 1 equiv) was added to a Schlenk flask. THF (75 mL) was added via cannula. Lithium aluminum hydride (288.0 mg, 6 equiv) was added portion-wise to the solution at 0 °C. The reaction was stirred for 12 h at room temperature. The mixture was quenched with water (6 mL), NaOH (1 M, 7 mL), and water (8 mL). The solution was stirred for 30 min. The organic layer was cannula transferred into a separate Schlenk flask, and the solvent was removed under vacuum to give an orange solid (905 mg, 91% yield). ¹H NMR (C₆D₆), δ, ppm:

1.57 (s, 18H, (CH₃)₃), 1.84 (s, 2H, NH), 3.23 (s, 4H, C N(CH₂)₂), 3.55 (s, 4H, ArCH₂N), 3.96 (t, 4H, CpH), 4.13 (s, 10H, CpH), 4.57 (t, 4H, CpH), 7.78 (s, 4H, ArH).

6.3.7 Synthesis of dimethyl ethane-1,2-diylbis((3-tert-butyl)-5-ethynylferrocene-2-hydroxybenzyl)carbamate (18)

17 (735 mg, 1 equiv) was added to a Schlenk flask, and dichloromethane (20 mL) was added via cannula. Pyridine (6 equiv) was added to the solution via syringe. The reaction was cooled to 0 °C before methyl chloroformate (6 equiv) was added via syringe. The mixture was slowly warmed to room temperature and stirred for 12 h. The reaction was quenched with water (5 mL), and the water layer was removed via cannula. The solvent was removed under vacuum to give an orange solid (515 mg, 70% yield). ¹H NMR (C₆D₆), δ, ppm: 1.53 (s, 18H, (CH₃)₃), 2.69 (s, 4H, N(CH₂)₂), 3.38 (s, 6H, CH₃), 3.92 (s, 4H, ArCH₂N), 3.96 (t, 4H, CpH), 4.12 (s, 10H, CpH), 4.57 (t, 4H, CpH), 7.11 (s, 2H, ArH), 7.82 (s, 2H, ArH), 9.95 (s, 2H, OH).

6.3.8 Synthesis of 6,6'-((ethane-1,2-diylbis(methylazanediyl))bis(methylene))bis(2-(tert-butyl)-4-ethynylferrocenophenol (11)

18 (415 mg, 1 equiv) was added to a Schlenk flask. THF (30 mL) was added via cannula, and the solution was cooled to 0 °C. LAH (181.7 mg, 10 equiv) was added portion-wise, and the solution was slowly warmed to room temperature and stirred for 12 h. The reaction was quenched with water (8 mL), NaOH (1 M, 4 mL), and water (5 mL) and stirred for an additional 30 min. The organic layer was removed by cannula, and the solvent was removed *in vacuo* to give an orange solid (191 mg, 62% yield). ¹H NMR (C₆D₆), δ, ppm: 1.55 (s, 18H, (CH₃)₃), 1.67 (s, 6H, CH₃), 1.95 (s, 4H, N(CH₂)₂), 3.08 (s, 4H, ArCH₂N), 3.96 (t, 4H, CpH), 4.13 (s, 10H, CpH), 4.55 (t, 4H, CpH), 7.14 (s, 2H, ArH), 7.76 (s, 2H, ArH), 11.20 (s, 2H, OH).

REFERENCES

- (1) Xie, T. Y.; Mcauley, K. B.; Hsu, J. C. C.; Bacon, D. W. "Gas-Phase Ethylene Polymerization - Production Processes, Polymer Properties, and Reactor Modeling". *Ind Eng Chem Res* **1994**, *33*, 449-479.
- (2) Cherian, A. E.; Rose, J. M.; Lobkovsky, E. B.; Coates, G. W. "A C₂-symmetric, living alpha-diimine Ni(II) catalyst: regioblock copolymers from propylene". *J. Am. Chem. Soc.* **2005**, *127*, 13770-13771.
- (3) Domski, G. J.; Rose, J. M.; Coates, G. W.; Bolig, A. D.; Brookhart, M. "Living alkene polymerization: New methods for the precision synthesis of polyolefins". *Prog Polym Sci* **2007**, *32*, 30-92.
- (4) Zhang, W.; Wei, J.; Sita, L. R. "Living Coordinative Chain-Transfer Polymerization and Copolymerization of Ethene, α -Olefins, and α,ω -Nonconjugated Dienes using Dialkylzinc as "Surrogate" Chain-Growth Sites". *Macromolecules* **2008**, *41*, 7829-7833.
- (5) Azoulay, J. D.; Schneider, Y.; Galland, G. B.; Bazan, G. C. "Living polymerization of ethylene and alpha-olefins using a nickel alpha-keto-beta-diimine initiator". *Chem Commun* **2009**, 6177-6179.
- (6) Natta, C. "Stereospecific Polymerizations". *J Polym Sci* **1960**, *48*, 219-239.
- (7) Ziegler, K.; Holzkamp, E.; Breil, H.; Martin, H. "The Mulheim Normal Pressure Polyethylene Process". *Angew Chem Int Edit* **1955**, *67*, 541-547.
- (8) Galli, P.; Vecellio, G. "Technology: driving force behind innovation and growth of polyolefins". *Prog Polym Sci* **2001**, *26*, 1287-1336.
- (9) Sinn, H.; Kaminsky, W.; Vollmer, H. J.; Woldt, R. "Living Polymers on Polymerization with Extremely Productive Ziegler Catalysts". *Angew Chem Int Edit* **1980**, *19*, 390-392.
- (10) Ittel, S. D.; Johnson, L. K.; Brookhart, M. "Late-metal catalysts for ethylene homo- and copolymerization". *Chem Rev* **2000**, *100*, 1169-1204.
- (11) Johnson, L. K.; Killian, C. M.; Brookhart, M. "New Pd(II)-Based and Ni(II)-Based Catalysts for Polymerization of Ethylene and Alpha-Olefins". *J Am Chem Soc* **1995**, *117*, 6414-6415.
- (12) Gibson, V. C.; Spitzmesser, S. K. "Advances in non-metallocene olefin polymerization catalysis". *Chem Rev* **2003**, *103*, 283-315.
- (13) Guan, Z.; Cotts, P. M.; McCord, E. F.; McLain, S. J. "Chain walking: A new strategy to control polymer topology". *Science* **1999**, *283*, 2059-2062.
- (14) Gates, D. P.; Svejda, S. A.; Oñate, E.; Killian, C. M.; Johnson, L. K.; White, P. S.; Brookhart, M. "Synthesis of Branched Polyethylene Using (α -Diimine)nickel(II)

Catalysts: Influence of Temperature, Ethylene Pressure, and Ligand Structure on Polymer Properties". *Macromolecules* **2000**, *33*, 2320-2334.

(15) Guan, Z. B. "Recent Progress of Catalytic Polymerization for Controlling Polymer Topology". *Chem-Asian J* **2010**, *5*, 1058-1070.

(16) Camacho, D. H.; Salo, E. V.; Ziller, J. W.; Guan, Z. B. "Cyclophane-based highly active late-transition-metal catalysts for ethylene polymerization". *Angew Chem Int Edit* **2004**, *43*, 1821-1825.

(17) Camacho, D. H.; Guan, Z. B. "Living polymerization of alpha-olefins at elevated temperatures catalyzed by a highly active and robust cyclophane-based nickel catalyst". *Macromolecules* **2005**, *38*, 2544-2546.

(18) Liu, F. S.; Hu, H. B.; Xu, Y.; Guo, L. H.; Zai, S. B.; Song, K. M.; Gao, H. Y.; Zhang, L.; Zhu, F. M.; Wu, Q. "Thermostable alpha-Diimine Nickel(II) Catalyst for Ethylene Polymerization: Effects of the Substituted Backbone Structure on Catalytic Properties and Branching Structure of Polyethylene". *Macromolecules* **2009**, *42*, 7789-7796.

(19) Alt, H. G.; Koppl, A. "Effect of the Nature of Metallocene Complexes of Group IV Metals on Their Performance in Catalytic Ethylene and Propylene Polymerization". *Chem Rev* **2000**, *100*, 1205-1222.

(20) Chen, E. Y.; Marks, T. J. "Cocatalysts for metal-catalyzed olefin polymerization: activators, activation processes, and structure-activity relationships". *Chem Rev* **2000**, *100*, 1391-1434.

(21) Coates, G. W. "Precise control of polyolefin stereochemistry using single-site metal catalysts". *Chem Rev* **2000**, *100*, 1223-1252.

(22) Killian, C. M.; Tempel, D. J.; Johnson, L. K.; Brookhart, M. "Living polymerization of alpha-olefins using Ni-II-alpha-diimine catalysts. Synthesis of new block polymers based on alpha-olefins". *J Am Chem Soc* **1996**, *118*, 11664-11665.

(23) Boffa, L. S.; Novak, B. M. "Copolymerization of polar monomers with olefins using transition-metal complexes". *Chem Rev* **2000**, *100*, 1479-1494.

(24) Johnson, L. K.; Mecking, S.; Brookhart, M. "Copolymerization of ethylene and propylene with functionalized vinyl monomers by palladium(II) catalysts". *J Am Chem Soc* **1996**, *118*, 267-268.

(25) Mecking, S.; Johnson, L. K.; Wang, L.; Brookhart, M. "Mechanistic studies of the palladium-catalyzed copolymerization of ethylene and alpha-olefins with methyl acrylate". *J Am Chem Soc* **1998**, *120*, 888-899.

- (26) Popeney, C. S.; Guan, Z. B. "A Mechanistic Investigation on Copolymerization of Ethylene with Polar Monomers Using a Cyclophane-Based Pd(II) alpha-Diimine Catalyst". *J Am Chem Soc* **2009**, *131*, 12384-12393.
- (27) Gates, D. P.; Svejda, S. K.; Onate, E.; Killian, C. M.; Johnson, L. K.; White, P. S.; Brookhart, M. "Synthesis of branched polyethylene using (alpha-diimine)nickel(II) catalysts: Influence of temperature, ethylene pressure, and ligand structure on polymer properties". *Macromolecules* **2000**, *33*, 2320-2334.
- (28) Anselment, T. M. J.; Vagin, S. I.; Rieger, B. "Activation of late transition metal catalysts for olefin polymerizations and olefin/CO copolymerizations". *Dalton Trans* **2008**, 4537-4548.
- (29) Coates, G. W.; Hustad, P. D.; Reinartz, S. "Catalysts for the living insertion polymerization of alkenes: Access to new polyolefin architectures using Ziegler-Natta chemistry". *Angew Chem Int Edit* **2002**, *41*, 2236-2257.
- (30) Younkin, T. R.; Connor, E. F.; Henderson, J. I.; Friedrich, S. K.; Grubbs, R. H.; Bansleben, D. A. "Scope of olefin polymerization nickel catalysts - Response". *Science* **2000**, *288*, 1750-1751.
- (31) Tempel, D. J.; Johnson, L. K.; Huff, R. L.; White, P. S.; Brookhart, M. "Mechanistic studies of Pd(II)-alpha-diimine-catalyzed olefin polymerizations". *J Am Chem Soc* **2000**, *122*, 6686-6700.
- (32) Mecking, S. "Cationic nickel and palladium complexes with bidentate ligands for the C-C linkage of olefins". *Coordin Chem Rev* **2000**, *203*, 325-351.
- (33) Berkefeld, A.; Mecking, S. "Deactivation Pathways of Neutral Ni(II) Polymerization Catalysts". *J Am Chem Soc* **2009**, *131*, 1565-1574.
- (34) Popeney, C. S.; Rheingold, A. L.; Guan, Z. B. "Nickel(II) and Palladium(II) Polymerization Catalysts Bearing a Fluorinated Cyclophane Ligand: Stabilization of the Reactive Intermediate". *Organometallics* **2009**, *28*, 4452-4463.
- (35) Gao, H. Y.; Hu, H. B.; Zhu, F. M.; Wu, Q. "A thermally robust amine-imine nickel catalyst precursor for living polymerization of ethylene above room temperature". *Chem Commun* **2012**, *48*, 3312-3314.
- (36) Meinhard, D.; Wegner, M.; Kipiani, G.; Hearley, A.; Reuter, P.; Fischer, S.; Marti, O.; Rieger, B. "New Nickel(II) diimine complexes and the control of polyethylene microstructure by catalyst design". *J Am Chem Soc* **2007**, *129*, 9182-9191.
- (37) Liu, H.; Zhao, W. Z.; Hao, X. A.; Redshaw, C.; Huang, W.; Sun, W. H. "2,6-Dibenzhydryl-N-(2-phenyliminoacenaphthylenylidene)-4-methylbenzenamine Nickel Dibromides: Synthesis, Characterization, and Ethylene Polymerization". *Organometallics* **2011**, *30*, 2418-2424.

- (38) Berthon-Gelloz, G.; Siegler, M. A.; Spek, A. L.; Tinant, B.; Reek, J. N. H.; Marko, I. E. "IPr* an easily accessible highly hindered N-heterocyclic carbene". *Dalton Trans* **2010**, 39, 1444-1446.
- (39) Cherian, A. E.; Lobkovsky, E. B.; Coates, G. W. "Chiral anilines: development of C-2-symmetric, late-transition metal catalysts for isoselective 2-butene polymerization". *Chem Commun* **2003**, 2566-2567.
- (40) Lee, L. S.; Ou, H. J.; Hsu, H. F. "The experiments and correlations of the solubility of ethylene in toluene solvent". *Fluid Phase Equilib* **2005**, 231, 221-230.
- (41) Azoulay, J. D.; Bazan, G. C.; Galland, G. B. "Microstructural Characterization of Poly(1-hexene) Obtained Using a Nickel α -Keto- β -diimine Initiator". *Macromolecules* **2010**, 43, 2794-2800.
- (42) Ittel, S. D.; Johnson, L. K.; Brookhart, M. "Late-metal catalysts for ethylene homo- and copolymerization". *Chem. Rev.* **2000**, 100, 1169-1203.
- (43) Harney, M. B.; Keaton, R. J.; Fettinger, J. C.; Sita, L. R. "Living Ziegler-Natta polymerization by early transition metals: Synthesis and evaluation of cationic zirconium alkyl complexes bearing beta-hydrogens as models for propagating centers". *J Am Chem Soc* **2006**, 128, 3420-3432.
- (44) Webster, O. W. "Living Polymerization Methods". *Science* **1991**, 251, 887-893.
- (45) Reinartz, S.; Mason, A. F.; Lobkovsky, E. B.; Coates, G. W. "Titanium Catalysts with Ancillary Phenoxyketimine Ligands for Living Ethylene Polymerization". *Organometallics* **2003**, 22, 2542-2544.
- (46) Makio, H.; Terao, H.; Iwashita, A.; Fujita, T. "FI catalysts for olefin polymerization--a comprehensive treatment". *Chem Rev* **2011**, 111, 2363-2449.
- (47) Long, B. K.; Eagan, J. M.; Mulzer, M.; Coates, G. W. "Semi-Crystalline Polar Polyethylene: Ester-Functionalized Linear Polyolefins Enabled by a Functional-Group-Tolerant, Cationic Nickel Catalyst". *Angew. Chem. Int. Ed.* **2016**, 55, 7106-7110.
- (48) Yu, S. M.; Mecking, S. "Extremely narrow-dispersed high molecular weight polyethylene from living polymerization at elevated temperatures with o-F substituted Ti enolatoimines". *J Am Chem Soc* **2008**, 130, 13204-13205.
- (49) Ali, E. M.; Abasaeed, A. E.; Al-Zahrani, S. M. "Optimization and control of industrial gas-phase ethylene polymerization reactors". *Ind Eng Chem Res* **1998**, 37, 3414-3423.
- (50) Camacho, D. H.; Guan, Z. "Living Polymerization of α -Olefins at Elevated Temperatures Catalyzed by a Highly Active and Robust Cyclophane-Based Nickel Catalyst". *Macromolecules* **2005**, 38, 2544-2546.

- (51) Zai, S.; Liu, F.; Gao, H.; Li, C.; Zhou, G.; Cheng, S.; Guo, L.; Zhang, L.; Zhu, F.; Wu, Q. "Longstanding living polymerization of ethylene: substituent effect on bridging carbon of 2-pyridinemethanamine nickel catalysts". *Chem Commun (Camb)* **2010**, *46*, 4321-4323.
- (52) Gao, H.; Hu, H.; Zhu, F.; Wu, Q. "A thermally robust amine-imine nickel catalyst precursor for living polymerization of ethylene above room temperature". *Chem. Commun.* **2012**, *48*, 3312-3314.
- (53) Hu, H.; Zhang, L.; Gao, H.; Zhu, F.; Wu, Q. "Design of Thermally Stable Amine–Imine Nickel Catalyst Precursors for Living Polymerization of Ethylene: Effect of Ligand Substituents on Catalytic Behavior and Polymer Properties". *Chem. Eur. J.* **2014**, *20*, 3225-3233.
- (54) Liu, J.; Chen, D.; Wu, H.; Xiao, Z.; Gao, H.; Zhu, F.; Wu, Q. "Polymerization of α -Olefins Using a Camphyl α -Diimine Nickel Catalyst at Elevated Temperature". *Macromolecules* **2014**, *47*, 3325-3331.
- (55) Hu, H.; Chen, D.; Gao, H.; Zhong, L.; Wu, Q. "Amine-imine palladium catalysts for living polymerization of ethylene and copolymerization of ethylene with methyl acrylate: incorporation of acrylate units into the main chain and branch end". *Polymer Chemistry* **2016**, *7*, 529-537.
- (56) Rhinehart, J. L.; Mitchell, N. E.; Long, B. K. "Enhancing α -Diimine Catalysts for High-Temperature Ethylene Polymerization". *ACS Catalysis* **2014**, *4*, 2501-2504.
- (57) Fan, L.; Yue, E.; Du, S.; Guo, C.-Y.; Hao, X.; Sun, W.-H. "Enhancing thermo-stability to ethylene polymerization: synthesis, characterization and the catalytic behavior of 1-(2,4-dibenzhydryl-6-chlorophenylimino)-2-aryliminoacenaphthylnickel halides". *RSC Advances* **2015**, *5*, 93274-93282.
- (58) Guan, Z. "Recent progress of catalytic polymerization for controlling polymer topology". *Chem. Asian. J.* **2010**, *5*, 1058-1070.
- (59) Anderson, W. C.; Rhinehart, J. L.; Tennyson, A. G.; Long, B. K. "Redox-Active Ligands: An Advanced Tool To Modulate Polyethylene Microstructure". *J. Am. Chem. Soc.* **2016**, *138*, 774-777.
- (60) Anderson, W. C.; Long, B. K. "Modulating Polyolefin Copolymer Composition via Redox-Active Olefin Polymerization Catalysts". *ACS Macro Letters* **2016**, *5*, 1029-1033.
- (61) Connelly, N. G.; Geiger, W. E. "Chemical redox agents for organometallic chemistry". *Chem Rev* **1996**, *96*, 877-910.
- (62) Rhinehart, J. L.; Brown, L. A.; Long, B. K. "A robust Ni(II) α -diimine catalyst for high temperature ethylene polymerization". *J Am Chem Soc* **2013**, *135*, 16316-16319.

- (63) Liu, F.-S.; Hu, H.-B.; Xu, Y.; Guo, L.-H.; Zai, S.-B.; Song, K.-M.; Gao, H.-Y.; Zhang, L.; Zhu, F.-M.; Wu, Q. "Thermostable α -Diimine Nickel(II) Catalyst for Ethylene Polymerization: Effects of the Substituted Backbone Structure on Catalytic Properties and Branching Structure of Polyethylene". *Macromolecules* **2009**, *42*, 7789-7796.
- (64) Rhinehart, J. L.; Brown, L. A.; Long, B. K. "A Robust Ni(II) α -Diimine Catalyst for High Temperature Ethylene Polymerization". *J Am Chem Soc* **2013**, *135*, 16316-16319.
- (65) Hicks, F. A.; Jenkins, J. C.; Brookhart, M. "Synthesis and ethylene polymerization activity of a series of 2-anilino-1-propanone-based neutral nickel(II) catalysts". *Organometallics* **2003**, *22*, 3533-3545.
- (66) Swift, G. "Directions for environmentally biodegradable polymer research". *Acc Chem Res* **1993**, *26*, 105-110.
- (67) Hayashi, T. "Biodegradable polymers for biomedical uses". *Prog Polym Sci* **1994**, *19*, 663-702.
- (68) Langer, R. "Biomaterials in Drug Delivery and Tissue Engineering: One Laboratory's Experience". *Acc Chem Res* **2000**, *33*, 94-101.
- (69) Auras, R.; Harte, B.; Selke, S. "An Overview of Polylactides as Packaging Materials". *Macromol Biosci* **2004**, *4*, 835-864.
- (70) Dechy-Cabaret, O.; Martin-Vaca, B.; Bourissou, D. "Controlled ring-opening polymerization of lactide and glycolide". *Chem Rev* **2004**, *104*, 6147-6176.
- (71) Garlotta, D. "A Literature Review of Poly(Lactic Acid)". *J Polym Environ* **2001**, *9*, 63-84.
- (72) Gregson, C. K. A.; Gibson, V. C.; Long, N. J.; Marshall, E. L.; Oxford, P. J.; White, A. J. P. "Redox control within single-site polymerization catalysts". *J Am Chem Soc* **2006**, *128*, 7410-7411.
- (73) Wang, X. K.; Thevenon, A.; Brosmer, J. L.; Yu, I. S.; Khan, S. I.; Mehrkhodavandi, P.; Diaconescu, P. L. "Redox Control of Group 4 Metal Ring-Opening Polymerization Activity toward L-Lactide and epsilon-Caprolactone". *J Am Chem Soc* **2014**, *136*, 11264-11267.
- (74) Biernesser, A. B.; Li, B.; Byers, J. A. "Redox-Controlled Polymerization of Lactide Catalyzed by Bis(imino)pyridine Iron Bis(alkoxide) Complexes". *J Am Chem Soc* **2013**, *135*, 16553-16560.
- (75) Lorkovic, I. M.; Duff, R. R.; Wrighton, M. S. "Use of the Redox-Active Ligand 1,1'-Bis(Diphenylphosphino)Cobaltocene to Reversibly Alter the Rate of the Rhodium(I)-Catalyzed Reduction and Isomerization of Ketones and Alkenes". *J Am Chem Soc* **1995**, *117*, 3617-3618.

- (76) Gregson, C. K. A.; Blackmore, I. J.; Gibson, V. C.; Long, N. J.; Marshall, E. L.; White, A. J. P. "Titanium-salen complexes as initiators for the ring opening polymerisation of rac-lactide". *Dalton Trans* **2006**, 3134-3140.
- (77) Cameron, P. A.; Jhurry, D.; Gibson, V. C.; White, A. J. P.; Williams, D. J.; Williams, S. "Controlled polymerization of lactides at ambient temperature using [5-Cl-salen]AlOMe". *Macromol Rapid Comm* **1999**, *20*, 616-618.
- (78) Idage, B. B.; Idage, S. B.; Kasegaonkar, A. S.; Jadhav, R. V. "Ring opening polymerization of dilactide using salen complex as catalyst". *Mater Sci Eng B-Adv* **2010**, *168*, 193-198.
- (79) Broderick, E. M.; Guo, N.; Vogel, C. S.; Xu, C. L.; Sutter, J.; Miller, J. T.; Meyer, K.; Mehrkhodavandi, P.; Diaconescu, P. L. "Redox Control of a Ring-Opening Polymerization Catalyst". *J Am Chem Soc* **2011**, *133*, 9278-9281.
- (80) Broderick, E. M.; Guo, N.; Wu, T. P.; Vogel, C. S.; Xu, C. L.; Sutter, J.; Miller, J. T.; Meyer, K.; Cantat, T.; Diaconescu, P. L. "Redox control of a polymerization catalyst by changing the oxidation state of the metal center". *Chem Commun* **2011**, *47*, 9897-9899.
- (81) Manna, C. M.; Kaplan, H. Z.; Li, B.; Byers, J. A. "High molecular weight poly(lactic acid) produced by an efficient iron catalyst bearing a bis(amidinato)-N-heterocyclic carbene ligand". *Polyhedron* **2014**, *84*, 160-167.
- (82) Allgeier, A. M.; Mirkin, C. A. "Ligand design for electrochemically controlling stoichiometric and catalytic reactivity of transition metals". *Angew Chem Int Edit* **1998**, *37*, 894-908.
- (83) Sussner, M.; Plenio, H. "Redox-switchable phase tags for recycling of homogeneous catalysts". *Angew Chem Int Edit* **2005**, *44*, 6885-6888.
- (84) Tennyson, A. G.; Lynch, V. M.; Bielawski, C. W. "Arrested Catalysis: Controlling Kumada Coupling Activity via a Redox-Active N-Heterocyclic Carbene". *J Am Chem Soc* **2010**, *132*, 9420-9429.
- (85) Ringenberg, M. R.; Nilges, M. J.; Rauchfuss, T. B.; Wilson, S. R. "Oxidation of Dihydrogen by Iridium Complexes of Redox-Active Ligands". *Organometallics* **2010**, *29*, 1956-1965.
- (86) Magenau, A. J. D.; Strandwitz, N. C.; Gennaro, A.; Matyjaszewski, K. "Electrochemically Mediated Atom Transfer Radical Polymerization". *Science* **2011**, *332*, 81-84.
- (87) Broderick, E. M.; Diaconescu, P. L. "Cerium(IV) catalysts for the ring-opening polymerization of lactide". *Inorg Chem* **2009**, *48*, 4701-4706.

- (88) Sauer, A.; Buffet, J. C.; Spaniol, T. P.; Nagae, H.; Mashima, K.; Okuda, J. "Switching the Lactide Polymerization Activity of a Cerium Complex by Redox Reactions". *Chemcatchem* **2013**, *5*, 1088-1091.
- (89) Hormnirun, P.; Marshall, E. L.; Gibson, V. C.; Pugh, R. I.; White, A. J. P. "Study of ligand substituent effects on the rate and stereoselectivity of lactide polymerization using aluminum salen-type initiators". *P Natl Acad Sci USA* **2006**, *103*, 15343-15348.
- (90) Alcazar-Roman, L. M.; O'Keefe, B. J.; Hillmyer, M. A.; Tolman, W. B. "Electronic influence of ligand substituents on the rate of polymerization of epsilon-caprolactone by single-site aluminium alkoxide catalysts". *Dalton Trans* **2003**, 3082-3087.
- (91) Qian, F.; Liu, K. Y.; Ma, H. Y. "Amidinate aluminium complexes: synthesis, characterization and ring-opening polymerization of rac-lactide". *Dalton Trans* **2010**, *39*, 8071-8083.
- (92) Pang, X.; Du, H. Z.; Chen, X. S.; Wang, X. H.; Jing, X. B. "Enolic Schiff base aluminum complexes and their catalytic stereoselective polymerization of racemic lactide". *Chem-Eur J* **2008**, *14*, 3126-3136.
- (93) Gong, S. G.; Ma, H. Y. "beta-diketiminato aluminium complexes: synthesis, characterization and ring-opening polymerization of cyclic esters". *Dalton Trans* **2008**, 3345-3357.
- (94) Shafir, A.; Fiedler, D.; Arnold, J. "Formation of 1 : 1 complexes of ferrocene-containing salen ligands with Mg, Ti and Zr". *J Chem Soc Dalton* **2002**, 555-560.
- (95) Gibson, V. C.; Gregson, C. K. A.; Halliwell, C. M.; Long, N. J.; Oxford, P. J.; White, A. J. P.; Williams, D. J. "The synthesis, coordination chemistry and ethylene polymerisation activity of ferrocenediyl nitrogen-substituted ligands and their metal complexes". *J. Organomet. Chem.* **2005**, *690*, 6271-6283.
- (96) Chen, H. Y.; White, P. S.; Gagne, M. R. "Synthesis and reactivity of titanium(IV)-salen complexes containing oxygen and chloride ligands". *Organometallics* **1998**, *17*, 5358-5366.
- (97) Clarkson, G. J.; Gibson, V. C.; Goh, P. K. Y.; Hammond, M. L.; Knight, P. D.; Scott, P.; Smit, T. M.; White, A. J. P.; Williams, D. J. "Group 4 catalysts for ethene polymerization containing tetradentate salicylaldiminato ligands". *Dalton Trans* **2006**, 5484-5491.
- (98) Sauer, A.; Kapelski, A.; Fliedel, C.; Dagorne, S.; Kol, M.; Okuda, J. "Structurally well-defined group 4 metal complexes as initiators for the ring-opening polymerization of lactide monomers". *Dalton Trans* **2013**, *42*, 9007-9023.
- (99) Thomson, R. K.; Scott, B. L.; Morris, D. E.; Kiplinger, J. L. "Synthesis, structure, spectroscopy and redox energetics of a series of uranium(IV) mixed-ligand metallocene complexes". *Cr Chim* **2010**, *13*, 790-802.

- (100) Appiah, W. O.; DeGreeff, A. D.; Razidlo, G. L.; Spessard, S. J.; Pink, M.; Young, V. G.; Hofmeister, G. E. "Linear Trimer Analogues of Calixarene as Chiral Coordinating Ligands: X-ray Crystallographic and NMR Spectroscopic Characterization of Chiral and Achiral Trisphenolates Complexed to Titanium(IV) and Aluminum(III)". *Inorg Chem* **2002**, *41*, 3656-3667.
- (101) Doisneau, G.; Balavoine, G.; Fillebeenkhan, T. "Synthesis and Some Reactions of Ferrocenylacetylenes". *J Organomet Chem* **1992**, *425*, 113-117.
- (102) Nielsen, M.; Gothelf, K. V. "Synthesis and catalytic properties of p-acylthio(phenylacetylene)(n) substituted chiral manganese salen complexes". *J Chem Soc Perk T 1* **2001**, 2440-2444.
- (103) Brown, L. A.; Rhinehart, J. L.; Long, B. K. "Effects of Ferrocenyl Proximity and Monomer Presence during Oxidation for the Redox-Switchable Polymerization of l-Lactide". *ACS Catal* **2015**, *5*, 6057-6060.
- (104) Anderson, W. C., Jr.; Rhinehart, J. L.; Tennyson, A. G.; Long, B. K. "Redox-Active Ligands: An Advanced Tool To Modulate Polyethylene Microstructure". *J Am Chem Soc* **2016**, *138*, 774-777.
- (105) Chen, M.; Yang, B.; Chen, C. "Redox-Controlled Olefin (Co)Polymerization Catalyzed by Ferrocene-Bridged Phosphine-Sulfonate Palladium Complexes". *Angew Chem Int Edit* **2015**, *54*, 15520-15524.
- (106) Gao, W.; Xin, L.; Hao, Z. Q.; Li, G. D.; Su, J. H.; Zhou, L. J.; Mu, Y. "The ligand redox behavior and role in 1,2-bis[[2,6-diisopropylphenyl]imino]-acenaphthene nickel-TMA(MAO) systems for ethylene polymerization". *Chem Commun* **2015**, *51*, 7004-7007.
- (107) Yamamoto, A.; Morifuji, K.; Ikeda, S.; Saito, T.; Uchida, Y.; Misono, A. "Diethylbis(bipyridine)iron. Butadiene cyclodimerization catalyst". *J Am Chem Soc* **1968**, *90*, 1878-1883.
- (108) Tshuva, E. Y.; Goldberg, I.; Kol, M. "Isospecific Living Polymerization of 1-Hexene by a Readily Available Nonmetallocene C2-Symmetrical Zirconium Catalyst". *J Am Chem Soc* **2000**, *122*, 10706-10707.
- (109) Tshuva, E. Y.; Goldberg, I.; Kol, M.; Goldschmidt, Z. "Zirconium Complexes of Amine-Bis(phenolate) Ligands as Catalysts for 1-Hexene Polymerization: Peripheral Structural Parameters Strongly Affect Reactivity". *Organometallics* **2001**, *20*, 3017-3028.
- (110) Segal, S.; Goldberg, I.; Kol, M. "Zirconium and Titanium Diamine Bis(phenolate) Catalysts for α -Olefin Polymerization: From Atactic Oligo(1-hexene) to Ultrahigh-Molecular-Weight Isotactic Poly(1-hexene)". *Organometallics* **2005**, *24*, 200-202.

- (111) Busico, V.; Cipullo, R.; Friederichs, N.; Ronca, S.; Talarico, G.; Togrou, M.; Wang, B. "Block Copolymers of Highly Isotactic Polypropylene via Controlled Ziegler–Natta Polymerization". *Macromolecules* **2004**, *37*, 8201-8203.
- (112) Busico, V.; Cipullo, R.; Friederichs, N.; Ronca, S.; Togrou, M. "The First Molecularly Characterized Isotactic Polypropylene-block-polyethylene Obtained via "Quasi-Living" Insertion Polymerization". *Macromolecules* **2003**, *36*, 3806-3808.
- (113) Cipullo, R.; Busico, V.; Fraldi, N.; Pellecchia, R.; Talarico, G. "Improving the Behavior of Bis(phenoxyamine) Group 4 Metal Catalysts for Controlled Alkene Polymerization". *Macromolecules* **2009**, *42*, 3869-3872.
- (114) Okuda, J. "Complexes with Sterically Demanding Ligands .11. Synthesis and Properties of Trimethyl[1,2,4-Tris(trimethylsilyl)cyclopentadienyl]Titanium". *Chem Ber* **1990**, *123*, 87-88.
- (115) Shapiro, P. J.; Bunel, E.; Schaefer, W. P.; Bercaw, J. E. "[((η -5-C₅Me₄)Me₂Si(η -1-Ncme₃))(Pme₃)Sch]₂ - a Unique Example of a Single-Component Alpha-Olefin Polymerization Catalyst". *Organometallics* **1990**, *9*, 867-869.
- (116) Cano, J.; Kunz, K. "How to synthesize a constrained geometry catalyst (CGC) - A survey". *J Organomet Chem* **2007**, *692*, 4411-4423.
- (117) Kleinschmidt, R.; Griebenow, Y.; Fink, G. "Stereospecific propylene polymerization using half-sandwich metallocene/MAO systems: a mechanistic insight". *J Mol Catal A: Chem* **2000**, *157*, 83-90.
- (118) Devore, D. D.; Timmers, F. J.; Hasha, D. L.; Rosen, R. K.; Marks, T. J.; Deck, P. A.; Stern, C. L. "Constrained-Geometry Titanium(II) Diene Complexes. Structural Diversity and Olefin Polymerization Activity". *Organometallics* **1995**, *14*, 3132-3134.
- (119) Lim, Y. K.; Wallace, S.; Bollinger, J. C.; Chen, X. F.; Lee, D. "Triferrocenes built on a C-3-symmetric ligand platform: Entry to redox-active pseudo-triphenylenes via chelation-driven stereoselection of triple Schiff bases". *Inorg Chem* **2007**, *46*, 1694-1703.
- (120) Wang, C.; Friedrich, S.; Younkin, T. R.; Li, R. T.; Grubbs, R. H.; Bansleben, D. A.; Day, M. W. "Neutral Nickel(II)-Based Catalysts for Ethylene Polymerization". *Organometallics* **1998**, *17*, 3149-3151.
- (121) Younkin, T. R.; Connor, E. F.; Henderson, J. I.; Friedrich, S. K.; Grubbs, R. H.; Bansleben, D. A. "Neutral, Single-Component Nickel (II) Polyolefin Catalysts That Tolerate Heteroatoms". *Science* **2000**, *287*, 460-462.
- (122) Bolm, C.; Legros, J.; Le Paih, J.; Zani, L. "Iron-catalyzed reactions in organic synthesis". *Chem Rev* **2004**, *104*, 6217-6254.

- (123) Bauer, I.; Knolker, H. J. "Iron Catalysis in Organic Synthesis". *Chem Rev* **2015**, *115*, 3170-3387.
- (124) Nakamura, E.; Sato, K. "Managing the scarcity of chemical elements". *Nat Mater* **2011**, *10*, 158-161.
- (125) Furstner, A. "Iron Catalysis in Organic Synthesis: A Critical Assessment of What It Takes To Make This Base Metal a Multitasking Champion". *ACS Central Sci* **2016**, *2*, 778-789.
- (126) Kamata, M.; Kudoh, T.; Kaneko, J.; Kim, H. S.; Wataya, Y. "Fe(II)-mediated fragmentation of 1,4-diaryl-2,3-dioxabicyclo[2.2.2]octanes through competitive single electron transfer pathway and Lewis acid pathway". *Tetrahedron Lett* **2002**, *43*, 617-620.
- (127) Liu, D. L.; Chen, H.; Yin, P.; Ji, N. Y.; Zong, G. X.; Qu, R. J. "Synthesis of Polyacrylonitrile by Single-Electron Transfer-Living Radical Polymerization Using Fe(0) as Catalyst and Its Adsorption Properties after Modification". *J Polym Sci Pol Chem* **2011**, *49*, 2916-2923.
- (128) Queensen, M. J.; Rabus, J. M.; Bauer, E. B. "Ferrocenium hexafluorophosphate as an inexpensive, mild catalyst for the etherification of propargylic alcohols". *J Mol Catal a-Chem* **2015**, *407*, 221-229.
- (129) Subramaniam, P.; Rose, J. J. S. J.; Rathinakumari, R. J. E. "A paradigm shift in rate determining step from single electron transfer between phenylsulfinylacetic acids and iron(III) polypyridyl complexes to nucleophilic attack of water to the produced sulfoxide radical cation: a non-linear Hammett". *J Phys Org Chem* **2016**, *29*, 496-504.
- (130) Toriyama, F.; Cornella, J.; Wimmer, L.; Chen, T. G.; Dixon, D. D.; Creech, G.; Baran, P. S. "Redox-Active Esters in Fe-Catalyzed C-C Coupling". *J Am Chem Soc* **2016**, *138*, 11132-11135.
- (131) Chirik, P. J.; Wieghardt, K. "Radical Ligands Confer Nobility on Base-Metal Catalysts". *Science* **2010**, *327*, 794-795.
- (132) Chirik, P. J. "Preface: Forum on Redox-Active Ligands". *Inorg Chem* **2011**, *50*, 9737-9740.
- (133) Knijnenburg, Q.; Gambarotta, S.; Budzelaar, P. H. M. "Ligand-centred reactivity in diiminepyridine complexes". *Dalton Trans* **2006**, 5442-5448.
- (134) Lyaskovskyy, V.; de Bruin, B. "Redox Non-Innocent Ligands: Versatile New Tools to Control Catalytic Reactions". *ACS Catal* **2012**, *2*, 270-279.
- (135) Blanchard, S.; Derat, E.; Desage-El Murr, M.; Fensterbank, L.; Malacria, M.; Mouries-Mansuy, V. "Non-Innocent Ligands: New Opportunities in Iron Catalysis". *Eur J Inorg Chem* **2012**, 376-389.

- (136) Chen, C. L.; Luo, S. J.; Jordan, R. F. "Cationic Polymerization and Insertion Chemistry in the Reactions of Vinyl Ethers with (α -Diimine) PdMe^+ Species". *J Am Chem Soc* **2010**, *132*, 5273-5284.
- (137) Williams, B. S.; Leatherman, M. D.; White, P. S.; Brookhart, M. "Reactions of vinyl acetate and vinyl trifluoroacetate with cationic diimine Pd(II) and Ni(II) alkyl complexes: Identification of problems connected with copolymerizations of these monomers with ethylene". *J Am Chem Soc* **2005**, *127*, 5132-5146.
- (138) Fedushkin, I. L.; Lukoyanov, A. N.; Dechert, S.; Schumann, H. "Synthesis and molecular structure of calcium difluoranthene, $[\text{Ca}(\text{THF})(6)][\text{C}_{16}\text{H}_{10}]_2$ center dot $2\text{C}_{16}\text{H}_{10}$ ". *Eur J Inorg Chem* **2004**, 2421-2424.
- (139) Fedushkin, I. L.; Skatova, A. A.; Chudakova, V. A.; Fukin, G. K. "Four-step reduction of dpp-bian with sodium metal: Crystal structures of the sodium salts of the mono-, di-, tri- and tetraanions of dpp-bian". *Angew Chem Int Edit* **2003**, *42*, 3294-3298.
- (140) Fedushkin, I. L.; Skatova, A. A.; Lukoyanov, A. N.; Khvoinova, N. M.; Piskunov, A. V.; Nikipelov, A. S.; Fukin, G. K.; Lysenko, K. A.; Irran, E.; Schumann, H. "1,2-Bis(imino)acenaphthene complexes of molybdenum and nickel". *Dalton Trans* **2009**, 4689-4694.
- (141) Khusniyarov, M. M.; Harms, K.; Burghaus, O.; Sundermeyer, J. "Molecular and electronic structures of homoleptic nickel and cobalt complexes with non-innocent bulky diimine ligands derived from fluorinated 1,4-diaza-1,3-butadiene (DAD) and bis(arylimino)acenaphthene (BIAN)". *Eur J Inorg Chem* **2006**, 2985-2996.
- (142) vanAsselt, R.; Elsevier, C. J.; Amatore, C.; Jutand, A. "Divalent palladium and platinum complexes containing rigid bidentate nitrogen ligands and electrochemistry of the palladium complexes". *Organometallics* **1997**, *16*, 317-328.
- (143) Cole, B. E.; Wolbach, J. P.; Dougherty, W. G.; Piro, N. A.; Kassel, W. S.; Graves, C. R. "Synthesis and Characterization of Aluminum- α -diimine Complexes over Multiple Redox States". *Inorg Chem* **2014**, *53*, 3899-3906.
- (144) Wekesa, F. S.; Arias-Ugarte, R.; Kong, L.; Sumner, Z.; McGovern, G. P.; Findlater, M. "Iron-Catalyzed Hydrosilylation of Aldehydes and Ketones under Solvent-Free Conditions". *Organometallics* **2015**, *34*, 5051-5056.
- (145) Stolt, M.; Sodergard, A. "Use of monocarboxylic iron derivatives in the ring-opening polymerization of L-lactide". *Macromolecules* **1999**, *32*, 6412-6417.
- (146) O'Keefe, B. J.; Monnier, S. M.; Hillmyer, M. A.; Tolman, W. B. "Rapid and controlled polymerization of lactide by structurally characterized ferric alkoxides". *J Am Chem Soc* **2001**, *123*, 339-340.

- (147) O'Keefe, B. J.; Breyfogle, L. E.; Hillmyer, M. A.; Tolman, W. B. "Mechanistic comparison of cyclic ester polymerizations by novel iron(III)-alkoxide complexes: Single vs multiple site catalysis". *J Am Chem Soc* **2002**, *124*, 4384-4393.
- (148) Gibson, V. C.; Marshall, E. L.; Navarro-Llobet, D.; White, A. J. P.; Williams, D. J. "A well-defined iron(II) alkoxide initiator for the controlled polymerisation of lactide". *J Chem Soc Dalton* **2002**, 4321-4322.
- (149) McGuinness, D. S.; Marshall, E. L.; Gibson, V. C.; Steed, J. W. "Anionic iron(II) alkoxides as initiators for the controlled ring-opening polymerization of lactide". *J Polym Sci Pol Chem* **2003**, *41*, 3798-3803.
- (150) Wang, X. Y.; Liao, K. R.; Quan, D. P.; Wu, Q. "Bulk ring-opening polymerization of lactides initiated by ferric alkoxides". *Macromolecules* **2005**, *38*, 4611-4617.
- (151) Reeske, G.; Hoberg, C. R.; Hill, N. J.; Cowley, A. H. "Capture of phosphorus(I) and arsenic(I) moieties by a 1,2-bis(arylimino)acenaphthene (aryl-BIAN) ligand. A case of intramolecular charge transfer". *J Am Chem Soc* **2006**, *128*, 2800-2801.
- (152) Bart, S. C.; Hawrelak, E. J.; Lobkovsky, E.; Chirik, P. J. "Low-valent alpha-diimine iron complexes for catalytic olefin hydrogenation". *Organometallics* **2005**, *24*, 5518-5527.
- (153) Muresan, N.; Lu, C. C.; Ghosh, M.; Peters, J. C.; Abe, M.; Henling, L. M.; Weyhermoller, T.; Bill, E.; Wieghardt, K. "Bis(alpha-diimine)iron complexes: Electronic structure determination by spectroscopy and broken symmetry density functional theoretical calculations". *Inorg Chem* **2008**, *47*, 4579-4590.
- (154) Khusniyarov, M. M.; Weyhermuller, T.; Bill, E.; Wieghardt, K. "Tuning the Oxidation Level, the Spin State, and the Degree of Electron Delocalization in Homo- and Heteroleptic Bis(alpha-diimine)iron Complexes". *J Am Chem Soc* **2009**, *131*, 1208-1221.
- (155) Butschke, B.; Fillman, K. L.; Bendikov, T.; Shimon, L. J. W.; Diskin-Posner, Y.; Leituss, G.; Gorelsky, S. I.; Neidig, M. L.; Milstein, D. "How Innocent are Potentially Redox Non-Innocent Ligands? Electronic Structure and Metal Oxidation States in Iron-PNN Complexes as a Representative Case Study". *Inorg Chem* **2015**, *54*, 4909-4926.
- (156) Supej, M. J.; Volkov, A.; Darko, L.; West, R. A.; Darmon, J. M.; Schulz, C. E.; Wheeler, K. A.; Hoyt, H. M. "Aryl-substituted BIAN complexes of iron dibromide: Synthesis, X-ray and electronic structure, and catalytic hydrosilylation activity". *Polyhedron* **2016**, *114*, 403-414.
- (157) Fedushkin, I. L.; Morozov, A. G.; Chudakova, V. A.; Fukin, G. K.; Cherkasov, V. K. "Magnesium(II) Complexes of the dpp-BIAN Radical-Anion: Synthesis, Molecular Structure, and Catalytic Activity in Lactide Polymerization". *Eur J Inorg Chem* **2009**, 4995-5003.
- (158) Jedrzekiewicz, D.; Czelusniak, I.; Wierzejewska, M.; Szafert, S.; Ejfler, J. "Well-controlled, zinc-catalyzed synthesis of low molecular weight oligolactides by ring opening reaction". *J Mol Catal a-Chem* **2015**, *396*, 155-163.

- (159) Ryner, M.; Stridsberg, K.; Albertsson, A. C.; von Schenck, H.; Svensson, M. "Mechanism of ring-opening polymerization of 1,5-dioxepan-2-one and L-lactide with stannous 2-ethylhexanoate. A theoretical study". *Macromolecules* **2001**, *34*, 3877-3881.
- (160) Delle Chiaie, K. R.; Yablon, L. M.; Biernesser, A. B.; Michalowski, G. R.; Sudyn, A. W.; Byers, J. A. "Redox-triggered crosslinking of a degradable polymer". *Polym Chem* **2016**, *7*, 4675-4681.
- (161) Nijenhuis, A. J.; Grijpma, D. W.; Pennings, A. J. "Lewis Acid-Catalyzed Polymerization of L-Lactide - Kinetics and Mechanism of the Bulk-Polymerization". *Macromolecules* **1992**, *25*, 6419-6424.
- (162) Kricheldorf, H. R.; Sumbel, M. V.; Kreiseraunders, I. "Polylactones .20. Polymerization of Epsilon-Caprolactone with Tributyltin Derivatives - a Mechanistic Study". *Macromolecules* **1991**, *24*, 1944-1949.
- (163) Kohn, F. E.; Vandenberg, J. W. A.; Vanderidder, G.; Feijen, J. "The Ring-Opening Polymerization of D,L-Lactide in the Melt Initiated with Tetraphenyltin". *J Appl Polym Sci* **1984**, *29*, 4265-4277.
- (164) Bassi, M. B.; Padias, A. B.; Hall, H. K. "The Hydrolytic Polymerization of Epsilon-Caprolactone by Triphenyltin Acetate". *Polym Bull* **1990**, *24*, 227-232.
- (165) Sheldrick, G. M. *SADABS* **2008**, v2008/1.
- (166) *CrystalClear-SM Expert* **2010**, v2.0.
- (167) Sheldrick, G. M. "A short history of SHELX". *Acta Crystallogr A* **2008**, *64*, 112-122.

APPENDICES

Appendix A –PROGRESS TOWARD OTHER REDOX ACTIVE LIGANDS

A.1 Introduction

The design of new redox active ligands will be imperative to move forward with this project. While the study of redox active catalysis during the formation of PLA will be continued to be studied, we would like to expand our understanding of the use of redox active catalysts into the realm of polyolefin production. Redox-active catalysts can be used to modulate polymerization behavior of lactide to change the rate of polymerization and to incorporate comonomers in a controlled fashion,^{72-74,79,80,103} and we hope to use the fundamental knowledge gained from this dissertation research to achieve similar results during olefin polymerizations in the future. To date, there have only been a few examples of the use of redox active catalysts for the polymerization of α -olefins, but most the catalysts explored contain a redox-active ligand that can only be reduced and usually the reduction is not reversible.^{60,104-106} Therefore incorporation of a ferrocenyl moiety whose redox behavior is easily understood and implemented by many known chemical oxidants and reductants could offer a path to achieve redox switchable polymerizations for α -olefins.⁶¹

All the redox-active moieties discussed in this section of the dissertation are ferrocene-based, which are quasi-reversible functionalities that can be oxidized from the ferrocene derivative (Fe^{II}) to ferrocenium species (Fe^{III}). However, most homogenous ethylene polymerization catalysts require activation by methylaluminoxane (MAO), which contains trialkyl aluminum impurities. Trialkyl aluminum species have been shown to act as a reductant to ferrocenium derivatives, which would mitigate all Fe^{III} species back to Fe^{II} species.¹⁰⁷ This reduction of the Fe^{III} species during polymerization activation prohibits the difference between catalytic electronic species to be observed during polymerization. However, this portion of the dissertation research will describe the design of redox-active ligands that can be used to make catalysts that may be used during the polymerization of α -olefins that would not require activation with MAO; therefore, the catalysts produced from these ligands may display two discrete Fe species during polymerization, so the catalyst's electronic variation using ferrocenyl moieties can be examined during polymerization. Three classes of ligands were chosen to be modified to contain redox active ferrocenyl moieties. The redox active ligands synthesized in this section can be seen in (**Figure A.1**) and described herein.

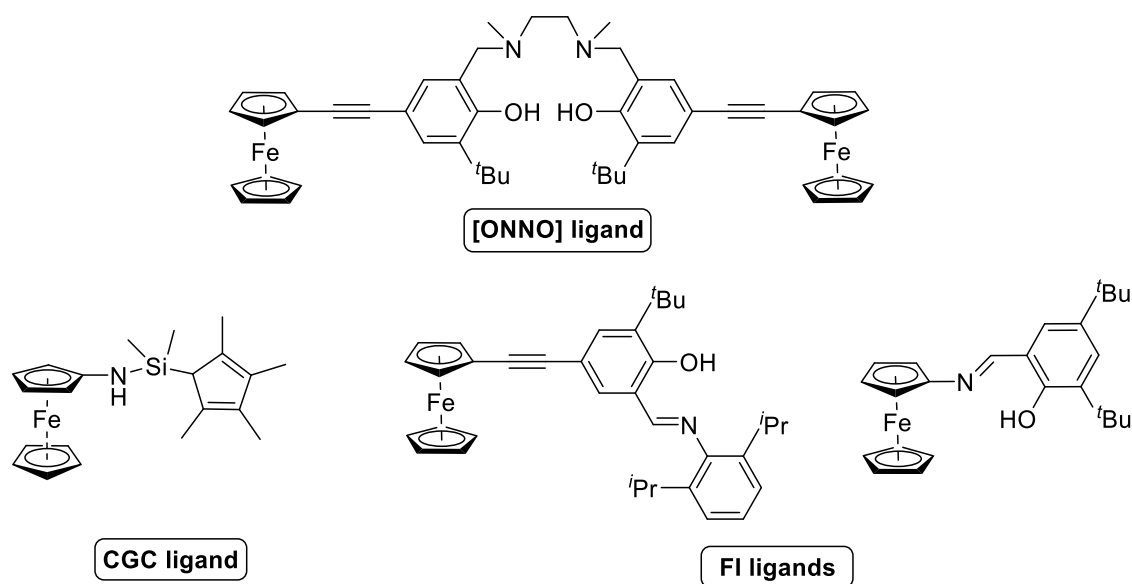


Figure A.1 Ligands synthesized which contain redox-active, ferrocenyl moieties.

A.2 Results and Discussion

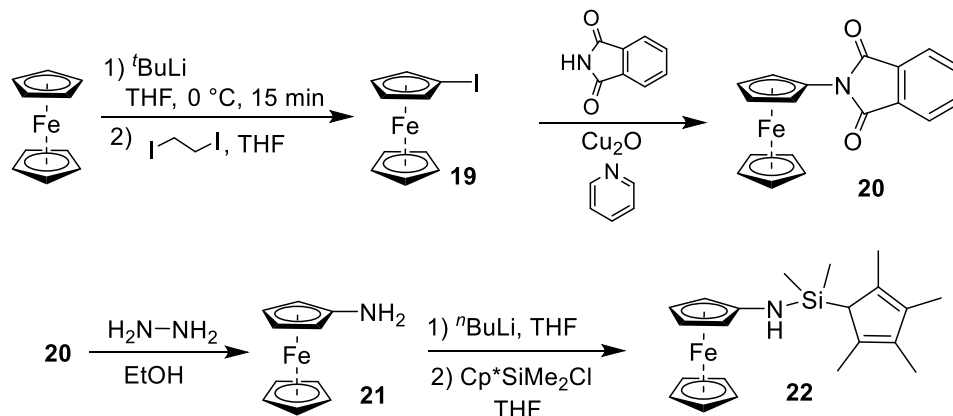
In 2000, Kol and coworkers synthesized tetradentate diamine bis(phenolate), or [ONNO] ligands, which were metallated with group 4 metals and observed their behavior for the polymerization of higher α -olefins, namely propylene and hexene.¹⁰⁸ This was the first example of the living olefin polymerization with a non-metallocene-based catalyst. Since their discovery for olefin polymerizations, it is well known that the ligand design can greatly affect the resultant polymer.¹⁰⁹⁻¹¹³ By changing substituents *para* to the phenol, oligomeric, atactic polyhexene or high molecular weight isospecific polyhexene could be achieved.¹¹⁰ Also, these catalysts were activated with tris(pentafluorophenyl)borane; thus, eliminating the need for MAO and other trialkyl aluminum species from the reaction.¹⁰⁸⁻¹¹⁰ While the electronics of these catalysts can be used to modulate the tacticity of the polymer during propylene and hexane polymerizations, two distinct catalysts must be synthesized to obtain the variation in polymeric material. Therefore, we propose to synthesize an [ONNO]-type ligand which contains redox-active ferrocenyl moieties *para* to the phenol, so the electronic nature of the resulting catalyst can be modulating using a single catalytic species. We hope that this ligand

can one day be used to vary the tacticity of polyolefins using a single catalyst. The synthesis of this ligand was previously described in **Chapter 6**.

Constrained geometry catalysts (CGC)s were introduced in 1990 for their use in ethylene polymerizations.^{114,115} CGCs are metallocene-like catalysts that contain a single cyclopentadienyl (Cp) ring that coordinates to the active metal center instead of two like traditional metallocene catalysts and typically contain a group 3 or 4 metal center. By only having one Cp ring, these ligands typically contain another site that can coordinate to the metal center. There has been several functionalities tested and an amido species was found to be the most optimal for ethylene polymerizations.¹¹⁶ Like traditional metallocene catalysts, CGCs are extremely active during ethylene polymerizations, but they are more thermally stable and can incorporate higher percentages of higher α -olefins comonomers during ethylene copolymerizations. Due to these enhanced features, academia and industry have found this class of catalysts very attractive and optimization of these complexes have been extensively studied. From these studies, it has been determined that the electronics of the catalyst, namely the substituents located on the ligand can have a dramatic effect on the polymerization activity.¹¹⁶⁻¹¹⁸ Therefore, the addition of a redox active moiety within the ligand could be used to modulate polymerization behavior. Thus, we propose ligand **22** which contains a ferrocenyl functionality pendant to the amido portion of the CGC ligand which could be used to vary the electronic nature of the ligand.

Ligand **22** was synthesized starting with commercially available ferrocene (**Scheme A.1**), which was iodinated with *tert*-butyl lithium (*t*BuLi) and 1,2-diiodoethane to give iodoferrocene.¹¹⁹ A substitution reaction of iodoferrocene with phthalimide afforded complex **20**, which underwent a Wolff-Kishner reduction to produce aminoferrocene (**21**).¹¹⁹ Aminoferrocene was reacted with *n*-butyl lithium and upon subsequent addition of chlorodimethyl-(2, 3, 4, 5-tetramethylcyclopenta-2,4-dien-1-yl)silane (Cp*Si(Me)₂Cl) to give ligand **22**.

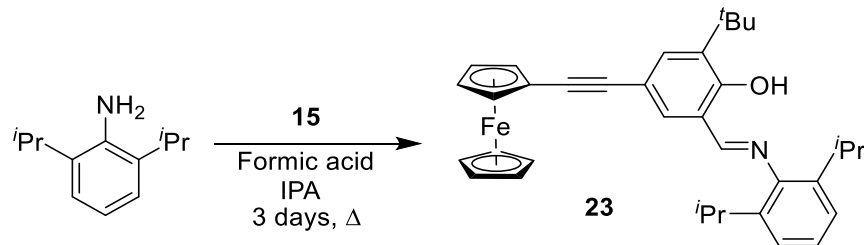
Grubbs and coworkers described the synthesis of phenoxyimine (FI) catalysts and described their use in the polymerization of olefins, specifically ethylene.^{120,121} Their FI ligands were typically metallated with either a group 4 or a group 10 species. The group 10 catalysts, namely the Ni-based catalysts, received attention because they could propagate via a neutral Ni^{II} center instead of the typical cationic species used propagate α -olefin



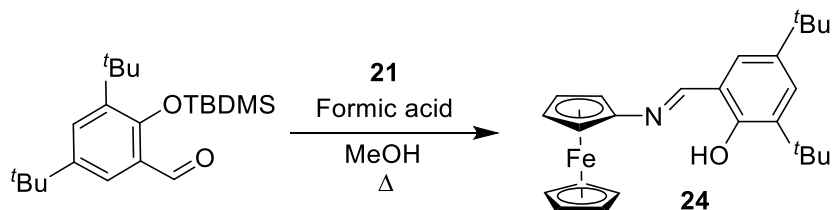
Scheme A.1 Synthesis of constrained geometry ligand **22**.

polymerizations. Because of this, there is no need for other co-catalysts or activators. Specifically, MAO is not needed to activate the polymerization; therefore, trialkyl aluminum species would not be present. However, due to the reduced electrophilic nature of the active metal center, the polymerizations tend to display decreased activity. Therefore, we believe that FI ligands would be a good target. The incorporation of a redox-active moiety that can be oxidized thereby increasing the electrophilicity of the active metal center could increase polymerization activity, which in combination that an activator or other co-catalysts are not needed make FI ligands an ideal target for redox switchable applications.

From this information, complexes **23** and **24** were designed as FI ligands which contained a single ferrocenyl moiety. Compound **23** contains ethynyl ferrocene of the phenol portion while compound **24** contains ferrocene off the imine portion of the ligand. We will use this difference to gain fundamental understanding of how the redox active placement effects olefin polymerization. Compound **23** was synthesized via an imine condensation of 2,6-diisopropylamine with **15** (**Scheme A.2**). Complex **24** was synthesized via imine condensation of aminoferrocene (**21**) with 3,5-di-*tert*-butyl-2((*tert*-butyldimethylsilyl)oxy)benzaldehyde (**Scheme A.3**).



Scheme A.2 Synthesis of FI ligand **23**, which contains a single ferrocenyl unit located on the phenol section of the ligand.



Scheme A.3 Synthesis of FI ligand **24**, which contains a single ferrocenyl moiety located in the imine portion of the ligand.

A.3 Conclusions

In this section, several ligands containing redox active ferrocenyl moieties were designed and synthesized for their potential use in α -olefin polymerizations. Three distinct classes of ligands were described and their potential benefit for incorporating redox activity into these catalyst systems. These ligands can be metallated with either group 4 or group 10 metals and can be activated for α -olefin polymerizations with borane or boranate complexes which will eliminate the use of MAO as a cocatalyst. By eliminating MAO from the polymerization, the reduction of the ferrocenium species to the ferrocene-derivative can be avoided thereby, the difference in polymerization activity may be observed between the two electronic species. These ligand designs will help to fundamentally develop the use of redox active ligands containing ferrocene for the polymerization of ethylene and higher α -olefins.

A.4 Experimental

A.4.1 General Considerations

All reactions were performed under inert nitrogen atmosphere using standard Schlenk technique or the glove box. All solvents were dried via standard solvent purification techniques and degassed via freeze/pump/thaw cycles (x3). All reagents and solvents were purchased from Fisher Scientific, Sigma Aldrich, or synthesized from previously reported methods. NMR spectra was obtained via either a Varian Mercury 300 MHz or a VNMRS 500 MHz instrument at 25 °C and referenced to residual solvent.

A.4.9 Synthesis of Iodoferrocene (19)

Ferrocene (133 mmol, 1 equiv) was added to a Schlenk flask in the glove box. Diiodoethane (1 equiv) was added to a separate Schlenk flask. THF (50 mL) was added to both flasks via cannula. *Tert*-butyl lithium (1 equiv, 1.9 M) was added dropwise to the flask containing ferrocene at 0°C via syringe. The solution was stirred for 15 min before the solution of diiodoethane was added via cannula. The solution was warmed to room temperature and quenched saturated sodium thiosulfate solution (20 mL). The organic layer was extracted with ethyl acetate, dried with magnesium sulfate, and filtered. Iodoferrocene (85% yield) was used without further purification and agreed with previous characterization data.¹¹⁹

A.4.10 Synthesis of *N*-ferrocenyl phthalimide (20)

19 (3.5 g, 10.9 mmol) was added to a Schlenk flask along with phthalimide (1.5 equiv), and copper(I) oxide (0.5 equiv). Pyridine (25 mL) was added via cannula, and the mixture was heated for 24 h at 135 °C. The solution was cooled to room temperature, and the solvent was removed *in vacuo*. The crude material was purified by column chromatography (10:90 ethyl acetate:hexanes) to give a solid product (30% yield). Characterization aligned with previous report.¹¹⁹

A.4.11 Synthesis of Aminoferrocene (21)

20 (600 mg, 1.8 mmol) was added to a Schlenk flask along with absolute ethanol (10 mL). Hydrazine (3.5 mL, 80% solution) was added by syringe, and the resulting mixture was heated at 70 °C for 2 h. The solution was cooled to room temperature and quenched with water (30 mL). The organic layer was extracted with diethyl ether, dried with magnesium sulfate, and filtered. The solvent was removed *in vacuo* to afford the product (82% yield). All characterization matched previous report.¹¹⁹

A.4.12 Synthesis of Ferrocenyldimethyl(2,3,4,5-tetramethylcyclopenta-2,4-dien-1-yl)silane (22)

Aminoferrocene (400 mg, 2 equiv) was added to a Schlenk flask. Pentanes (15 mL) and chlorodimethyl(2,3,4,5-tetramethylcyclopenta-2,4-dien-1-yl)silane (Cp*Si(Me)₂Cl) (1.1 equiv) were added to the flask via syringe at 0 °C. The reaction was slowly warmed to room temperature over 16 h, and the solvent was removed under vacuum. Hexanes was added via cannula and the mixture was filtered. The yellow/orange product was recovered upon removal of hexanes *in vacuo* (189.7 mg, 30% yield). ¹H NMR (C₆D₆), δ, ppm: 0.09 (s, 6H, Si(CH₃)₂), 1.82 (s, 6H, ArCH₃), 1.93 (s, 6H, ArCH₃), 3.77 (t, 2H, CpH), 3.78 (t, 2H, CpH), 4.09 (s, 5H, CpH).

A.4.13 Synthesis of (E)-2-(tert-butyl)-6-(((2,6-diisopropylphenyl)imino)methyl-4-ethynlferrocenophenol (23)

15 (1.0 g, 1 equiv) was added to a 20 mL vial. Isopropanol (5 mL) and 2,6-diisopropylaniline (1.1 equiv) were added the vial. Formic acid (10 drops) was added to the mixture. The solution was refluxed for 2 d. The reaction was cooled to room temperature and the yellow/orange precipitate was filtered. The crude material was purified by column chromatography (10:90 DCM:hexanes) to give an orange solid (1.01 g, 71% yield). ¹H NMR (CDCl₃), δ, ppm: 1.03 (d, 12H, CH(CH₃)₂), 1.43 (s, 9H, (CH₃)₃), 2.95 (sept, 1H, CH(CH₃)₂), 3.98 (t, 2H, CpH), 4.14 (s, 5H, CpH), 4.56 (t, 2H, CpH), 7.09 (s, 3H, ArH), 7.35 (s, 1H, ArH), 7.81 (s, 1H, ArH), 7.92 (s, 1H, HC=N), 14.34 (s, 1H, OH).

**A.4.14 Synthesis of (E)-2,4-di-tert-butyl-6-
(((ethynylferrocene)imino)methyl)phenol (24)**

Aminoferrocene (250 mg, 1 equiv) and 3,5-di-*tert*-butyl-2((*tert*-butyldimethylsilyloxy)benzaldehyde (1 equiv) were added to a Schlenk flask. Methanol was added via cannula. Formic acid (10 drops) was added via syringe, and the mixture was heated at 65 °C for 12 h. The solution was cooled to room temperature, and the product was filtered and washed with MeOH to give a pink solid (498 mg, 96% yield). ¹H NMR (C₆D₆), δ, ppm: 1.34 (s, 9H, (CH₃)₃), 1.69 (s, 9H, (CH₃)₃), 3.95 (s, 5H, CpH), 3.97 (t, 2H, CpH), 4.34 (t, 2H, CpH), 7.10 (s, 1H, ArH), 7.83 (s, 1H, ArH), 8.42 (s, 1H, HC=N).

Appendix B–POLYMERIZATION OF LACTIDE WITH AN IRON CATALYST

A version of this chapter has been submitted to a peer-reviewed journal for review by Lauren A. Brown, Francis S. Wekesa, Daniel K. Unruh, Michael Findlater, and Brian K. Long:

Lauren A. Brown, Francis S. Wekesa, Daniel K. Unruh, Michael Findlater, and Brian K. Long. "BIAN-Fe(η^6 -C₆H₆): Synthesis, Characterization, and L-Lactide Polymerization." *Submitted*.

I was responsible for the synthesis and characterization of all polymers reported, kinetic studies and analysis, and preparation of the manuscript. Francis S. Wekesa and Daniel K. Unruh were responsible for the synthesis and characterization of the catalyst. Dr. Brian Long and Dr. Michael Findlater advised this work.

B.1 Abstract

The α -diimine-ligated Fe-complex, **BIAN-Fe(C₆H₆)**, was synthesized and evaluated for the polymerization of L-lactide. Characterization of **BIAN-Fe(C₆H₆)** reveals that it is redox non-innocent and suggests that it is an Fe(I) species bearing a radical-anionic ligand. Furthermore, we demonstrate that **BIAN-Fe(C₆H₆)** is active for the ring-opening polymerization (ROP) of L-lactide, and that polymer is produced with, or without, the use of an added external initiator. Interestingly, very high molecular weight polymers are produced in the absence of external initiator whereas polymer molecular weights that agree with theoretical calculations are produced in the presence of external initiator. To the best of our knowledge, **BIAN-Fe(C₆H₆)** is the first iron α -diimine catalyst reported to be active for the polymerization of L-lactide.

B.2 Introduction

The direct replacement of precious metals with 1st row, Earth-abundant congeners has become an area of intense research interest.^{122,123} Beyond the obvious economic motivations, the environmental costs associated with the extraction of rare elements from the Earth's crust concomitant with the geopolitical nature of supply and distribution of such elements are also important drivers in this field.¹²⁴ However, the unparalleled activity, selectivity and general ease of handling has rendered precious metal catalysts among the

most widely utilized systems in synthetic chemistry. While somewhat simplistic, the ease with which noble metals undergo 2-electron transfer processes is often invoked as the dominant factor in their underlying success.¹²⁵ In contrast, although base metals (like iron) may undergo 2-electron processes, 1-electron chemistry is competitive and, in many cases, the preferred reaction mode.¹²⁶⁻¹³⁰ Thus, the management of redox events via metal-ligand cooperativity through the use of redox non-innocent ligands has become an increasingly popular strategy to render nobility to base metal chemistry.¹³¹⁻¹³⁵

It is in this vein that we began to explore the use of iron complexes of the bis(arylimino)-acenaphthene (BIAN) ligands. Such ligands, formed from the fusion of an α -diimine fragment with naphthalene, have found widespread use in coordination chemistry and catalysis.^{60,64,136,137} Moreover, they are known to undergo multiple, successive electron-accepting redox events making it an attractive ligand scaffold to deploy in redox non-innocent applications.^{60,104,106,138-143} Our initial forays into this field have focused on the generation of **BIAN-Fe(arene)** complexes as pre-catalysts in the hydrosilylative reduction of carbonyl-containing moieties.¹⁴⁴

Inspired by recent reports in which related redox-active iron complexes have been successfully shown to mediate polymerizations of cyclic esters,^{78,145-150} we hypothesized that these unique **BIAN-Fe(arene)** complexes may also be suitable catalyst for this application. In particular, the ring-opening polymerization (ROP) of L-lactide has become a central reaction for the evaluation of catalysts containing non-innocent ligands. Thus, herein we will describe the synthesis and evaluation of **BIAN-Fe(C₆H₆)** as a catalyst for the ROP of L-lactide. We will demonstrate that poly(lactic acid) (PLA) molecular weights greater than 300,000 g/mol could be achieved using **BIAN-Fe(C₆H₆)** in the absence of an external initiator, whereas addition of an external initiator permitted precise control over polymer molecular weights. The ability to reach such high PLA molecular weights (> 30,000 g/mol) has traditionally proven to be difficult.^{73,76,79} Lastly, to the best of our knowledge, **BIAN-Fe(C₆H₆)** is the first example of an Fe-based α -diimine catalyst to generate polylactide with or without the use of an external initiator.

B.3 Results and Discussion

B.3.1 Synthesis and Characterization of *BIAN-Fe(C₆H₆)*

Treatment of a pentane/benzene solution of **BIAN-FeCl₂**¹⁴⁴ with sodium-mercury amalgam for 48 h at ambient temperature resulted in a deep red reaction mixture which, upon workup, afforded the desired η^6 -arene complex, **BIAN-Fe(C₆H₆)** in moderate yield (**Figure B.1**). The formally Fe(0), 18- electron complex was characterized using multinuclear NMR spectroscopy and single crystal X-ray diffraction experiments. The ¹H NMR spectrum of **BIAN-Fe(C₆H₆)**, shown in , is consistent with a structure which displays C_{2v} symmetry. Also of note is the upfield-shifted resonance at 5.3 ppm corresponding to the hydrogens on the bound benzene. This is confirmed by preparation of the benzene-D₆ compound, where the bound arene is observed at 5.3 ppm in the ¹H NMR spectrum recorded in benzene. **BIAN-Fe(C₆H₆)** crystallizes as red blocks from pentane solution in the triclinic space group P-1. The solid state comprises monomers of **BIAN-Fe(C₆H₆)** (**Figure B.2**) and there are no short intermolecular contacts. Unsurprisingly, the benzene cap adopts the η^6 -binding motif which gives rise to an 18-electron metal complex. The C-C and C-N bond distances of the diimine fragment are 1.407(2) and 1.340(2) Å, respectively. The C-C and C-N bond lengths in the diimine ligand backbone are considered an important measure of the oxidation state of this type of ligand.¹⁵¹⁻¹⁵⁵ In **BIAN-Fe(C₆H₆)** these distances are intermediate between a neutral diimine ligand (two short C=N bonds and one long C-C bond) and those with a fully reduced dianionic diimine ligand (two long C-N bonds and one short C=C bond). These values are suggestive of the occurrence of a single electron-transfer event to afford a radical-anionic ligand and a (formally) Fe(I) center. This conclusion is supported by recent theoretical calculations¹⁵⁶ reported for the **BIAN-Fe(C₇H₈)**¹⁴⁴ toluene capped analogue.

B.3.2 *L*-lactide Polymerization

Initial polymerizations of *L*-lactide using **BIAN-Fe(C₆H₆)** were performed in benzene-D₆ and monitored via variable temperature ¹H NMR spectroscopy. Each polymerization was conducted at 90 °C and studied as a function of monomer concentration (0.75, 0.5, and 0.25 M). As a note, monomer concentrations below 0.25 M resulted in

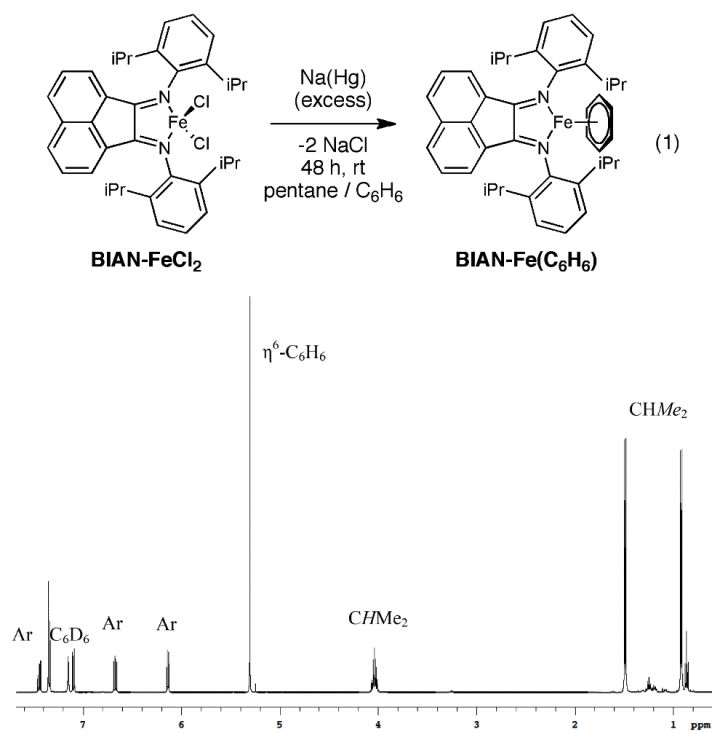


Figure B.1 ¹H NMR spectrum of **BIAN-Fe(C₆H₆)** illustrating η⁶-bound benzene and apparent diamagnetic nature of complex.

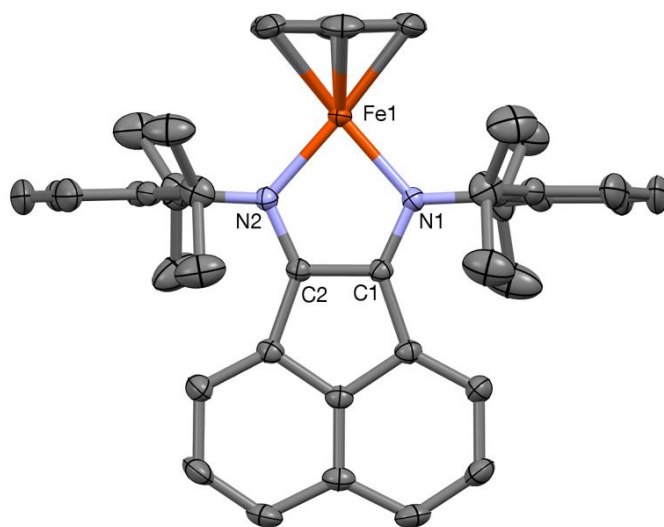


Figure B.2 Molecular structure of **BIAN-Fe(C₆H₆)**. Thermal ellipsoids are drawn at the 30% level for optimal viewing. Hydrogen atoms are excluded for clarity.

remarkably long reaction times, while monomer concentrations above 0.75 M resulted in polymerization rates too fast to be easily monitored by ^1H NMR spectroscopy.

These initial NMR scale experiments showed that **BIAN-Fe(C₆H₆)** readily polymerized L-lactide, and that monomer conversions exceeded 90% for all concentrations investigated (**Figure B.3**). However unexpectedly, upon reaching approximately 30% monomer conversion for each concentration evaluated, a dramatic acceleration in polymerization rate was observed which was accompanied by a simultaneous dramatic increase in polymerization solution viscosity. Based on these observations, we hypothesize that the observed rate acceleration is due to the so called 'gel effect' and autoacceleration. A similar increase in polymer solution viscosity has also been reported for L-lactide polymerization using an analogous magnesium(II) complex containing a dpp-BIAN (dpp-BIAN = 1,2-bis[(2,6-diisopropylphenyl)imino]acenaphthene) ligand.¹⁵⁷ Furthermore, an induction period was observed for each polymerization but decreased as a function of increasing monomer concentration.

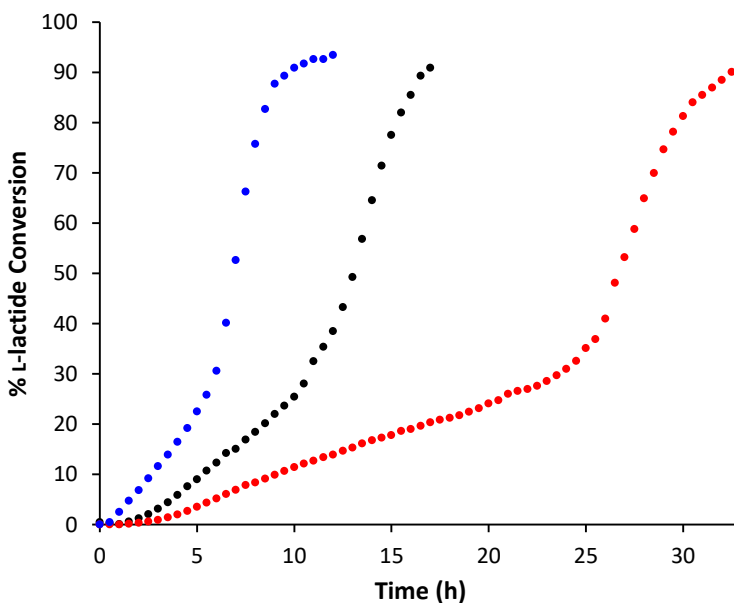


Figure B.3 Plot of percent conversion versus time for the polymerization of L-lactide (50 equiv) at 90 °C using **BIAN-Fe(C₆H₆)** as the catalyst with varying concentrations of monomer 0.75 M (blue), 0.5 M (black), and 0.25 (red) in C₆D₆.

Though these preliminary results clearly suggest that **BIAN-Fe(C₆H₆)**, is a competent catalyst for the polymerization of L-lactide, the mechanistic role of the Fe-complex in these polymerizations was somewhat unclear. For transition-metal mediated polymerizations of L-lactide, multiple mechanisms have been either proposed or proven. Examples of these include coordination-insertion based mechanism and even simple Lewis acid based mechanism which are often referred to as an “activated monomer mechanism”.^{70,158,159} Catalysts that initiate and propagate via coordination-insertion based mechanisms are those that typically contain nucleophilic or alkoxide-derived ligands. These catalysts propagate via a sequential series of monomer coordination and intramolecular insertion at the active metal center. In contrast, catalysts that proceed via Lewis acid catalysis simply involve coordination of the monomer to the electrophilic transition metal center. This coordination activates the monomer towards nucleophilic attack by another species in solution, such as an added external initiator (i.e. R-OH), in an intermolecular fashion.^{74,81,160}

Due to the absence of any nucleophile or alkoxide-based ligands in **BIAN-Fe(C₆H₆)** or presence of externally added initiating source, we hypothesize that our polymerizations likely proceed via an activated monomer mechanism and that the polymerizations shown in **Figure B.3** are likely initiated by miniscule amounts of adventitious H₂O or other nucleophilic species present in the monomer or solvent being used. It should be noted that many reports exist in which the true nature of the initiating species is unclear, and many also speculate the presence of trace impurities are the likely source of initiation.¹⁶¹⁻¹⁶⁴

Operating under this hypothesis, we utilized variable temperature ¹H NMR spectroscopy (90 °C) to study L-lactide polymerizations using **BIAN-Fe(C₆H₆)** as a function of added external initiator in an effort to better understand the initiation process for these polymerizations (**Figure B.4**). For these studies, we chose 4-methoxyphenol as our external initiator as it has been used successfully for lactide polymerizations with other Fe-based catalysts containing non-innocent ligands.^{74,81,160} When 4-methoxyphenol was added to our polymerizations, plots of monomer conversion versus time showed that no autoacceleration occurred and the polymerization solution no longer became extremely viscous (**Figure B.4**), which was in stark contrast to what was previously observed in the absence of added external initiator (**Figure B.3**). Detailed PLA end-group analysis via ¹H NMR spectroscopy clearly

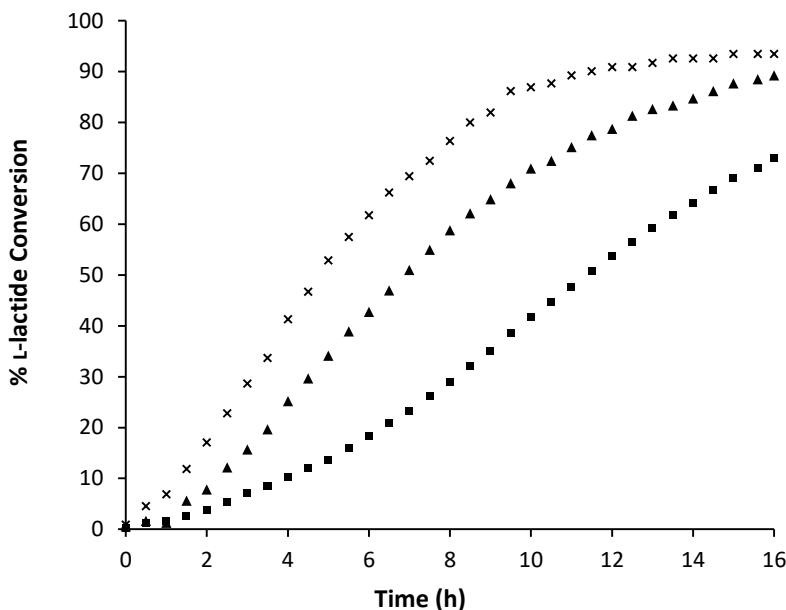


Figure B.4 Plot of percent conversion versus time for the polymerization of lactide (50 equiv, 0.5 M) in C_6D_6 at 90 °C using **BIAN-Fe(C₆H₆)** with either 2 equiv (triangle), 1 equiv (square), or 0.5 equiv (x) or 4-methoxyphenol present.

showed that presence of 4-methoxyphenol substituents at the polymer chain ends (**Figure B.5**) suggesting that a nucleophilic species is required to initiate polymerization. However, it does not differentiate if: (1) **BIAN-Fe(C₆H₆)** proceeds via a Lewis acidic mechanism with subsequent nucleophilic attack of activated monomer by the phenolic species, or (2) if an Fe-alkoxide species is produced upon reaction with the added phenolic initiator that is then the active species that polymerizes via a coordination-insertion based mechanism.

Further analysis of polymerization rates when using **BIAN-Fe(C₆H₆)** revealed that upon addition of 0.5 equiv of 4-methoxyphenol (relative to **BIAN-Fe(C₆H₆)**), the polymerization reached approximately 93% monomer conversion after 16 h. However, when 1.0 or 2.0 equiv of 4-methoxyphenol were added, a dramatic decrease in the polymerization rate was observed, ultimately reaching 89% or 73% conversion after 16 h, respectively. This suggests that **BIAN-Fe(C₆H₆)** displays a negative rate-order dependence with respect to 4-methoxyphenol (**Figure B.6**).

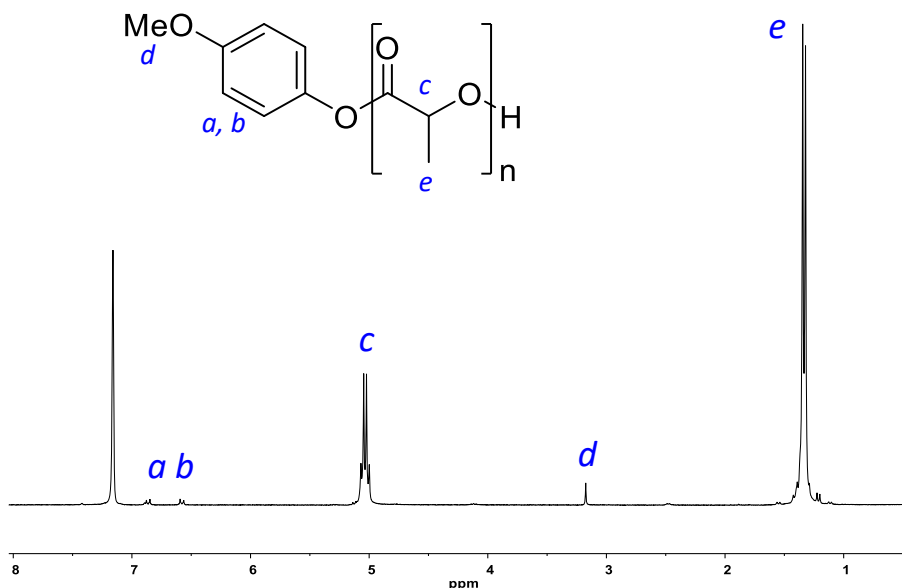


Figure B.5 ^1H NMR spectrum of end-group analysis for polymer obtained with L-lactide (50 equiv, 0.5 M) in C_6D_6 at 90°C using **BIAN-Fe(C₆H₆)** (1 equiv) and 4-methoxyphenol (2 equiv).

To better understand the source of this unusual negative polymerization rate dependence as a function of added initiator, we used ^1H NMR spectroscopy to detect any possible deleterious side-reactions between **BIAN-Fe(C₆H₆)** and 4-methoxyphenol. Using reaction concentrations and temperatures (90°C) identical to the polymerization conditions examined, it became apparent that one or more new paramagnetic species were being generated in-situ, as was evidenced by the resultant broad and complex ^1H NMR spectrum (**Figure B.7**). Based on this observation, we hypothesize that the observed negative rate-order dependence of polymerization rate on added initiator can be attributed to deactivation and/or decomposition of **BIAN-Fe(C₆H₆)** by reaction with 4-methoxyphenol. Additionally, these paramagnetic species complicated further attempts to measure additional kinetic aspects of this polymerization.

With these pieces in hand, larger scale polymerization studies were conducted in order to evaluate the PLA molecular weight (M_n) and molecular weight dispersities (\mathcal{D}) formed using **BIAN-Fe(C₆H₆)** (**Table B.1**). PLA produced using **BIAN-Fe(C₆H₆)** without any added 4-methoxyphenol reached a remarkable 319 kg/mol, which is roughly 45 times higher

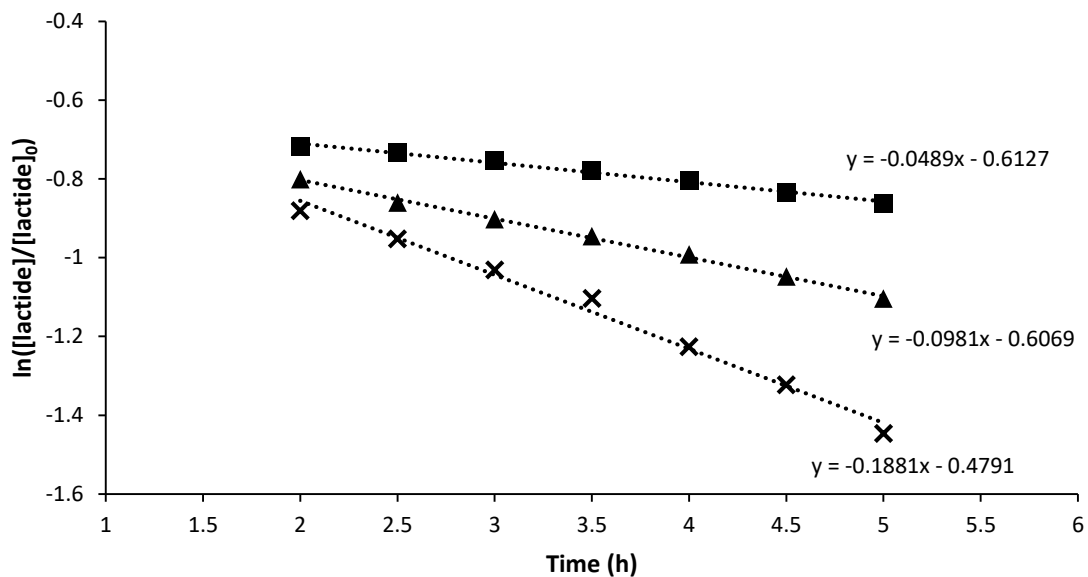


Figure B.6 Kinetic study L-lactide polymerization using **BIAN-Fe(C₆H₆)** and either 2 equiv (square), 1 equiv (triangle), or 0.5 equiv (x) of 4-methoxyphenol.

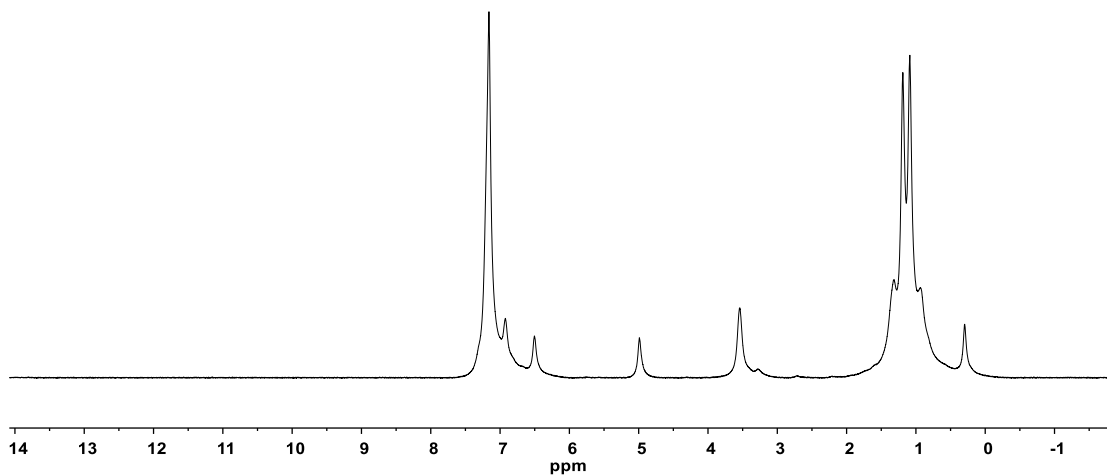


Figure B.7 ¹H NMR spectrum of **BIAN-Fe(C₆H₆)** (1 equiv, 9 μmol) and 4-methoxyphenol (2 equiv) in C₆D₆ after being heated for 90 °C for 5 h.

than theoretical molecular weight calculated on the basis of monomer conversion and assuming one chain per Fe center ($M_n^{\text{theo}} = 6.9 \text{ kg/mol}$) (**Table B.1**, entry 1). Addition of 4-methoxyphenol as an external initiator to L-lactide polymerizations using **BIAN-Fe(C₆H₆)** provided PLA with significantly lower molecular weights ($M_n = 35.1 - 6.7 \text{ kg/mol}$) (**Table B.1**, entries 2-4).

The polymers produced using **BIAN-Fe(C₆H₆)** and added 4-methoxyphenol were found to decrease in a linear fashion relative to the concentration of external initiator used. Molecular weights determined via gel permeation chromatography (GPC) agreed closely with those estimated via ¹H NMR spectroscopy, strongly suggesting that all polymer chains are indeed initiated by the added 4-methoxyphenol. Furthermore, it was noted that the molecular weights obtained via GPC and NMR were consistently twice that of their theoretical values (M_n^{theo}), though still following the expected decreasing trend predicted as initiator concentration is increased. Lastly, the molecular weight dispersity for each sample remained relatively narrow ($D < 1.75$) for all PLA produced when using **BIAN-Fe(C₆H₆)** with and without added external initiator.

Table B.1 L-lactide Polymerization using **BIAN-Fe(C₆H₆)**^a

entry	time (h)	BIAN-Fe(C₆H₆) : init. ^a	conv. ^b (%)	M_n^c (kg/mol)	$M_n^{\text{NMR}d}$ (kg/mol)	$M_n^{\text{theo}e}$ (kg/mol)	M_w/M_n^c
1	17	1 : 0.0	96	319.1	–	6.9	1.72
2	17	1 : 0.5	97	35.1	36.2	13.6	1.60
3	17	1 : 1.0	94	12.4	12.1	6.7	1.67
4	17	1 : 2.0	95	6.7	5.8	3.4	1.55

^aPolymerization conditions: **BIAN-Fe(C₆H₆)** (0.014 mmol), monomer (0.7 mmol, 0.5 M), initiator, 1,3,5-trimethoxybenzene (0.035 mmol), 0.7 mL of C₆H₆. ^bConversion was determined using ¹H NMR at 90 °C. ^cDetermined using gel permeation chromatography at 40 °C in THF and are reported relative to polystyrene standards. ^dDetermined using ¹H NMR spectroscopy via integration of phenolic signals to those of the PLA backbone. ^eTheoretical M_n was calculated on the basis of conversion and assuming one chain per initiator species.

B.4 Conclusions

In summary, we have synthesized an Fe-based α -diimine complex, **BIAN-Fe(C₆H₆)**, and investigated its behavior for the polymerization of L-lactide. In the absence of any added

external initiator, very high molecular weight PLA was obtained (>300 kg/mol). When 4-methoxyphenol was added as an external initiator, PLA molecular weights were found to be linearly dependent on initiator concentration and were consistent with theoretical molecular weights (M_n^{theo}). It is clear from ^1H NMR analysis of the PLA formed, that *p*-methoxy phenoxide end groups are present, thereby highlighting the role of this initiating species. Based on this information, and due to the formation of paramagnetic iron complexes arising from reactions between 4-methoxyphenol and **BIAN-Fe(C₆H₆)**, we were unable to conclusively determine the mechanistic role of **BIAN-Fe(C₆H₆)** in these L-lactide polymerizations. Further studies are currently being pursued to elucidate the identity of the catalytically active species and mechanism of these polymerizations.

B.5 Experimental

B.5.1 General Considerations

All reagents were purchased from commercial vendors, and were used without further purification unless otherwise noted. CH₃CN was distilled from CaH₂. BIAN-FeCl₂ was prepared according to literature methods.¹⁴⁴ L-lactide was purchased from Fisher Scientific and recrystallized twice in toluene prior to use. 1,3,5-trimethoxybenzene (TMB) was purchased from Fisher Scientific and recrystallized in diethyl ether twice prior to use. All manipulations of oxygen- and moisture-sensitive materials were conducted with a standard Schlenk technique or in a glovebox. Flash column chromatography was performed using silica gel (230-400 mesh). Analytical thin layer chromatography (TLC) was performed on 60 F254 (0.25 mm) plates and visualization was accomplished with UV light (254 and 354 nm) and/or an aqueous alkaline KMO₄ solution followed by heating. Proton and carbon nuclear magnetic resonance spectra (^1H NMR and ^{13}C NMR) were recorded on a Jeol 400 MHz spectrometer with Me₄Si or solvent resonance as the internal standard (^1H NMR, Me₄Si at 0 ppm, CHCl₃ at 7.26 ppm, C₆D₆ at 7.15 ppm, CD₂Cl₂ at 5.32 ppm; ^{13}C NMR, Me₄Si at 0 ppm, CDCl₃ at 77.0 ppm, C₆D₆ at 128.4 ppm, CD₂Cl₂ at 53.8 ppm). ^1H NMR data are reported as follows: chemical shift, multiplicity (s = singlet, d = doublet, t = triplet, q = quartet, quint = quintet, sext = sextet, sept = septet, br = broad, m = multiplet), coupling constants (Hz), and integration. Gas chromatography-mass spectrometry (GC-MS) and high-resolution mass spectrometry

(HRMS) was performed on an electron ionization ISQ™ QD mass spectrometer. Melting points were recorded using a capillary melting point apparatus and are uncorrected. Molecular weights (M_n) of the polymers were determined using a Tosoh EcoSEC GPC at 40 °C in THF and referenced to polystyrene standards. ^1H NMR of the polymers were recorded on a Bruker 400 MHz spectrometer at 90 °C; chemical shifts are reported with respect to residual solvent peaks, 7.16 ppm (C_6D_6).

B.5.2 X-ray crystallography

Data for **BIAN-Fe(C_6H_6)** were obtained on a Bruker Smart Apex II CCD diffractometer. All data were collected at 100 K using graphite-monochromated Mo- $\text{K}\alpha$ radiation ($\lambda = 0.71073 \text{ \AA}$). Intensity data were collected using ω -steps accumulating area detector images spanning at least a hemisphere of reciprocal space. All the data were corrected for Lorentz polarization effects. A multi-scan absorption correction was applied using SADABS¹⁶⁵ or CrystalClear.¹⁶⁶ Structures were solved by direct methods and refined by full-matrix least squares against F^2 (SHELXTL¹⁶⁷). All hydrogen atoms were assigned riding isotropic displacement parameters and constrained to idealized geometries. CCDC-1451878 contains the supplementary crystallographic data for this paper. These data can be obtained free of charge from the Cambridge Crystallographic Data Center (CCDC).

B.5.3 Preparation of BIAN-Fe(C_6H_6)

In a dry box, a 100mL round-bottom flask was charged with 57.699 g Hg (288 mmol) and approximately 10 mL pentane. With stirring, 0.289 g Na (12.5 mmol) was added, and the amalgam was stirred for 30 minutes. Then, 1.564g (2.49 mmol) of **BIAN-FeCl₂** were added with 20 mL of pentane and 10 mL of benzene. The resulting solution was allowed to stir for 48 h under ambient conditions to form a red solution. The reaction mixture was decanted and filtered through Celite®. The filtrate was collected, and the solvent was removed in vacuum to yield 0.745g (46.0%) crude red product. ^1H NMR (C_6D_6): δ 0.92 (d, 7.0Hz, 12H, $\text{CH}(\text{CH}_3)_2$), 1.49 (d, 6.5Hz, 12H, $\text{CH}(\text{CH}_3)_2$), 4.04 (sept, 6.5Hz, 4H, $\text{CH}(\text{CH}_3)_2$), 5.41 (s, 6H, C_6H_6), 6.14 (d, 6.5Hz, 2H), 6.67 (dd, 7.0Hz, 2H), 7.10 (d, 8.0Hz, 2H), 7.34 (d, 7.5Hz, 4H), 7.44 (t, 8Hz, 2H). ^{13}C NMR (C_6D_6): δ 24.30, 25.51, 28.51, 81.60, 118.96, 123.97, 124.17, 126.70, 130.80, 132.48, 136.87, 141.52, 152.34, 152.85.

B.5.4 General Procedure for NMR Scale Polymerizations

In a glove box, L-lactide (75, 50, or 25 equiv), **BIAN-Fe(C₆H₆)** (1 equiv), 1,3,5-trimethoxybenzene (internal standard, 2.5 equiv), and C₆D₆ (0.7 mL) was added to a J. Young NMR tube. As appropriate, 4-methoxyphenol (0.5, 1, or 2 equiv) was added J Young tube. The NMR tube was removed from the glove box, and the polymerization was monitored by ¹H NMR spectroscopy for up to 17 hours by placing the sample in a preheated Bruker Avance 400 MHz NMR at 90 °C. The command “multizg” was used to collect data every 10 or 30 minutes. The data was processed with XWinNMR3.6. Conversion of L-lactide was monitored by ¹H NMR where the methine peak of the monomer was compared to the methyl peak of the internal standard, 1,3,5-trimethoxybenzene.

B.5.5 General Procedure for Larger Scale Polymerizations

In a glove box, L-lactide (50 equiv), **BIAN-Fe(C₆H₆)** (1 equiv), 1,3,5-trimethoxybenzene (internal standard, 2.5 equiv), and C₆H₆ (1.4 mL) was added to a vial. As appropriate, 4-methoxyphenol (0.5, 1, or 2 equiv) was added to the vial. The polymerization was performed in the glovebox. After 17 hours, the polymerization was quenched and conversion was determined by ¹H NMR spectroscopy. The data was processed with XWinNMR3.6. Conversion of L-lactide was determined by comparing the integration of the methine peak of the monomer to the methyl peak of the internal standard, 1,3,5-trimethoxybenzene.

B.5.6 Procedure for BIAN-Fe(C₆H₆) Decomposition Study

In the glove box, **BIAN-Fe(C₆H₆)** (1 equiv, 9 μmol) and 4-methoxyphenol (2 equiv) were added to a J. Young NMR tube along with 0.7 mL of C₆D₆. All NMR spectra for this procedure was obtained on a Varian 500 MHz NMR at 25 °C. ¹H NMR was taken prior to heating, after 30 min of heating at 90 °C, and after 5 h of heating at 90 °C.

B.6 Supporting Information

B.6.1 ^1H NMR Spectroscopy

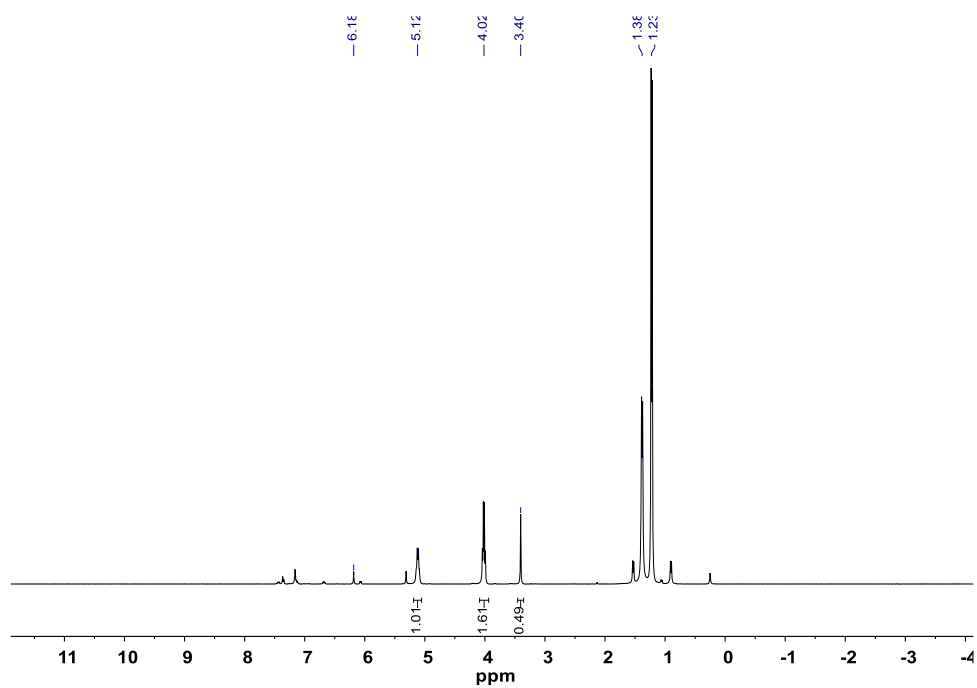


Figure B.8 Representative ^1H NMR spectrum (400 MHz, 90 °C, C_6D_6) of polymerization with 50 equiv. of L-lactide and **BIAN-Fe(C_6H_6)**.

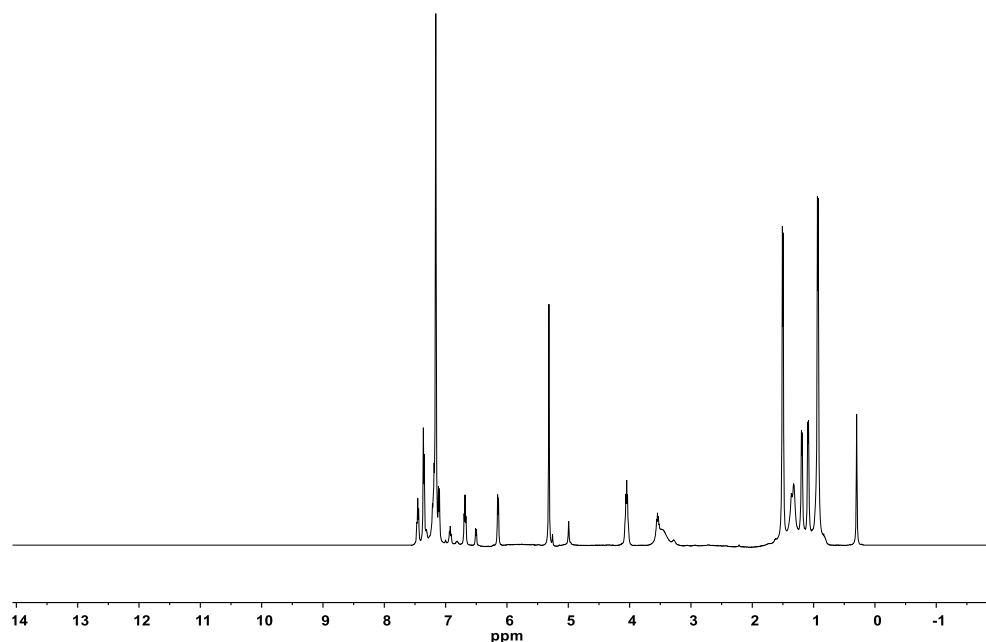


Figure B.9 ^1H NMR spectrum of **BIAN-Fe(C₆H₆)** (1 equiv, 9 μmol) and 4-methoxyphenol (2 equiv) in C_6D_6 after being heated for 90 $^\circ\text{C}$ for 30 minutes.

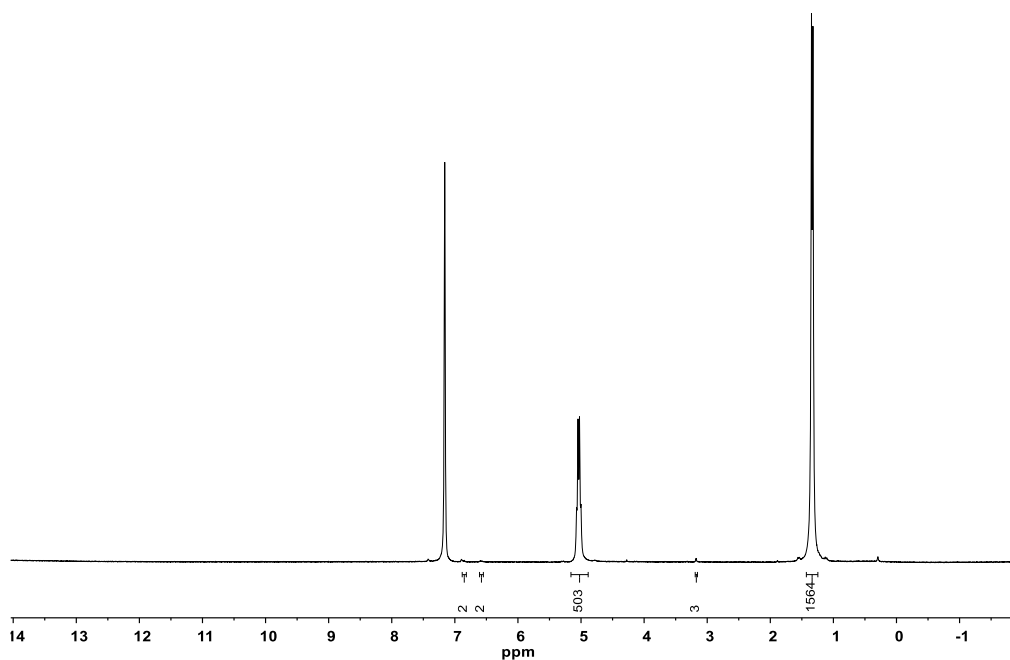


Figure B.10 ^1H NMR spectrum of PLA (**Table B.1**, entry 2) produced with **BIAN-Fe(C₆H₆)** (1 equiv, 9 μmol) and 4-methoxyphenol (0.5 equiv) in C_6D_6 . Used to calculate M_n^{NMR} .

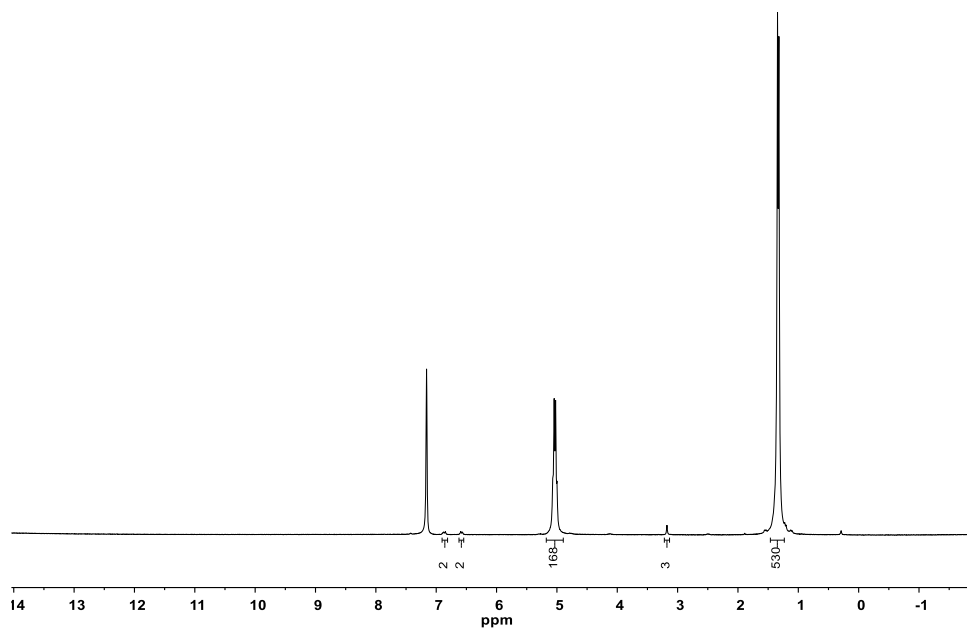


Figure B.11 ¹H NMR spectrum of PLA (**Table B.1**, entry 3) produced with **BIAN-Fe(C₆H₆)** (1 equiv, 9 μmol) and 4-methoxyphenol (1.0 equiv) in C₆D₆. Used to calculate M_n^{NMR} .

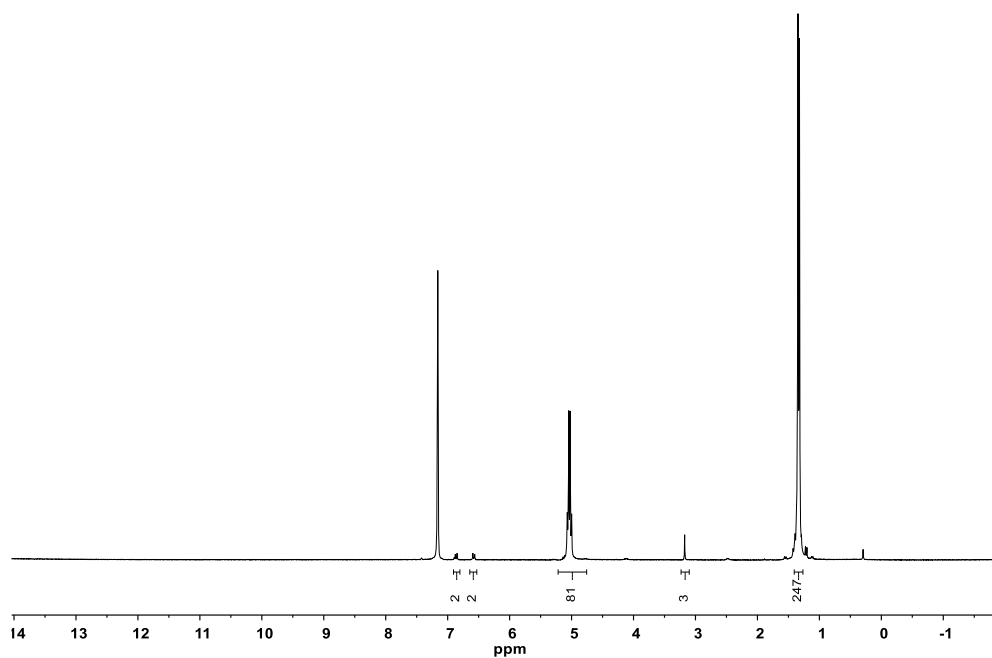
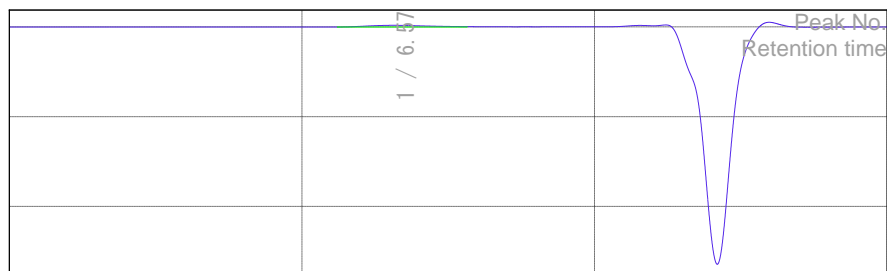


Figure B.12 ¹H NMR spectrum of PLA (**Table B.1**, entry 4) produced with **BIAN-Fe(C₆H₆)** (1 equiv, 9 μmol) and 4-methoxyphenol (2.0 equiv) in C₆D₆. Used to calculate M_n^{NMR} .

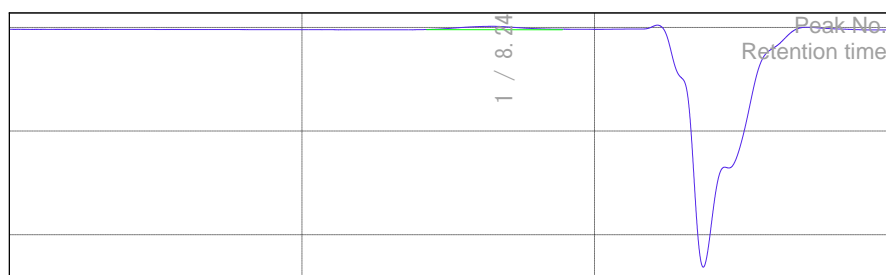
B.6.2 Gel Permeation Chromatography



Result of molecular weight calculation (RI)
Peak 1 Valley Peak

	min]	[mV	[mol	Mn	
Peak start	5.603	0.108	3,189,997	Mw	319,065
Peak top	6.570	3.683	519,099	Mz	548,542
Peak end	7.828	0.671	83,756	Mz+1	859,393
				Mv	1,177,542
Height [mV]			3.824	Mp	548,542
Area [mV*sec]			280.583	Mz/Mw	483,595
Area% [%]			100.000	Mw/Mn	1.567
[eta]			548541.51880	Mz+1/Mw	1.719
					2.147

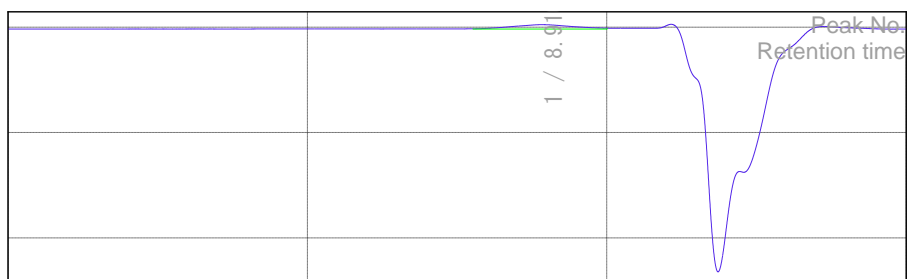
Figure B.13 GPC trace of PLA formed with **BIAN-Fe(C₆H₆)**. Samples measured in THF at 40 °C and referenced to polystyrene standards (**Table B.1**, Entry 1).



Result of molecular weight calculation (RI)
Peak 1 Valley Peak

	min]	[mV	[mol	Mn	
Peak start	7.125	-	203,100	Mw	35,075
Peak top	8.248	1.140	46,619	Mz	55,931
Peak end	9.455	-	7,378	Mz+1	78,877
		1.674		Mv	99,893
Height [mV]			3.279	Mp	55,931
Area [mV*sec]			241.655	Mz/Mw	53,747
Area% [%]			100.000	Mw/Mn	1.410
[eta]			55930.93380	Mz+1/Mw	1.595
					1.786

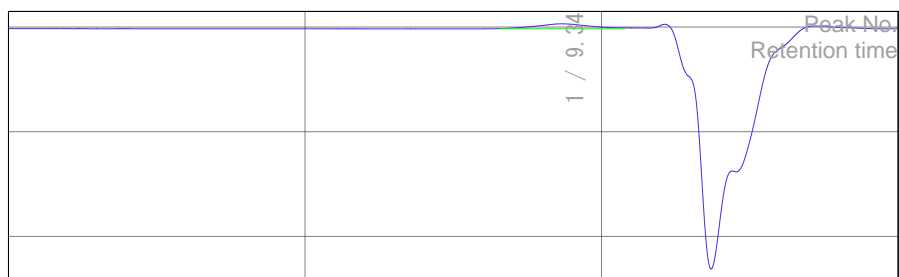
Figure B.14 GPC trace of PLA formed with **BIAN-Fe(C₆H₆)** and 0.5 equiv of 4-methoxyphenol. Samples measured in THF at 40 °C and referenced to polystyrene standards (**Table B.1**, Entry 2).



Result of molecular weight calculation (RI)
Peak 1 Valley Peak

	[min]	[mV]	[mol]		
Peak start	7.760	1.439	91,093	Mn	12,393
Peak top	8.910	2.490	17,258	Mw	20,676
Peak end	10.008	0.851	3,121	Mz	31,901
				Mz+1	43,500
				Mv	20,676
Height [mV]			4.174	Mp	17,258
Area [mV*sec]			299.325	Mz/Mw	1.543
Area% [%]			100.000	Mw/Mn	1.668
[eta]			20675.53598	Mz+1/Mw	2.104

Figure B.15 GPC trace of PLA formed with **BIAN-Fe(C₆H₆)** and 1 equiv of 4-methoxyphenol. Samples measured in THF at 40 °C and referenced to polystyrene standards (**Table B.1**, Entry 3).



Result of molecular weight calculation (RI)
Peak 1 Valley Peak

	min]	[mV	[mol	Mn	
Peak start	8.267	1.495	45,407	Mw	10,348
Peak top	9.348	3.097	8,714	Mz	15,101
Peak end	10.400	0.792	1,672	Mz+1	20,197
Height [mV]			4.681	Mv	10,348
Area [mV*sec]			293.829	Mp	8,715
Area% [%]			100.000	Mz/Mw	1.459
[eta]			10348.19026	Mw/Mn	1.548
				Mz+1/Mw	1.952

Figure B.16 GPC trace of PLA formed with **BIAN-Fe(C₆H₆)** and 2 equiv of 4-methoxyphenol. Samples measured in THF at 40 °C and referenced to polystyrene standards (**Table B.1**, Entry 4).

Appendix C –EXPERIMENTAL AND SUPPORTING INFORMATION

C.1 Supporting Information – Chapter 2

C.1.1 X-ray Crystallography Data

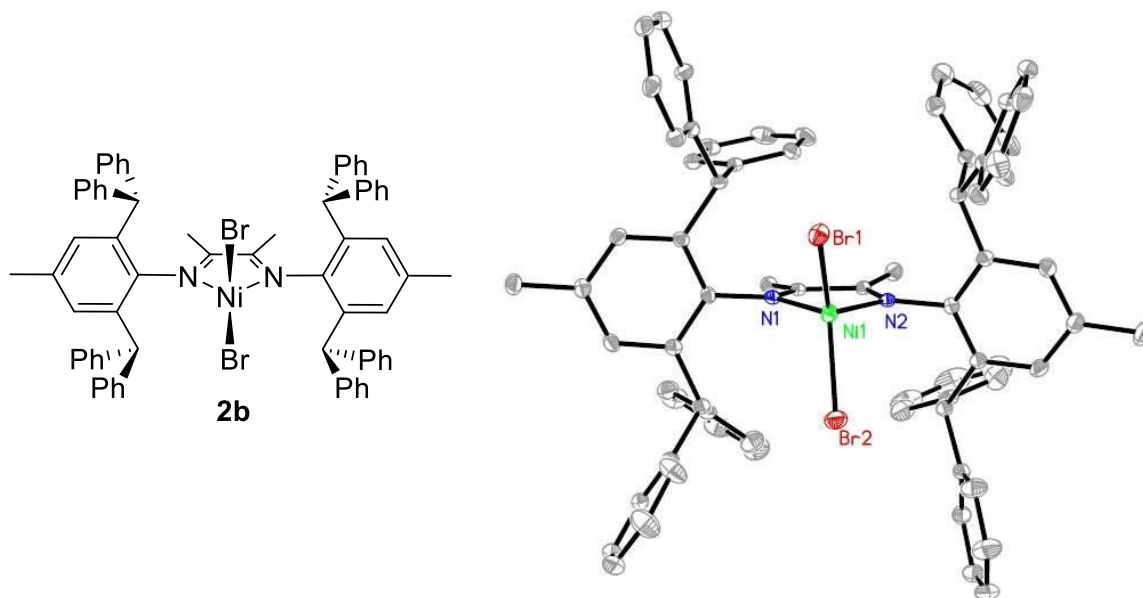


Figure C.1 ORTEP representation of precatalyst **2b** with thermal ellipsoids drawn at 50% probability. Hydrogens were omitted for clarity. X-ray quality single crystals of complex **2b** were grown overnight at ambient temperature by layering a saturated methylene chloride solution with pentanes. The observed bond lengths are typical for α -diimine Ni^{II} complexes with N1–Ni = 1.9978(15) Å and N2–Ni = 2.0020(15) Å. The Ni–Br bond lengths were 2.3286(3) and 2.3351(3) Å for Ni–Br1 and Ni–Br2, respectively. Complex **2b** displayed a distorted tetrahedral geometry with a N1–Ni–N2 angle of 80.76(6)° and a Br1–Ni–Br2 angle of 125.767(12)°. Crystal data for C₇₀H₆₀Br₂N₂Ni (1147.77 g/mol); monoclinic; space group P2₁/c; *a* = 18.3734(8) Å; *b* = 18.2988(8) Å; *c* = 17.9527(8) Å; α = 90°; β = 98.511(2)°; γ = 90°. Data for this structure can be obtained free of charge from the Cambridge Crystallographic Data Center (CCDC) under CCDC1570782.

C.1.2 NMR Spectroscopy

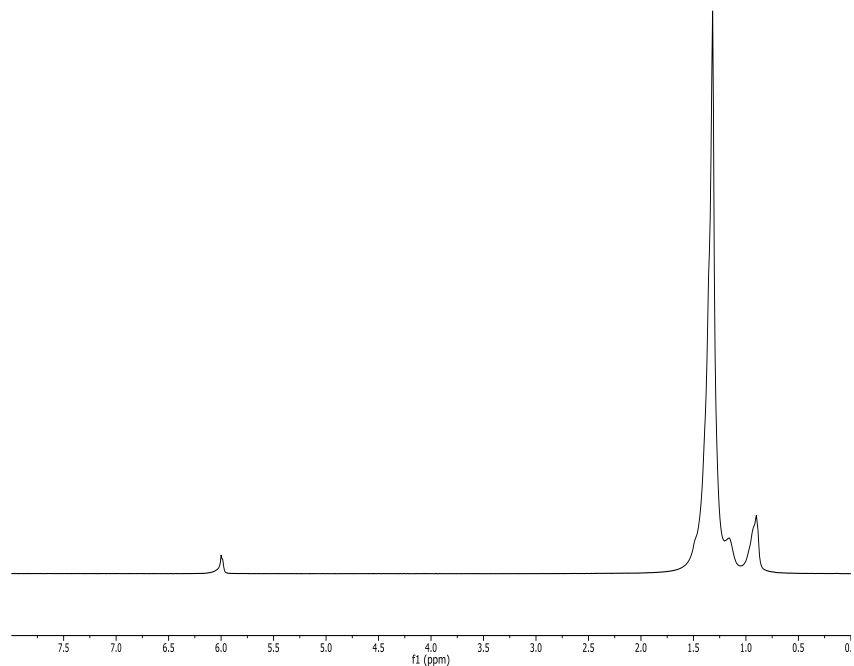


Figure C.2 ^1H NMR spectrum of polyethylene made by catalyst **2b** (Table 2.3, Entry 4).

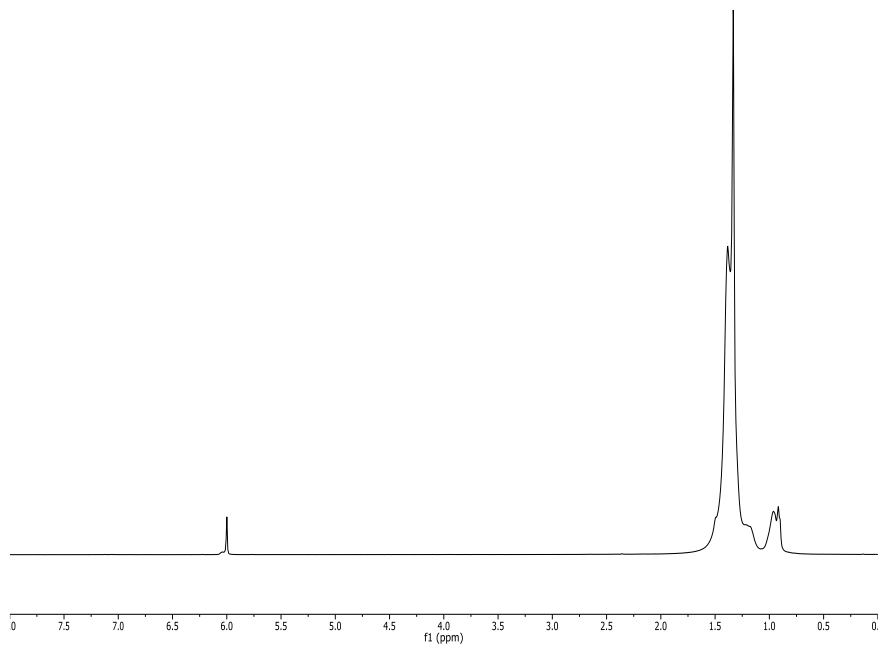


Figure C.3 ^1H NMR spectrum of polyethylene made by catalyst **2b** (Table 2.3, Entry 8)

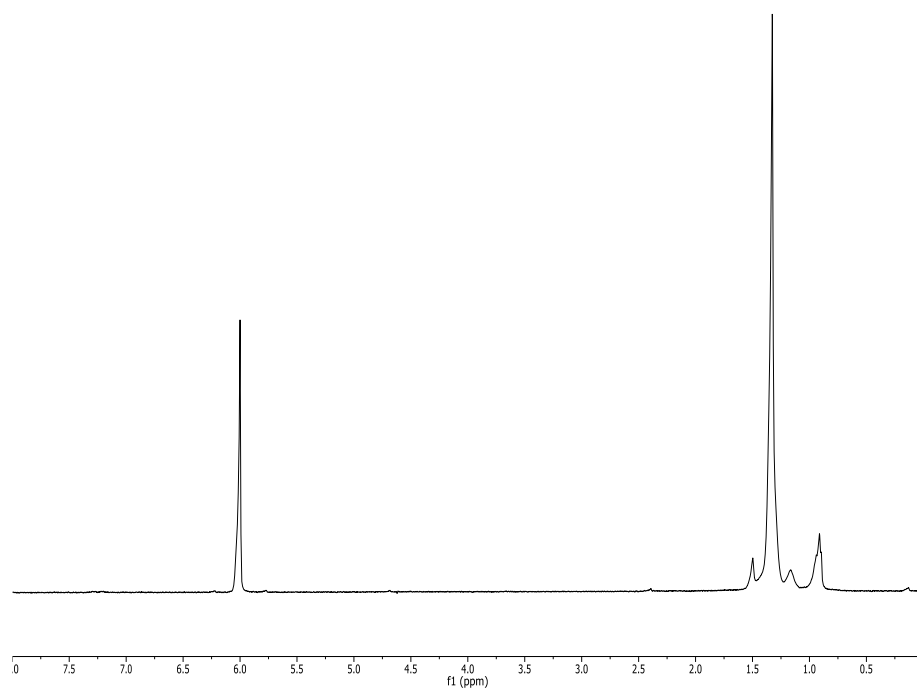


Figure C.4 ^1H NMR spectrum of polyethylene made by catalyst **2b** (Table 2.3, Entry 12).

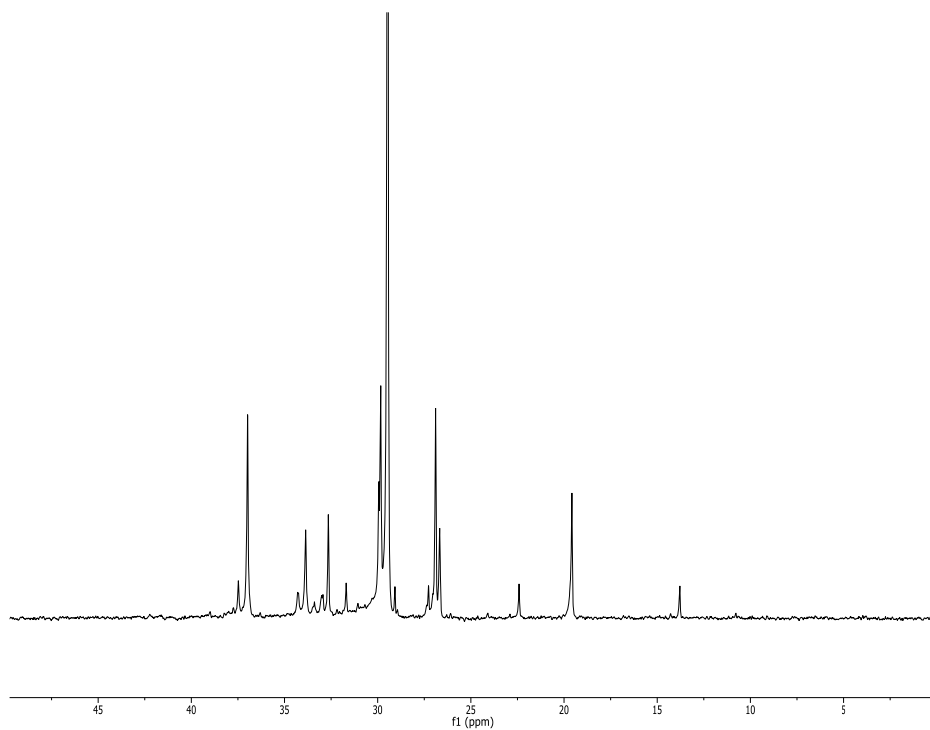


Figure C.5 ^{13}C NMR Spectrum of polyethylene made by catalyst **2b** (Table 2.3, Entry 8).

C.2 Supporting Information – Chapter 3

C.2.1 NMR Spectroscopy

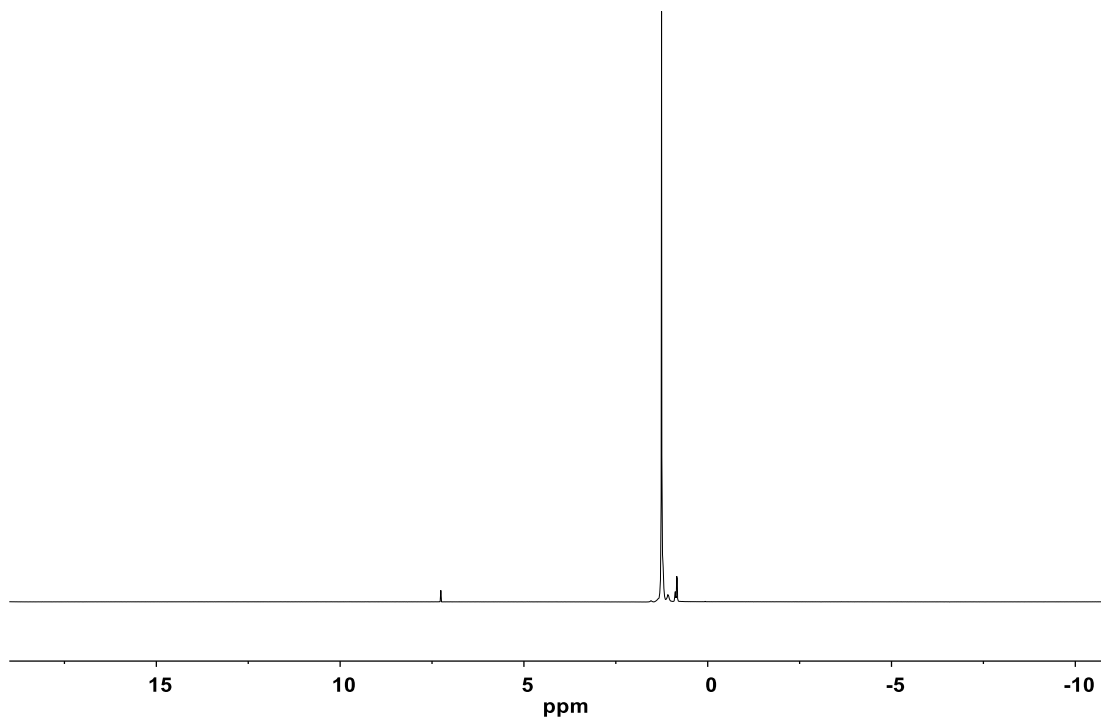


Figure C.6 Representative ^1H NMR of polyethylene at 70 °C. (**Table 3.1**, Entry 3).

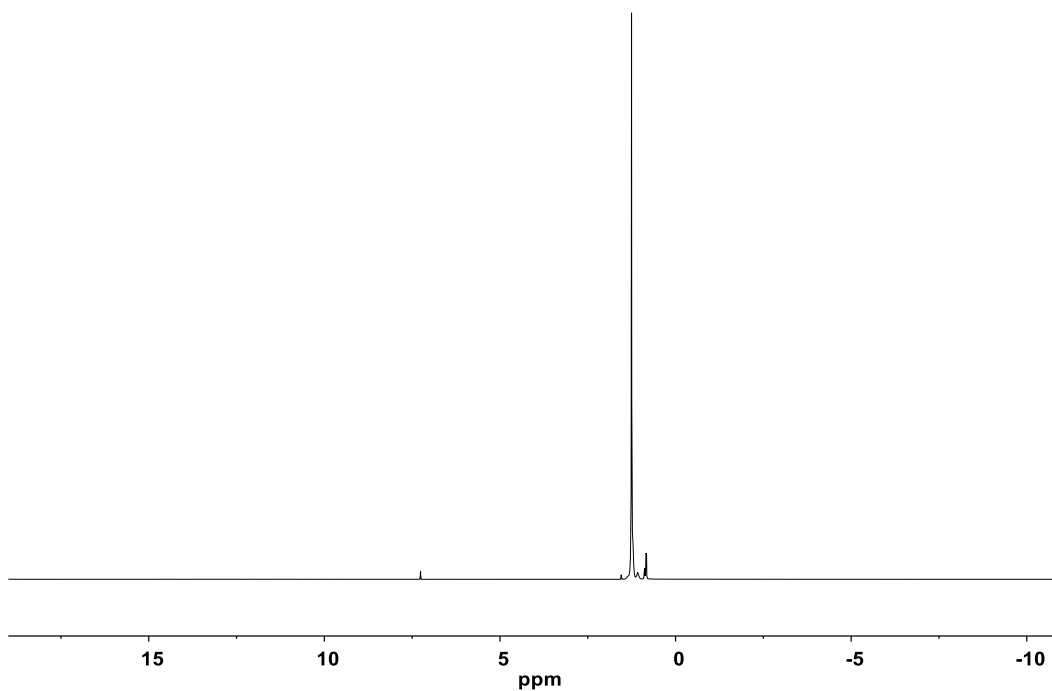


Figure C.7 Representative ¹H NMR of polyethylene at 75 °C. (**Table 3.1**, Entry 8).

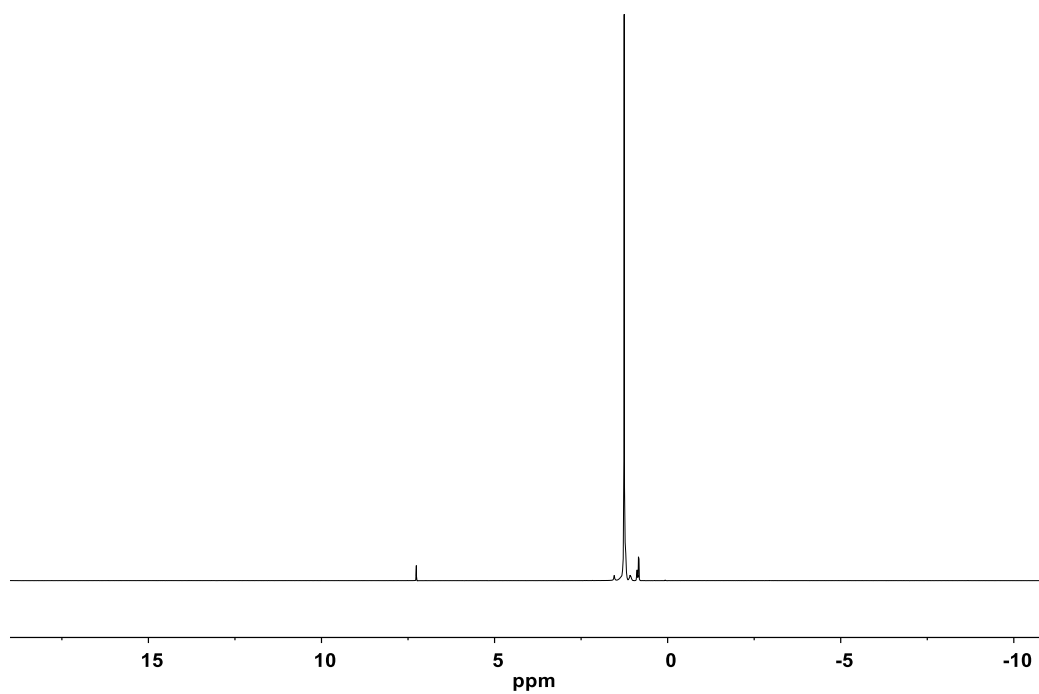


Figure C.8 Representative ¹H NMR of polyethylene at 80 °C. (**Table 3.1**, Entry 11)

C.2.2 Gel Permeation Chromatography

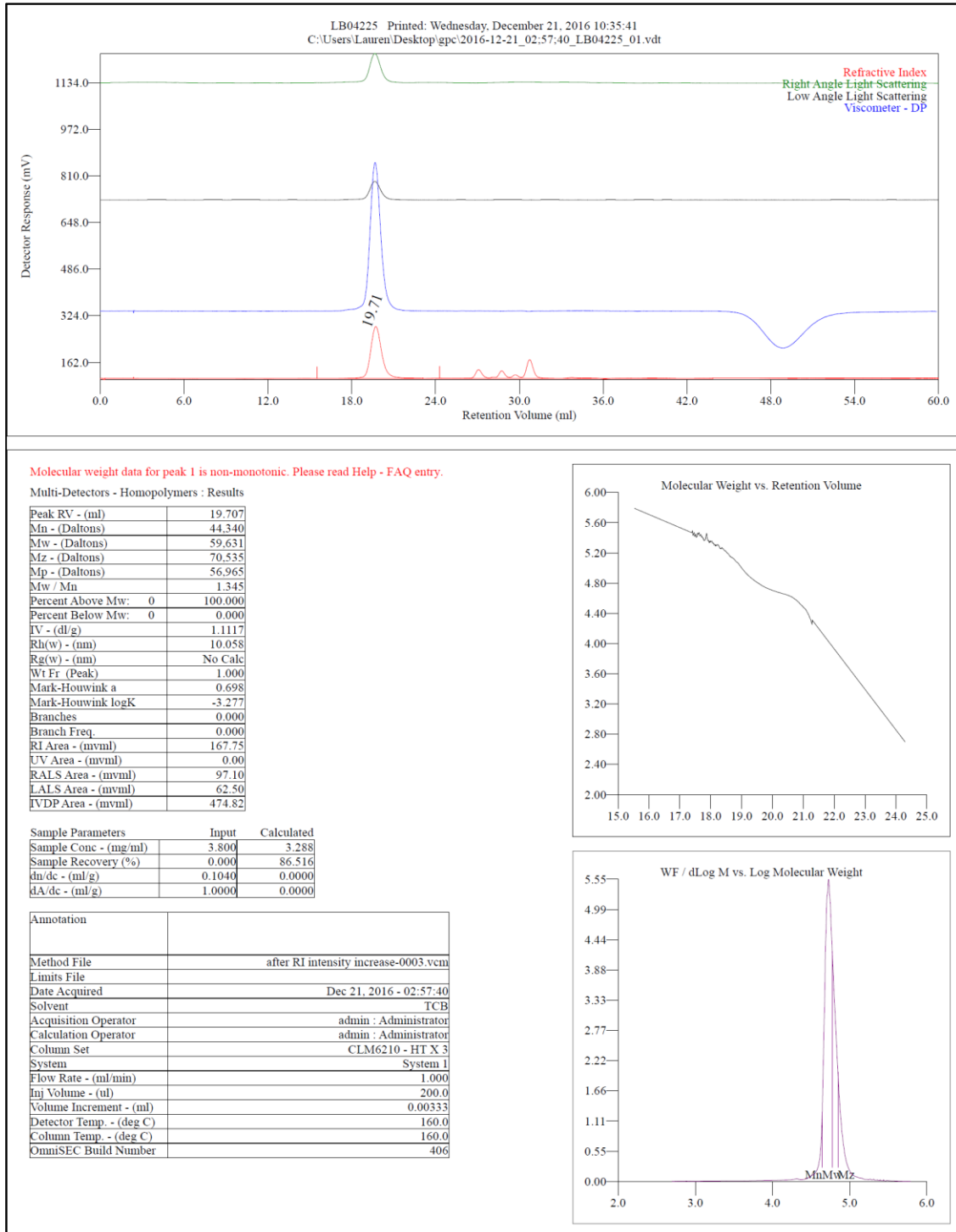


Figure C.9 GPC of polyethylene. (Table 3.1, Entry 1)

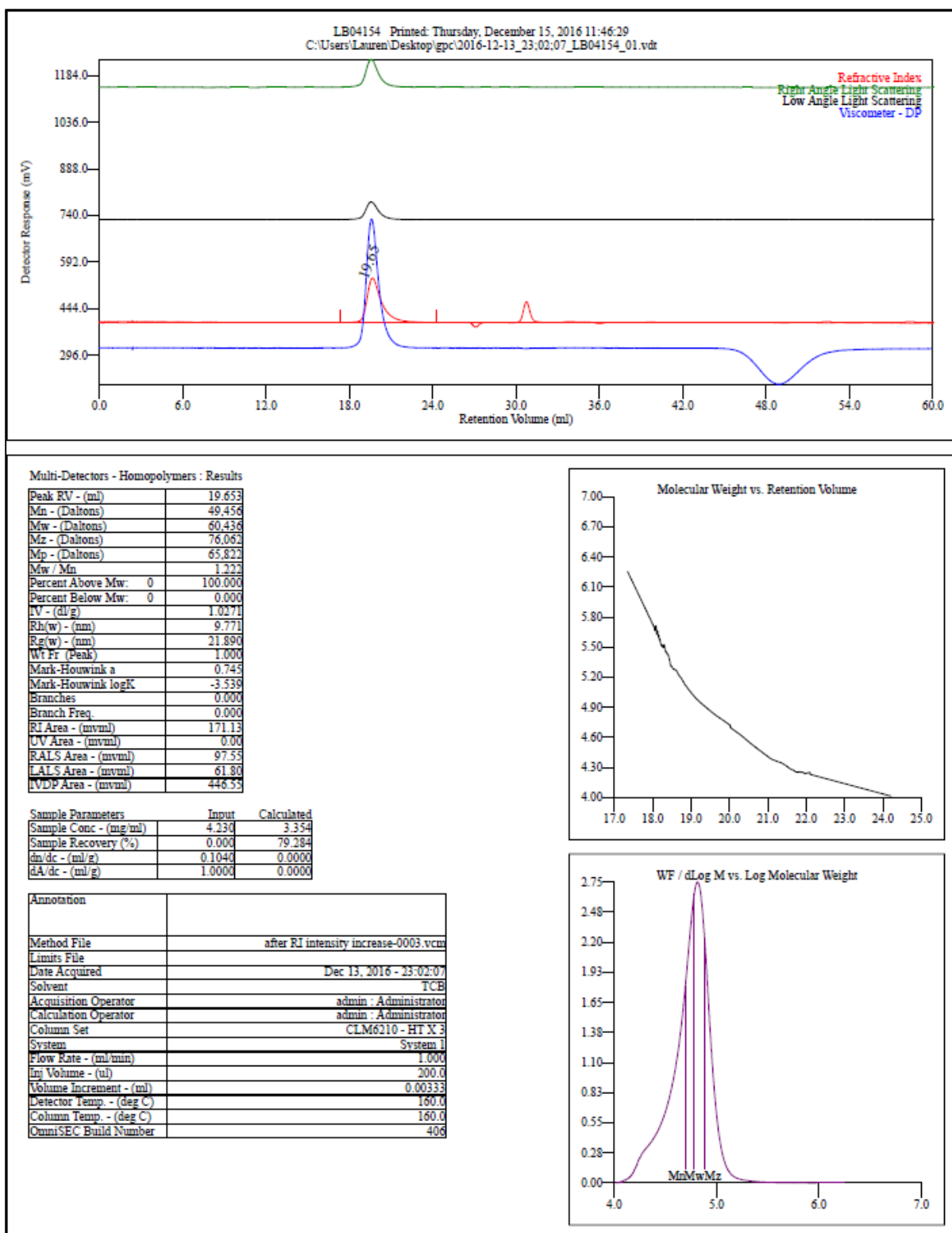
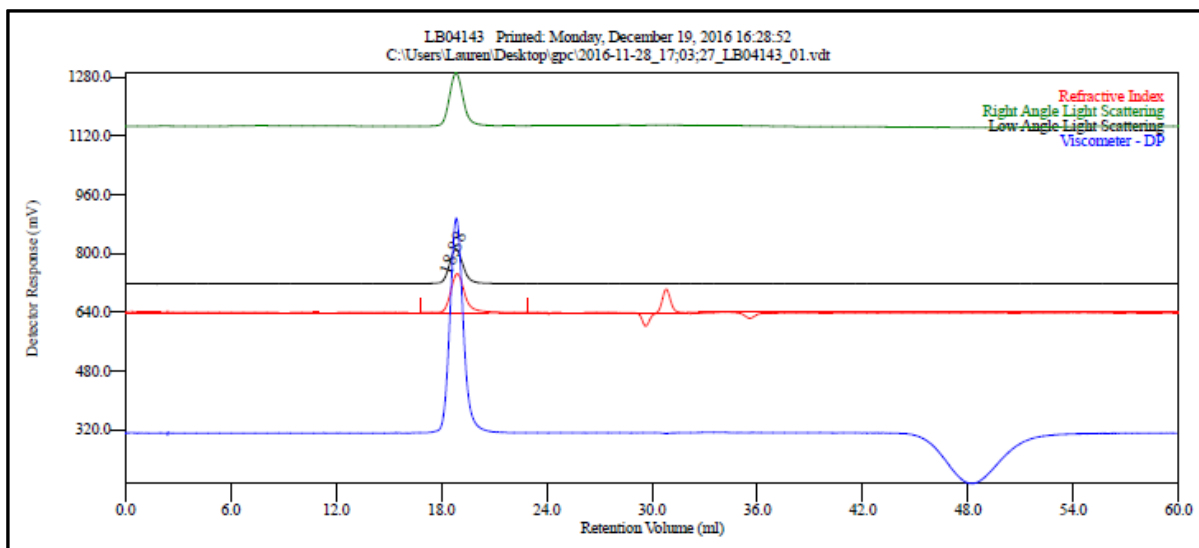


Figure C.10 GPC of polyethylene. (Table 3.1, Entry 2)



Multi-Detectors - Homopolymers : Results

Peak RV - (ml)	18.883
Mn - (Daltons)	128,197
Mw - (Daltons)	146,658
Mz - (Daltons)	158,072
Mp - (Daltons)	148,166
Mw / Mn	1.144
Percent Above Mw:	0 100.000
Percent Below Mw:	0 0.000
IV - (dl/g)	2.0571
Rh(w) - (nm)	16.703
Rg(w) - (nm)	24.630
Wt Fr (Peak)	1.000
Mark-Houwink a	0.770
Mark-Houwink logK	-3.660
Branches	0.000
Branch Freq.	0.000
RI Area - (mVml)	98.63
UV Area - (mVml)	0.00
RALS Area - (mVml)	130.80
LALS Area - (mVml)	85.92
IVDP Area - (mVml)	516.59

Sample Parameters	Input	Calculated
Sample Conc - (mg/ml)	2.450	1.933
Sample Recovery (%)	0.000	78.895
dn/dc - (ml/g)	0.1040	0.0000
dA/dc - (ml/g)	1.0000	0.0000

Annotation	
Method File	after RI intensity increase-0003.vcm
Limits File	
Date Acquired	Nov 28, 2016 - 17:03:27
Solvent	TCB
Acquisition Operator	admin : Administrator
Calculation Operator	admin : Administrator
Column Set	CLM6210 - HT X 3
System	System 1
Flow Rate - (ml/min)	1.000
Inj Volume - (ul)	200.0
Volume Increment - (ml)	0.00333
Detector Temp. - (deg C)	160.0
Column Temp. - (deg C)	160.0
OmniSEC Build Number	406

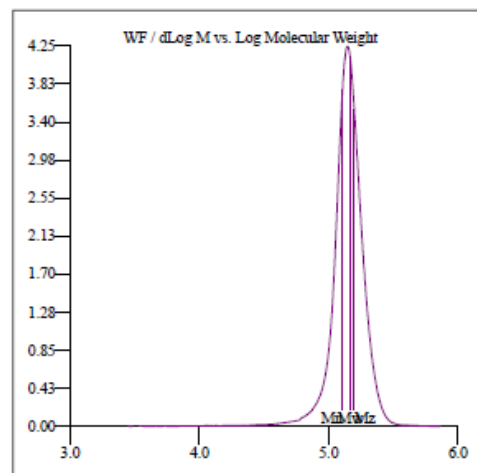
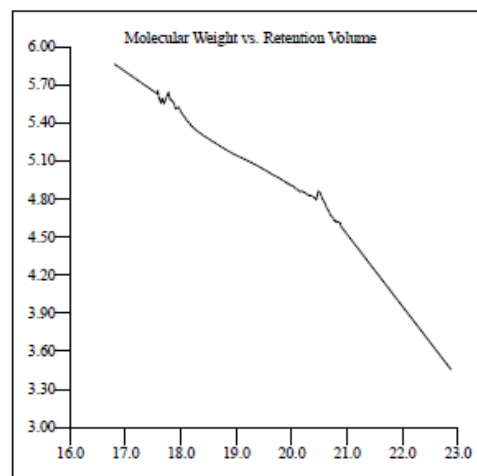
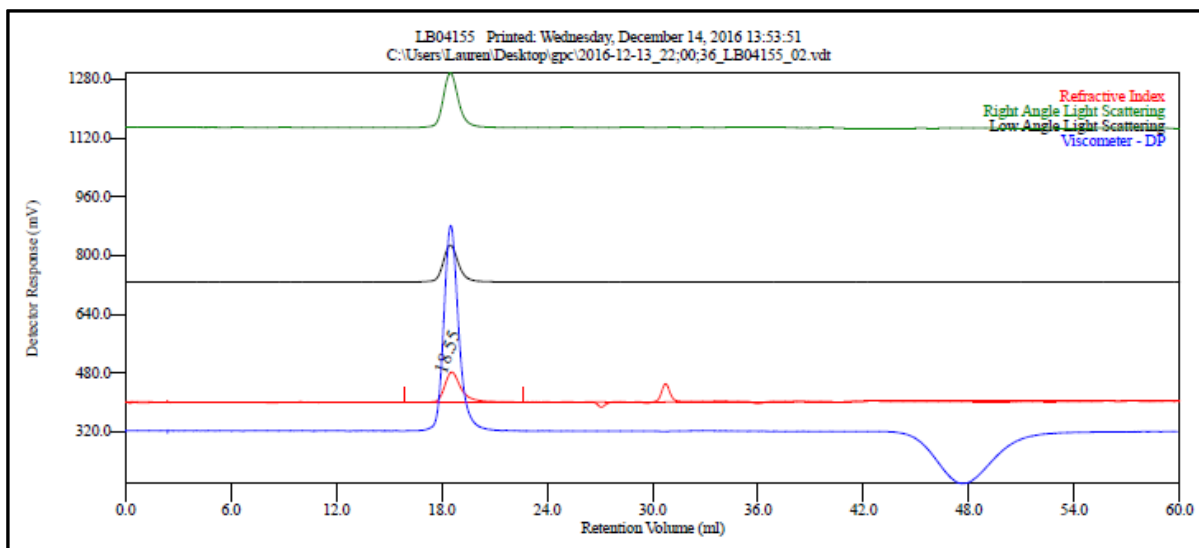


Figure C.11 GPC of polyethylene. (Table 3.1, Entry 3)



Multi-Detectors - Homopolymers : Results

Peak RV - (ml)	18.550
Mn - (Daltons)	163,983
Mw - (Daltons)	192,785
Mz - (Daltons)	244,962
Mp - (Daltons)	202,667
Mw / Mn	1.176
Percent Above Mw:	0 100.000
Percent Below Mw:	0 0.000
IV - (dl/g)	2.4351
Rh(w) - (nm)	19.241
Rg(w) - (nm)	28.722
Wt Fr (Peak)	1.000
Mark-Houwink a	0.781
Mark-Houwink logK	-3.731
Branches	0.000
Branch Freq	0.000
RI Area - (mVml)	88.80
UV Area - (mVml)	0.00
RALS Area - (mVml)	149.88
LALS Area - (mVml)	100.87
IVDP Area - (mVml)	550.33

Sample Parameters	Input	Calculated
Sample Conc - (mg/ml)	2.010	1.740
Sample Recovery (%)	0.000	86.584
dn/dc - (ml/g)	0.1040	0.0000
dA/dc - (ml/g)	1.0000	0.0000

Annotation	
Method File	after RI intensity increase-0003.vcm
Limits File	
Date Acquired	Dec 13, 2016 - 22:00:36
Solvent	TCB
Acquisition Operator	admin : Administrator
Calculation Operator	admin : Administrator
Column Set	CLM6210 - HT X 3
System	System 1
Flow Rate - (ml/min)	1.000
Inj Volume - (ul)	200.0
Volume Increment - (ml)	0.00333
Detector Temp. - (deg C)	160.0
Column Temp. - (deg C)	160.0
OmniSEC Build Number	406

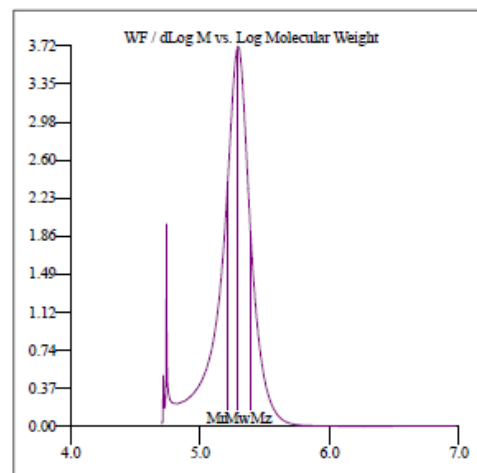
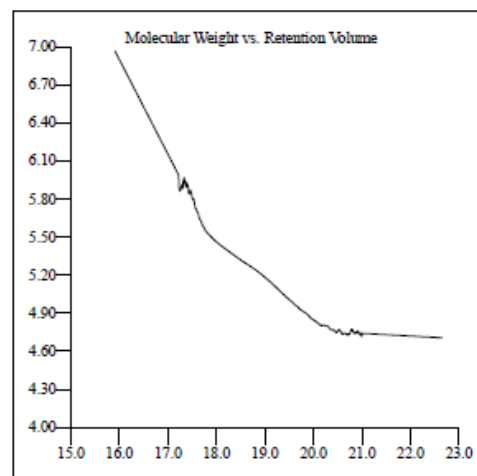
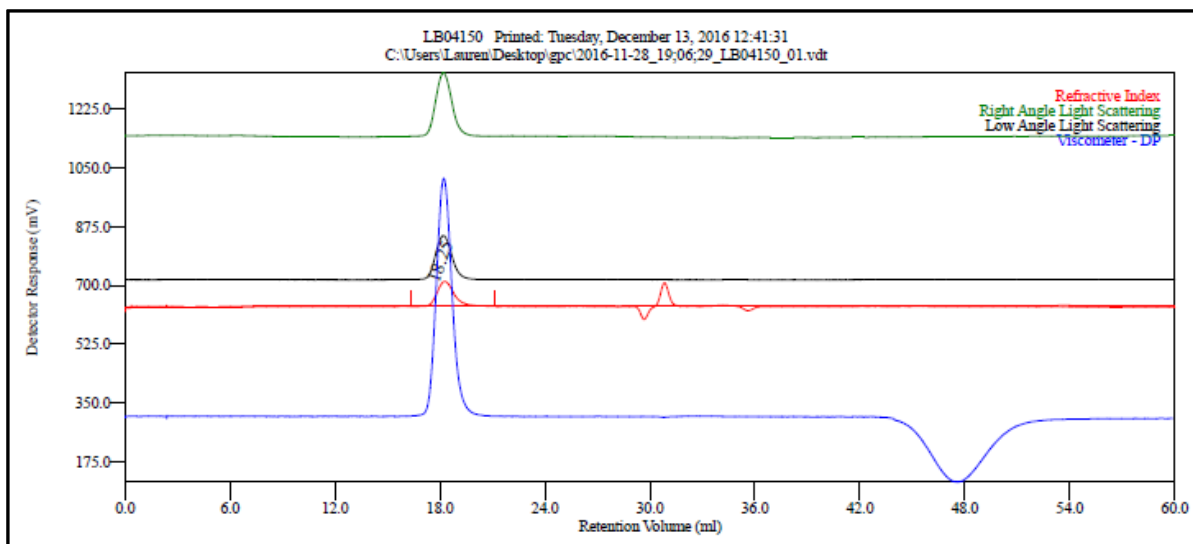


Figure C.12 GPC of polyethylene. (Table 3.1, Entry 4)



Multi-Detectors - Homopolymers : Results

Peak RV - (ml)	18.250
Mn - (Daltons)	244,076
Mw - (Daltons)	285,631
Mz - (Daltons)	312,428
Mp - (Daltons)	296,670
Mw / Mn	1.170
Percent Above Mw:	0 100.000
Percent Below Mw:	0 0.000
IV - (dl/g)	3.4779
Rh(w) - (nm)	24.816
Rg(w) - (nm)	33.330
Wt Fr (Peak)	1.000
Mark-Houwink a	0.797
Mark-Houwink logK	-3.806
Branches	0.000
Branch Freq.	0.000
RI Area - (mVml)	82.65
UV Area - (mVml)	0.00
RAIS Area - (mVml)	201.92
LALS Area - (mVml)	140.56
IVDP Area - (mVml)	739.40

Sample Parameters	Input	Calculated
Sample Conc - (mg/ml)	2.220	1.620
Sample Recovery (%)	0.000	72.964
dn/dc - (ml/g)	0.1040	0.0000
dA/dc - (ml/g)	1.0000	0.0000

Annotation	
Method File	after RI intensity increase-0003.vcm
Limits File	
Date Acquired	Nov 28, 2016 - 19:06:29
Solvent	TCB
Acquisition Operator	admin : Administrator
Calculation Operator	admin : Administrator
Column Set	CLM6210 - HT X3
System	System 1
Flow Rate - (ml/min)	1.000
inj Volume - (ul)	200.0
Volume Increment - (ml)	0.00333
Detector Temp. - (deg C)	160.0
Column Temp. - (deg C)	160.0
OmniSEC Build Number	406

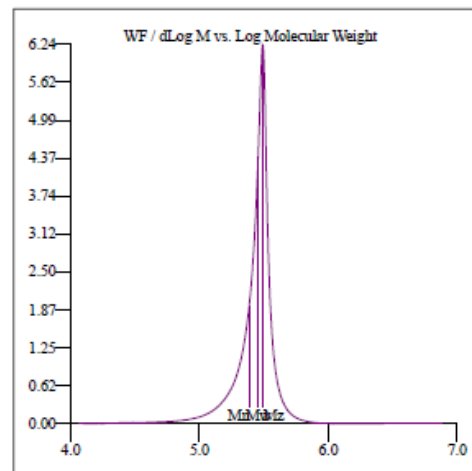
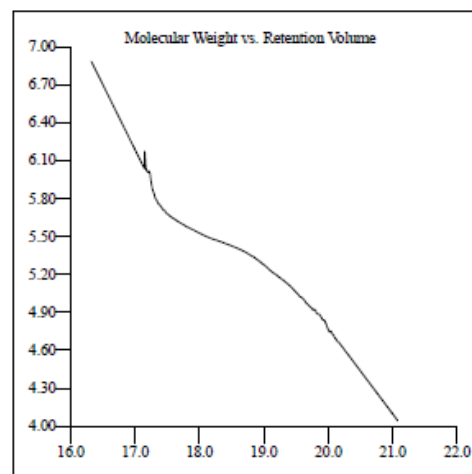
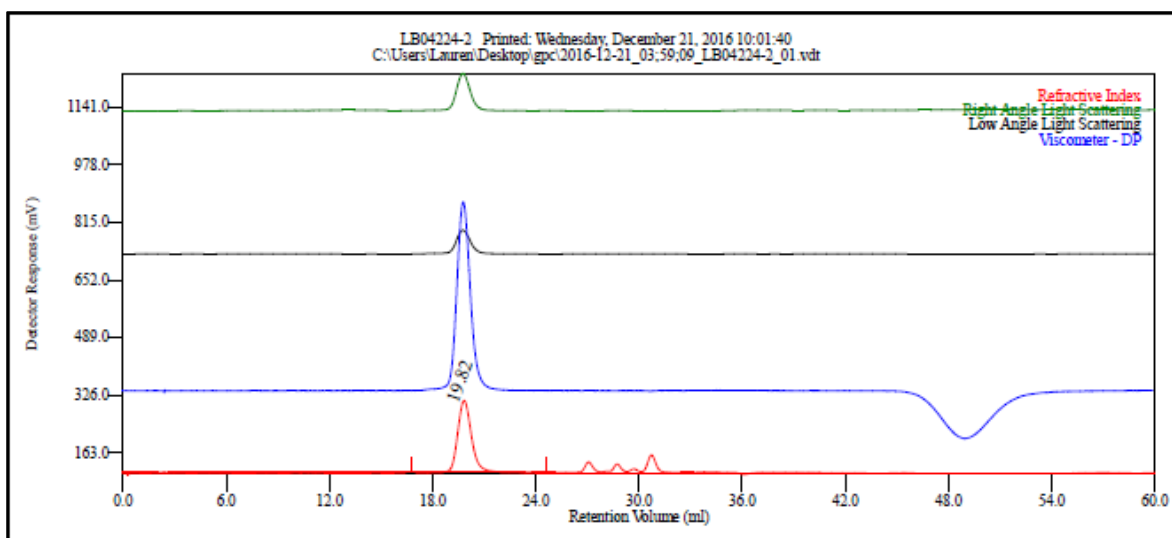


Figure C.13 GPC of polyethylene. (Table 3.1, Entry 5)



Multi-Detectors - Homopolymers : Results

Peak RV - (ml)	19.817
Mn - (Daltons)	40.284
Mw - (Daltons)	55.187
Mz - (Daltons)	63.085
Mp - (Daltons)	55.011
Mw / Mn	1.370
Percent Above Mw:	0 100.000
Percent Below Mw:	0 0.000
IV - (dl/g)	1.0082
Rh(w) - (nm)	9.482
Rz(w) - (nm)	22.300
WT Fr (Peak)	1.000
Mark-Houwink a	0.657
Mark-Houwink logK	-3.013
Branches	0.000
Branch Freq.	0.000
RI Area - (mVmin)	192.56
UV Area - (mVmin)	0.00
RALS Area - (mVmin)	98.78
LALS Area - (mVmin)	64.81
IVDP Area - (mVmin)	492.48

Sample Parameters	Input	Calculated
Sample Conc - (mg/ml)	4.460	3.774
Sample Recovery (%)	0.000	84.613
dn/dc - (ml/g)	0.1040	0.0000
dA/dc - (ml/g)	1.0000	0.0000

Annotation	
Method File	after RI intensity increase-0003.vcm
Limits File	
Date Acquired	Dec 21, 2016 - 03:59:09
Solvent	TCE
Acquisition Operator	admin : Administrator
Calculation Operator	admin : Administrator
Column Set	CLM6210 - HT X 3
System	System 1
Flow Rate - (ml/min)	1.000
Inj Volume - (ul)	200.0
Volume Increment - (ml)	0.00333
Detector Temp. - (deg C)	160.0
Column Temp. - (deg C)	160.0
OmniSEC Build Number	408

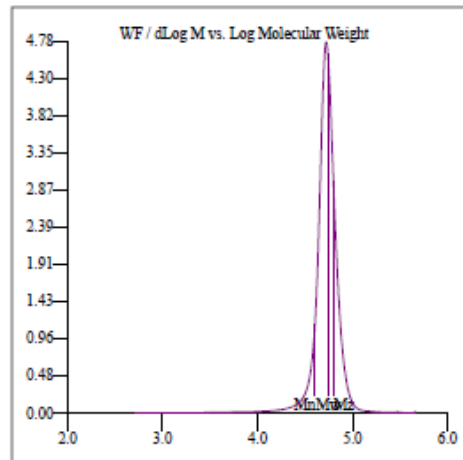
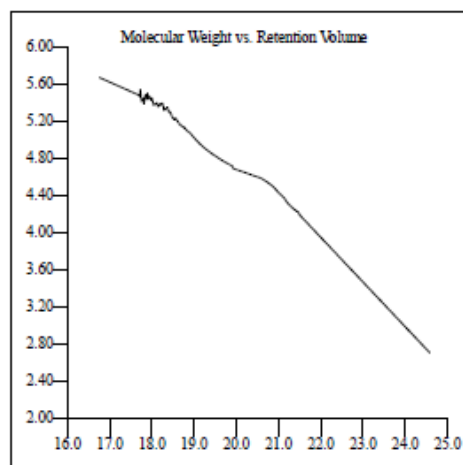
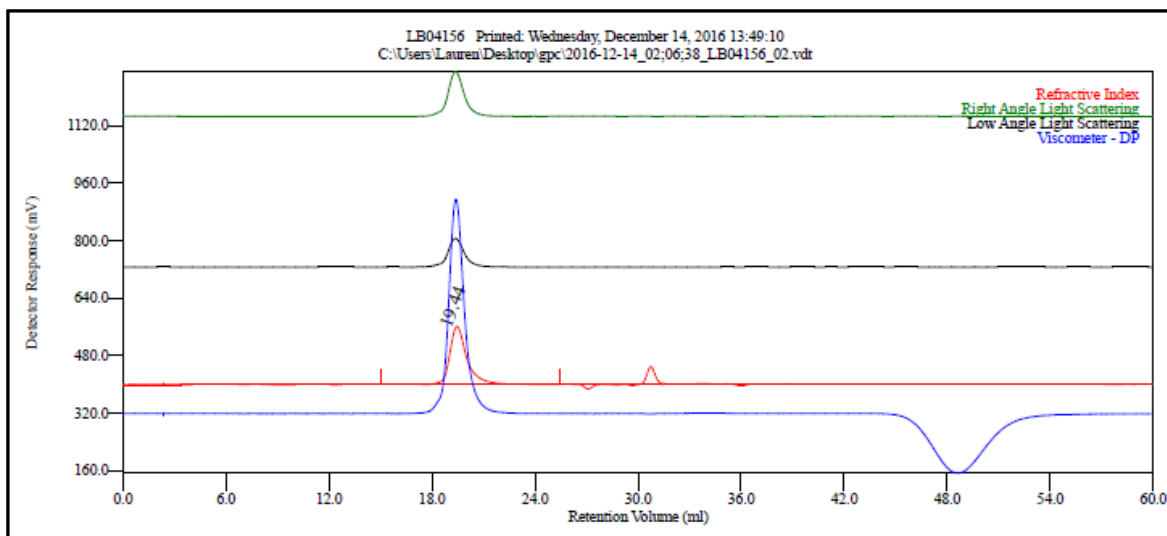


Figure C.14 GPC of polyethylene. (Table 3.1, Entry 6)



Multi-Detectors - Homopolymers : Results

Peak RV - (ml)	19.443
Mn - (Daltons)	67.160
Mw - (Daltons)	80.607
Mz - (Daltons)	99.680
Mp - (Daltons)	82.091
Mw / Mn	1.200
Percent Above Mw:	0
Percent Below Mw:	0
IV - (dl/g)	1.3366
Rh(w) - (nm)	11.768
Rg(w) - (nm)	23.754
WT Fr (Peak)	1.000
Mark-Houwink a	0.703
Mark-Houwink logK	-3.318
Branches	0.000
Branch Freq.	0.000
RI Area - (mVml)	187.79
UV Area - (mVml)	0.00
RALS Area - (mVml)	139.73
LALS Area - (mVml)	90.81
IVDP Area - (mVml)	640.91

Sample Parameters	Input	Calculated
Sample Conc - (mg/ml)	4.400	3.680
Sample Recovery (%)	0.000	83.644
dn/dc - (ml/g)	0.1040	0.0000
dA/dc - (ml/g)	1.0000	0.0000

Annotation	
Method File	after RI intensity increase-0003.vcm
Limits File	
Date Acquired	Dec 14, 2016 - 02:06:38
Solvent	TCB
Acquisition Operator	admin : Administrator
Calculation Operator	admin : Administrator
Column Set	CLM6210 - HT X 3
System	System 1
Flow Rate - (ml/min)	1.000
inj Volume - (ul)	200.0
Volume Increment - (ml)	0.00333
Detector Temp. - (deg C)	160.0
Column Temp. - (deg C)	160.0
OmniSEC Build Number	408

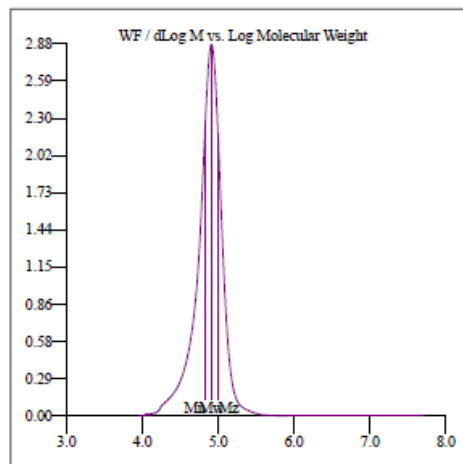
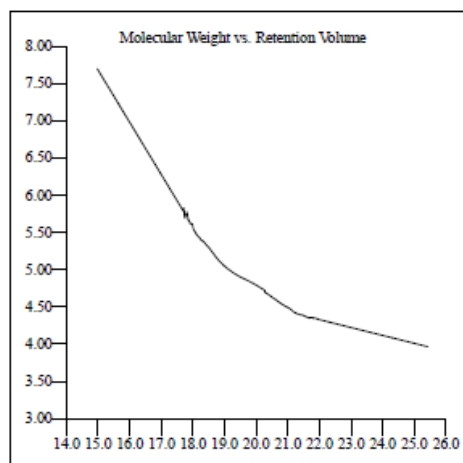
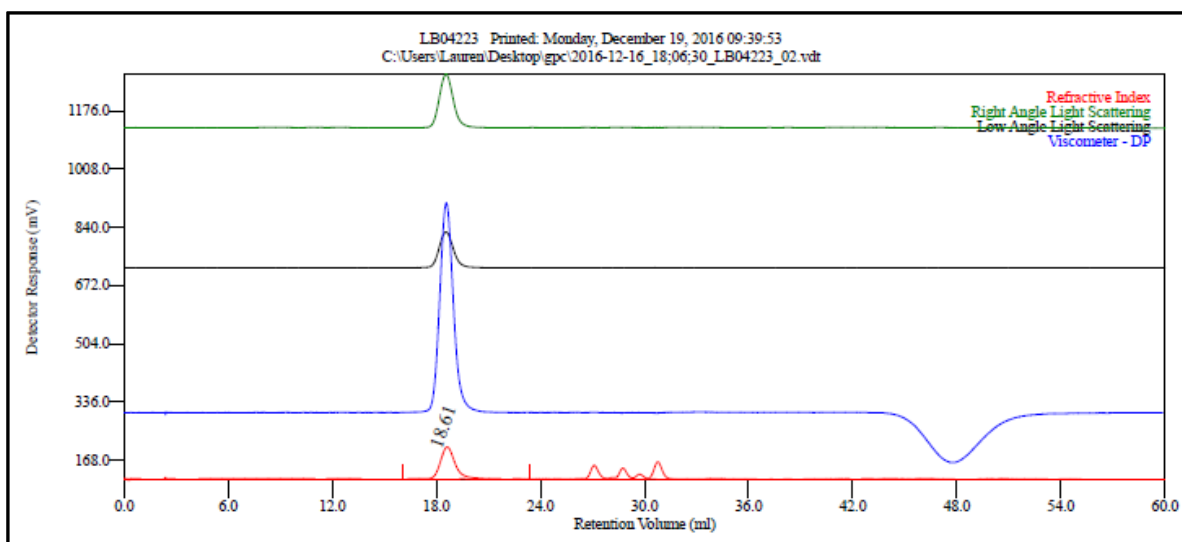


Figure C.15 GPC of polyethylene. (Table 3.1, Entry 7)



Molecular weight data for peak 1 is non-monotonic. Please read Help - FAQ entry.

Multi-Detectors - Homopolymers : Results

Peak RV - (ml)	18.613
Mn - (Daltons)	154.545
Mw - (Daltons)	181.453
Mz - (Daltons)	195.478
Mp - (Daltons)	187.728
Mw / Mn	1.174
Percent Above Mw	0
Percent Below Mw	0
IV - (dl/g)	2.3853
Rh(w) - (nm)	18.832
Rg(w) - (nm)	34.274
Wt Fr (Peak)	1.000
Mark-Houwink a	0.768
Mark-Houwink logK	-3.658
Branches	0.000
Branch Freq	0.000
RI Area - (mVml)	91.69
UV Area - (mVml)	0.00
RALS Area - (mVml)	144.76
LALS Area - (mVml)	98.39
IVDP Area - (mVml)	559.66

Sample Parameters	Input	Calculated
Sample Conc - (mg/ml)	1.980	1.797
Sample Recovery (%)	0.000	90.754
dn/dc - (ml/g)	0.1040	0.0000
dA/dc - (ml/g)	1.0000	0.0000

Annotation	
Method File	after RI intensity increase-0003.vcu
Limits File	
Date Acquired	Dec 16, 2016 - 18:06:30
Solvent	TCB
Acquisition Operator	admin : Administrator
Calculation Operator	admin : Administrator
Column Set	CLM6210 - HT X3
System	System 1
Flow Rate - (ml/min)	1.000
Inj Volume - (ul)	200.0
Volume Increment - (ml)	0.00333
Detector Temp. - (deg C)	160.0
Column Temp. - (deg C)	160.0
OmniSEC Build Number	406

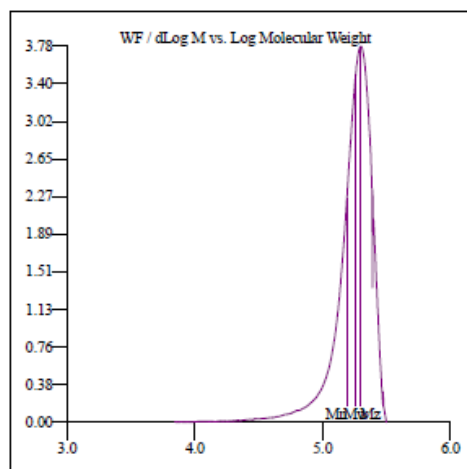
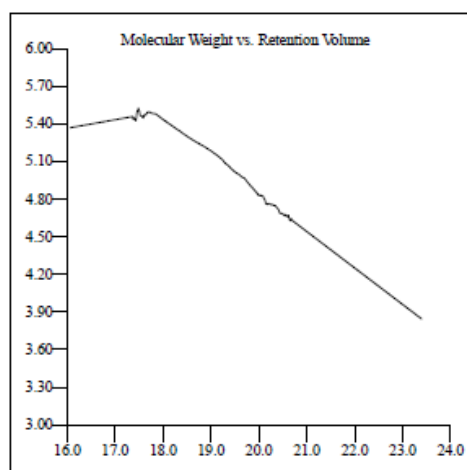


Figure C.16 GPC of polyethylene. (Table 3.1, Entry 8)

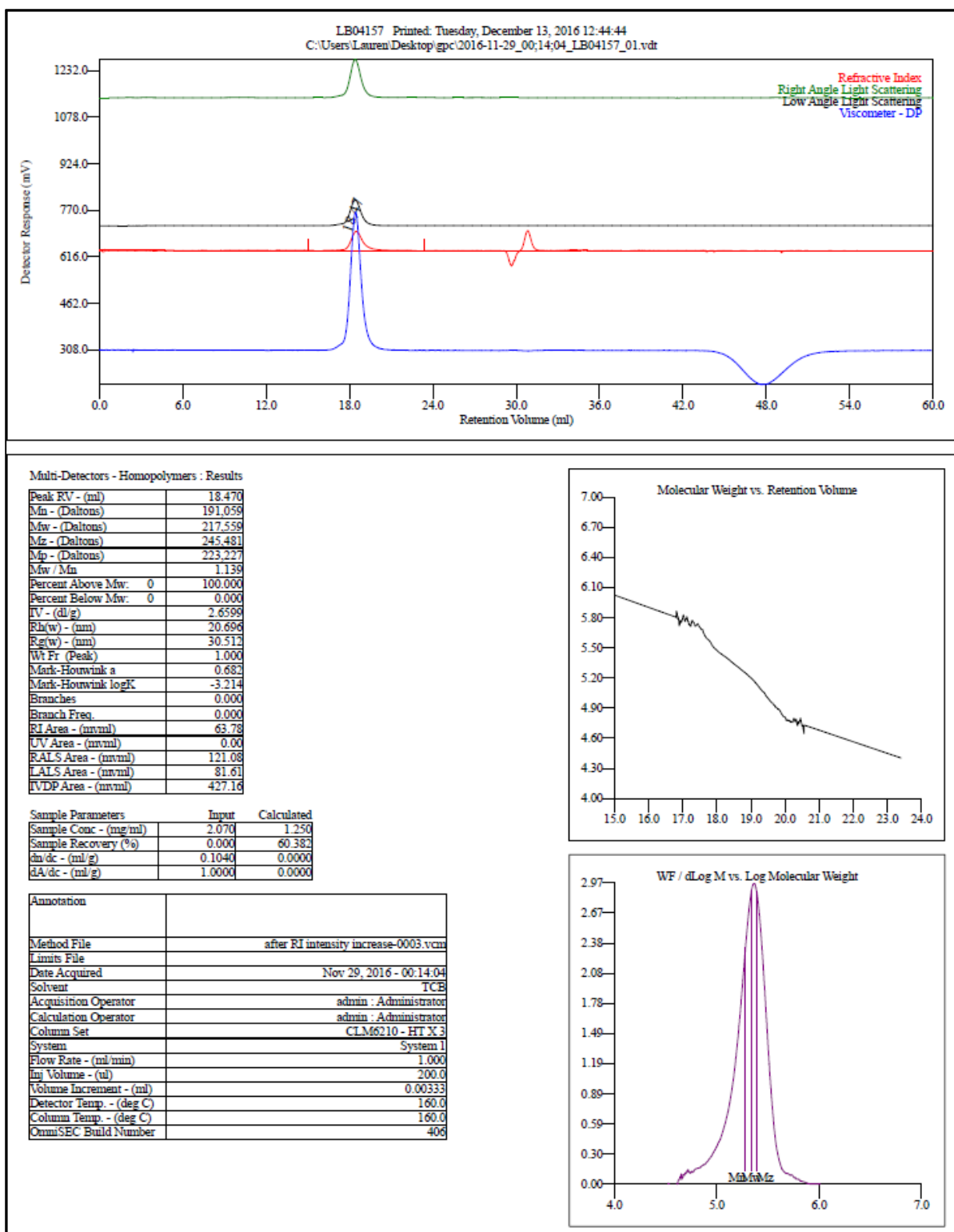
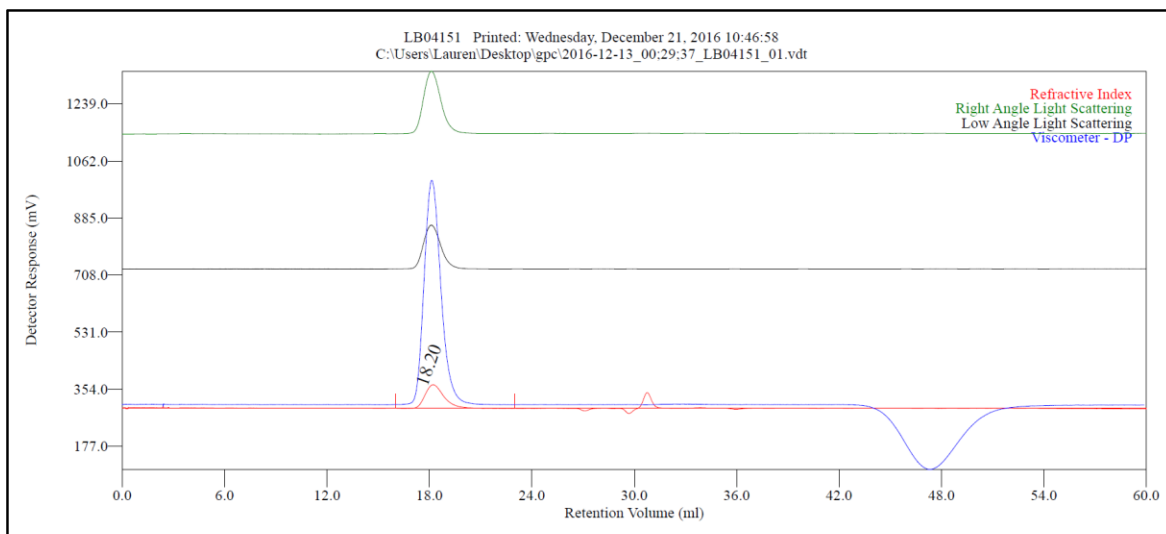


Figure C.17 GPC of polyethylene. (Table 3.1, Entry 9)



Molecular weight data for peak 1 is non-monotonic. Please read Help - FAQ entry.

Multi-Detectors - Homopolymers : Results

Peak RV - (ml)	18.203
Mn - (Daltons)	253,440
Mw - (Daltons)	290,065
Mz - (Daltons)	321,609
Mp - (Daltons)	308,691
Mw / Mn	1.145
Percent Above Mw: 0	100.000
Percent Below Mw: 0	0.000
IV - (dl/g)	3.3094
Rh(w) - (nm)	24.498
Rg(w) - (nm)	34.271
Wt Fr (Peak)	1.000
Mark-Houwink a	0.851
Mark-Houwink logK	-4.123
Branches	0.000
Branch Freq.	0.000
RI Area - (mVml)	93.52
UV Area - (mVml)	0.00
RAIS Area - (mVml)	229.84
LALS Area - (mVml)	162.33
IVDP Area - (mVml)	796.62

Sample Parameters	Input	Calculated
Sample Conc - (mg/ml)	2.320	1.833
Sample Recovery (%)	0.000	79.002
dn/dc - (ml/g)	0.1040	0.0000
dA/dc - (ml/g)	1.0000	0.0000

Annotation	
Method File	after RI intensity increase-0003.vcm
Limits File	
Date Acquired	Dec 13, 2016 - 00:29:37
Solvent	TCB
Acquisition Operator	admin : Administrator
Calculation Operator	admin : Administrator
Column Set	CLM6210 - HT X 3
System	System 1
Flow Rate - (ml/min)	1.000
Inj Volume - (ul)	200.0
Volume Increment - (ml)	0.00333
Detector Temp. - (deg C)	160.0
Column Temp. - (deg C)	160.0
OmniSEC Build Number	406

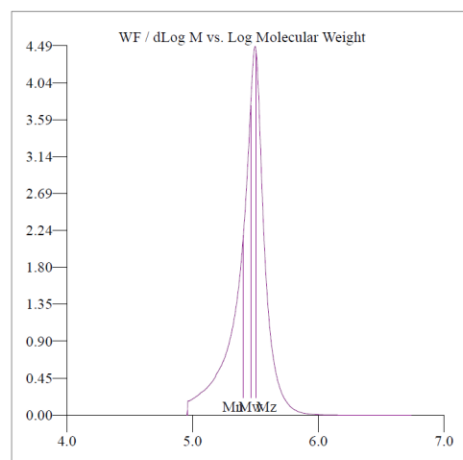
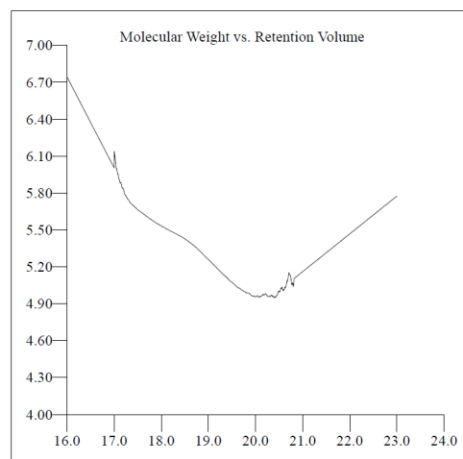
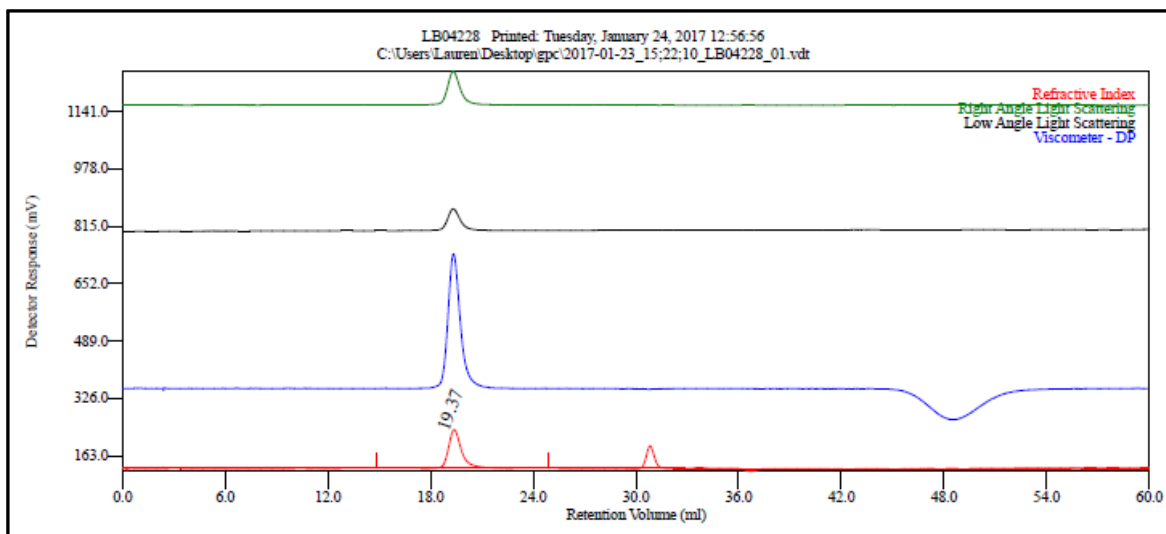


Figure C.18 GPC of polyethylene. (Table 3.1, Entry 10)



Multi-Detectors - Homopolymers : Results

Peak RV - (ml)	19.367
Mn - (Daltons)	69.570
Mw - (Daltons)	76.312
Mz - (Daltons)	87.100
Mp - (Daltons)	76.598
Mw / Mn	1.097
Percent Above Mw:	0 100.000
Percent Below Mw:	0 0.000
IV - (dl/g)	1.1574
Rh(w) - (nm)	10.981
Rg(w) - (nm)	No Calc
Wt Fr (Peak)	1.000
Mark-Houwink a	0.586
Mark-Houwink logK	-2.798
Branches	0.000
Branch Freq.	0.000
RI Area - (mVml)	97.98
UV Area - (mVml)	0.00
RALS Area - (mVml)	84.12
LALS Area - (mVml)	55.53
IVDP Area - (mVml)	329.68

Sample Parameters	Input	Calculated
Sample Conc - (mg/ml)	2.300	0.000
Sample Recovery (%)	0.000	83.720
dn/dc - (ml/g)	0.1040	0.0000
dA/dc - (ml/g)	1.0000	0.0000

Annotation	
Method File	Long Group 1-9-16-0000.vcm
Limits File	
Date Acquired	Jan 23, 2017 - 15:22:10
Solvent	TCB
Acquisition Operator	admin : Administrator
Calculation Operator	admin : Administrator
Column Set	CLM6210 - HT X3
System	System 1
Flow Rate - (ml/min)	1.000
Inj Volume - (ul)	200.0
Volume Increment - (ml)	0.00333
Detector Temp. - (deg C)	160.0
Column Temp. - (deg C)	160.0
OmniSEC Build Number	406

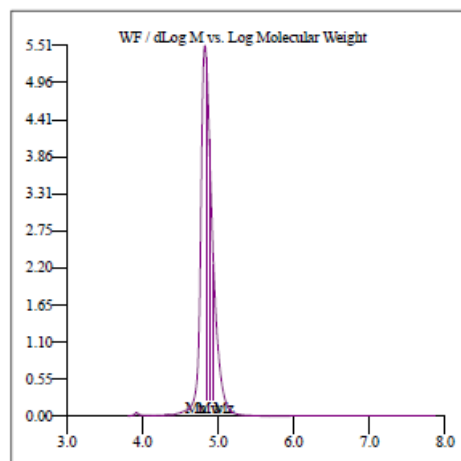
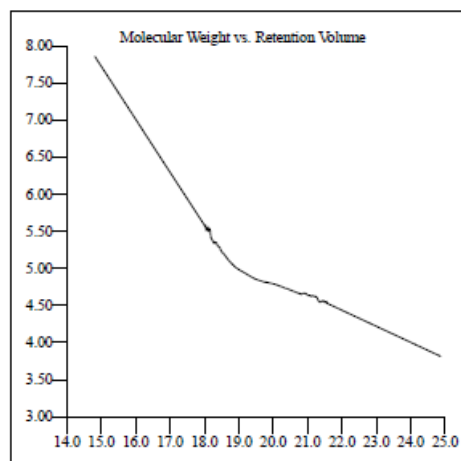
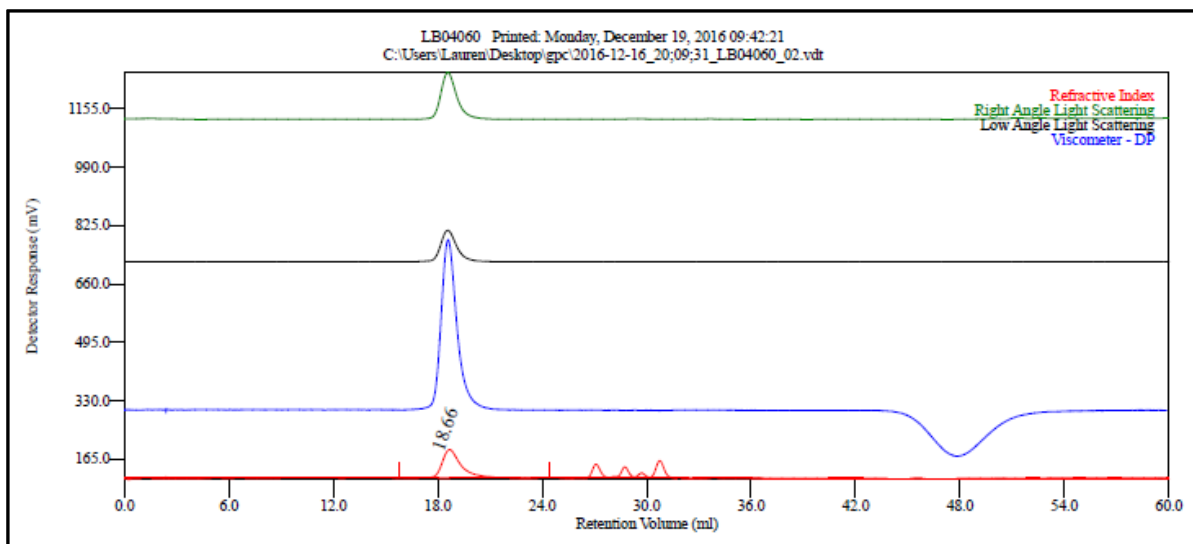


Figure C.19 GPC of polyethylene. (Table 3.1, Entry 11)



Multi-Detectors - Homopolymers : Results

Peak RV - (ml)	18.663
Mn - (Daltons)	113,544
Mw - (Daltons)	162,221
Mz - (Daltons)	192,266
Mp - (Daltons)	183,057
Mw / Mn	1.429
Percent Above Mw	0
Percent Below Mw	0
IV - (dl/g)	2.0336
Rh(w) - (nm)	17.003
Rg(w) - (nm)	29.339
Wt Fr (Peak)	1.000
Mark-Houwink a	0.814
Mark-Houwink logK	-3.921
Branches	0.000
Branch Freq.	0.000
RI Area - (mVml)	99.64
UV Area - (mVml)	0.00
RALS Area - (mVml)	140.15
LALS Area - (mVml)	96.09
IVDP Area - (mVml)	514.12

Sample Parameters	Input	Calculated
Sample Conc - (mg/ml)	2.050	1.953
Sample Recovery (%)	0.000	95.257
dn/dc - (ml/g)	0.1040	0.0000
dA/dc - (ml/g)	1.0000	0.0000

Annotation	
Method File	after RI intensity increase-0003.vcm
Limits File	
Date Acquired	Dec 16, 2016 - 20:09:31
Solvent	TCB
Acquisition Operator	admin - Administrator
Calculation Operator	admin - Administrator
Column Set	CLM6210 - HT X3
System	System 1
Flow Rate - (ml/min)	1.000
Inj Volume - (ul)	200.0
Volume Increment - (ml)	0.00333
Detector Temp. - (deg C)	160.0
Column Temp. - (deg C)	160.0
OmniSEC Build Number	406

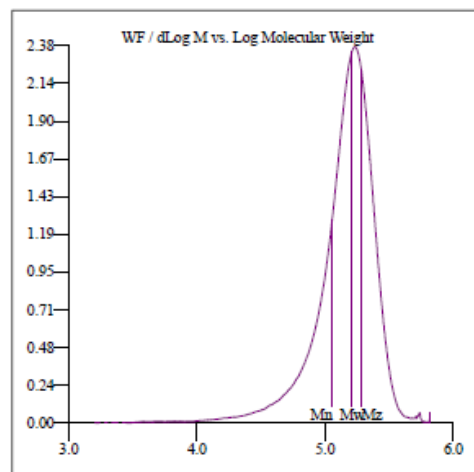
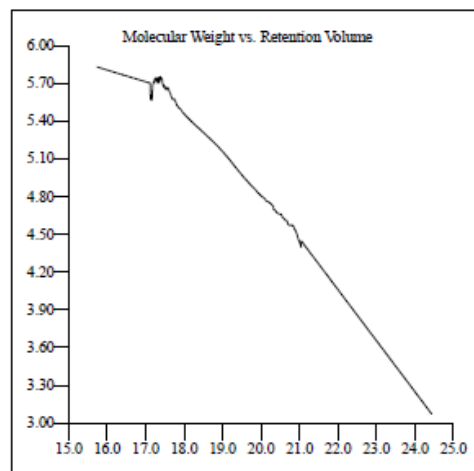
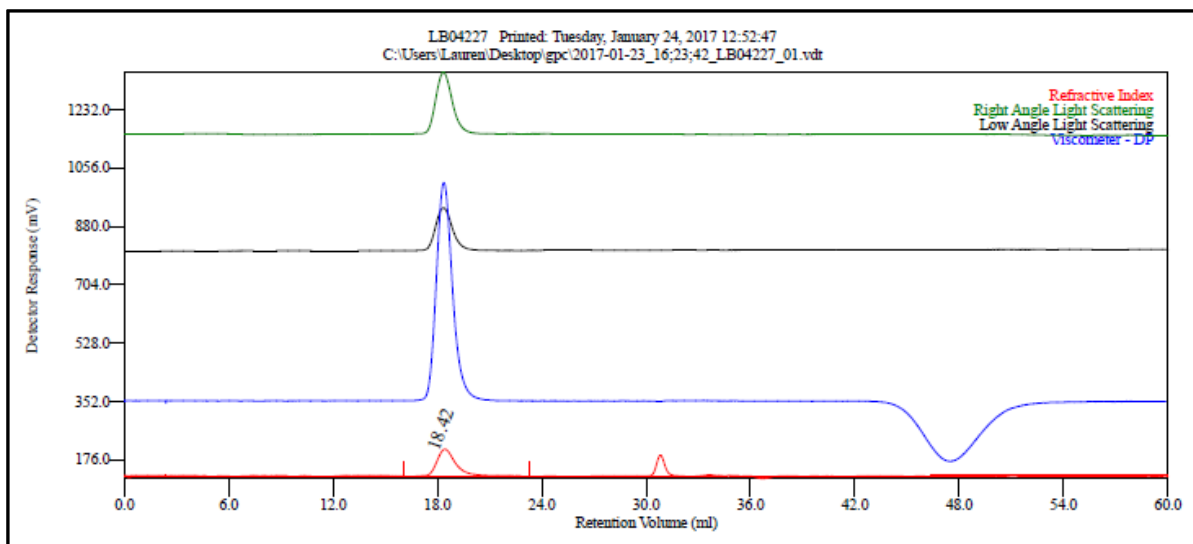


Figure C.20 GPC of polyethylene. (Table 3.1, Entry 12; Table 3.2, Entry 3)



Multi-Detectors - Homopolymers : Results

Peak RV - (ml)	18.420
Mn - (Daltons)	161,556
Mw - (Daltons)	200,523
Mz - (Daltons)	223,178
Mp - (Daltons)	217,887
Mw / Mn	1.241
Percent Above Mw.	0
Percent Below Mw.	0
IV - (dl/g)	2.3981
Rh(w) - (nm)	19.417
Rg(w) - (nm)	27.824
Wt Fr (Peak)	1.000
Mark-Houwink a	0.806
Mark-Houwink logK	-3.884
Branches	0.000
Branch Freq.	0.000
RI Area - (mVml)	99.20
UV Area - (mVml)	0.00
RAIS Area - (mVml)	205.48
LALS Area - (mVml)	145.34
IVDP Area - (mVml)	713.06

Sample Parameters	Input	Calculated
Sample Conc - (mg/ml)	2.310	0.000
Sample Recovery (%)	0.000	84.398
dn/dc - (ml/g)	0.1040	0.0000
dA/dc - (ml/g)	1.0000	0.0000

Annotation	
Method File	Long Group 1-9-16-0000.vcm
Limits File	
Date Acquired	Jan 23, 2017 - 16:23:42
Solvent	TCB
Acquisition Operator	admin - Administrator
Calculation Operator	admin - Administrator
Column Set	CLM6210 - HT X 3
System	System 1
Flow Rate - (ml/min)	1.000
inj Volume - (ul)	200.0
Volume Increment - (ml)	0.00333
Detector Temp. - (deg C)	160.0
Column Temp. - (deg C)	160.0
OmniSEC Build Number	406

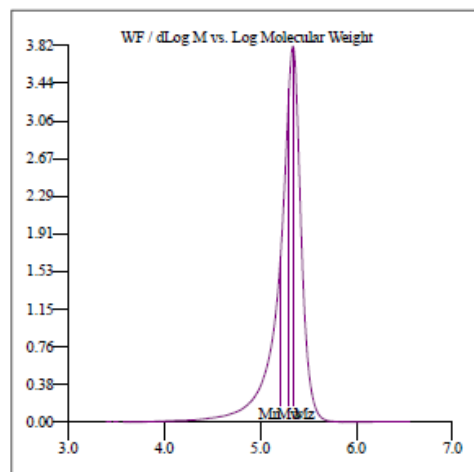
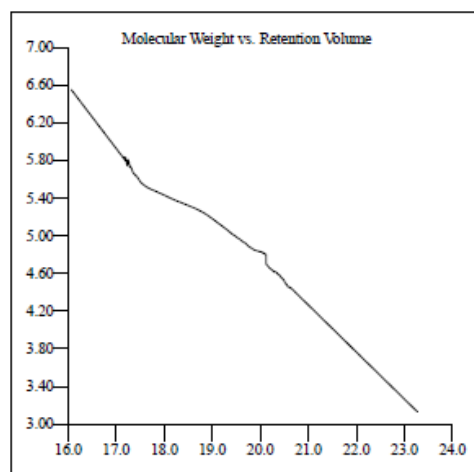
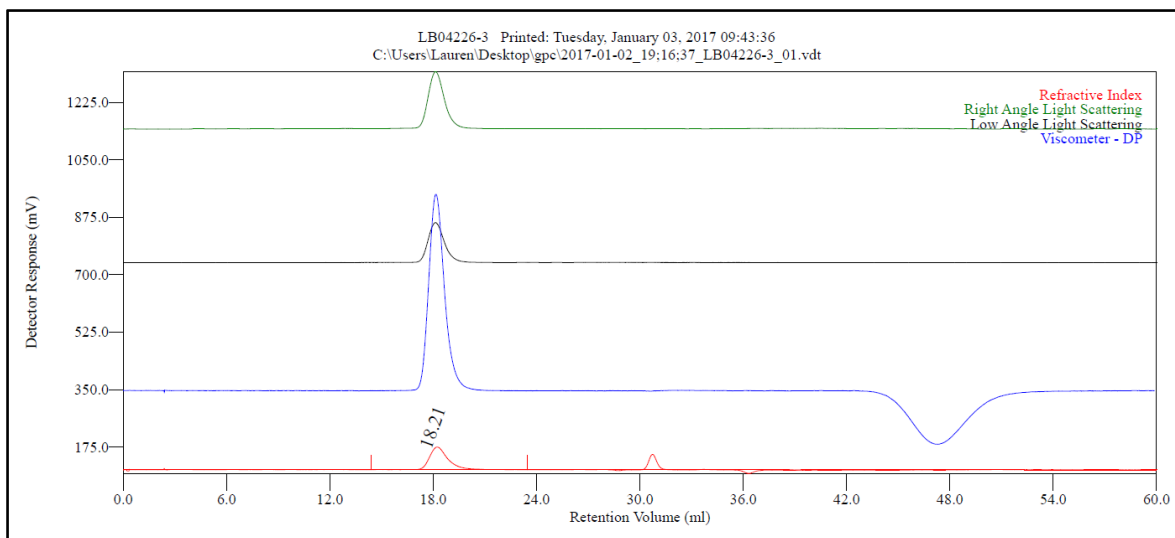


Figure C.21 GPC of polyethylene. (Table 3.1, Entry 13)



Multi-Detectors - Homopolymers : Results

Peak RV - (ml)	18.213
Mn - (Daltons)	192.793
Mw - (Daltons)	255.586
Mz - (Daltons)	292.681
Mp - (Daltons)	283.614
Mw / Mn	1.326
Percent Above Mw:	0
Percent Below Mw:	0
IV - (dl/g)	2.9555
Rh(w) - (nm)	22.488
Rg(w) - (nm)	No Calc
Wt Fr (Peak)	1.000
Mark-Houwink a	0.747
Mark-Houwink logK	-3.561
Branches	0.000
Branch Freq.	0.000
RI Area - (mVml)	85.46
UV Area - (mVml)	0.00
RALS Area - (mVml)	190.64
LALS Area - (mVml)	133.65
IVDP Area - (mVml)	643.32

Sample Parameters	Input	Calculated
Sample Conc - (mg/ml)	2.200	1.675
Sample Recovery (%)	0.000	76.133
dn/dc - (ml/g)	0.1040	0.0000
dA/dc - (ml/g)	1.0000	0.0000

Annotation	
Method File	after RI intensity increase-0003.vcm
Limits File	
Date Acquired	Jan 02, 2017 - 19:16:37
Solvent	TCB
Acquisition Operator	admin : Administrator
Calculation Operator	admin : Administrator
Column Set	CLM6210 - HT X 3
System	System 1
Flow Rate - (ml/min)	1.000
Inj Volume - (ul)	200.0
Volume Increment - (ml)	0.00333
Detector Temp. - (deg C)	160.0
Column Temp. - (deg C)	160.0
OmniSEC Build Number	406

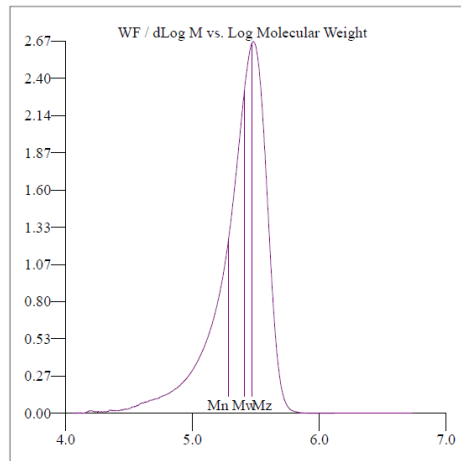
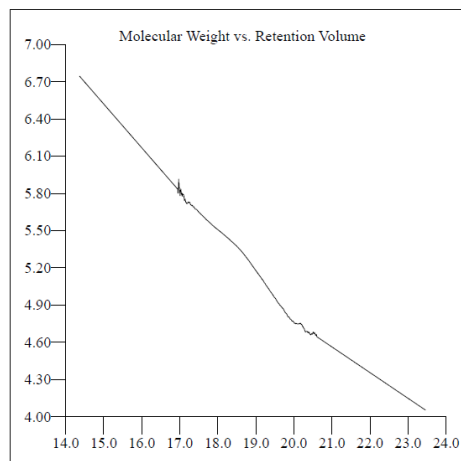
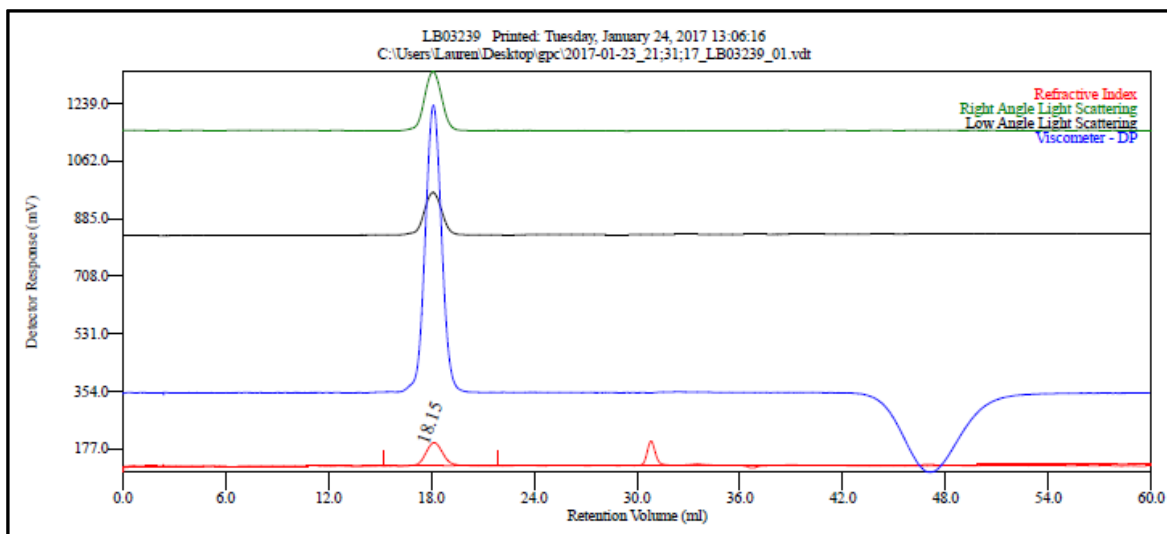


Figure C.22 GPC of polyethylene. (Table 3.1, Entry 14)



Multi-Detectors - Homopolymers : Results

Peak RV - (ml)	18.150
Mn - (Daltons)	204.427
Mw - (Daltons)	230.345
Mz - (Daltons)	245.254
Mp - (Daltons)	222.518
Mw / Mn	1.127
Percent Above Mw:	0 100.000
Percent Below Mw:	0 0.000
IV - (dl/g)	3.4764
Rh(w) - (nm)	23.182
Rg(w) - (nm)	33.890
Wt Fr (Peak)	1.000
Mark-Houwink a	0.621
Mark-Houwink logK	-2.791
Branches	0.000
Branch Freq.	0.000
RI Area - (mVml)	82.71
UV Area - (mVml)	0.00
RALS Area - (mVml)	209.67
LALS Area - (mVml)	156.74
IVDP Area - (mVml)	985.35

Sample Parameters	Input	Calculated
Sample Conc - (mg/ml)	2.180	0.000
Sample Recovery (%)	0.000	74.568
dn/dc - (ml/g)	0.1040	0.0000
dA/dc - (ml/g)	1.0000	0.0000

Annotation	
Method File	Long Group 1-9-16-0000.vcm
Limits File	
Date Acquired	Jan 23, 2017 - 21:31:17
Solvent	TCE
Acquisition Operator	admin : Administrator
Calculation Operator	admin : Administrator
Column Set	CLM6210 - HT X3
System	System 1
Flow Rate - (ml/min)	1.000
Inj Volume - (ul)	200.0
Volume Increment - (ml)	0.00333
Detector Temp. - (deg C)	160.0
Column Temp. - (deg C)	160.0
OmniSEC Build Number	406

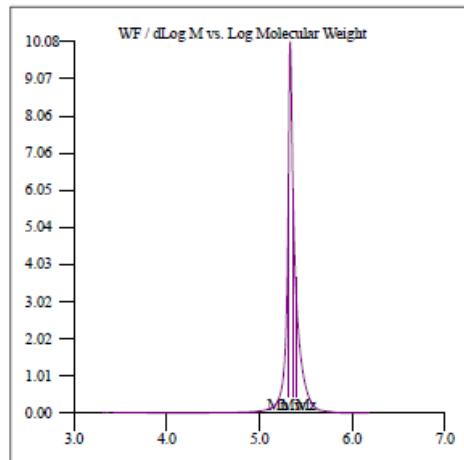
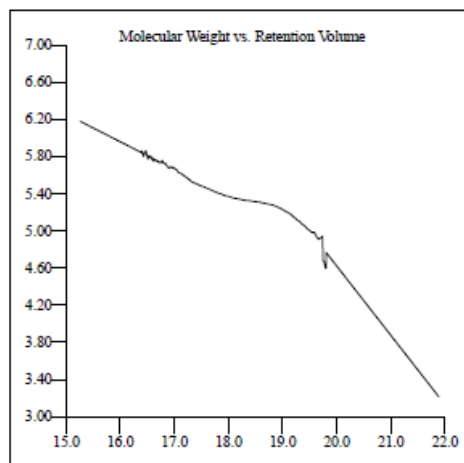


Figure C.23 GPC of polyethylene. (Table 3.2, Entry 1)

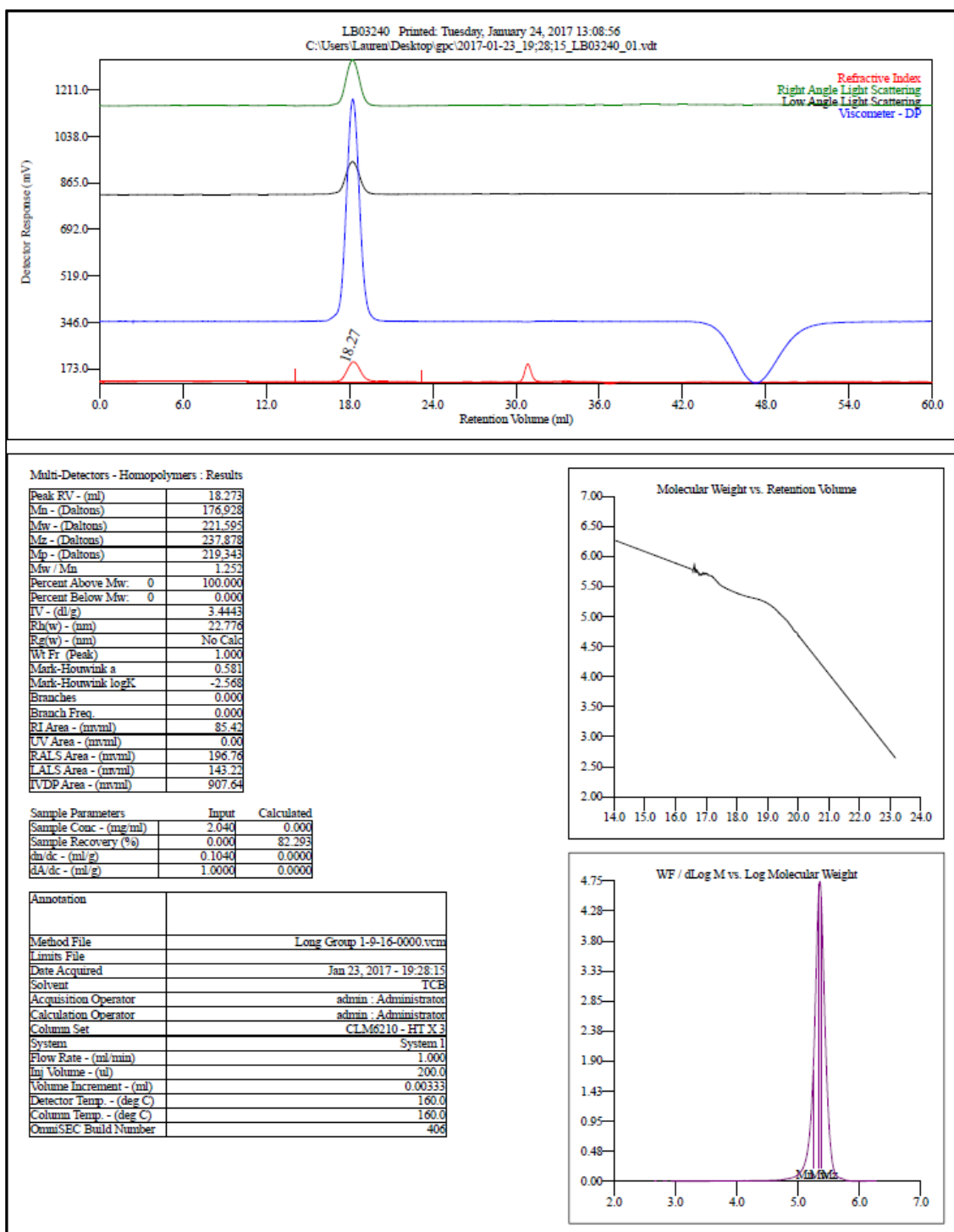


Figure C.24 GPC of polyethylene. (Table 3.2, Entry 2)

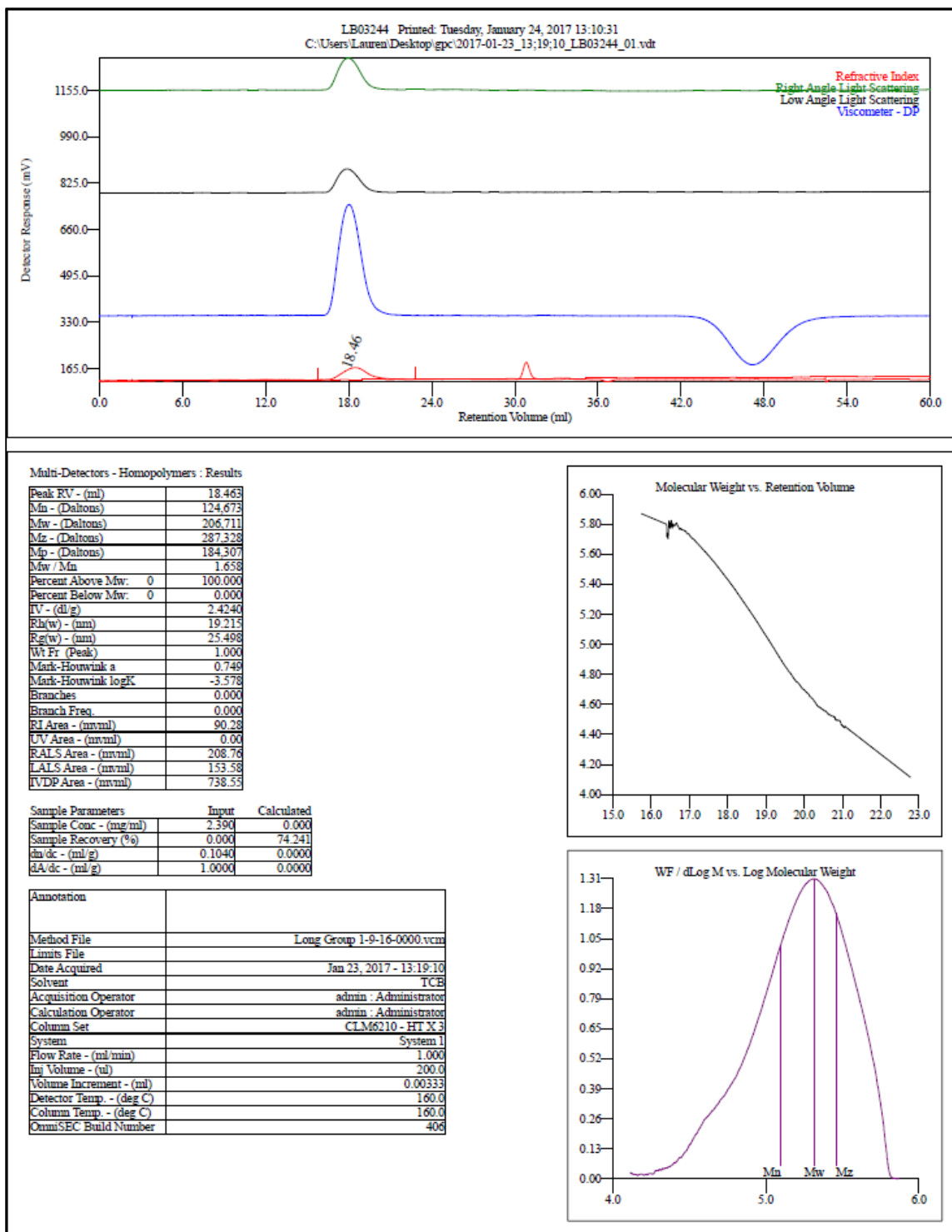


Figure C.25 GPC of polyethylene. (Table 3.2, Entry 4)

C.3 Supporting Information – Chapter 5

C.3.1 X-ray Crystallography Data

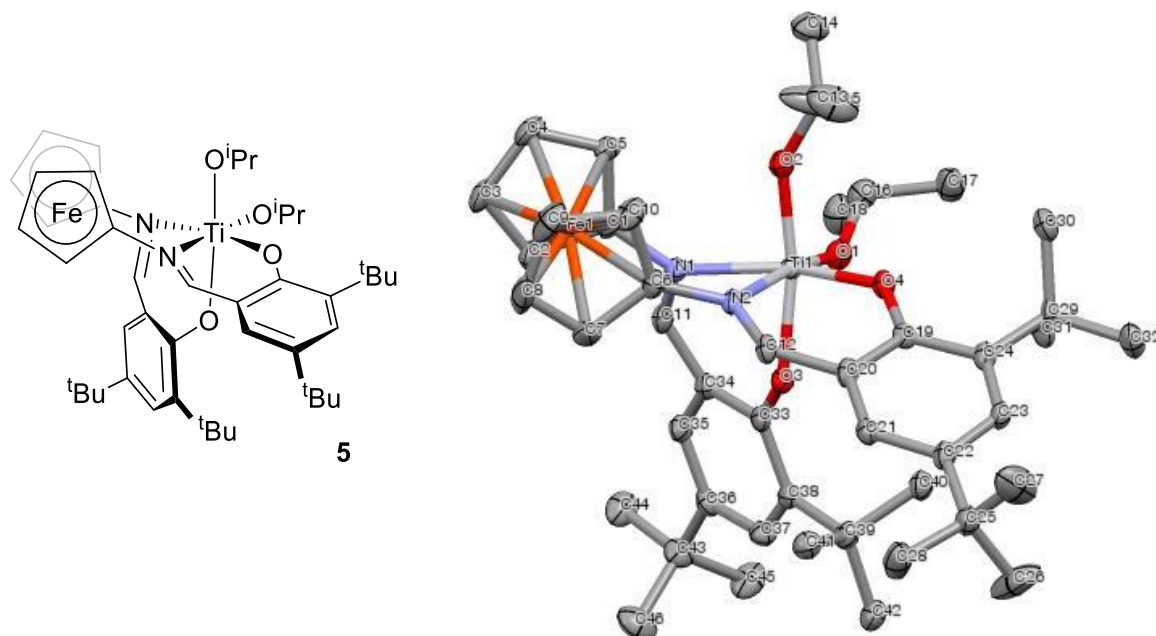
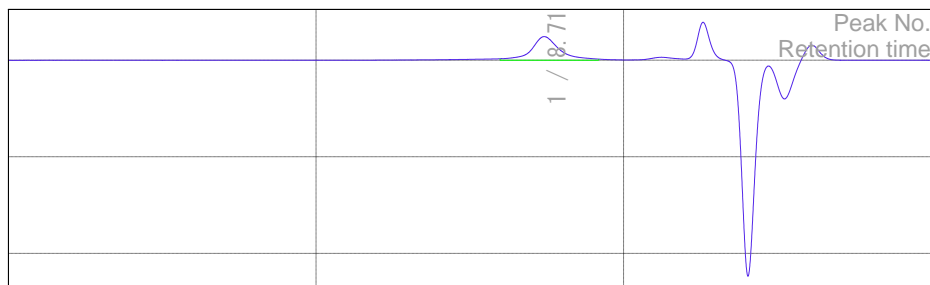


Figure C.26 ORTEP representation of (salfen)Ti(OⁱPr)₂ (**5_{red}**) with thermal ellipsoids drawn at 50% probability. Hydrogens were omitted for clarity. X-ray quality single crystals of complex **5_{red}** were grown overnight at ambient temperature from a concentrated hexanes solution. Crystal data for C₄₆H₆₄FeN₂O₄Ti (812.74 g/mol); orthorhombic; space group P-2₁; *a* = 10.8375(13) Å; *b* = 14.8073(18) Å; *c* = 27.377(3) Å; α = 90°; β = 90°; γ = 90°; *V* = 4393.3(9) Å³; *Z* = 4; *T* = 273(2) K; λ = 0.71073 Å; μ = 0.554 mm⁻¹; *R*₁ = 0.0505, *wR*₂ = 0.1255 for 8408 reflections; GOF = 0.901. Data for this structure can be obtained free of charge from the Cambridge Crystallographic Data Center (CCDC) under CCDC1570783.

C.3.2 Gel Permeation Chromatography



Result of molecular weight calculation (RI)

Peak 1 Valley Peak

	[min]	[mV]	[mol]		Mn	
Peak start	7.990	0.740	45,634		Mw	13,319
Peak top	8.713	12.245	15,515		Mz	15,959
Peak end	9.593	0.586	3,911		Mz+1	18,869
Height [mV]			12.257		Mv	22,276
Area [mV*sec]			394.108		Mp	15,959
Area% [%]			100.000		Mz/Mw	15,633
[eta]			15958.97509	w	Mw/Mn	1.182
					Mz+1/M	1.198
						1.396

Result of molecular weight calculation (RI)

Total

	[min]	[mV]	[mol]		Mn	
Peak start	7.990	0.740	45,634		Mw	13,319
Peak top	8.713	12.245	15,515		Mz	15,959
Peak end	9.593	0.586	3,911		Mz+1	18,869
Height [mV]			12.257		Mv	22,276
Area [mV*sec]			394.108		Mp	15,959
Area% [%]			100.000		Mz/Mw	15,633
[eta]			15958.97509	w	Mw/Mn	1.182
					Mz+1/M	1.198
						1.396

Figure C.27 Representative GPC trace of PLA formed with rereduced catalyst **5_{red}**. Samples measured in THF at 40 °C and referenced to polystyrene standards (**Table 5.1**, Entry 6)

VITA

Lauren Ashley Brown was born and raised in Easley, South Carolina. After graduating high school in 2007, Lauren began studying at Wofford College in Spartanburg, South Carolina where she earned a B.S. in chemistry. After she graduated Wofford in 2011, Lauren started working for Milliken and Company in Spartanburg, South Carolina. She was a technical laboratory specialist for the applications section of polymeric colorants and additives. In fall of 2012, Lauren started graduate studies at the University of Tennessee. Lauren worked for Dr. Brian K. Long, and during her tenure at UTK, she published several manuscripts, attended national and regional ACS conferences, and earned multiple awards for her accomplishments, including the Chancellor Fellowship, Jerome Eastham Award for Organic Chemistry, Eli Lilly/Women Chemists Committee Travel Award, and Excellence in Polymer Research Award.